Engineering Cytochrome $P450_{BM3}$ into a Drug Metabolising Enzyme

Jake Yorke

St. Peter's College

University of Oxford

Trinity 2012

A thesis submitted to the Board of the Faculty of Physical Sciences in partial fulfilment of the requirements for the degree of Doctor of Philosophy in the University of Oxford

Engineering Cytochrome $P450_{BM3}$ into a Drug Metabolising Enzyme

Jake Yorke D. Phil. Thesis Abstract

St. Peter's College Trinity, 2012

Directed evolution studies by Whitehouse *et al.* identified several variants of $P450_{BM3}$ (CYP102A1) with enhanced substrate oxidation rates across a range of substrates. This thesis describes the use of these 'generic accelerator' variants, in combination with selectivity altering mutations to engineer $P450_{BM3}$ for the oxidation of pharmaceuticals. Using engineered variants the non-steroidal anti-inflammatory drug diclofenac was metabolised to the primary human metabolites 4′- and 5-hydroxydiclofenac, with total conversion of 2 mM substrate by 5 μM enzyme. The local-anaesthetic lidocaine and the steroid testosterone were similarly metabolised to human metabolites. This is the first report of a drug compound being totally converted to the human metabolites by a $P450_{BM3}$ variant, and is also the first report of lidocaine metabolism by a $P450_{BM3}$ variant. The engineered variants are akin to CYP3A4, the primary human drug metabolising enzyme, as they show activity towards a range of compounds including anionic, cationic and neutral drugs. This range of activity is at the expense of NADPH coupling, which remains low with these substrates.

In order to more fully understand the origin of the rate enhancing properties of the generic accelerator variants, spectroelectrochemical, stopped-flow and kinetic studies were performed. A custom optically transparent thin layer electrode system was designed and fabricated for use in spectroelectrochemical titrations. A spectroelectrochemical cell and gold mesh electrode were designed and used in spectroelectrochemical investigations of $P450_{BM3}$ variants, as well as other P450s and their redox partners. These spectroelectrochemical, stopped-flow and kinetic studies, in combination with X-ray

crystal structures provided insight into the origin of the rate enhancing properties of these enzymes and supplied the first example of the complete characterization of the thermodynamic and kinetic properties of WT and mutant $P450_{BM3}$ for the oxidation of a non-natural substrate. The generic accelerator variants are, in the resting state, in a more catalytically ready conformation than the WT enzyme, and reorganization energy barriers appear to be lowered, so that fewer substrate-induced structural changes are required to promote electron transfer and initiate the catalytic cycle.

Acknowledgements

First and foremost I would like to thank my supervisor Dr. Luet Wong, whose enthusiasm and outstanding attitude has been an inspiration. Without his guidance, support and patience I could not have completed this thesis and it has been a privilege to work with such an outstanding supervisor.

Many thanks to Dr. Stephen Bell for always having a helpful answer, seemingly never running out of patience with me and teaching me how to work efficiently. Thanks to Dr. Christopher Whitehouse for teaching me the ins and outs of molecular biology, pleasant chats over coffee and an encyclopaedic knowledge of the literature.

To Eachan: thanks for always being up for a coffee break and keeping me entertained in the lab. It's been a pleasure. Thanks to Nicki, Dom, Chris, Anthony S., Adrian, Clare, Anthony B., Rachel, Ben, Emma, James, Larry, Laura, Emily, Kouji and Sophia, who have been a joy to work with.

A special thank you to Dr. Christopher Blanford for teaching me electrochemistry and potentiometric titrations, and to Dr. Peter Leigh for letting me play with the photolithography kit in engineering. Thanks to Dr. Nick Rees for running NMR spectra and Dr. Colin Sparrow for running Mass Spec. Thanks go to Mr. Keith Waters and Ms. Terri Adams for fabrication of custom equipment. Particular thanks to Professor Zihe Rao and his group in Nankai University in China for solving crystal structures. Thank you to the Rhodes Trust and the Natural Sciences and Engineering Research Council of Canada for funding.

Thank you to OUPLC and MMRFC, for keeping me busy and acting as perfect stress releases during the past 4 years.

Finally, thank you to Gillian, for constant support, reassurance and understanding that science is a fickle mistress. Thank God for Skype.

Table of Contents

List of Figures

List of Tables

Abbreviations

AdR: adrenodoxin reductase

Adx: adrenodoxin

AU: absorbance unit

CPO: chloroperoxidase

CPR: cytochrome P450 reductase

CTAB: hexadecyltrimethylammonium bromide

CYP: cytochrome P450

DMDA: dimethyldioctadecylammonium, bromine salt

DSS: dioctylsulfosuccinate

DTT: dithiothreirol

FAD: flavin adenine dinucleotide

FMN: flavin mononucleotide

GC: gas chromatography

HPLC: high performance liquid chromatography

IPTG: isopropyl-β-D-thiogalactopyranoside

Kan: kanamycin

LB: Luria-Bertani Broth

$NAD(P)^+$: nicotine adenine dinucleotide (phosphate)

NAD(P)H: nicotine adenine dinucleotide (phosphate), reduced form

NMR: nuclear magnetic resonance

NOS: nitric oxide synthase

NPG: *N*-palmitoyl glycine

NSAID: non-steroidal anti-inflammatory drug

OTTLE: optically transparent thin layer electrode

PCR: polymerase chain reaction

PDB: protein data bank

PdR: putidaredoxin reductase

Pdx: putidaredoxin

PFR: produce formation rate

SB: Substrate-bound

SF: Substrate-free

PMMA: poly-methylmethacrylate

TFB: transformation buffer

Tris: 2-Amino-2-hydroxymethyl-propane-1,3-diol

TTN: total turnover number

WT: wild type (i.e. mutation-free)

Chapter One

Introduction

1.1 General background

1.1.1 Cytochrome P450 enzymes

Cytochrome P450 monooxygenases (P450s) are heme *b* containing enzymes found in nearly all forms of life. The typical P450 reaction involves the insertion of one atom of atmospheric dioxygen into a C—H bond, generating the corresponding alcohol, with the other atom being reduced to water.

$$R—H + 2H^+ + O_2 + 2e^- \longrightarrow R—OH + H_2O$$

This contrasts with iron containing dioxygenases which incorporate both atoms of dioxygen into the substrate. The two electrons required for dioxygen activation are commonly derived from NAD(P)H and shuttled to the heme by electron transfer partners.

This unique functionality endows P450 enzymes with a myriad of physiological roles, from activity in metabolic pathways of bacteria to the biosynthesis of antibiotics, vitamins and steroids in higher organisms. Many biologically active secondary plant metabolites, such as the antimalarial agent artemisinin[1], are products of P450 reactions. Though involved in a staggering number of physiologically important reactions, P450s are perhaps best known for the metabolism of xenobiotics in humans[2]. Nearly 80% of the drugs currently on the market are metabolised by just five human P450s[3].

Given the vast number of identified P450s (over 18,000 *CYP* genes are found in genome databases) there is an understandably diverse functional range across the superfamily. Some P450 enzymes operate with a high degree of substrate specificity, oxidizing a small range of substrates with high regio- and stereo- selectivity. Examples of highly specific P450s include $P450_{cam}$ which selectively oxidizes camphor to 5-*exo*-hydroxycamphor,

and those P450s involved in steroid biosynthesis. Others, such as those found in the human liver, are active across a broad range of substrates. While the insertion of an oxygen atom into a C—H bond is the signature P450 reaction, there are other known reaction types, including epoxidation, desaturation, dearomatization, dealkylation, ring expansion, C—C bond formation[4] and heteroatom oxidation[5-7].

Cytochromes P450, so named for the intense absorption band at 450 nm in the CO-bound, reduced form of the enzyme, display a huge variety in primary structure, with only the heme ligating cysteine residue being conserved[8]. However, the tertiary structure is highly conserved, giving P450s a distinct protein fold. Figure 1.1 shows this conserved tertiary structure across four P450s with different reactivities. Within the conserved protein fold there are structural differences between membrane bound and soluble proteins[9], but even these structures are broadly similar. The conserved protein fold in the P450 superfamily may point towards a common ancestor and mechanism of oxygen activation, while the variation in the substrate binding pocket attests to the variation in function demonstrated by these enzymes[10].

Traditionally, P450 enzymes were named after their host organism, as in $P450_{FOXY}$ from *Fusarium oxysporum*; their substrate, as in $P450_{cam}$, the camphor oxidizing P450 from *Pseudomonas putida*; or the order in which they were isolated from their host, as in $P450_{BM3}$, the third P450 isolated from *Bacillus megaterium.* However, as more than 18,000 *CYP* genes are presently known, a more systematic nomenclature has been adopted.

Presently, P450 enzymes and the genes encoding them are designated with the CYP prefix. This is followed by a number denoting the family of cytochrome, where members of the same family share 40% sequence identity. The subfamily, those enzymes with 55% sequence identity, is specified with a letter, and an additional number denotes the

individual gene within that family. Thus, the enzyme $P450_{cam}$ is designated CYP101A1, while $P450_{BM3}$ is CYP102A1. The CYP designation of a P450 enzyme also indicates the type of organism from which the gene is isolated, with 1–49 designating an animal, 51–69 for lower eukaryotes, 71–99 for plants and 101 and upward for bacteria, though this system is not sufficient to allow for the correct designation of all *CYP* genes being discovered, as the field is expanding rapidly and new family numbers will have to be implemented to accommodate overflow[11]. Throughout this thesis, P450s will be referred to by their CYP designations, with the exception of those widely known by their older name, such as $P450_{BM3}$.

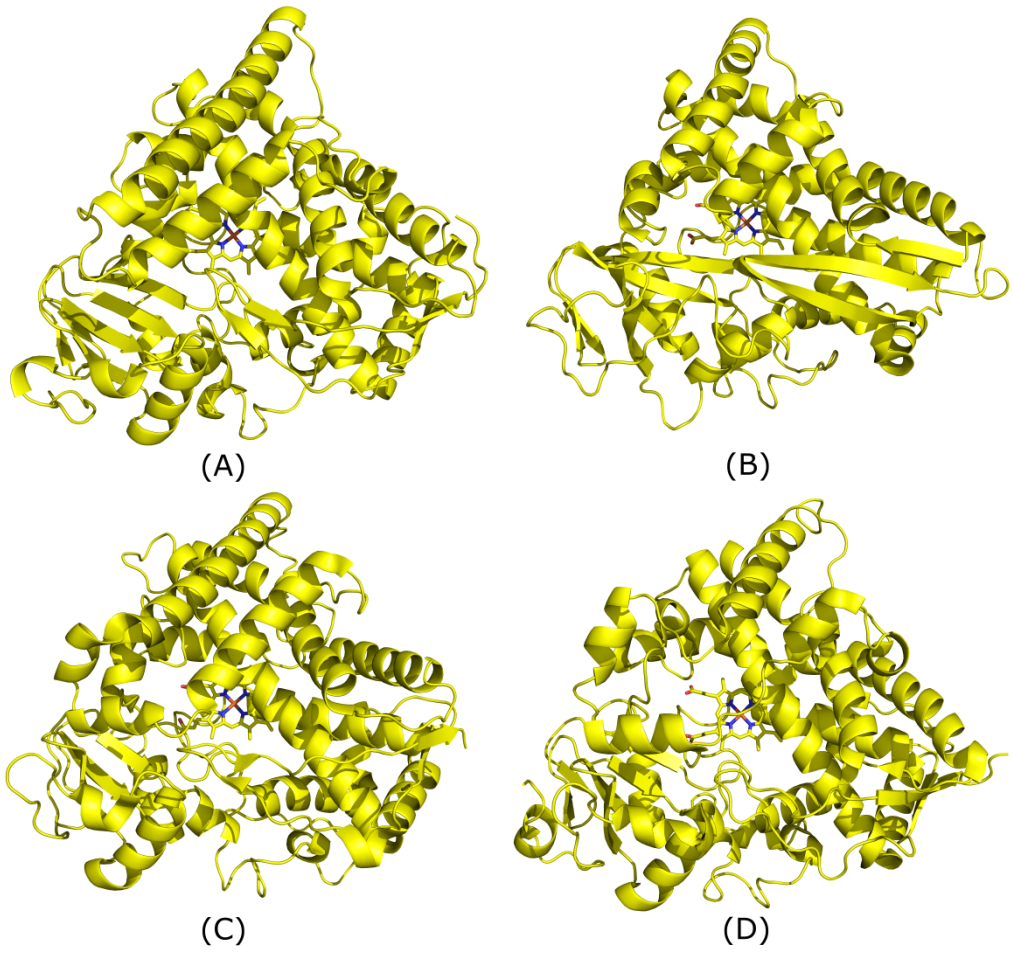

Figure 1.1. Conserved structure of P450 enzymes. **(A)** $P450_{BM3}$ heme domain[12] (PDB code 1BU7); **(B)** Camphor-bound (omitted) $P450_{cam}$[13] (PDB code 2CPP); **(C)** CYP2C9[14] (PDB code 1OG2); **(D)** CYP3A4[15] (PDB code 1TQN).

1.1.2 Electron transfer in P450s

The heme in most P450s cannot directly accept electrons from NAD(P)H, though hydrogen peroxide is able to deliver electrons and act as the source of an oxygen atom, as in the case of fatty acid alpha-hydroxylase (FAAH)[16] and other peroxygenases. Most P450s require redox partners to deliver electrons. P450 enzymes were therefore divided into two broad classes based on the nature of their redox partners; those obtaining electrons from NADPH via a diflavin reductase naturally found in liver microsomes[17], and the mitochondrial P450s accepting electrons from NADPH via adrenodoxin reductase and adrenodoxin[18, 19]. As more P450s were discovered, it became obvious that two classes could not account for the extreme diversity across the Cytochrome P450 superfamily. Now, some ten classes are required to cover the wide range of electron transfer chains[20]. These classes are summarized in Table 1.1 and fundamentally represent different permutations of P450 enzymes with primarily ferredoxin or flavodoxin electron transport proteins, though other distinct classes (such as the phthalate dioxygenase reductase domain-fused systems) do exist.

The two types of electron transfer chains directly relevant to this thesis are the classic PdR/Pdx/$P450_{cam}$ type (Class I) three-component system and the fused, single polypeptide $P450_{BM3}$ type system (Class VIII), which are shown schematically in Figure 1.2.

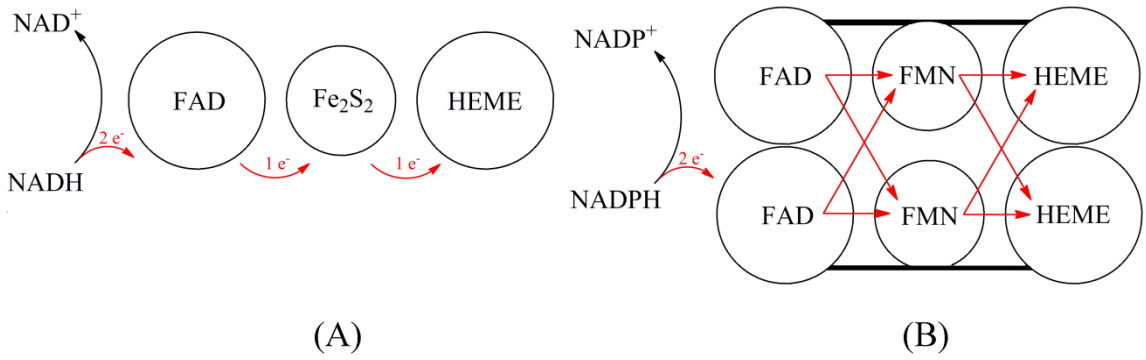

Figure 1.2. Schematic showing the most relevant electron transfer systems in this thesis. **(A)** A PdR/Pdx/$P450_{cam}$ type electron transfer system; **(B)** $P450_{BM3}$ electron transfer, where the red arrows indicate possible pathways for electron transfer in the dimer.

In the PdR/Pdx/$P450_{cam}$ type electron transfer system the initial electron receptor is a flavin adenine dinucleotide (FAD)-containing ferredoxin reductase which receives two electrons from NADH. The electrons are then passed sequentially to the [Fe_2S_2]-ferredoxin Pdx which shuttles them to the terminal electron acceptor, $P450_{cam}$. Another well characterized three component ferredoxin reductase/ferredoxin/P450 system is the AdR/Adx/CYP24A1 system, which has also been completely structurally characterized[21, 22].

In systems such as $P450_{BM3}$, the heme domain is fused to a reductase domain containing both FAD and flavin mononucleotide (FMN) binding domains. Electron transfer between domains in $P450_{BM3}$ is fast, which supports the highest substrate oxidation rates of any P450 class (3200 nmol (nmol $P450_{BM3}$)$^{-1}$ min^{-1} with arachidonate)[23]. The rapid electron transfer observed in $P450_{BM3}$ is not solely the result of the three component domains being fused in a single polypeptide, however, as $P450_{BM3}$ is functionally a dimer[24-26]. Indeed, at least one of the electron transfer steps is across the dimer interface, but it is not clear between which domains this occurs[27].

Table 1.1. Electron transfer classes in P450s[20].

Class/Source	Electron transport chain	Remarks	Example P450
Class I			
Bacterial	NAD(P)H ▸[FdR] ▸[Fdx] ▸[P450]	Cytosolic, soluble	$P450_{cam}$
Mitochondrial	NADPH ▸[FdR] ▸[Fdx] ▸[P450]	P450 membrane bound, FdR membrane associated, FdX soluble	CYP11A1
Class II			
Bacterial	NADH ▸[CPR] ▸[P450]	Cystolic, soluble, most common eukaryotic type	CYP105A3
Microsomal	NADPH ▸[CPR] ▸[P450]	Membrane anchored	CYP2B1
Class III			
Bacterial	NAD(P)H ▸[FdR] ▸[Fldx] ▸[P450]	Cystolic, soluble	CYP176A1
Class IV			
Bacterial	Pyruvat, CoA ▸[OFOR] ▸[Fdx] ▸ [P450]	Cytosolic, soluble, found only in extremophiles	CYP119
Class V			
Bacterial	NADH ▸[FdR]▸ [Fdx–P450]	Cytosolic, soluble, ferredoxin reductase unknown, only one known example	CYP51
Class VI			
Bacterial	NAD(P)H ▸[FdR] ▸[Fldx–P450]	Cytosolic, soluble, fused flavodixin and and P450 domains	*xplA*
Class VII			
Bacterial	NADH ▸[PFOR–P450]	Cytosolic, soluble, P450 C-terminally fused to a phthalate dioxygenase reductase domain	CYP116B2
Class VIII			
Bacterial, fungal	NADPH ▸[CPR–P450]	Cytosolic, soluble, catalytically self sufficient	$P450_{BM3}$
Class IX			
Fungal	NADH ▸[P450]	Cytosolic, soluble, only one known example	CYP55
Class X			
Mammalian, plant	[P450]	Membrane bound, independent of other electron transport proteins	CYP74A

The $P450_{BM3}$ type fused electron transfer system is rare among P450s, but not the only example in nature. Nitric-oxide synthase (NOS) is the enzyme responsible for the generation of NO in mammals, and is very similar to the enzymes in the P450 family[28]. NOS is also a heme-thiolate protein, fused to the diflavin reductase domain[29] and like $P450_{BM3}$ shows high activity[30].

Typically, the redox partner systems are highly specific, transferring electrons efficiently only to their natural partners. For example, if the ferredoxin PuxB from *Rhodopseudomonas palustris* is used to transfer electrons to CYP199A2 in lieu of the physiological ferredoxin from the same organism, Pux, the turnover activity drops to 99 nmol (nmol P450)$^{-1}$min^{-1} for 4-methoxybenzoic acid oxidation compared with 1,438 nmol (nmol P450)$^{-1}$min^{-1} [31]. Similarly, Adx cannot be used to reconstitute $P450_{cam}$ activity in lieu of Pdx[32]. This is not always the case, however, as the ferredoxin Arx from *Novosphingobium aromaticivorans* transfers electrons efficiently to five P450s[33]. In humans, cytochrome P450 reductase (CPR) effectively transfers electrons to over a dozen P450 enzymes[34, 35], in addition to several other metabolically important human enzymes[36] such as cytochrome b_5[37], fatty acid elongase[38] and heme oxygenase[39].

1.1.3 The P450 catalytic cycle

The catalytic cycle of P450s, shown in Figure 1.3, has been extensively studied and is therefore believed to be well understood[40]. In the resting state (**I**) the iron is six-coordinate and low-spin ($S=\frac{1}{2}$). When a viable substrate in introduced, the axial water ligand is displaced and the ferric iron becomes five-coordinate (**II**). This is accompanied by a spin-state shift to high-spin ($S=\frac{5}{2}$) which can be observed by monitoring the change in the UV-visible spectrum of the enzyme. The low-spin form has a Soret maximum at 418 nm, while the five-coordinate high-spin form has a Soret maximum at 395 nm. The

displacement of the axial water ligand also shifts the reduction potential of the heme iron to more oxidising values. This facilitates electron transfer to the heme to give the ferrous state (**III**).

The binding of oxygen (**IV**) and subsequent addition of a second electron yields the ferric peroxy complex (**V**). Upon protonation of the terminal oxygen atom the hyperoxy adduct 'Compound 0' is obtained (**VI**). A second protonation leads to cleavage of the O—O bond, the loss of water and the formation of a ferryl species, 'Compound I' (**VII**). Both Compound 0 and Compound I have been characterized[41-44], and it has been shown that Compound I is the active oxidant in most P450 reactions[45]. A hydrogen atom is abstracted from the substrate (**VIII**) and following radical-rebound, the product alcohol is released and the heme iron atom returns to the ferric resting state.

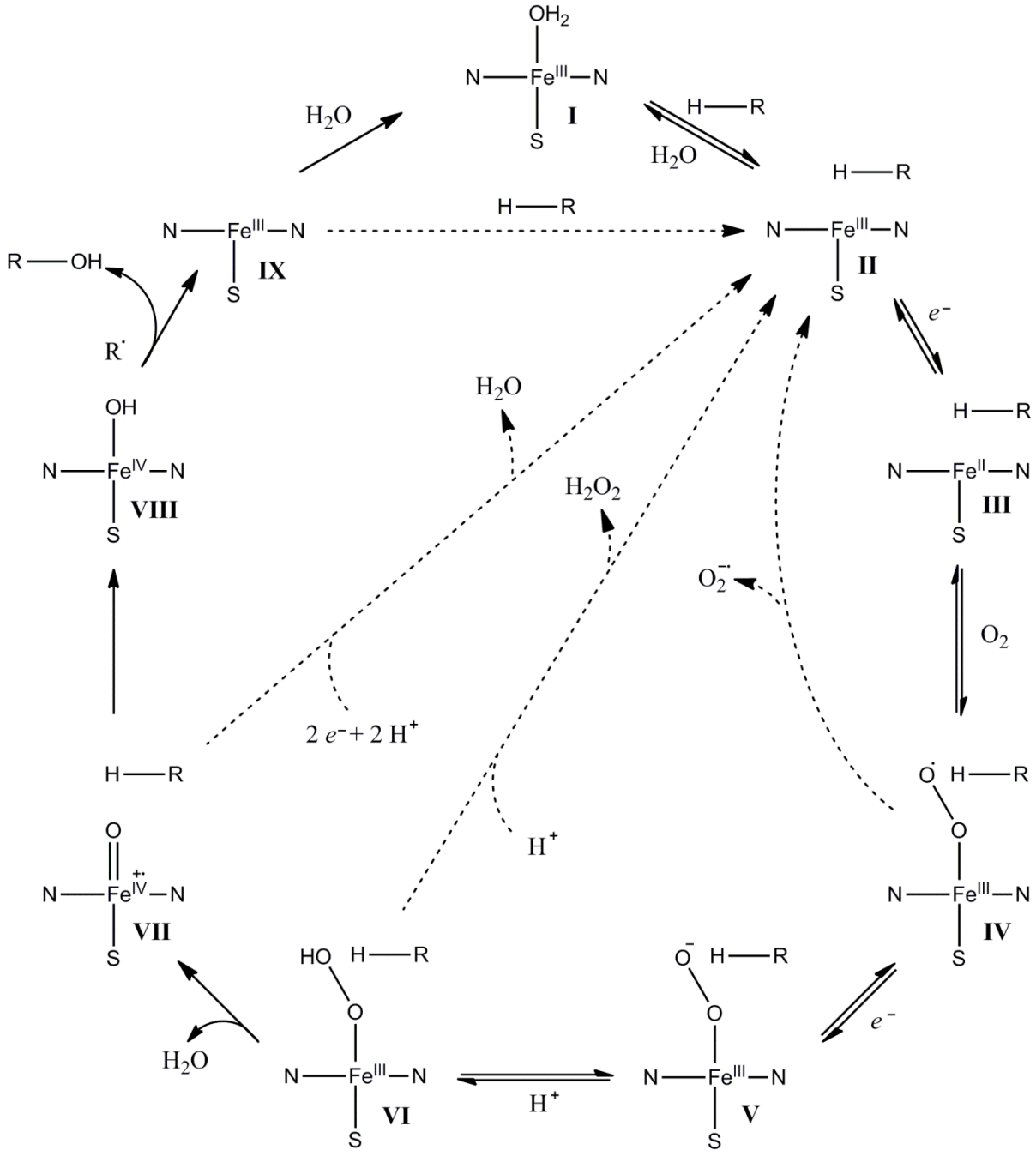

Figure 1.3. The catalytic cycle of P450 enzymes.

In some situations, NAD(P)H consumption is uncoupled from the catalytic process; the electrons provided by the cofactor are not used in the formation of product. This can happen through several routes. If the second electron transfer is slow, the superoxide may be lost, leading to superoxide uncoupling. Oxidase uncoupling occurs if a substrate without a readily available hydrogen is present, and leads to the reduction of Compound I.

One possible uncoupling reaction of the catalytic cycle can actually be used to drive the reactions. If Compound 0 is protonated, but the substrate is not tightly bound in the active site and fails to force the formation of Compound I, hydrogen peroxide is released, in a process called peroxide uncoupling. At high peroxide concentrations (mM), the peroxide uncoupling pathway may reverse, leading to the turnover of substrate driven by peroxide, rather than NAD(P)H and atmospheric oxygen. This 'peroxide shunt' is seen in the peroxidase enzymes, which have been studied and reviewed[46-48].

1.2 $P450_{BM3}$

1.2.1 Background

Perhaps the most extensively studied P450 enzyme is $P450_{BM3}$, the subject of this thesis. Several reviews have been published on this enzyme alone[40, 49-56]. The 119 kDa enzyme[57] is comprised of a 65 kDa reductase domain fused on the N-terminus to a 55 kDa heme domain by a short linker sequence[58]. $P450_{BM3}$ was initially found to oxidize medium- to long- chain fatty acids at sub-terminal positions, requiring only NADPH and oxygen to function[59]. However, it was soon found to epoxidize unsaturated fatty acids[60] and oxidize fatty amides and alcohols[61], hydroxylated fatty acids[62] and branched fatty acids[63]. It is now known that wild-type (WT) $P450_{BM3}$ is active towards a broad range of substrates[40].

1.2.2 Crystal structure and the identification of key residues

In 1993 the Peterson laboratory published the first crystal structure of the heme domain of $P450_{BM3}$ (PDB code 2HPD)[64], only the second P450 crystal structure available (the first being that of $P450_{cam}$)[13]. In 1997 Li and Poulos published a structure of the palmitoleate bound form of the heme domain (PDB code 1FAG)[65]. Since these structures were published, nearly 40 crystal structures have been reported for $P450_{BM3}$ variants. Figure

1.4 shows the active site of $P450_{BM3}$, both in the substrate-free (SF) and substrate-bound (SB) forms, highlighting key residues.

There are, not unexpectedly, several structural differences between the SF and SB forms of the enzyme. In the first $P450_{BM3}$ structure, the two molecules of the asymmetric unit displayed poor alignment in the region of the F- and G-helices and the F/G loop, indicating a great deal of fluidity in this region[64]. This area is less disordered in the palmitoleate bound form[65], and the F- and G- helices have also been rotated along their axes by roughly half a turn, which breaks a salt-bridge between Lys224-Asp251 that links the G and I-helices in the SF form. The N-palmitoylglycine (NPG)-bound structure (PDB code 1JPZ)[66] shows further changes in the I-helix (Figure 1.4 B). Specifically, the kink angle of the I-helix is reduced from 13° to 5°, disrupting an extensive network of hydrogen bonds within the active site[40]. This same hydrogen-bond network disruption leads to the I-helix withdrawing by 1.7 Å from the heme iron, compared to the SF WT structure.

The NPG-bound structure reveals further conformational changes in the area of the G-helix. As a result of this helix being shifted to a position closer to the C-terminus of the E-helix, the side chain of Ile219 impacts the aromatic ring of Phe158. This begins the 'phenylalanine cascade,' as the side chain of Phe158 rotates through *ca.* 90° to relieve steric constraints of Ile219 (Figure 1.4 C). This rotation impinges on the aromatic ring of Phe261, which also rotates by *ca.* 90°. It has been proposed that substrates exit the active site through a hole beside Phe261[67], though the rotation does not appear to enlarge this opening, so the exact functional role of the phenylalanine cascade is unknown.

The axial water ligand found in the SF WT is no longer present in the NPG-bound structure, and instead an ordered water molecule is located 3.5 Å from the heme iron (Figure 1.4 D). This water molecule is hydrogen-bound to the carbonyl oxygen of

Ala264, as is the axial water ligand in the SF WT structure, and it is proposed that the axial water ligand is relocated to this alternative binding site by substrate-induced conformational changes[66].

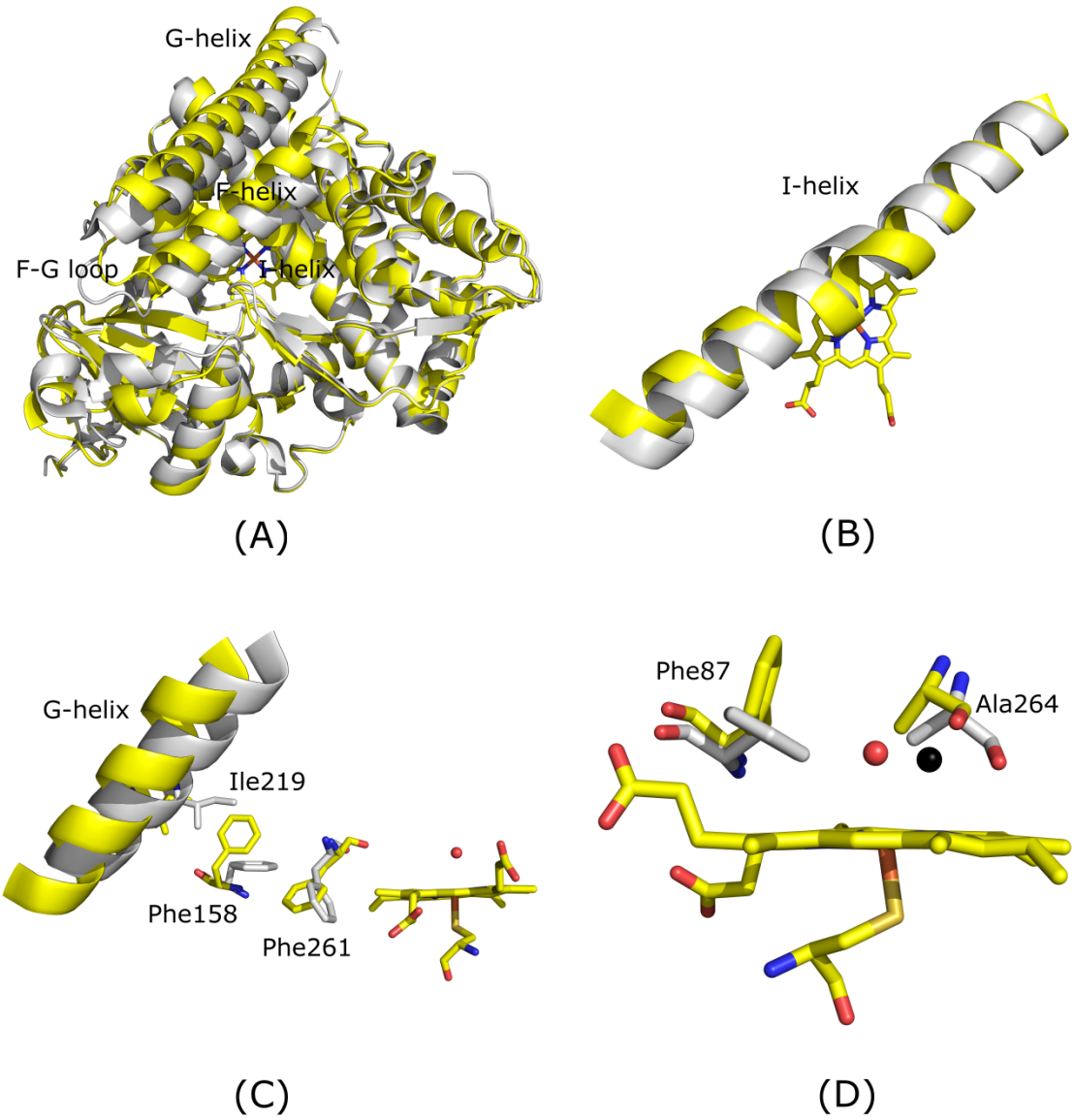

Figure 1.4. Overlay of the crystal structure of SF WT (PDB code: 1BU7) with the NPG-bound WT (PDB code: 1JPZ). SF WT is shown in yellow with waters as red spheres. NPG-bound WT is shown in grey with waters as black spheres. **(A)** full overlay; **(B)** top-down view of the I-helix, showing the reduction in the kink angle and the movement away from the heme in the NPG-bound form; **(C)** shows the phenylalanine cascade in the NPG-bound form; **(D)** show the rotation of Phe87 and displacement of axial water ligand in the NPG-bound form.

The displacement of the axial water ligand shifts the spin-state of the heme iron to high-spin, and this shift is accompanied by a corresponding shift in the heme reduction potential to a more oxidizing value. These substrate induced structural changes also activate the heme to electron transfer, though the precise mechanism of this activation is unknown. In three-component systems, such as PdR/Pdx/$P450_{cam}$, it is believed that conformational changes are key in activating the enzyme towards electron transfer from the ferredoxin[32], and it appears that a similarly important conformational gate is in effect here.

The SF structure shows a substrate access channel lined with hydrophobic residues, which contrasts to the $P450_{cam}$ structure, where no clear substrate access channel can be identified[13]. The SB structure shows the fatty acid substrate extending through the access channel. However, the terminal carbon atoms lie too far from the heme iron for oxidation[65]. It has been proposed that the enzyme only adopts a catalytically ready conformation upon heme reduction[68], when the substrate moves a full 7 Å towards the ferrous iron. Indeed, the spin-state of the NPG-bound is temperature-dependent, and it has been proposed that the substrate remains bound at all temperatures but, upon cooling, moves from a position near the heme where the ligating water is displaced to a more distant position which restores the ligating water and lowers the spin-state[69].

Lying above the heme, in a position leucine typically occupies in microsomal fatty acid hydroxylases[52], is a phenylalanine, Phe87. The side chain of Phe87 extends into the active site, and undergoes a *ca*. 90° rotation upon substrate binding[70, 71]. The addition of a substrate to $P450_{BM3}$ induces a spin-state shift, indicating displacement of the axial water. However, as noted above, the substrate binds too far away from the heme to cause the displacement of the water ligand. It has been proposed that the rotation of Phe87 which is induced by the binding of substrate causes the water displacement, and therefore the spin-

state shift[66]. Phe87 may have other roles in addition to the displacement of the ligating water, including promoting sub-terminal oxidation by isolating the terminal carbon in long-chain fatty acids in a binding pocket between Phe87 and Phe81[60, 61, 72, 73]. One study showed that terminal oxidation could be achieved by substituting the phenylalanine for alanine[74], supporting the hypothesis that Phe87 sequesters the terminal carbon of fatty acids. However, subsequent studies were unable to reproduce terminal oxidation[49, 71, 75-78], and it was noted that the F87A substitution tends to shift selectivity towards the centre of the fatty acid, rather than the terminus, it is now generally agreed that the sequestering of the terminal carbon is not a functional role of Phe87[40].

As soon as the hydrophobic substrate access channel was found, it was proposed that there must be an anchoring site for the hydrophilic head of the fatty acid substrates[61]. Indeed, the residues Arg47 and Tyr51 were shown to be closely associated with the carboxylate of the fatty acid and are believed to be involved in the initial recognition and subsequent sequestering of natural substrates.

Ala264, in the middle of the I-helix, is hydrogen-bonded to the water molecule that lies closest to the heme in most of the published $P450_{BM3}$ structures. Ala264 remains associated to this water molecule even if the water is not axially coordinated to the heme, or in the presence of substrate, indicating the residue may be key in pulling the water away from the axially coordinating site when the I-helix withdraws from the heme iron upon substrate binding[66].

Several active site residues are involved in key steps in the catalytic cycle. Glu267 and Thr268, a pair of residues with highly conserved functionality across the P450 family[79], are implicated in proton delivery, stabilizing the oxy-ferrous complex and activation of dioxygen[80, 81]. However, this may not uniquely require an acidic residue at this position, as variants including E267V[82] or T268A[80] are active. Phe393 may regulate the rates of

oxygen binding and heme reduction[83, 84], while Phe42 may have a role in capping off the active site access channel upon substrate binding[65].

Crystal structures of $P450_{BM3}$ show the enzyme to be dynamic, with the F/G loop and F- and G-helices being particularly mobile, as exemplified by the SF structure (2HPD)[85], where the average *B* factor for residues in this area is 80 $Å^2$, compared to 25 $Å^2$ for the structure as a whole[40]. This open structure is likely a predominant form in solution, as the enzyme must be accessible to substrate. The conformational changes induced by substrate binding result in the enzyme switching to a closed conformation and serve to raise the heme reduction potential to a more oxidizing value, displace the axial water ligand and close the active site to bulk solvent, which is important in preventing side reactions when Compound I is generated[66].

1.2.3 Engineering of $P450_{BM3}$

1.2.3.1 Engineering of key residues

P450s are attractive candidates for use in biotechnology, and several have been developed for commercial application, including fine-chemical synthesis and bioremediation[86, 87]. The crystal structures of both the SF and SB forms of $P450_{BM3}$ allowed for the identification of residues likely to be important in substrate recognition, binding and turnover. This enabled rational mutagenesis of residues with targeted aims of altering substrate specificity, regio- and chemo-selectivity, and substrate oxidation rate. Using rational redesign combined with random mutagenesis, $P450_{BM3}$ has been engineered to oxidize a range of non-natural substrates including polycyclic aromatic hydrocarbons[88], alkanes[89], terpenes[90] and drugs[91].

One of the most obvious targets for mutagenesis is Phe87, which lies above the heme and appears to limit access to the heme iron (Section 1.2.2). F87A was the first Phe87

mutation described[92], and this residue has been targeted in numerous site saturation mutagenesis studies[93-95] and its mutants are involved in many variants with altered specificity.

With focus on admitting larger, non-polar substrates to the active site the hydrophilic binding residues Arg47 and Try51 were targeted. The double hydrophobic substitution R47L and Y51F (RLYF) increased activity towards polycyclic aromatic hydrocarbons more than 40-fold[88], such as an increase in product formation rate with phenanthrene from 0.5 min^{-1} with the WT to 22 min^{-1} with the RLYF variant.

While opening the active site near the heme improves activity with larger substrates, it can be important to restrict the active site to promote oxidation of small molecules or alter product profile. Mutations at Ala328, such as A328L, which promotes terminal oxidation of octane[96], or A328V, which increases oxidation of nerylacetone 2-fold[97], have been shown to be important in altering product profile. Often, combinations of mutants opening one side of the active site above the heme, and closing the active site on the opposite side, produce large shifts in selectivity and activity.

Of mutants produced from early mutagenesis work on $P450_{BM3}$ one of the most active is the A74G/F87V/L188Q 'Schmid' variant[98], which is the result of an error-prone PCR study, followed by site saturation at the three sites found to be common among the mutants active in the screen. While the screening process was a test of indigo formation, the Schmid mutant and the mutations found therein have been shown to oxidize a range of compounds including polycyclic aromatic hydrocarbons[99], pesticides[100, 101] and branched fatty acids[102], among others[103-106].

Though the vast majority of mutagenesis studies have been carried out on the heme domain, there have been studies carried out on the reductase domain. Residue Gly570,

which controls FMN binding[107], has been utilized to investigate electron transfer in the $P450_{BM3}$ dimer by preventing FMN incorporation using the G570D variant[108]. Trp1046 controls specificity of the co-factor, and a substitution for alanine or histidine switches the pyridine nucleotide specificity in $P450_{BM3}$ from NADPH to NADH[27, 109].

1.2.3.2 Engineering $P450_{BM3}$ for alkane oxidation

The oxidation of C—H bonds in alkanes is synthetically difficult, often requiring heterogeneous catalysts using high temperatures and pressures. This often results in further oxidation products including aldehydes and deep oxidation to carbon dioxide[110]. In efforts to develop green catalysts for mild, controlled oxidation of alkanes there has been widespread interest in developing monoogygenase (both heme[7] and non-heme[111]) based biocatalysts.

Though certain strains of yeast contain P450s capable of oxidizing C_8 to C_{16} alkanes[112], notably the alkane-inducible CYP52 family[113], there are no P450s that naturally oxidize gaseous alkanes. $P450_{cam}$ has been engineered to oxidize small chain, even gaseous alkanes, including hexane and pentane[114, 115], butane and propane[116], and even ethane[110]. The crystal structure of a precursor variant (F87W/Y96F/V247L) to the 9-mutation ethane monooxygenase, F87W/Y96F/T101L/T185M/L244M/V247L/G248A/L294M/ L1358P has been determined. This precursor variant shows a restricted active site containing only three water molecules, compared to the six found in the wild-type[110]. The restricted active site is key for the oxidation of small molecules, particularly alkanes.

$P450_{BM3}$ has also been engineered as an alkane hydroxylase[40]. Indeed, WT BM3 displays some activity towards hexane and octane[117], and the Schmid variant[118] improves on this activity. Propane oxidation has been achieved using a directed evolution variant which has more than 20 site mutations[119]. Ethane oxidation by $P450_{BM3}$ has also been shown,

though at a rate three orders of magnitude slower than propane[120]. The exceedingly slow oxidation of ethane compared to propane demonstrates the difficulty in activating small molecules and the importance of restricting the active site in order to promote alkane oxidation.

Restricting the active site is achieved through mutagenesis by substituting for residues with larger or more rigid side chains. This is not the only way to reduce active site volume, however, and it has been reported that an inert co-substrate can also be used to fill the active site. Watanabe *et al*. showed that using a perfluorocarboxylic acid, which binds tightly to the enzyme, but is inert towards oxidation, the gaseous alkanes butane and propane were oxidized by WT $P450_{BM3}$[121]. Using this same method and carrying out the reaction under 10 bar pressure methane oxidation was also reported for the WT[122].

1.2.3.3 Engineering $P450_{BM3}$ for fine chemical synthesis

Sesquiterpenes, the largest class of terpenoids and constituents of essential plant oils, are derived from farnesyl pyrophosphate (FPP) and synthesized by >100 reported terpene synthase enzymes in nature[123]. P450 enzymes are involved in further processing of terpenes to alcohols or ketones in nature, such as the conversion of (–)-limonene to (–)-carvone by CYP71D18 in spearmint[124], and these oxidation products are often value-added. Oxidation of terpene precursors to the value-added products offers a difficult synthetic challenge[125]. Chemical means of oxidation have been investigated[126-128], though it is more desirable to use biocatalysts. A biocatalyst is preferable, as any compound synthesized using chemical means of oxidation or environmentally harmful reagents or solvents cannot be marketed as 'natural,' which, owing to market pressure, is undesirable[125].

WT $P450_{cam}$ has been shown to be active towards the terpenes α-pinene[129] and (–)-limonene[130]. Protein engineering of $P450_{cam}$ improves the product formation rate with (+)-α-pinene nearly 15-fold, from 18.6 min^{-1} for the WT to 271 min^{-1} with the Y96F/V247L variant[129]. Though WT $P450_{cam}$ is not active towards the sesquiterpene (+)-valencene, it was engineered to oxidize at the 2 position, giving the value-added (+)-*trans*-nootkatol and (+)-nootkatone, with a PFR of nearly 10 min^{-1} with the F87A/Y96F/L244A variant[90].

In the same study, Sowden *et al*. also engineered $P450_{BM3}$ to oxidize (+)-valencene, though it was shown to be less selective, generating *cis*-(+)-valencene-1,10-epoxide and nootkatone-13*S*,14-epoxide, as well as three unidentified products, in addition to (+)-*cis*- and (+)-*trans*-nootkatol and (+)-nootkatone[90]. The WT enzyme gives primarily an unidentified product and (+)-*cis*-valencene-1,10-epoxide, though it also forms (+)-*trans*-nootkatol. The RLYF variant shifts selectivity from (+)-*trans*- to (+)-*cis*-nootkatol, though the primary product remains the unidentified product formed by WT. Adding F87A to RLYF promotes epoxide formation, and also the further oxidation of (+)-nootkatol to (+)-nootkatone. The I263A mutation shifts selectivity towards the 2 position, with 34.3% of the total products of the RLYF/I263A variant being a (+)-nootkatol or (+)-nootkatone. (+)-Nootkatone, a grapefruit fragrance, has been the target of numerous synthetic studies, both chemical and biological, and these have been reviewed[125], though there is currently no industrial process for the generation of (+)-nootkatone.

Urlacher *et al*. developed a small library of variants which showed improved or shifted chemo-, regio- or stereo-selectivity toward terpenes[97]. This library was developed by analysing molecular dynamics simulations of $P450_{BM3}$ with (+)-α-pinene[104], and a study of 31 crystal structures and 6300 *CYP* sequences which reported that the residue in the

position equivalent to 328 in $P450_{BM3}$ lies near the heme in 98% of cases. Indeed, Ala328 mutations have been shown to be important in affecting the enantio- and regio-selectivity towards alkanes[96]. Thus, residues Phe87 and Ala328 were targeted and a small library of variants was generated featuring only mutations at these sites. The resulting library was screened for activity with four terpene substrates: (+)-valencene, geranylacetone, nerylacetone and (*R*)-limonene[97].

The A328F and F87A/A328V variants did not display activity towards any of the substrates tested, whereas the F87A/A328I, F87L/A328I, F87V and F87V/A328V variants were as active or more active towards all substrates than the WT. Selectivity towards geranylacetone was most improved by the F87A/A328L variant, which promotes terminal oxidation to the alcohol, rather than forming the epoxide and unidentified products favoured by the WT. Activity towards geranylacetone, however, was reduced by all variants compared to the WT. Only the A328V variant gave significant shifts in selectivity with nerylacetone, strongly favouring (>97%) terminal oxidation, versus <15% for the WT.

For the oxidation of (*R*)-limonene, both the F87A/A328F and F87V/A328F variants give over 90% (*R*)-limonene-8,9-epoxide, whereas the WT gives only 7% of this compound. Each of these variants also increased the total conversion of limonene to >65%, while the WT converts <50% of 200 μM limonene after 1 h with 500 nM enzyme. (+)-Valencene was the most challenging substrate, with only 7 variants showing activity towards the larger sesquiterpene. The WT enzyme, which does not show an NADPH depletion rate faster than the leak rate in the presence of (+)-valencene, nonetheless was found to generate four products from the compound, with 29% oxidation at C2. The four most selective engineered variants, however, all revealed >85% selectivity towards C2,

generating (+)-nootkatol or (+)-nootkatone. The F87A/A328I variant converted more than 50% of 200 μM limonene after 1 h with 500 nM enzyme.

1.2.3.4 Engineering $P450_{BM3}$ for steroid oxidation

P450 enzymes catalyse both the synthesis of steroids and steroid hormones, as in the case of pregnenolone synthesis from cholesterol by CYP11A1[131], and the initial steps of catabolism to bile acids by CYP3A4, among others[132]. As steroids, and steroid derivatives, are industrially important compounds, there has been widespread interest in selectively oxidizing steroid compounds, both chemically and biochemically[133].

Recent efforts have focused on developing $P450_{BM3}$ for activity towards steroids[134]. $P450_{BM3}$ variant F1, which contains some 17 mutations, was shown to be active towards trimethylestriol[135]. Testosterone has been the focus of several studies, and oxidation was achieved with the R47L/F87V/L188Q variant, showing a product formation rate nearly double that of CYP3A4 and three primary hydroxylation products, 15β-, 16β- and 2β-hydroxytestosterone in a 53:29:18 ratio[136]. A site saturation study at position 87 was carried out by Vermeulen *et al*. and this study revealed that this site is key in controlling selectivity of testosterone oxidation[137]. Substituting phenylalanine for asparagine, for example, shifts selectivity completely towards 2β-hydroxytestosterone, though also lowers activity by an order of magnitude, while the F87A variant produces a >10-fold excess of 15β- hydroxytestosterone compared to 16β-hydroxytestosterone[137].

Recently, Reetz *et al*. applied Combinatorial Active-site Saturation Test (CAST) screening (Section 1.2.4) with the goal of altering selectivity of the F87A variant towards testosterone in whole cell reactions[138]. A variant in this study, F87A /A330W, gave 97% 2β-hydroxytestosterone and converted 79% of 1 mM testosterone. R47Y/T49F/V78L/A82M/F87A, by contrast, gave 96% 15β-hydroxytestosterone and

85% conversion at 1 mM testosterone. The same variant library was then screened for activity towards progesterone[138]. The F87A/A330W variant, interestingly, showed the highest 16β-regioselectivity at 91%, while V78V/A82N/F87A gave 100% 2β-hydroxyprogesterone[138].

1.2.4 Screening strategies for directed evolution libraries

Directed evolution allows for enzyme stability, activity and selectivity to be enhanced[139]. Since it involves random mutagenesis across an entire protein gene, expression and screening of the new enzyme libraries require high-throughput techniques to identify active variants worthy of further pursuit.

In 1999, Gillam *et al*. described a method for screening variants of CYP2A6 using indigo formation[140]. *E. coli* cultures can produce indigo from indole, particularly when grown in complex media such as LB broth, as indole is a product of tryptophan metabolism. F87V-containing variants of $P450_{BM3}$ were shown to oxidize indole to indigo, while the WT displays no such activity[98]. Thus, indigo formation in cell cultures containing $P450_{BM3}$ is an indication of altered substrate specificity and has been used as a screening protocol for high-throughput initial analysis of large mutant libraries[106, 141, 142].

High-throughput screening methods for $P450_{BM3}$ libraries are not limited to monitoring indigo formation. When a library is developed using a previously evolved variant as the starting point, it is common to screen for activity with a substrate towards which the parent variant is particularly active. An example of this is the naproxen metabolising variants derived from variants 21B3 and 5H6 (Appendix 1), which were screened for activity with *p*-nitrophenoxycarboxylic acid[143]. Other studies use benzyloxyresorufin oxidation (BROD) as a measure of enzyme activity, and have identified drug compounds

which inhibit $P450_{BM3}$ using high-throughput screening of BROD activity[144]. Activity towards 7-ethoxycoumarin has also been used to screen for $P450_{BM3}$ activity[82].

One further assay commonly used to screen $P450_{BM3}$ libraries for activity is the alkali assay, developed by Gilardi *et al.*[145], which is used to detect $NADP^+$ produced by the enzyme during substrate turnover. This method is perhaps preferable to other high-throughput screening methods described, as it can be used as a screen for activity directly with the compounds of interest and does not rely on the developed library retaining activity towards a specific substrate. Though there is a possibility of an increased number of false-positives from this screen if, for example, a variant has a particularly rapid leak rate, it is preferable to analyse a variant with a high leak rate for activity than to exclude a variant from further analysis based on activity with a substrate that is not the focus of the study. The alkali assay has been applied in screening libraries for drug activity towards ibuprofen, diclofenac and tolbutamide[146]. Another assay which uses NAD(P)H depletion as a marker for activity was developed by Glieder, and uses nitroblue tetrazolium salts to form dyes upon reduction with residual NAD(P)H, so colonies with active variants do not form dyed areas on a plate[147].

Not only has high-throughput screening been used to identify variants worthy of further investigation, it has also been applied to screening for protein folding. This is achieved by reduction of the P450 and binding of CO with rapid analysis of the absorbance at 450 nm to determine if the protein folds correctly[143].

Alternative methods for developing small libraries of variants displaying improved chemo- or regio-selectivity or a wider range of substrate acceptance have also been developed[97, 148]. These methods use crystallographic data to select residues which appear to play a role in substrate interaction, and develop a small library of variants targeting these residues (rational mutagenesis). For example, Urlacher *et al.* developed a small (25

variant) library which showed shifted and/or improved chemo-, regio- or stereo-selectivity toward terpenes[97], as discussed in Section 1.2.3.3

A second method, the Combinatorial Active-site Saturation Test (CAST), described by Reetz *et al.* involves selecting multiple pairs of residues which are in the active site of an enzyme[148]. Randomization of the side chains at these sites leads to a relatively small (saturation at two sites yields a 400 variant library, compared to libraries of over 8000 which are screened by some groups[94, 149]), yet structurally diverse, library which can be screened for activity against target compounds. This method has been applied to improve the range of substrates accepted by the lipase from *Pseudomonas aeruginosa* (PAL)[148]. Combining beneficial mutants discovered through CAST screening can further increase activity towards difficult substrates, as once again demonstrated using PAL[150].

Not only is high-throughput screening for initial variant activity important, it is also key to develop a method of rapidly screening reaction mixtures for products of turnover reactions. Indeed, high-throughput HPLC, complete with automated injection and data analysis has been used in the screening of $P450_{BM3}$ variants for activity towards drug compounds[151].

1.3 Drug metabolism by P450s

1.3.1 General background

Phase I oxidative metabolism, the first reaction a xenobiotic undergoes in the body, can have many effects on ingested compounds. Phase I metabolism is responsible for the oxidation of pro-drugs into active oxidized species (as with the bioactivation of cancer pro-drug tegafur to 5-fluorouracil)[152], detoxification[153] and, in some cases such as acetonitrile, toxicification[154]. P450s are responsible for the phase I oxidative metabolism of over 90% of drugs in current clinical use[155]. Indeed, P450s are responsible for the

generation of 60% of active or toxic metabolites, with the other metabolites being produced primarily by oxidoreductases, hydrolases and transferases[156].

Though each liver P450 does display a degree of substrate specificity, it is not atypical for a single drug to be metabolized by multiple enzymes[157], with each enzyme usually oxidizing the drug at a unique site. For example, warfarin is oxidized to 6- and 8-hydroxywarfarin by CYP1A2, to 10-hydroxywarfarin by CYP3A4, while the *S*-warfarin enantiomer is selectively hydroxylated to 7-hydroxywarfarin by CYP2C9[158].

The enzymes primarily responsible for drug metabolism in humans include CYP1A2, CYP2A6, CYP2B6, CYP2C8, CYP2C9, CYP2C19, CYP2D6, CYP2E1 and CYP3A4[159]; with minor roles being played by 5 other P450s[160, 161]. Many of the P450s involved in drug metabolism also have other physiological roles, such as steroid synthesis[162]. Of the 57 human P450s the two most highly expressed in the liver are CYP2C9[163] and CYP3A4[164]. Drug metabolism in humans is primarily carried out in hepatic cells, though it is important to consider that many liver P450s are also expressed in the small intestine, lungs and skin[165]. Drug clearance in intestinal microsomes is 4.5- to 50-fold lower than hepatic estimates[166], though intestinal P450s still play a role in primary metabolism, such as the bioactivation of the pro-drug terfenadine[167].

The generation of drug metabolites of human P450s is a key step in drug design and testing, as it allows for the toxicity, secondary metabolism, and potential metabolite activity to be assessed. Currently, animal models, including primates, are used in the pre-clinical testing of new drugs. Beginning with Russell and Burch in 1959 there has been a call to refine, reduce and replace the use of animal models[168] and this '3Rs' principle has spurred research interest in developing alternative methods to animal testing in the drug development process[169, 170]. Generation of drug metabolites is one area in particular where less reliance on animal models can be achieved by using biotechnological applications.

It would, therefore, be advantageous to have large amounts of human P450 available to generate the required metabolites *in vitro*. Unfortunately, human microsomes are not suited to the task of large scale synthesis for several reasons, including batch-to-batch variation and inhibition difficulties[171, 172]. This has led to great interest in developing convenient synthetic techniques including expressing human P450s in yeast[173], and the engineering of microbial P450s into drug metabolizing systems, which will be discussed in more detail in Chapter 3.

1.3.2 Crystal structure of CYP2C9

CYP2C9 is responsible for the oxidation of 15–20% of clinical drugs[174], and typical substrates are anionic and lipophilic[175]. Metabolism by CYP2C9 has a large role in causing clinical adverse drug reactions, a product of unexpected alterations to P450 activity by metabolically based drug-drug interactions[176]. The crystal structure of CYP2C9 has been solved for both the substrate-free form and ligated to *S*-warfarin[14], the isoform of the drug responsible for its anticoagulation properties.

In the substrate-free form of the enzyme, eleven residues in the F/G loop (residues 212–222) form the F′- and G′-helices, which are previously unreported in P450 structures[14]. Though the enzyme exhibits preference for anionic substrates, the access channel appears to be composed of hydrophobic residues with no polar or positively charged residues which may be involved in binding a negatively charged substrate. As CYP2C19, a related drug metabolising human enzyme, shows no preference for acidic substrates[177], it is likely that substrate selectivity is not the result of active site residues. Instead, the key may be the entrance to the substrate access channel, where Lys72 in CYP2C9 is a glutamate in the equivalent position in CYP2C19[14], which may exclude anionic compounds from entering the active site.

Unlike in $P450_{BM3}$ the binding of substrate, in this case warfarin, to CYP2C9 does not induce major conformational changes in the protein structure, though there are some localized changes, such as π-π stacking of warfarin with the side chain of Phe437. As with fatty-acid bound $P450_{BM3}$ where the substrate is bound in a catalytically non-productive position, the site of oxidation in *S*-warfarin remains 10 Å from the heme iron. The lack of large scale structural changes associated with substrate binding noted with the complexation of CYP2C9 with *S*-warfarin may be because *S*-warfarin does not bind in the region traditionally believed to be the substrate binding pocket (Figure 1.5). Indeed, *S*-warfarin is located in a new binding pocket, which indicates that CYP2C9 may accommodate multiple ligands during its biological functions[14]. This is not uncommon among the drug-metabolising human P450s, as CYP3A4 is also known to accept multiple ligands during its function[178], and is consistent with the observation that a two-site binding model is necessary to explain the kinetic behaviour of CYP2C9 with other substrates, such as dapsone[179, 180]. Other P450s have been shown to accommodate multiple substrates, including $P450_{BM3}$, which displays chain length-dependent cooperativity in fatty acid binding and oxidation under low ionic strength conditions[181].

The structure of CYP2C9 has also been solved with the non-steroidal anti-inflammatory drug (NSAID) flurbiprofen[182]. This structure reveals several structural perturbations compared to both the substrate-free and *S*-warfarin-bound structures described above. One of the most notable structural differences is a distinctly altered conformation of the B- and C-helices, which repositions Arg108, allowing it to stabilize the binding of flurbiprofen[182]. The structure shows that flurbiprofen lies 4.9 Å from the heme iron, while the unusual G′-helix fails to form.

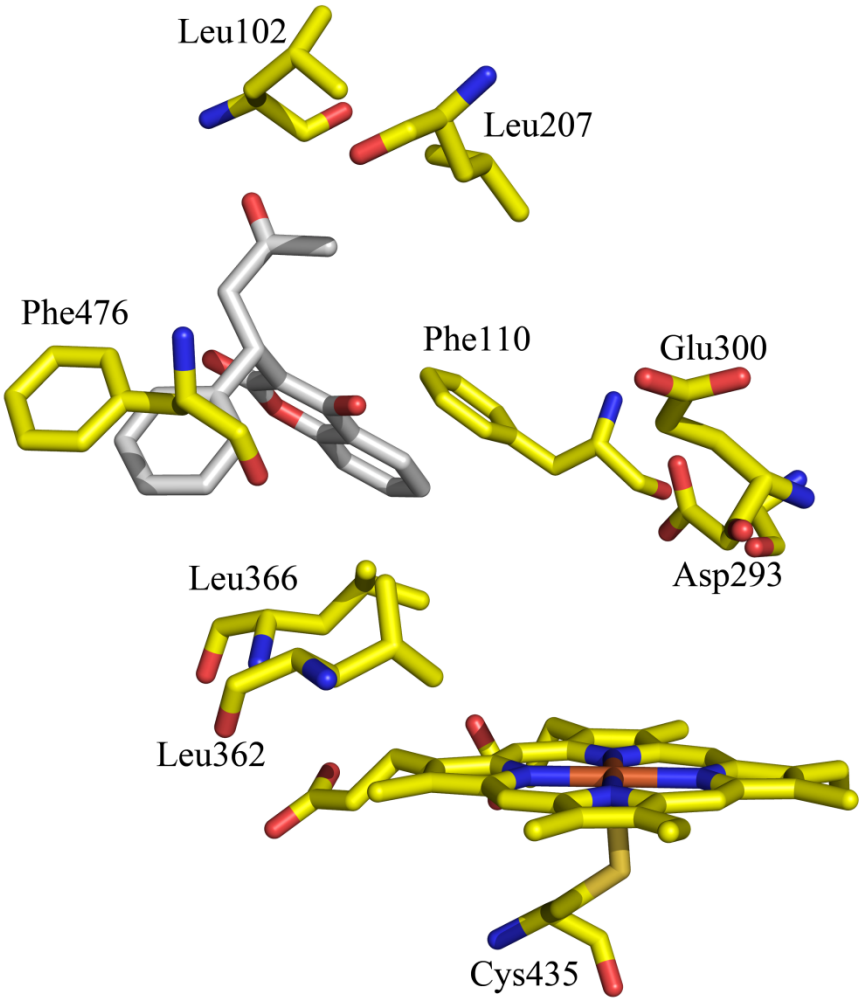

Figure 1.5 Active site of warfarin-bound CYP2C9 (PDB code: 1OG5). Warfarin is shown in grey.

1.3.3 Crystal structure of CYP3A4

CYP3A4 is arguably the most important enzyme for drug metabolism in humans[155] as it is the most highly expressed in the liver and small intestine and thus highly involved in the metabolism of oral drugs. Among the most promiscuous P450s[183], reactivity of CYP3A4 has been extensively studied with well over 100 compounds[184], though a single suitable drug probe for marker activity has not yet been identified[185, 186]. The crystal structure of CYP3A4 has been solved, both in the absence of substrate[15, 187], in the presence of ketoconazole and erythromycin[188], and with a substrate (progesterone) and an inhibitor

(metyrapone) occupying the active site[187]. Like CYP2C9, it shows the capacity for binding multiple ligands in the active site[188].

Given that some CYP3A4 substrates are very large, such as the 1,203 Da cyclosporine, a surprising feature of the CYP3A4 structure is a cluster of seven phenylalanine residues lying above the active site and forming a hydrophobic core (Figure 1.6)[187]. This reduces the calculated active site volume to 520 Å^3, much smaller than would be expected. However, as mutagenesis studies on many of these phenylalanine residues show that they play a role in substrate metabolism, it is likely that their relocation or displacement is possible, particularly by large substrates[189].

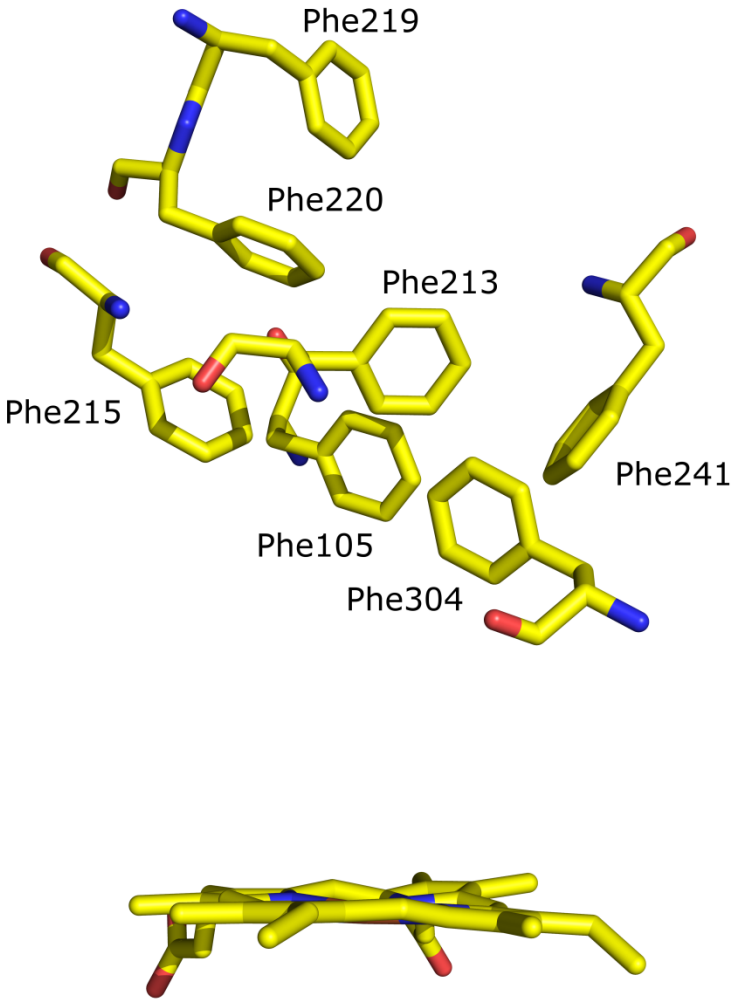

Figure 1.6. Active site of CYP3A4 (PDB code: 1TQN), showing the 'phenylalanine cluster.'

Another interesting feature of the substrate-free CYP3A4 structure is a lack of an axial water ligand, which would be expected for a low-spin heme. If the enzyme was reduced by X-rays, as is known to be possible[190], then a 5-coordinate iron atom would be expected to be non-planar with the porphyrin, though this does not appear to be the case, at the resolution at which this structure was determined. A second structure for substrate-free CYP3A4 was independently determined at the same time[15] as the structure determined by Williams and co-workers discussed here, though these structures are very similar[191].

Like the CYP2C9 structure with *S*-warfarin, neither the binding of the inhibitor metyrapone nor the substrate progesterone induce conformational changes in CYP3A4[187]. The progesterone molecule is bound 17 Å from the heme at a binding site near the phenylalanine cluster. This peripheral binding site may play a role in substrate recognition, binding of effector molecules (such as α-naphthoflavone, which promotes substrate release[192]), and enzyme cooperativity.

Also like the structure of CYP2C9, large conformational changes in CYP3A4 are observed with other substrates[188]. Notably, the phenylalanine cluster noted in the substrate-free structures is disrupted, with some of the residues being exposed to the protein surface in the ketoconazole bound structure. Interestingly, two molecules of ketoconazole were located in the active site, with one being nitrogen-bound to the heme iron through the imidazole group. Since kinetic studies with ketoconazole do not suggest CYP3A4 binds multiple substrate molecules, this may be an artefact of the high concentration of ketoconazole required during crystallization.

An erythromycin bound structure was also determined and showed similar, if less exaggerated, conformational changes in CYP3A4[188]. Though accurate determination of the location of erythromycin could not be completed, electron density modelling suggested that the substrate was docked close to the heme, but the D-desoamine group,

which is demethylated by CYP3A4, was oriented away from the heme and 17 Å distant. Thus, the substrate was not bound in a productive orientation.

The crystal structures of CYP2C9 and CYP3A4 show enzymes with large active sites which are not binding-optimized towards specific substrates. The enzymes are active across a broad range of substrates, many of which induce only modest spin-state shifts. This suggests that binding optimization of an enzyme active site may limit the overall range of substrates the enzyme is capable of oxidizing.

1.4 Electrochemistry of proteins

1.4.1 General background

Electrochemical studies of redox active proteins have gained widespread interest as they provide insight into not only intrinsic thermodynamic and kinetic properties, but also structural requirements for electron transfer[193]. Cytochrome *c* was the first protein to be reduced at the surface of an electrode in 1958[194], though further developments were slow due to two technical difficulties. Firstly, proteins often adsorb onto unmodified electrode surfaces, or are denatured upon application of a potential, making analysis problematic. Secondly, redox centres in proteins are typically buried within polypeptide chains, making electron transfer directly from an electrode difficult as the distances involved are large.

As a means of overcoming these difficulties, spectroelectrochemistry was developed as a method for analysing redox processes in proteins[193]. Spectroelectrochemistry combines optical and electrochemical techniques to allow simultaneous measurement of an electrical property (current, potential, etc.) and a spectral change (IR, UV-vis). There are two primary methods applied to spectroelectrochemistry: cyclic voltammetry and

potentiometric titrations, which can be achieved using chemical titrants or an optically transparent thin layer electrode (OTTLE).

Cyclic voltammetry, the process of monitoring current change as applied potential is linearly varied between two set points, has been used to measure the reduction potential of P450s including the heme domain of $P450_{BM3}$ (BMP), $P450_{cam}$[195] and CYP2C9[196], among others[197, 198]. This technique often requires immobilization of the protein in a film[199] or on the electrode[200]. One problem with using this technique is that the protein is easily denatured, e.g. into the P420 form, which subsequently dominates the signal[201].

Measuring electrochemical properties of soluble bacterial P450s is slightly less problematic than investigating membrane-associated proteins such as the mammalian drug-metabolising enzymes. In order to solubilize membrane-associated proteins, electrochemical studies must employ the use of surfactants[202]. Unusually, when measured using cyclic voltammetry using surfactants or liposomes, several P450s, including CYP3A4, were shown not to undergo a substrate induced change in reduction potential[203-205].

Recently, work in the Sligar laboratory has developed a nano-scale membrane bi-layer disc (nanodisc), which was used to stabilize CYP3A4[206]. Using the nanodisc, the reduction potential of CYP3A4, in the absence of substrate and with several drug molecules bound was measured. These experiments showed that the reduction potential of CYP3A4 does indeed shift upon the binding of substrate, though the extent of the shift depends on the substrate, correlating to the substrate-induced spin-state shifts[206]. Substrate-free CYP3A4 has a reduction potential of –220 ± 10 mV vs. SHE, which is shifted to –137 ± 5 mV vs. SHE by bromocriptine binding, and to –140 ± 5 mV vs. SHE by testosterone binding while no potential shift was observed in the erythromycin-bound form (–210 ± 10 mV vs. SHE).

In a potentiometric titration, the potential of the bulk solution is held until the components reach equilibrium. The protein will reach equilibrium between the oxidized and reduced forms and, providing the oxidized and reduced forms display different spectra, the equilibrium can be monitored spectroscopically[193]. Determining the ratio between the reduced and oxidized forms ([R]/[O]) at several potentials allows for the determination of the heme reduction potential, using the Nernst equation (**Eq. 1**). Using Beer's Law the ratio of [R]/[O] can be replaced with measurable absorption values. Methods of potentiometric titrations will be described in detail in Chapter 4.

$$E = E° - \frac{RT}{nF} \ln \frac{[R]}{[O]}$$

Equation 1.1. The Nernst equation. E is the applied potential, E^o is the midpoint potential, R is the gas constant, T is the temperature, n is the number of electrons involved in the process, F is Faraday's constant, [R] and [O] are the concentration of the reduced and oxidized species respectively.

1.5 Thesis aims

The principal aim of this thesis was to develop new variants of $P450_{BM3}$ which display increased activity towards commercial drug compounds, and generate the oxidation products common in human P450 metabolism. Combining mutants known to improve activity towards non-natural substrates and drugs, such as R47L/Y51F, F87V and E267V with the generic accelerator mutation I401P produced a $P450_{BM3}$ variant which was capable of completely converting 2 mM diclofenac (1 mL solution volume, 5 μM enzyme) to the two human metabolites, 4′- and 5-hydroxydiclofenac. Total turnover with this enzyme towards drugs is low, as even the total conversion of diclofenac was only 400 turnovers. This variant was also shown to be active towards several other drug compounds, such as testosterone and lidocaine.

While establishing variants active towards drug metabolism, various biochemical properties of the most successful variants were investigated. The reduction potential, first electron transfer rate constant and kinetic parameters for several generic accelerator mutants were determined. The KT2 (A191T/N239H/I259V/A276T/L353I) variant was shown to have a reduction potential, in the absence of substrate, similar to that of the WT. Substrate-free I401P however, has a reduction potential shifted to the value for WT bound with palmitate. Substrate-free KT2 and I401P also show accelerated rates of first electron transfer. The crystal structures of I401P and KT2 reveal that the rate accelerating properties displayed by these variants may stem from catalytically ready conformation the enzymes adopt. A method for reliably determining heme reduction potentials using an OTTLE cell was established and extended for use in determining the reduction potential of other P450s and their redox partners.

Chapter Two

Materials and Methods

2.1 Chemicals and Equipment

2.1.1 Chemicals

General reagents and chemicals were from Alfa-Aesar, Fisher Scientific and Sigma-Aldrich. HPLC grade solvents were from Sigma-Aldrich and Merck. Media components were from Melford Laboratories, Sigma-Aldrich and VWR International. Buffer components were from Amresco, Fisher Scientific and VWR International. Kanamycin (kan) was from Melford Laboratories. NADPH (tetrasodium salt) was from Apollo Scientific or Melford Laboratories, and NADH (disodium salt) from Roche Diagnostics. Isopropyl-β-D-thiogalactopyranoside (IPTG) was from Melford Laboratories or Roche Diagnostics. Bovine liver catalase was from Sigma-Aldrich. Restriction enzymes, T4 DNA ligase and the associated buffers were from New England Biolabs. Oligonucleotides were supplied by Eurofins Genetic Services, UK. Platinum mesh, 100 mesh, wire diameter 3×10^{-3} in, was supplied by Alfa-Aesar. Gold mesh, 500 wires per in, wire diameter 4.5×10^{-4} in, 60% transmission, was from InterNet Ltd.

2.1.2 Growth media and buffers

Water was purified using Millipore Elix systems. First-stage water (Resistivity ≥8 MΩ.cm) was used for the preparation of growth media while second-stage water (≥18 MΩ.cm) was used for buffers and in DNA preparations and transformations. Growth and expression media components are shown in Table 2.1. All media were sterilised in an autoclave at 121 °C for 15 min prior to use. LB_{kan}, $2YT_{kan}$ and EMM_{kan} included 30 mg L^{-1} kanamycin, which was added after cooling to ambient temperature. Buffer components are shown in Table 2.2.

Table 2.1. Growth and expression media components.

Medium	Components (per Litre)
LB	10 g tryptone, 5 g yeast extract, 10 g NaCl
LB-agar	As LB, with 15 g bacto-agar
2YT	16 g tryptone, 10 g yeast extract, 5 g NaCl
Trace Elements Solution	0.74 g $CaCl_2 \cdot H_2O$, 0.18 g $ZnSO_4 \cdot 7H_2O$, 0.132 g $MnSO_4 \cdot 4H_2O$, 20.1 g Na_2EDTA, 16.7 g $FeCl_3 \cdot 6H_2O$, 0.10 g $CuSO_4 \cdot 5H_2O$, 0.25 g $CoCl_2 \cdot 6H_2O$
$FB_{glycerol}$	14.7 g anhydrous K_2HPO_4, 3.6 g NaH_2PO_4, 2.5 g $(NH_4)_2SO_4$, 2.0 g Na_2SO_4, Na_3citrate$\cdot 2H_2O$, 0.5 g NH_4Cl, 5 mL glycerol. Autoclave, then when cool: 2 mL 1 M $MgSO_4 \cdot 7H_2O$, 3 mL trace elements solution, 1 mL 10% Thamine:HCl (all filter-sterilized)
$M9_{agar}$	12.8 g $Na_2HPO_4 \cdot 7H_2O$, 3 g KH_2PO_4, 0.5 g NaCl, 1 g NH_4Cl, 15 g bacto-agar. Autoclave, then when cool: 20 mL 20% w/v glucose, 2 mL 1 M $MgSO_4$, 100 µL 1 M $CaCl_2$, 1 mL 1 M thiamine-HCl (all filter-sterilized)
SOB	20 g tryptone, 5 g yeast extract, 0.5 g NaCl, 10 mL 250 mM KCl. Adjusted to pH 7.0 using 10 M NaOH.
SOC	SOB with 20 mL 20% w/v glucose (filter sterilized)

Table 2.2. Buffer components.

Buffer	Buffer components (per Litre)
Tris (1 M)	121.1 g Tris, pH corrected using HCl
Buffer P	6.45 g $K_2HPO_4 \cdot 3H_2O$, 1.6 g KH_2PO_4, pH corrected using H_3PO_4
Buffer G	Buffer P with 0.154 g DTT
TFB1	100 mM RbCl, 50 mM $MnCl_2$, 30 mM KOAc, 10 mM $CaCl_2$
TFB2	10 mM MOPS, 10 mM RbCl, 75 mM $CaCl_2$, 30 % v/v glycerol

2.1.3 Equipment

UV-visible spectra, enzyme quantitations, activity assays, spin shifts and spectroelectrochemical titrations were run on Varian Cary 50 and Cary 1E spectrophotometers. Sonication was carried out using a Misonix 3000 sonicator.

Mutagenesis and PCR reactions were carried out in a Techne TC-312 thermocycler. Gas chromatography (GC) was carried out on Thermo Finnigan instruments equipped with flame-ionization detectors (FIDs), using helium as the carrier gas. Potentiometric titrations were carried out using an Ivium CompactStat or Autolab analogue potentiostat with a UE9 computer interface from LabJack to measure current and apply potential. ^{1}H NMR spectra were acquired on a Varian UnityPlus 500 MHz spectrometer and kindly obtained by Dr. Nick Rees. Mass spectra were obtained on a Micromass GC TOF mass spectrometer and kindly obtained by Dr. Colin Sparrow. Fused silica strips were obtained from UQG Optics Ltd. Mr. Keith Waters fabricated the custom wire housing for the patterned gold electrodes and the PMMA solution well for the spectroelectrochemical cell. The custom 4-way neck was fabricated by Ms. Terri Adams.

2.2 DNA techniques

2.2.1 Oligonucleotide design

Each mutagenesis reaction required the design of two complementary primers, which consisted of 30-50 bases. Table 2.3 contains a list of designed primers used in this thesis. Melting temperatures were calculated using equation 2.1, supplied in the Stratagene mutagenesis protocol.

$$T_m\ (^{o}C) = 81.5 - (675/N) + (0.41 \times \%GC) - \%M$$

Equation 2.1.

T_m is the melting temperature, N is the primer length (in bases), %GC is the percentage of the primer made up of guanine and cytosine and %M is the percentage of bases altered. A melting temperature >78 °C is required for optimal annealing, though PCR was performed with primers with a lower melting temperature.

2.2.2 Mutagenesis

All variants described in this thesis are cloned into the pET28a vector, which has a T7 promoter. Mutagenesis was performed using Novagen KOD Hot Start DNA Polymerase kit, according to the manufacturer's protocol. The PCR mixture (50 μL total) was comprised of 37.5 μL second-stage water, 5 μL 10× polymerase buffer, 5 μL deoxynucleotide triphosphates (dNTPs, each at 2 mM), 2 μL 25 mM $MgSO_4$, 2 μL DMSO, 2 μL 0.05 μg/μL parent DNA, 1.5 μL 0.1 μg/μL mixture of the two primers, 1 μL KOD polymerase in a thin walled microcentrifuge tube.

PCR was performed in a Techne TC-312 thermocycler using 18 × 15.5 min cycles consisting of 0.5 min at 94 °C, 1 min at 45 °C and 14 min at 68 °C, to allow for strand separation, primer annealing and extension, respectively. This was followed by a final 10 min hold at 68 °C. Gel electrophoresis (2.2.3) confirmed the resulting amplicon was of the correct length and the PCR mixture was digested overnight at 37 °C by *Dpn* I, a restriction enzyme which cleaves methylated DNA, while leaving intact the desired unmethylated DNA.

2.2.3 Heme domain preparation

The PCR protocol used for heme domain preparation was identical to the mutagenesis protocol, except that amplification was by 30 cycles of strand separation at 95 °C for 30 s, annealing at 50 °C for 30 s and extension at 68 °C for 105 s. Amplified DNA was purified using the Qiagen QIAquick kit, in accordance with the manufacturer's protocol, followed by a restriction digest using *Nco* I and *Spe* I and containing 16.8 μL DNA. A standard digest using the same two restriction enzymes was also carried out on the heme domain of the wild-type enzyme in pET28. The *ca.* 1440 bp fragment from the first digest and the

long fragment from the second digest were isolated via agarose gel electrophoresis and ligated.

2.2.4 Gel electrophoresis

1×TAE buffer was prepared by 2:98 dilution of commercial 50×TAE stock. 0.5 g agarose was dissolved in 50 mL of 1×TAE buffer by microwave heating. Once sufficiently cool but not set, a staining agent was added (2.5 μL of a 10 mg/mL solution of ethidium bromide or 2.5 μL of RedSafe from Chembio, UK) and the gel was poured to set. 250 mL 1×TAE was used as a running buffer, and contained 5 μL ethidium bromide if this was used as the stain. Samples (10 μL PCR product) were mixed with 2 μL 6×blue-orange load-dye from Promega and loaded into 25 μL wells and run along with 10 μL of Promega 1 kbp DNA ladder. Gels were run for 90 min at 90 mV and analysed under UV light.

2.2.5 DNA transformation

2 μL of the PCR product plasmid, post-digestion with *Dpn* I, was mixed with 150 μL competent JM109 or DH5α *E. coli* cells. For purified DNA transformations for use in protein expression, 0.25 μL DNA was mixed with 150 μL competent BL21(DE3) *E. coli* cells. The following steps are unchanged for post-mutagenesis or pure DNA transformations. Competent cells had been stored at –80 °C and were thawed on ice before adding DNA. Cells were then left on ice for 45 min and heat-shocked at 42 °C for 45 s and placed back on ice for 2 min. 200 μL filter-sterilized SOC was added and the cells were incubated at 37 °C while shaking at 200 rpm for 1 h. Following incubation the cells were spread onto a LB-agar plate containing 30 μg/mL kanamycin and incubated at 37 °C overnight.

Table 2.3. Primers designed for use in this thesis. Sequence reads from 5′ to 3′ and the mutated base(s) are highlighted.

Primer name	Sequence	T_M (°C)
V78F	AGTCAAGCGCTTAAATTTTTCCGTGATTTTGCAGGAGACGGG	81.6
V78F reverse	CCCGTCTCCTGCAAAATCACGGAAAAATTTAAGCGCTTGACT	81.6
F81W	GCGCTTAAATTTGTACGTGATTGGGCAGGAGACGGGTTATTTACA	80.3
F81W reverse	TGTAAATAACCCGTCTCCTGCCCAATCACGTACAAATTTAAGCGC	80.3
F87V	CGTGATTTTGCAGGAGACGGGTTAGTAACAAGCTGG	72.6
F87V reverse	CCAGCTTGTTACTAACCCGTCTCCTGCAAAATCACG	72.6
I263A	CGCTATCAAATTATTACATTCTTAGCCGCGGGACAC	74.9
I263A reverse	GTGTCCCGCGGCTAAGAATGTAATAATTTGATAGCG	74.9
E267V	CTTAATTGCGGGACACGTAACAACAAGTGGTCTTTT	77.1
E267V reverse	AAAAGACCACTTGTTGTTACGTGTCCCGCAATTAAG	77.1
A328I	CTGCGCTTATGGCCAACTATTCCTGCGTTTTCCC	77.5
A328I reverse	GGGAAAACGCAGGAATAGTTGGCCATAAGCGCAG	77.5

2.2.6 DNA purification

DNA was purified using solutions from the Promega Wizard Plus SV Minipreps kit and a modified version of the manufacturer's protocol. A single colony from an LB_{agar} plate was grown overnight at 37 °C in 40 mL LB_{kan}, shaking at 200 rpm. The cells were harvested by centrifugation at 9250 *g* for 5 min and the resulting cell pellet was resuspended in 1200 µL Resuspension Solution. Cells were divided evenly into 4 aliquots in microcentrifuge tubes and lysed by the addition of 300 µL Cell Lysis Solution. 10 µL Alkaline Protease Solution was added and the mixture was incubated for 5 min. 350 µL Neutralization Solution was added and cell debris was removed by centrifugation at

21,100 *g* for 20 min. The lysate was transferred to a Wizard SV minicolumn, and the four columns were centrifuged at 11000 *g* for 1 min. 750 μL Column Wash Solution was eluted through the columns by centrifugation at 11,000 *g* for 1 min. A further 250 μL Column Wash Solution was similarly eluted through the column, following which the columns were spun for an additional 2 min at 11,000 *g*. 100 μL Nuclease Free Water was added to each column and collected into a new microcentrifuge tube by centrifugation at 11,000 *g* for 1 min.

DNA was concentrated by adding 40 μL 3 M NaOAc and 800 μL 100% ethanol and chilling at –20 °C for 2 h. The mixture was centrifuged at 21,100 *g* for 20 min. and the supernatant was discarded. The resulting DNA pellet was washed with 500 μL 70% ethanol by vortexing, and then centrifuging at 21,100 *g* for 5 min. Supernatant was discarded and the pellet dried by placing the microcentrifuge tube in a 42 °C heating block for 45 s. 50 μL second-stage water was added and the pellet dissolved by pipette mixing. The DNA solution concentrate was determined by UV-vis spectroscopy. After dilution by a factor of 100, each absorbance unit at 260 nm corresponded to a concentration of 5 μg μL^{-1}. Purity was considered acceptable when A_{260}/A_{280} fell between 1.5 and 1.8.

2.2.7 DNA sequencing

Purified PCR plasmid products were sequenced by Geneservice, UK using the standard T7F and custom BM3FP2 primers. The T7F primer binds to the T7 promoter in the vector, while the BM3FP2 primer binds to the bases in the $P450_{BM3}$ gene coding for the residues 188-195, and the sequences of these primers are shown in Table 2.4.

Table 2.4. Nucleotide sequences of the T7F and BM3FP2 primers.

Primer	Sequence
T7F	TAATACGACTCACTATAGG
BM3FP2	CTGCAGCGAGCAAATCCAGACGAC

2.3 Protein expression, purification and quantification

2.3.1 Competent cell preparation

Cells of the desired strain were streaked onto an $M9_{agar}$ plate which contained no antibiotic, and incubated for 36–48 h at 37 °C. A single colony was grown in 5 mL LB overnight. This culture was poured into 200 mL LB and grown until optical density of 0.8–1.0 (*ca.* 3 h). Cells were collected by centrifuging in 4 sterile 50 mL centrifuge tubes at 5000 *g* for 5 min, at 4 °C. The supernatant was discarded and the tubes were centrifuged again for 1 min and any remaining supernatant removed by sterile pipette. Working on ice, each cell pellet was resuspended gently in 8 mL filter sterilized TFB1 and left to stand for 1 h, followed by centrifugation at 2500 *g* for 5 min at 4 °C. The supernatant was again discarded, and the cell pellets were gently resuspended in 4 mL TFB2. After standing on ice for 1 h, the cells were transferred in 150 µL aliquots to sterilized microcentrifuge tubes and flash-frozen in liquid nitrogen and stored at –80 °C.

2.3.2 Protein Expression

4 – 8 2 L Erlenmeyer flasks containing $2YT_{kan}$ or $FB_{glycerol/kan}$ were inoculated with single colonies of BL21(DE3) cells containing the appropriate plasmid and incubated at 37 °C for 18–24 h while shaking at 110 rpm. After sufficient cell growth, the incubator temperature was lowered to 20 °C, shaking speed was reduced to 100 rpm and protein expression induced by the addition of IPTG to a final concentration of 55 µM. Cells were

harvested, after 24 h for 2YT growths or after 24–48 h for $FB_{glycerol}$ growths, by centrifugation at 5250 *g* for 10 min at 4 °C. Collected cell pellets were stored at –20 °C until needed.

2.3.3 Protein purification

Cell pellets were defrosted and resuspended in 200 mL Buffer G. Cells were lysed on ice by sonication and cell debris was separated by centrifugation at 37,500 *g* for 25 min at 4 °C. The supernatant was loaded onto a GE Healthcare DEAE Fast Flow Sepharose column (200 × 50 mm) pre-equilibrated with Buffer G. The protein was eluted using a linear gradient of 80–400 mM ammonium sulphate in Buffer G. Fractions containing P450 (assayed by UV-vis spectrophotometry) were collected and concentrated in an amicon using a 30 kDa cut-off cellulose membrane. A Sephadex G-25 column pre-equilibrated with Buffer G was used to remove ammonium sulphate from the solution, which was then concentrated using the amicon. The resulting solution was centrifuged at 9250 *g* and filter sterilized through a 0.2 micron filter. The protein was loaded onto a GE Healthcare Source-Q column (120 × 26 mm) and purified using a linear gradient of 0−30% 16× Buffer G. Fractions with A_{404}/A_{280} >0.25 were collected, concentrated by ultrafiltration, mixed to 50% v/v with sterilized glycerol and filter-sterilised before being stored at –20 °C. Immediately prior to use glycerol was removed by running the protein down a 5-mL PD-10 gel filtration column which was pre-equilibrated with 50 mM Tris, pH 7.4.

2.3.4 Protein quantification – The P450 assay

Purified protein was saturated with CO by gentle bubbling and reduced with sodium dithionite. Additional CO was bubbled until A_{450} was maximized. The protein was

quantified using an extinction coefficient of 91000 $M^{-1}cm^{-1}$ for the absorbance at A_{450}-A_{490}.

2.4 Activity assays

2.4.1 *In vitro* assays

2.4.1.1 NADPH turnover assays

NADPH turnovers were run in 1250 μL of oxygenated 50 mM Tris, pH 7.4 containing 0.1 – 0.5 μM P450, 125 μg bovine liver catalase (added as a 10 mg/mL stock in 50% v/v Tris/glycerol) and 1 mM substrate added from a 100 mM stock in DMSO. This solution was equilibrated at 30 °C for 1 min, followed by the addition of 1 AU NADPH (ca. 160 μM). Rate of decay of A340 (Δ) was measured, from which an NADPH consumption rate (N) was determined using the Equation 2.2, where [P450] is the concentration of enzyme in μM; 6.22 is the millimolar extinction coeffiecient of NADPH at 340 nm.

$$N = \frac{1000\,\Delta}{(6.22\times[\mathrm{P_{450}}])}$$

Equation 2.2

2.4.1.2 Determination of kinetic parameters

K_M and k_{cat} values were obtained by measuring NADPH consumption rates with 0.1 μM P450 and various substrate concentrations. Turnovers were run as above, with the following alterations: 1 mL total volume and catalase was omitted. The resulting NADPH consumption rates were fitted to the Michaelis–Menten hyperbolic function.

2.4.1.3 Assays using an NADH regeneration system

Assays using a yeast alcohol dehydrogenase NADH regeneration system were performed with (+)-valencene using 0.5 μM P450 in 1 mL 50 mM Tris, pH 7.4, in a 7 mL glass vial. 1 – 2 mM (+)-valencene was added from a 100 mM DMSO stock. 2 units of yeast alcohol dehydrogenase were added, along with 50 μL ethanol or hexanol. NADH was added to a final concentration of 0.2 mg/mL and the reactions were shaken at 200 rpm overnight at 37 °C.

2.4.1.4 Assays of (+)-valencene using an NADPH regeneration system

Assays using a glucose dehydrogenase NADPH regeneration system were performed with (+)-valencene using 0.5 μM P450 in 1 mL 50 mM Tris, pH 7.4, in a 7 mL glass vial. 1 – 2 mM (+)-valencene was added from a 100 mM DMSO stock. 2 units of glucose dehydrogenase were added, along with glucose to a final concentration of 100 mM, from a 1 M stock in Tris. NADPH was added to a final concentration of 0.2 mg/mL and the reactions were shaken at 200 rpm overnight at 37 °C. For tests involving a second phase, 400 μL undecane was added to the vial. For second phase reactions with surfactants, 4.8 % w/v surfactant was added.

2.4.1.5 Assays of drug compounds using an NADPH regeneration system

Assays using an NADPH regeneration system were performed with pharmaceuticals using 0.25 – 5 μM P450 in 250 μL – 10 mL 50 mM Tris. 0.5 – 2 mM substrate was added from a 50 mM ethanol stock (testosterone) or a 100 mM ethanol stock (all others). 2 units/mL of glucose dehydrogenase were added, along with glucose to a final concentration of 100 mM, from a 1 M stock in Tris. NADPH was added to a final concentration of 0.2 mg/mL and the reactions were shaken at 200 rpm overnight at 37 °C.

In one experiment, glucose-6-phosphate and glucose-6-phosphate dehydrogenase were used in the same concentrations as in the reaction using glucose dehydrogenase.

2.4.2 *In vivo* assays

2.4.2.1 Whole cell reactions with diclofenac

Proteins were expressed as described in section 2.3.1, but cell pellets were not frozen. The collected cell pellets were resuspended in one tenth growth volume of $FB_{glycerol/kan}$ or, in one case 2YT. 50 mL of the 10× cell density cultures were incubated for 24 h with 1 mM diclofenac (added as a 100 mM stock in ethanol) and shaken at 110 rpm in a 250 mL conical flask.

2.5 Product isolation and analysis

2.5.1 Reactions with (+)-valencene

2.5.1.1 NADPH turnover assays

1000 µL of the reaction mixture resulting from an NADPH turnover assay with (+)-valencene was removed and 3 µL of a 100 mM stock of *p*-benzyphenol in DMSO was added as an internal standard. 400 µL EtOAc was added and the mixture was vortexed to mix, then centrifuged at 21,000 *g* for 3 min. 250 µL of the organics was removed and dried over anhydrous $MgSO_4$ for 15 minutes. Solids were separated by centrifugation at 21,000 *g* for 3 minutes and the supernatant was analysed by GC, using a 15-m DB-1 column and the following oven conditions: 100 °C initial temperature hold for 1 min, 15 °C/min ramp to 220 °C, hold for 4 min. Product concentrations were calculated using a calibration curve generated by Mr. Christopher Douse[207].

2.5.1.2 NAD(P)H regeneration system assays

Products from reactions using an NAD(P)H regeneration system were isolated and analysed in the manner described in section 2.5.1.1.

2.5.1.3 NADPH regeneration system assays with a second phase

Organics were removed from the reaction by pipette and centrifuged for 5 min at 21,000 *g* in a 1.5 mL microcentrifuge tube. The organics were analysed by GC as described above. The aqueous phase was analysed as described in section 2.5.1.1, though did not show any reaction products.

2.5.1.4 NADPH regeneration system with a second phase and surfactant

Products from reactions using an NADPH regeneration system with a second phase and surfactant were isolated and analysed in the manner described in section 2.5.1.3.

2.5.2 Oxidation of pharmaceuticals

2.5.2.1 *In vitro*

Reactions were stopped by the addition of 50% of the reaction volume of cold (–20 °C) methanol. Precipitated protein was removed by centrifugation at 21,000 *g* for 5 min. The supernatant was removed from the protein pellet and evaporated to dryness using a Buchi rotary evaporator. The resulting solids were extracted with 3 × 200 μL methanol, which was combined and concentrated to *ca*. 50 μL. The resulting solution was analysed by HPLC on a Pursuit XRS C18, 4.6×150 mm, 5μm column from Agilent. The mobile phase was comprised of A) 99:0.8:0.2 water:acetonitrile:formic acid and B) 99:0.8:0.2 acetonitrile:water:formic acid. The elution gradient was run at 1 mL/min and consisted of 2 min 100 % A, a 10 min ramp to 100 % B, a 2 min ramp to 100 % A for a 2 min hold.

2.5.2.2 *In vivo*

In vivo reactions with pharmaceuticals were stopped by the centrifugation of the reaction mixture at 9250 *g* for 5 min at 4 °C to remove cells. The supernatant was removed and work up proceeded as described in section 2.5.2.1.

2.6 Potentiometric titrations

2.6.1 Experimental details

To prepare the analyte enzyme solution, the previously prepared enzyme stock solutions, which are 50:50 glycerol:phosphate buffer, was eluted on a 5-mL PD-10 gel filtration column, which serves to remove the glycerol and exchange the buffer with 50 mM Tris, pH 7.4. The resulting Tris solution was then concentrated to a volume of *ca*. 200 μL in a centricon. This concentrated solution was transferred to a glove box. A fresh analyte solution was used for each titration.

To prepare the cocktail of electrochemical mediators, a 1 mM solution of the mediators was prepared by weighing 0.0037 g methylene blue, 0.0031 g anthraquinone-2-sulfonate, 0.0041 g each of anthraquinone-1,5-disulfonate and anthraquinone-2,6-disulfonate and 0.0026 g methyl viologen into a vial, and transferring this to a Belle Technology glove box under nitrogen atmosphere (O_2 <5 ppm). 10 mL 50 mM Tris, pH 7.4, which was stored in the glove box, was added and the solids dissolved. 10 μL of this mixture was then added to a 310 mM solution of NaCl, which is used as the supporting electrolyte. 830 μL of the resulting mediator/salt solution was added to the enzyme solution. A fresh mediator solution was prepared for most experiments.

A 1 M stock of glucose was prepared by weighing solid glucose and adding 50 mM Tris, pH 7.4 in the glove box. This solution was sealed and stored in a freezer. 130 μL of this

solution was added to the mediator/protein solution prepared above. A solution containing 1 mg/mL glucose oxidase and 2 mg/mL catalase was also prepared and stored in a freezer. 13 μL of this solution was added to the protein mixture, and the final volume of the protein solution was madde up to 1300 μL. This gives final concentrations of 5 μM for each of the five mediators, 10 mM glucose, 0.1 mg/mL glucose oxidase, 0.2 mg/mL bovine liver catalase, 200 mM NaCl. Enzyme concentration was *ca.* 30 μM for P450s (heme domain only for $P450_{BM3}$) or *ca.* 70 μM for ferredoxins.

The saturated colomel reference electrode is assembled into the Luggin capilary outside of the glovebox, with the capilary containing a 0.1 M KCl solution. All other cell assembly is carried out in the glove box to minimize the presence of oxygen in the cell. The titrations were carried out in a custom-built optically transparent thin-layer electrode (OTTLE) cell constructed from a quartz cuvette of 0.1 cm path length. The working electrode was a gold mesh (500 wires per in, wire width 4.5×10^{-4} in, 60% transmission) attached to gold wire (0.2 mm diameter) with cyanoacrylate adhesive and insulated with paraffin film. A poly(methyl-methacrylate) solution well was attached to the top of the cuvette by silicone sealant. The counter electrode was a platinum mesh (100 mesh, 0.003 in wire diameter) in solution. Anaerobic conditions were maintained by purging the system continually with argon that had first been sparged through a *ca.* 10 cm column of room-temperature water to hydrate the gas and keep cell solution levels constant and component concentrations steady. Spectra were acquired for 40 – 80 min to allow equilibration and cell temperature was maintained at 25 °C.

2.6.2 Data analysis

Data analysis is also described in Chapter 4. Spectral data were corrected for baseline drifts by a 0^{th} order adjustment based on the average optical density from 775–800 nm.

Because the absorbance of the peaks in the Soret band was convoluted by contributions from the reduced form of methyl viologen (λ_{max} = 395 nm), the absorbances at 450 nm, 465 nm and 550 nm were used for data analysis. Data were fitted to Equation 2.3, a sigmoid derived from the Nernst equation:

$$A(E) = \frac{A(E_{max}) - A(E_{min})}{1+\exp[(E_m - E_{appl})/(RT/nF)]} + A(E_{min})$$

Equation 2.3

where $A(E)$ is the absorbance for a given potential, $A(E_{max})$ and $A(E_{min})$ are the optical densities for the fully oxidized and fully reduced chromophore, E_m and E_{appl} are the midpoint and applied potentials, R the gas constant, T the cell temperature, n the number of electrons transferred for the redox couple, and F Faraday's constant. The values of $A(E_{max})$, $A(E_{min})$ and E_m were determined by minimising the square of the difference between the measured value and the predicted value, assuming equal weighting of the data. The value of n was fixed to 1. When n was allowed to vary, values ranged from 0.80 to 1.35. All potentials relate to the standard hydrogen electrode, using a +242 mV correction, at 25 °C.

2.7 Stopped flow spectrophotometry

2.7.1 Experimental details

Experimental details are given in Chapter 5. To prepare the analyte enzyme solution, the previously prepared enzyme stock solutions, which are 50:50 glycerol:phosphate buffer, was eluted on a 5-mL PD-10 gel filtration column, which serves to remove the glycerol and exchange the buffer with 50 mM Tris, pH 7.4. The resulting solution was diluted to *ca.* 4 μM. This sample was transferred to a 15 mL centrifuge tube. The second sample tube contained NADPH (200 μM). For substrate-bound complexes, both tubes contained

2 % v/v DMSO and 200 μM substrate. The tubes were sealed using a rubber septum and paraffin film, and the solution was then saturated with CO by gently bubbling for 5 min and then purging the headspace for a further 5 min. The tubes were transferred to a glove box and gas-tight syringes used to remove the solutions from the tubes, maintaining CO saturation. The syringes were loaded into an Applied Photophysics SX20 stopped-flow spectrophotometer in single-wavelength mode set at 450 nm and components were mixed in a 1:1 ratio. The stopped-flow cell is held at 25.0 ± 0.1 °C. Data acquisition times ranged from 0.16–6 s.

2.7.2 Data analysis

Data were fitted using Pro-data Viewer software (Applied Photophysics) and could be deconvoluted into up to three distinct phases, a "fast" phase associated with high-spin heme, a "slow" phase associated with low-spin heme (*ca.* 1 s^{-1} for WT and ca. 12 s^{-1} for KT2) , and a "denatured" phase associated with CO bubbling (*ca.* 30 s^{-1}). Following deliberate vigorous and prolonged bubbling of CO through enzyme solutions, only the 30 s^{-1} phase was observed (Chapter 5). Although the relative amplitude of this phase varied between experiments, the rate constant derived from multiphasic fits always fell within a narrow range for each enzyme.

2.8 Fabrication of patterned gold electrodes

2.8.1 Deposition of Cr and Au layers

Prior to deposition of the metal layers the fused silica strips were cleaned by a 'standard cleaning' protocol to prepare surfaces for metal deposition[208]. The strips were cleaned for 15 min at 75 °C in a 5:1:1 mixture of double-distilled water: concentrated hydrochloric acid: 30% hydrogen peroxide and rinsed with double-distilled water. This was followed

by 15 min at 75 °C in a 5:1:1 mixture of double-distilled water: 20% ammonia: 30% hydrogen peroxide followed with rinsing in double-distilled water. The strips were dried by heating to 120 °C for 30 min and sent for metal deposition.

The deposition of the Cr and Au layers were performed by Dr. Robert Jacobs of the Department of Chemistry, University of Oxford. The metals were depositied by chemical vapour deposition in an Edwards Auto 306 Cryo Evaporator.

2.8.2 Photolithography

Photolithographic masks were printed on acetate sheets by Oxford University Computing Services. Positive photoresist was coated over the plates and distributed evenly by centrifugation at 2500 *g* for 30 s. The resist was dried by heating at 80 °C for 5 min. The resist was exposed to UV light for 5 seconds through a mask containing the electrode design and developed using positive photoresist developer. The exposed gold was etched using Gold Etchant, and, after rinsing with water the exposed chromium was etched using Etch 18. The photoresist was removed using acetone.

Chapter Three

Engineering $P450_{BM3}$ for the Oxidation of Pharmaceuticals and High Value Chemicals

3.1 Generic accelerator variants

3.1.1 Engineering and Evolution

The two ways of achieving increased activity towards a non-natural substrate are through protein engineering and evolution. The goal is to produce an enzyme where the active site admits a range of compounds which displace the axial water ligand and promote electron transfer to initiate the P450 catalytic cycle. The altered active site must keep the substrate close to the heme to improve coupling, but should not bind the substrate too tightly, as this can lead to product inhibition or limit the diversity of substrates oxidized. Enzymes can be evolved to specifically oxidize a small number of substrates selectively at a certain position, such as the specific propane oxidase evolved by Arnold *et al*[119], though for specific selectivity and activity towards a single product protein engineering is often used, such as the efforts towards (+)-nootkatone production from (+)-valencene by Sowden *et al*[90], and Urlacher *et al*[97].

Directed evolution is often the strategy used for mutant library development, as a relatively large number of variants can be screened for activity towards a particular substrate or multiple substrates and a library of variants active towards these compounds is generated. Once the mutations which influence selectivity and activity are identified, site-saturation studies, or more selective mutagenesis studies, can be used to test the influence of individual mutation sites towards overall activity.

Variants which display increased activity to a substrate are a good basis for engineering product selectivity, especially when the variants are active towards a range of compounds.

In humans, drug metabolism is carried out primarily by just five enzymes, so an enzyme which displays high activity across a range of compounds is an excellent candidate for engineering human P450-like activity.

Directed evolution and screening by Whitehouse *et al*. identified four $P450_{BM3}$ variants that display enhanced oxidation activity towards a broad range of substrates: KSK19 (F87A/H171L/Q307H/N319Y)[209], KT2 (A191T/N239H/I259V/A276T/L353I)[209], A330P (AP)[209] and I401P(IP)[78]. The development of these variants for the metabolism of drugs is the subject of this chapter.

3.1.2 The generic accelerator variants

The study in which these variants were identified used indigo formation as an initial screen, with blue colonies being selected for *in vivo* activity tests towards naphthalene and propylbenzene[209]. Figure 3.1 shows an example of this increased oxidation activity with propylbenzene as the substrate. Additional mutations on these generic accelerator variants can further increase oxidation rate or alter substrate selectivity. In particular the R47L/Y51F combination can increase not only NADPH consumption rate and product formation rate (PFR), but also coupling efficiency of the KT2 variant with propylbenzene[210].

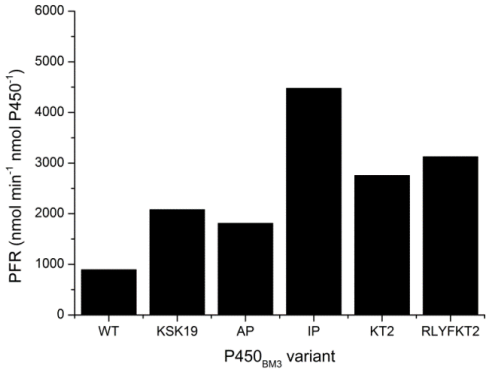

Figure 3.1. Product formation rates with propylbenzene.

3.1.2.1 KSK19

Of the generic accelerator variants identified by Whitehouse *et al*., KSK19 is the only one that contains a mutation at Phe87. KSK19 displays the same altered selectivity as the F87A variant alone, indicating the mutations at His171, Gln307 and Asn319 do not have a large impact on product selectivity. A crystal structure of KSK19 has not yet been solved so the reason these particular mutations impart their rate enhancing effects is unknown. These mutations lie far from the active site, near the beginning of the F helix (His171) and in the K helix (Gln307 and Asn319), though interestingly His171 and Gln307 are fully conserved across the CYP102A subfamily. Asn319 lies near the proposed FMN domain binding site[12], indicating domain-domain interactions may play a role in the activity enhancing properties of KSK19. However, a threonine mutation at Asn319 has been reported to play no significant role in activity enhancement[91].

From previous work in this group, the F87A mutation is known to limit total turnover number of $P450_{BM3}$ (not shown), while demonstrating large shifts in selectivity. For example, when oxidizing 3-methylpentane WT gives 7% 3-methyl-3-pentanol, while F87A gives 90% 3-methyl-3-pentanol[210]. This indicates that the active site in F87A-based variants is more open and the substrate is more free to adopt multiple orientations. As a result, the ferryl oxygen can access most, if not all parts of the substrate, and oxidation occurs at the most activated C—H bond.

3.1.2.2 KT2

Like KSK19, KT2 contains mutations not found in the active site with no immediately obvious reason for imparting rate enhancing effects. Several of the individual mutations in KT2 are known (I259V[211] and N239H[212]), and other substitutions at Ala191[213, 214] and Leu353[215] have been reported as part of directed evolution studies. As with many

multiple-mutation variants, insight into the catalytic activity can be obtained from the crystal structure, which has been solved[216]. The SF KT2 crystal structure resembles the SB-WT structure and this is likely the origin of the rate enhancing effects. The crystal structure will be discussed in detail in Chapter 5.

In contrast to the Schmid mutant (A74G/F87V/L188Q), which displays high product formation rates (PFRs) mostly due to accelerated NADPH consumption rates, high PFRs are observed with KT2 owing to improved coupling with substrates such as ethylbenzene or naphthalene[210]. With these substrates, KT2 was up to twice as efficient at utilizing NADPH.

KT2 rarely alters the product profile compared to the WT enzyme, which increases its use as an accelerator base mutant, as selectivity-altering mutation can be used in combination to give accelerated rates and targeted selectivity changes. For example, with propylbenzene F87A/KT2 and F87V/KT2 give the product profiles of F87A and F87V respectively[210, 217].

3.1.2.3 I401P

The single proline mutant, I401P, displays vastly enhanced substrate oxidation rates[218]. The position of the mutation, immediately adjacent to the heme ligating cysteine (Cys400), is occupied by proline in chloroperoxidase as well as several other P450s[33, 219]. The $P450_{cam}$ ethane hydroxylase has an analogous mutation[110], and many other single proline mutations on $P450_{BM3}$ have been investigated by this group[207]. The crystal structure of I401P has also been determined and, like KT2, shows resemblances to the SB-WT, suggesting that the enzyme is in a catalytically ready conformation even without a substrate, as will be discussed in detail in Chapter 5.

The PFR of the RLYF/I401P variant with propylbenzene was determined to be 5074 min^{-1}, one of the highest reported with variants of this enzyme and any substrate[210]. The total turnover number (TTN) with propylbenzene is 114,000. This is the highest reported TTN for $P450_{BM3}$ as well, nearly doubling the previously highest reported value, which was 66,700 with lauric acid[210, 220]. Coupling with this substrate was also among the highest reported among non-natural substrates, at 90%[210].

3.1.2.4 A330P

Ala330 was not identified as an access channel residue in the initial studies of the substrate-free crystal structure[64], though was shown to make contact with the substrate in the palmitoleic acid bound structure[65]. The crystal structure of A330P has been solved and will be discussed in detail in Chapter 5, though some features will be discussed here in order to understand the selectivity shifts demonstrated by the A330P variant.

Pro329 is a highly conserved residue among eukaryotic P450s[210] and a key residue in the substrate access channel. Proline is a highly rigid amino acid often found in β-turns and the terminus of α-helices. In the A330P mutant, Pro329 is relocated into the active site, restricting access to the heme iron. The constricted active site, while preventing activity with fatty acids, imparts A330P with enhanced activity towards small molecules such as toluene and pentane, while altering product profiles with other substrates[5, 209].

Restriction of the active site is not the only means by which activity towards small molecules is promoted. With propane I401P shows a PFR of 25 min^{-1}, and RLYF/I401P has a PFR of 106 min^{-1}. When these mutations are combined with A330P, a PFR of 430 min^{-1} is achieved with propane, which is very near the activity reported (455 min^{-1}) by Arnold *et al.* with a 24-mutation variant specifically evolved for propane oxidation[119].

3.2 Metabolism of Drugs by $P450_{BM3}$

3.2.1 General background

As many drug metabolites are themselves biologically active, understanding the activity, toxicity and bio-availability of a drug metabolite is a key step in evaluating the efficacy of a pharmaceutical[221]. Studies of drug metabolites require large quantities of pure metabolites which are not always easy to synthesize. There has therefore been widespread interest in developing a convenient synthetic route to human metabolites of drug compounds.

One such alternate synthetic route is to use P450s to generate the primary drug metabolites. An obvious approach is to use liver microsomes as a source of human P450s. However, their limited availability and variable expression levels make their use as a preparative-scale synthetic method impractical[93]. Alternative methods of expressing human P450s have been explored, including the expression of human P450s and CPR in yeast[173], *E. coli*[222, 223] and insect cells[224]. These methods remain impractical, however, owing to low enzyme stability and reaction rates[225].

As expression of human enzymes is difficult several research groups have focused instead on engineering $P450_{BM3}$ to metabolise drug compounds. The results of these efforts are summarized below. The mutations present in drug metabolizing variants of $P450_{BM3}$ are summarized in Appendix 1, and drugs towards which $P450_{BM3}$ has been reported to show activity are summarized in Appendix 2.

3.2.2 Approaches by Arnold and co-workers

Arnold and co-workers have developed variants of the $P450_{BM3}$ heme-domain (BMP) capable of utilizing hydrogen peroxide, in place of the reductase domain and NADPH, to

drive oxidation of fatty acids[212]. These 'P450 peroxygenases' have been evolved through a combination of site-specific and random mutagenesis to produce human metabolites of propranolol[93]. The starting BMP variant had fourteen mutations, notably F87A and N239H, while seven additional sites, including R47 and V78, were targeted for site-directed mutagenesis[93]. A 17-mutation variant oxidized propranolol to 4′- and 5′-hydroxypropranolol and desisopropylpropranolol, which were detected by HPLC, with 20% conversion, using 5 μM enzyme and 5 mM propranolol (Figure 3.2)[93].

Directed evolution studies have also been carried out with the aim of metabolising non-steroidal anti-inflammatory drugs (NSAIDs) such as ibuprofen and naproxen[143, 149]. The BMP peroxygenases described above showed activity towards naproxen and were further evolved through directed-evolution, using high-throughput screening with *p*-nitrophenoxycarboxylic acid as a screen substrate. 8160 variants were screened for activity with propranolol and naproxen. Of these, one variant (5H6-13C9, see Appendix 1) showed activity towards naproxen, though activity was low, at 12.9 nmol product formed by 0.4 nmol enzyme in 2 h[143]. Propranolol oxidation was achieved by 10 variants with the most active (21B3-14C10) forming 23.2 nmol product with 0.4 nmol enzyme in 2 h[143].

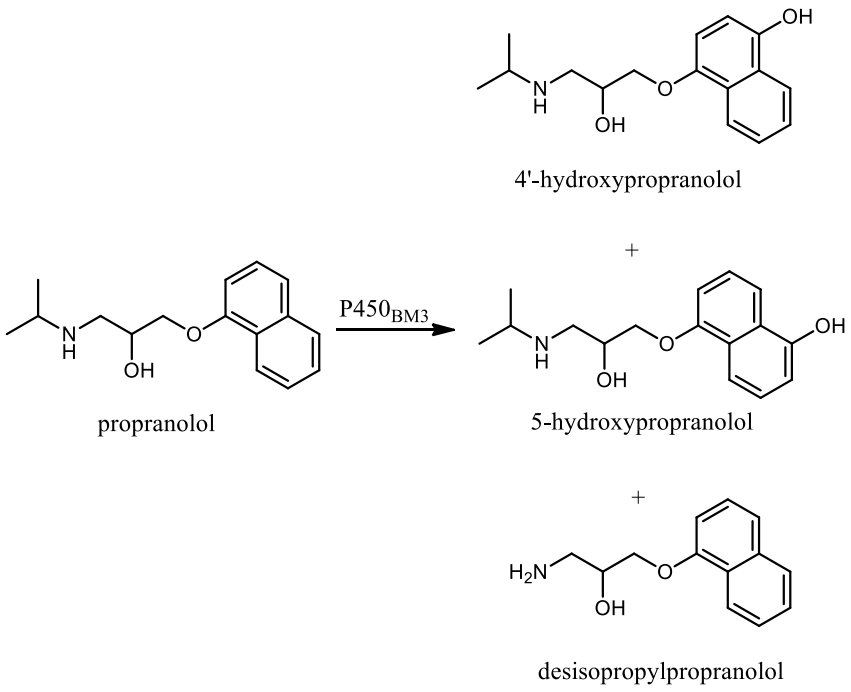

Figure 3.2. Metabolism by $P450_{BM3}$ of propranolol to 4′- and 5-hydroxypropranolol and desisopropylpropranolol.

Efforts were made to engineer $P450_{BM3}$ into a CYP2C9 mimic, as this is the second most highly expressed human P450 in liver microsomes. Activity was eventually achieved towards ibuprofen and improved towards naproxen[149], and was increased by re-attaching the reductase domain (BMR) to the BMP 'peroxygenases' and using an NADPH regeneration system. Conversions of up to 20% for naproxen (3 mM substrate, 0.033 mol% enzyme, generating desmethylnaproxen) were achieved with variant W7D8, which also displayed the highest TTN value with ibuprofen, at 650, producing 2- and 3-hydroxyibuprofen[149]. These drugs and metabolites are shown in Figure 3.3.

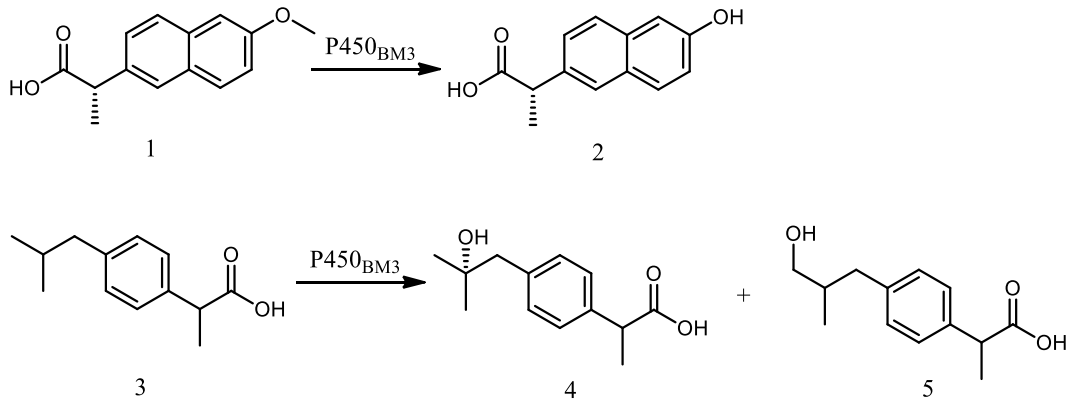

Figure 3.3. Metabolism by $P450_{BM3}$ of: naproxen (**1**) to desmethylnaproxen (**2**) and, ibuprofen (**3**) to 2- hydroxyibuprofen (**4**) and 3-hydroxyibuprofen (**5**).

Chimeras, fusions of BMP with the heme domains of CYP102A2 or CYP102A3, have also been studied by Arnold *et al* for activity towards verapamil and astemizole [226]. In all but one case, of the 120 variants screened the non-chimera based variants displayed better conversion of the target substrates. Of the screened variants, twenty-eight displayed activity towards verapamil, with D6H10 displaying a substrate conversion of 78% (all other conversions were less than 50%). Thirty variants displayed activity towards astemizole, with F87I and 9-10A showing 50% conversion. The variant 9-10A F87L was purified and used to generate 9.4 mg of a purified metabolite from 25 mg verapamil with a TTN for the enzyme of 1560, though the obtained metabolite was not formed by human microsomes (Figure 3.4)[226].

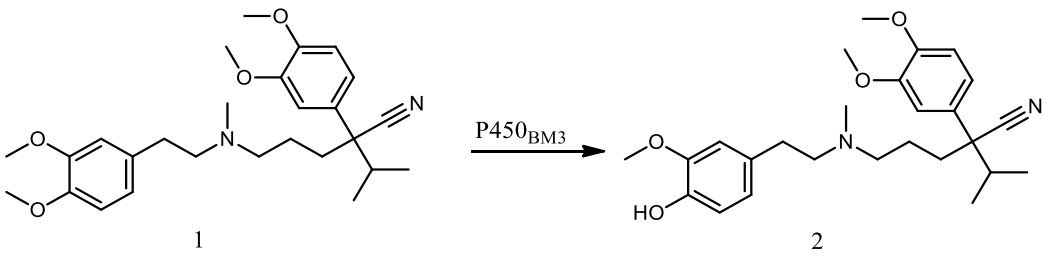

Figure 3.4. Metabolism by $P450_{BM3}$ of verapamil (1) to (2), a metabolite not generated by human P450s.

3.2.3 Approaches by Gilardi and co-workers

Much of the drug metabolism work carried out in the Gilardi laboratory has focused on the fusion of human drug metabolising enzymes to BMR[227, 228], though $P450_{BM3}$ variants have been screened to target metabolite synthesis[146, 229].

The first human P450 to be fused to BMR was CYP2E1[227], which is responsible for metabolism of a relatively small number of compounds, though its substrates include paracetemol and chlorzoxazone[230, 231]. The CYP2E1-BMR fusion was successfully expressed and shown to be soluble and retain activity towards chlorzoxazone (K_M = 0.65 ± 0.08 mM and k_{cat} = 0.95 ± 0.10 min^{-1} for 6-hydroxychlorzoxazone formation). Subsequently, CYP2C9-BMR, CYP2C19-BMR and CYP3A4-BMR fusion proteins were developed and also shown to be catalytically self-sufficient and maintain the activity of the native human P450[228].

The Gilardi group has also shown that WT $P450_{BM3}$ is active towards several drug compounds with comparable V_{max} values to human drug metabolising P450s, albeit with K_M values three orders of magnitude higher. Chlorzoxazone, propranolol, nifedipine and aniline were all oxidized by WT $P450_{BM3}$, while the enzyme showed no activity with terfenadine, acetophenetidine, erythromycin, propafenone, sparteine, debrisoquine, perhexiline, diclofenac, ibuprofen, tolbutamide, sulphamethoxazole, warfarin, caffeine, or theophylline.

Recently, a double mutant variant of $P450_{BM3}$, A2, was shown to hydroxylate diclofenac, ibuprofen and tolbutamide to their CYP2C9 products[146]. The WT enzyme shows no activity towards these compounds, though the A2 variant shows an NADPH consumption rate of 428 min^{-1}, 146 min^{-1} and 231 min^{-1} respectively for diclofenac, ibuprofen and tolbutamide, the k_{cat} values for product formation were considerably lower, and K_M values

were also high[146]. The increased activity of the A2 variant towards drug compounds is unexpected as neither of the mutation sites (Asp251 or Gln307) are in the active site, though as with the variants KSK19 (which contains a mutation at Gln307) and KT2[216], mutations far from the active site can have large impact on the enzyme structure and function. Section 1.2.2 discussed structural changes induced in $P450_{BM3}$ by substrate binding, including the breaking of a salt-bridge between Asp251 and Lys224, which could be an explanation for the effects of mutations at this site.

3.2.4 Approaches by Vermeulen and co-workers

The Vermeulen group, like the Arnold group, applies high-throughput screening methods to identify potential target substrates. Indeed, this group was the first to show that drug compounds may act as ligands to $P450_{BM3}$, after a 7-benzlyoxyresorufin oxidation (BROD) screen of the triple mutant R47L/F87V/L188Q with 45 drug-like compounds identified eight potential substrates[232].

After identifying potential R47L/F87V/L188Q substrates, the group showed that this variant, though not the WT, is active towards testosterone, amodiaquine, dextromethorphan, acetaminophen, and 3,4-methylenedioxymethylamphetamine (MDMA)[136]. These compounds were believed to be oxidized to the human metabolites (determined by co-elution with human enzyme turnovers on HPLC), but activity was one- to two-orders of magnitude lower for the $P450_{BM3}$ variant.

MDMA and dextromethorphan activity was improved nearly 200-fold with the addition of three mutations to the triple variant: F81I, E267V and L86I[91]. Discovered through a BROD screen of a library of random mutagenesis variants with the R47L/F87V/L188Q triple mutant as the starting point, M01, M02, M05 and M11 were discovered to be highly active towards MDMA and dextromethorphan and, while other mutations were present in

these variants, many of the other mutations were shown to not affect activity by removing them with directed mutagenesis (variants M01a, M02a and M02b)[67, 91].

His-tagged versions of M01, M02, M05 and M11 were used to generate metabolites of diclofenac, clozapine and acetaminophen[3, 233]. The metabolites were determined through the formation of glutathione (GSH) adducts by LC-MS/MS analysis, and compared to those generated by rat and human liver microsomes. Though activity of the $P450_{BM3}$ variants was nearly 70-fold higher than the human liver microsomes, total conversion remained low. $M11_{his}$ was also shown to generate human metabolites of trimethoprim[234] and troglitazone[235].

Further high-throughput screening identified four further $P450_{BM3}$ variants, based on the M01-M11 library, which demonstrated activity towards several drug compounds, but only produced metabolites from buspirone[236]. Following this, a large scale screen was completed wherein six $P450_{BM3}$ variants were tested for activity with 43 drug molecules, and nine of these drugs were in turn used to study the activity of a 14 variant library in more detail[151]. Metabolites were produced from all but two of the screened drugs, with 33 of the drugs being more than 20% converted. Of these variants, it was shown that mutations at Leu437 and Ser72 seemed to have a large impact on the type of drug metabolised, with the S72D and L437S mutations increasing activity towards cationic drug compounds.

3.2.5 Approaches by Yun and co-workers

Yun *et al.* have reported that WT $P450_{BM3}$ is capable of generating piceatannol, the human metabolite of resveratrol, though k_{cat} is less than 1 min^{-1}. The group also performed a study using many previously reported variants to generate human metabolites of 7-ethoxycoumarin, a typical substrate of human P450s[82]. The same

variants improved activity towards resveratrol, the most active variant, R47L/L86I/F87V/L188Q, had a 4.0 min^{-1} product formation rate[237].

Using an indigo-formation-based screening protocol, a library of variants generated through random mutagenesis was developed, which showed activity towards coumarin, 7-ethoxycoumarin, chlorzoxazone, phenacetin and *p*-nitrophenol[141]. A library of existing variants was also evaluated towards simvastatin and lovastatin, with the M11 variant from the Vermeulen group giving the highest PFR among the screened variants[238].

3.2.6 Common mutation sites and drug types

From the large number of $P450_{BM3}$ variants that have been shown to oxidize drug compounds, there are several mutation sites and specific substitutions that appear across several libraries. As each laboratory develops their own criteria for mutant screening, if a mutation appears in several random mutagenesis studies, it is likely to have an important effect in engineering $P450_{BM3}$ to oxidize drug compounds.

The most obvious site which appears in multiple studies is Phe87. So important is this site that a site-saturation mutagenesis study was undertaken using the active M11 variant, which has the F87V mutation, as the template[137]. This study showed that F87V and F87W were among the most active substitutions, though alterations in regioselectivity occur across mutants. Another site, which has also been reported as a target earlier[239], is Glu267. The E267V variant, reported by Richard Kenny in 2004 as a Part II student in this group[239], appears in eight of the drug metabolising $P450_{BM3}$ variants, including perhaps the most robust and active, M11. R47L, another mutation first described by this group[88], is also widely used in the drug metabolising libraries. Substitutions at Ala82, as well as those at the Schimid mutant sites A74 and L188 are also prevalent. The location of these residues is shown in Figure 3.5.

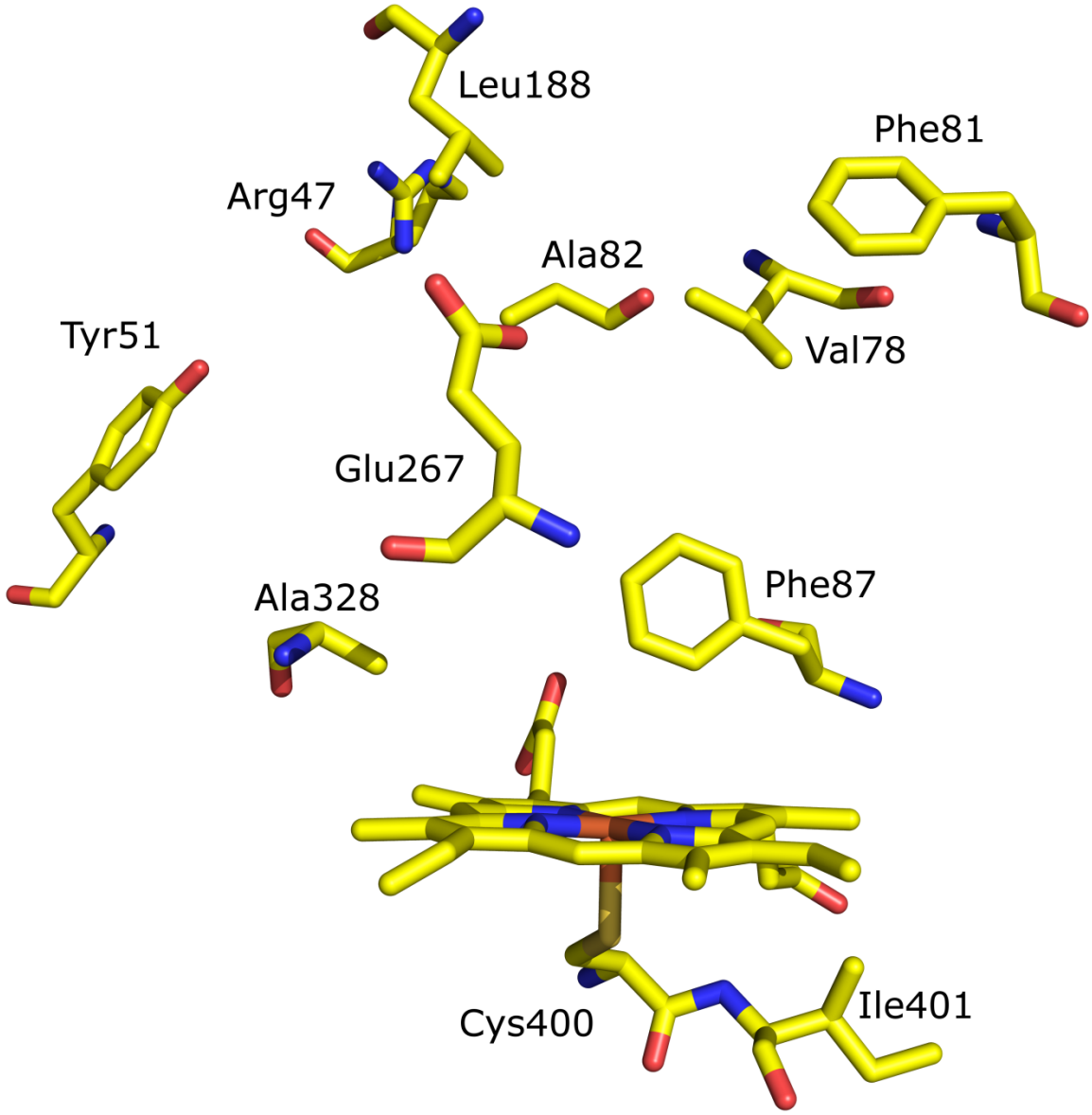

Figure 3.5. Active site of SF WT (PDB code: 1BU7) showing residues commonly mutated in drug metabolizing variants.

Though initial screens with $P450_{BM3}$ libraries focused on small molecules such as 7-ethoxyresorufin, chlorzoxazone or acetaminophen, recent studies have expanded this set to include molecules of a variety of structures, sizes and chemical types. The drugs towards which $P450_{BM3}$ shows activity are shown in Appendix 2. Many of these compounds have been involved in only one large scale screen for base activity, while some have been heavily studied, such as ibuprofen and diclofenac. However, in spite of

concerted efforts by several groups, oxidation of compounds containing a charged carboxylate moiety, remain a challenge: "There has been no report on a $P450_{BM3}$ variant exhibiting good activity on these charged molecules[149]."

3.3 Oxidation of pharmaceuticals by I401P variants

3.3.1 Initial screening of generic accelerator variants.

The variants I401P, KT2, RLYF/A330P and KSK19 were screened for oxidation of the drug compounds propranolol, theophylline, caffeine, phenetidine and chlorzoxazone[240]. These substrates, shown in Figure 3.6, were selected as they have a range of size, structural features and charges. High NADPH consumption rates (*N*) were observed with I401P, which displayed an $N > 1100$ min^{-1} for chlorzoxazone, while other variants had *N* values between 20 and 210 min^{-1}. Though turnovers were assayed by GC and HPLC, no metabolite was detected in any reaction in this screen[240].

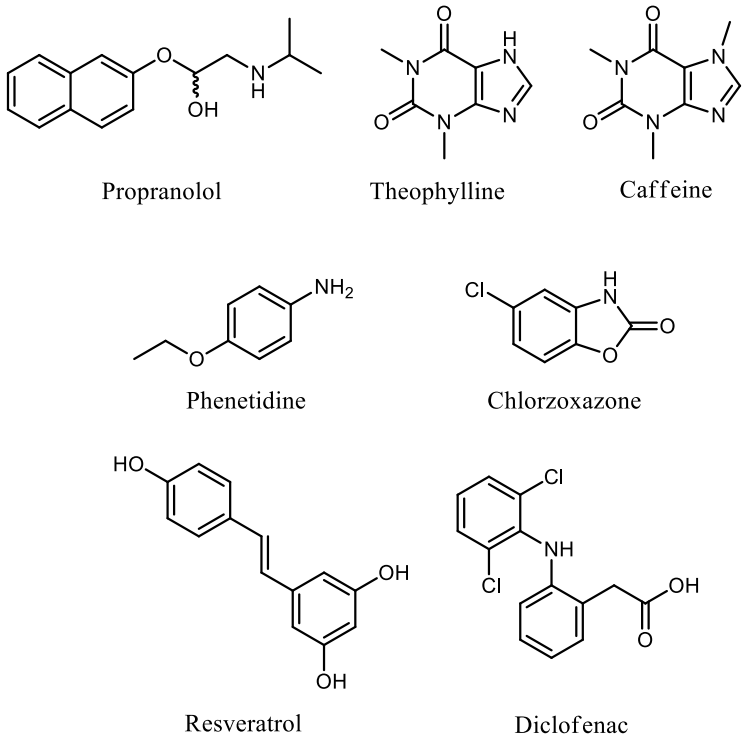

Figure 3.6. Drugs selected for initial screening of $P450_{BM3}$ variants.

A secondary screen was performed using the variants KSK19/I263A, I401P, F87A/I401P and RLYF/I401P (RP) and the drug compounds propranolol, resveratrol, diclofenac and chlorzoxazone (Figure 3.6). In all but one case, there was no trace of metabolism by the screened variants by HPLC analysis. The exception was the drug diclofenac with the RP variant, which showed a small peak in the HPLC (Figure 3.7). Thus, the RP variant was selected as a template for the addition of other mutations shown to promote drug oxidation. Interestingly, no metabolites were observed with propranolol, a drug towards which the WT enzyme has been reported to metabolize. This could indicate that the analysis protocols were not sufficiently optimized for product detection.

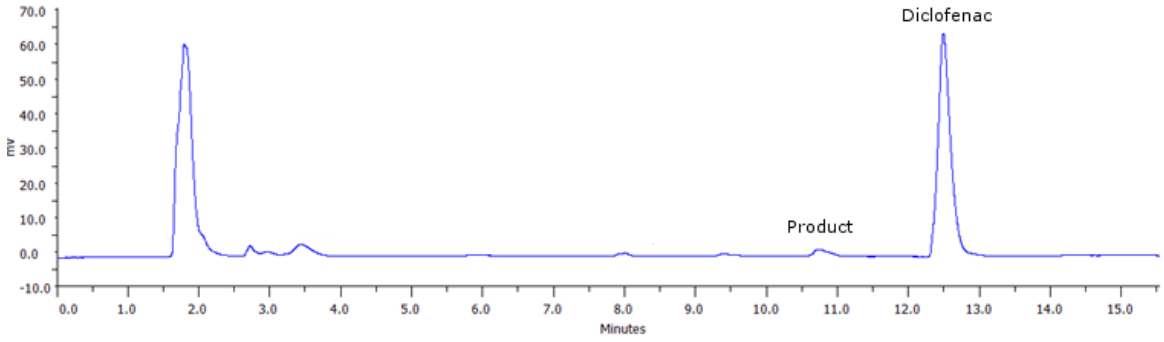

Figure 3.7. HPLC trace of 1 mM diclofenac metabolized by 5 µM RP, pH 7.4, 1 h, 20 °C. Analysed with a 1 mL/min elution gradient.

Diclofenac, a common NSAID, is metabolized primarily by CYP2C9 and CYP3A4 into 4′- and 5-hydroxydiclofenac, as shown in Figure 3.8. As noted above, diclofenac is a challenging substrate towards which $P450_{BM3}$ variants have been screened but for which activity has been low[149]. The most active $P450_{BM3}$ variant towards diclofenac is MT35 (Appendix 1) which contains mutations at sites R47, F87, E267 and L188, among others. This enzyme oxidized 50% of 40 µM diclofenac over 90 min, with 0.5 µM enzyme.

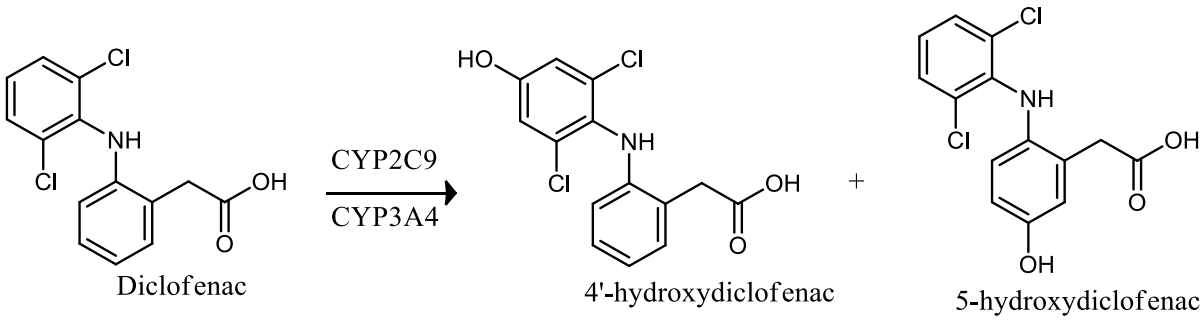

Figure 3.8. Diclofenac and the two human metabolites, 4′- and 5-hydroxydiclofenac.

3.3.2 Library development

The RP variant showed hints of activity towards diclofenac and so was selected as the template for library development with the aim of generating a small library of mutants that shows high conversion of diclofenac to the human metabolites. The F87V and E267V mutations have been reported to improve the activity of $P450_{BM3}$ towards drugs and are present in the MT35 variant[151]. These mutations were added to the RP variant to create three new variants, which were tested for *in vitro* activity towards diclofenac. The results of this are shown in Table 3.1.

NADPH consumption rates were not studied, as RP-based variants tend to have high leak rates and the enzyme is highly uncoupled with these substrates. Therefore, the reactions were performed on a larger scale using an NADPH regeneration system with the target of achieving high conversion of the drug compounds into human metabolites.

Reactions were performed in a 1.5 mL microcentrifuge tube, in 50 mM Tris, pH 7.4 with 250 μL total reaction volume. Enzyme concentration was varied (either 1, 2 or 5 μM) and diclofenac concentration was 1 mM. NADPH was regenerated using 1 unit/mL glucose dehydrogenase and 100 mM glucose. The reactions were shaken at 37 °C for 1 h at 200 rpm. The addition of 125 μL cold methanol stopped the reaction, and the mixture was centrifuged at 21,100 *g* for 3 minutes to remove the precipitated protein. The supernatant

was evaporated to dryness and the resulting solids were extracted with 3 × 200 µL methanol. This methanol was concentrated to a volume of *ca.* 50 µL and analysed by reverse phase HPLC on a C18 column (4.6 × 150 mm, 5 µm bead size, Agilent Technologies) equipped with a 20 µL injection loop. The mobile phase was comprised of (v/v) A) 99: 0.8: 0.2 water: acetonitrile: formic acid and B) 99: 0.8: 0.2 acetonitrile: water: formic acid. The elution gradient was run at 0.4 mL/min and consisted of 5 min 100% A, a 25 min ramp to 100% B, a 5 min ramp to 100% A for a 5 min hold. Conversion is based on the ratio of the diclofenac peak to the total peak area (product + substrate peak areas) in the HPLC trace and, where conversion was over 10%, rounded to the nearest 0.5%. Control experiments where no $NADP^+$ was added showed no conversion of diclofenac (not shown).

Table 3.1. *In vitro* conversion of diclofenac by variants of $P450_{BM3}$, 1 h reaction time, pH 7.4.

$P450_{BM3}$ variant	Enzyme concentration (µM)	Conversion (%)
RP	5	1.2
RP/F87V	1	3.5
	2	8.7
	5	18.0
RP/E267V	1	7.9
	2	13.5
RP/F87V/E267V	1	10.5
	2	19.5

The starting variant, RP, showed low conversion (1.2%) of diclofenac at 5 µM enzyme concentration. The addition of the F87V mutation increases the activity nearly 18-fold, converting 18% of diclofenac in 1 h at 5 µM enzyme. The diclofenac oxidation activity

scaled with enzyme concentration, with 1 µM enzyme converting 3.5% of 1 mM diclofenac and 2 µM converting 8.7% after 24 h. The E267V mutation improved the activity of the RP variant further, converting 7.9% of 1 mM diclofenac at 1 µM enzyme. Combining the two mutations on RP further improved the activity towards diclofenac, with RP/F87V/E267V (henceforth referred to as RP/FV/EV) converting 10.5% of diclofenac at 1 µM enzyme concentration. Figure 3.9 shows the HPLC traces for the conversion of diclofenac by RP/FV/EV at various enzyme concentrations. A single product peak was observed in all reactions. It should be noted that the diclofenac peak in all HPLC traces is not quantitative, owing to variations in injection volume and sample preparation.

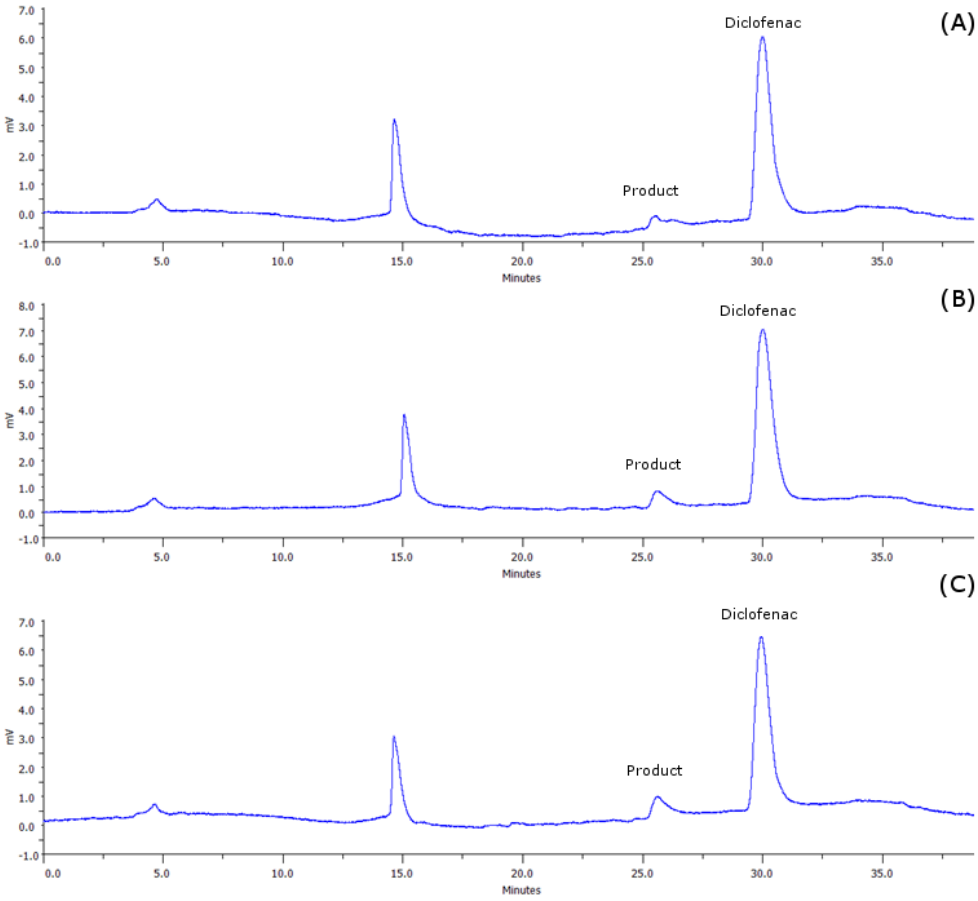

Figure 3.9. HPLC traces of 1 mM diclofenac, pH 7.4 metabolized in 1 h by 1 µM **(A)** RP/F87V; **(B)** RP/E267V; **(C)** RP/FV/EV. All samples run with a 0.4 mL/min elution gradient.

These tests were carried out using glucose dehydrogenase as an NADPH regeneration system, though previous studies with drug metabolising variants of $P450_{BM3}$ utilized glucose-6-phosphate dehydrogenase. Therefore, a side-by-side comparison of the two systems was undertaken using the RP/F87V variant, to determine which was better suited to support drug metabolism by $P450_{BM3}$. The results are summarized in Table 3.2.

Table 3.2. Effect of NADPH regeneration system on conversion of diclofenac by the RP/FV variant. 1 mM diclofenac, 1 μM enzyme, 250 μL volume, shaken at 37 °C for 1 h at 200 rpm in a 1.5 mL microcentrifuge tube.

Regeneration system	Concentration (units/mL)	Initial $NADP^+$ concentration (mg/mL)	Conversion (%)
Glucose Dehydrogenase	1	0.2	3.5
Glucose-6-phosphate dehydrogenase	1	0.2	3.8
	2	2	8.1

This study showed that glucose-6-phosphate did not improve diclofenac conversion over glucose dehydrogenase as the NADPH regeneration system, though higher conversion could be achieved by raising the concentration of the regeneration system and initial $NADP^+$ concentration. As glucose-6-phosphate and glucose-6-phosphate dehydrogenase are significantly more expensive than glucose dehydrogenase and glucose, it was decided that future reactions would be carried out using glucose dehydrogenase.

At 5 μM enzyme concentration, the RP/FV/EV variant could convert 55.5% of 1 mM diclofenac in a 250 μL reaction volume. The reactions were tested on a 1 mL scale, to determine if the reaction could be scaled up to larger volumes. The reactions were also run over 2 h, to examine the effect of reaction time, and these results are summarized in Table 3.3.

Reactions were performed in a 7 mL glass vial, in 50 mM Tris, pH 7.4 with 1 mL total reaction volume. Enzyme concentration was varied (0.25 and 2 μM) and the diclofenac concentration was 1 mM. NADPH was regenerated using 2 unit/mL glucose dehydrogenase and 100 mM glucose. The reactions were shaken at 37 °C for 1 h at 200 rpm. The addition of 500 μL cold methanol stopped the reaction, and the mixture was centrifuged at 14800 rpm for 3 minutes to remove the precipitated protein. The supernatant was evaporated to dryness and the resulting solids were extracted with 3 × 200 μL methanol. This methanol was concentrated to a volume of *ca.* 50 μL and analysed by the same method described above. As shown in Table 3.3, not only did enzyme perform as well on a larger scale, but it was more efficient at the 1 mL scale. At 2 μM enzyme concentration the RP/FV/EV variant converted 19.5% diclofenac at the 250 μL scale, while at the 1 mL scale 34.4% of the diclofenac was converted. This improvement was likely due to increased oxygen transport and mixing in the larger vials compared to a 1.5 mL microcentrifuge tube.

Table 3.3. *In vitro* conversion of diclofenac by the RP/FV/EV variant on a 1 mL scale.

Enzyme concentration (μM)	Reaction time (h)	Conversion (%)
0.25	1	2.4
2	1	17.0
0.25	2	5.5
2	2	34.5

3.3.3 Characterization of the product of diclofenac metabolism and enzyme kinetics

The RP/FV/EV variant was capable of metabolizing 34.5% of 1 mM diclofenac in a 1 mL reaction, and preparative (prep)-scale HPLC was used to isolate the product peak from the

reaction. Five such 1 mL reactions, were carried out with 2 μM RP/FV/EV, as described above, with the supernatants being combined for analysis. Prep-scale HPLC was performed using the same column and elution gradient as analytical HPLC and a 20 μL injection was used to test the fraction collector and confirm presence of a product peak. The HPLC was then fitted with a 1 mL injection loop and 2 × 100 μL samples were injected for analysis and collection. The product fractions were collected, combined and evaporated to dryness. The resulting solids were dissolved in acetone-d^6.

The ^{1}H NMR spectra of the diclofenac metabolite of the RP/FV/EV variant showed that, rather than a single oxidation product, the single observed product peak was a mixture of two singly oxidized compounds, 4′- and 5-hydroxydiclofenac. This is the first example of a single $P450_{BM3}$ variant being confirmed to produce two human drug metabolites in sufficient quantity for characterization. The NMR spectrum, along with peak assignments, is shown in Figure 3.10. The peak assignments were made by comparing the obtained NMR spectrum to literature spectra of chemically synthesized 4′- and 5-hydroxydiclofenac[241].

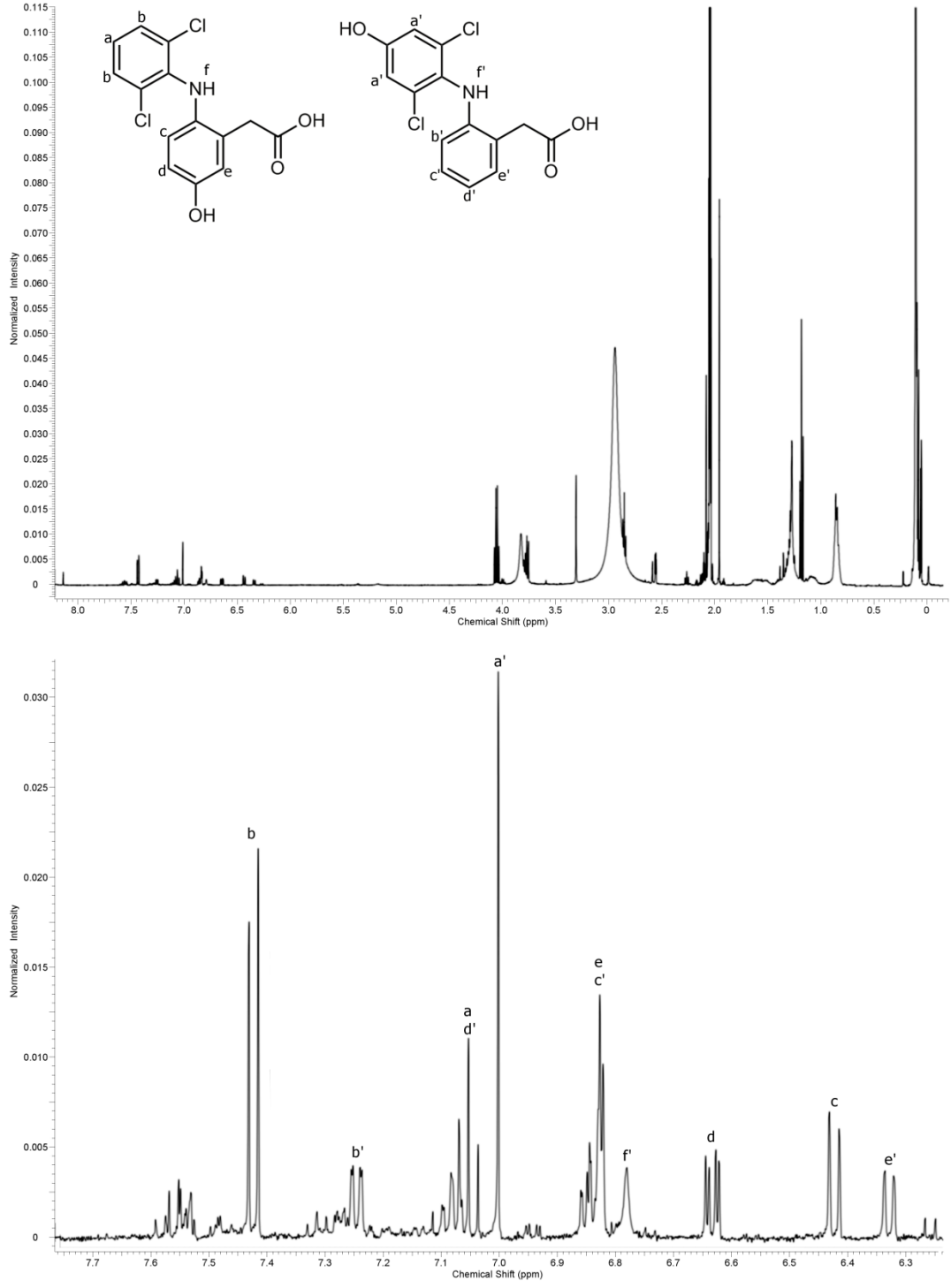

Figure 3.10. The ^{1}H NMR spectrum of the RP/FV/EV metabolites of diclofenac (top), with peak assignments in the aromatic region (bottom).

2 μL of the acetone-d^6 solution was added to 198 μL acetonitrile for accurate molecular mass determination. The theoretical mass of hydroxydiclofenac is 310.0043 Da, and the accurate mass of the RP/FV/EV metabolite was 310.0035 Da, confirming that the product was a monooxygenated metabolite. The mass spectral data is shown in Appendix 3.

Attempts to separate the two components in the product mixture were unsuccessful. Samples of purified product were analysed by HPLC, using the same elution buffers with an isocratic method of 20% B. 30% and 40% isocratic methods were also tried, but the two products consistently co-eluted.

Diclofenac induces a small shift in the heme spin-state of the RP/FV/EV variant (Figure 3.11). This shift towards the low-spin form is either the result of a type-II shift where the substrate coordinates to the heme iron or an inverse type-I shift, where the substrate forces the water ligand to interact more strongly with the heme iron. More work would be required to identify the nature of this shift. The kinetic parameters K_M and k_{cat} were determined for RP/FV/EV with diclofenac, and this is shown in Figure 3.12. The k_{cat} for RP/FV/EV with diclofenac was 39.9 ± 0.4 s^{-1} and the K_M was 18.2 ± 1.3 μM. The obtained K_M value is lower than that of the WT enzyme with palmitate, which gives a K_M = 42.4 ± 8.5 μM[242]. However, the leak rate of this enzyme is also very high, at 18.8 s^{-1}, meaning that at low diclofenac concentrations when the enzyme is not fully saturated the observed rate is a mixture of the leak rate and diclofenac-induced NADPH consumption rate. Thus, at low concentrations of diclofenac the rate is less reliable, though the high observed k_{cat} is more so, as the enzyme is sufficiently saturated at these concentrations.

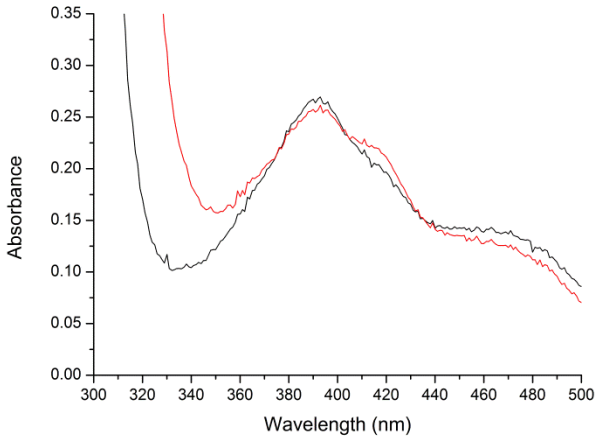

Figure 3.11. Diclofenac-induced spin state shift of RP/FV/EV with SF RP/FV/EV in black and RP/FV/EV in the presence of 5 mM diclofenac in red.

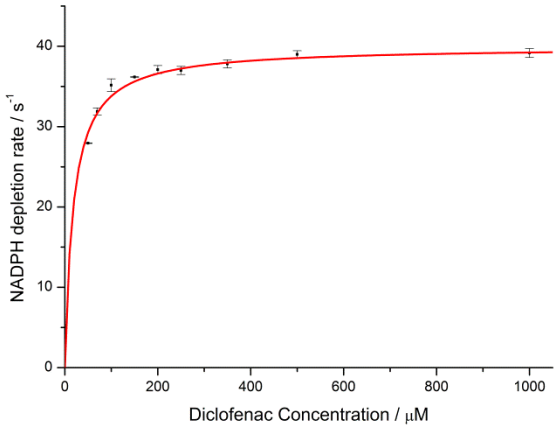

Figure 3.12. Determination of K_M and k_{cat} of diclofenac with RP/FV/EV.

3.3.4 Second generation variants

To attempt to improve activity and alter selectivity towards diclofenac, a second generation library was developed by adding selectivity-altering mutations to the RP/FV/EV variant. A328I, V78F and F81W were added to the RP/FV/EV variant and screened for activity towards diclofenac, the results of which are shown in Table 3.4, with Figure 3.13 showing the obtained HPLC traces. The reactions were performed using the same conditions described above for the 1 mL RP/FV/EV reactions, and used 5 μM P450. The samples were eluted at 0.8 mL/min, with a 2.5 min 100% A, a 12.5 min ramp to

100% B, a 2.5 min ramp to 100% A for a 2.5 min hold. This ensures the same peak separation is achieved as in the former method, though is twice as fast, as the elution gradient times are half the original method, while the gradient is being run twice as quickly.

Table 3.4. *In vitro* activity of second generation $P450_{BM3}$ variants towards diclofenac. 5 μM P450, pH 7.4, 2 h reaction time.

P450BM3 variant	Conversion (%)
RP/FV/EV	55.5
RP/FV/EV/A328I	22.0
RP/FV/EV/V78F	45.5
RP/FV/EV/F81W	68.0

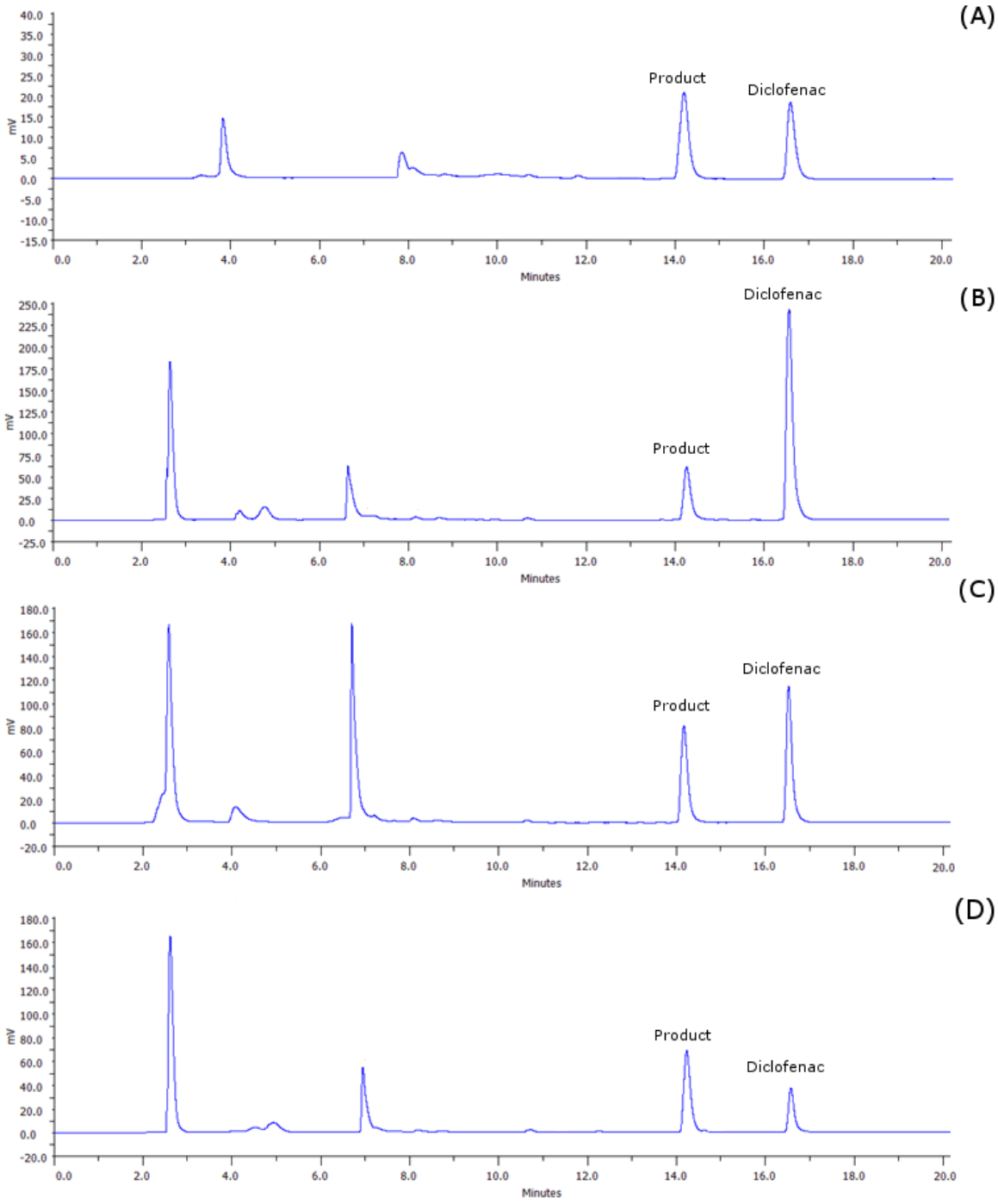

Figure 3.13. HPLC traces 1 mM diclofenac metabolized in 2 h at pH 7.4 by 5 µM **(A)** RP/FV/EV; **(B)** RP/FV/EV/A328I; **(C)** RP/FV/EV/V78F; **(D)** RP/FV/EV/F81W.

The A328I mutation lowered activity of the RP/FV/EV variant with diclofenac, in a similar manner that activity of KSK19 was lowered towards (+)-valencene upon the inclusion of this mutation (Section 3.5). The V78F variant also slightly lowered activity,

giving 45.5% conversion, whereas the F81W variant improved oxidation activity, giving 68.0% conversion of 1 mM diclofenac. The effect of these mutations on 4′- vs. 5-selectivity could not be assessed, as the products could not be separated on the HPLC.

In vitro oxidation of drug compounds requires the purification of the variants being tested, which can be time consuming. *In vivo* oxidation, by contrast, does not require purification of the enzymes, though potentially suffers from difficulties in mass transport across the cell membrane and low expression of the P450. To test the effectiveness of the drug metabolising variants for *in vivo* reactivity, a screen of several $P450_{BM3}$ variants was conducted, also assessing reaction volume and medium. The results of this screen are summarized in Table 3.5.

Drug metabolizing variants were expressed in BL21(DE3) *E. coli* cells containing the appropriate plasmid, which were inoculated into 2 L Erlenmeyer flasks containing 500 mL $2YT_{kan}$ or $FB_{glycerol/kan}$ and incubated at 37 °C for 18–24 h at 110 rpm. After sufficient cell growth (O.D. 0.8–1), the temperature was lowered to 20 °C, shaking speed was reduced to 100 rpm and protein expression induced by the addition IPTG to a final concentration of 55 μM. Cells were harvested, after 24 h for 2YT growths or after 24–48 h for $FB_{glycerol}$ growths, by centrifugation at 5000 rpm for 10 min at 4 °C. Cell pellets were resuspended in one tenth growth volume of $FB_{glycerol/kan}$ or 2YT. The 10× cell density cultures were incubated for 24 h with 1 mM diclofenac (added as a 100 mM stock in ethanol) and shaken at 110 rpm in a 250 mL conical flask. A control experiment was performed with *E. Coli* cells expressing a non-catalytic protein, and showed no conversion of diclofenac (not shown).

Table 3.5. *In vivo* activity of $P450_{BM3}$ variants towards diclofenac over 24 h.

$P450_{BM3}$ variant	Reaction medium	Reaction volume (mL)	Conversion (%)
RP/FV	2YT	50	3.9
RP/EV	2YT	50	3.8
RP/FV/EV	2YT	50	13.5
	2YT	1	3.5
	$FB_{glycerol}$	50	3.8
RP/FV/EV/A328I	2YT	50	8.4
RP/FV/EV/V78F	2YT	50	11.5
RP/FV/EV/F81W	2YT	50	11.5
	2YT	1	4.7
	$FB_{glycerol}$	50	6.0

In all cases, *in vivo* oxidation leads to lower conversion than the *in vitro* assays. $FB_{glycerol}$ gave lower conversion than the complex medium 2YT, likely due to lower expression of the P450 enzyme in this medium. Similarly, a 1 mL scale reaction also displayed lower conversion than a 50 mL scale reaction, possibly due to slower mass transport or oxygen saturation in the reduced volume. The RP/FV/EV variant gave the highest conversion of all the tested variants at 13.5%, with the second generation variants RP/FV/EV/V78F and RP/FV/EV/F81W converting 11.5%. These tests showed that *in vitro* oxidation is likely the better method to test the conversion of diclofenac by $P450_{BM3}$ variants.

The RP/FV/EV and RP/FV/EV/F81W variants were also tested for activity over 24 h, with 2 mM diclofenac (Table 3.6). Reactions were set up in the same manner described for standard 1 mL scale reactions and set to shake at 20 °C. One reaction using 5 μM RP/FV/EV/F81W was set up at a 10 mL scale. This reaction used identical concentrations of reagents and was set up in a 50 mL round-bottom flask.

Table 3.6. *In vitro* conversion of diclofenac by $P450_{BM3}$ variants over 24 h with 5 µM P450, pH 7.4.

$P450_{BM3}$ variant	Reaction volume (mL)	Diclofenac concentration (mM)	Conversion (%)
RP/FV/EV	1	2	90.5
RP/FV/EV/F81W	1	2	>99.0
	10	1	66.5

The longer incubation time allowed for total conversion of 2 mM diclofenac by the RP/FV/EV/F81W variant, and conversion of over 90% with RP/FV/EV on a 1 mL scale. On a 10 mL scale the enzyme was less effective, with RP/FV/EV/F81W converting 66.5% of 1 mM diclofenac, though this lower conversion may be the result of imperfect conditions, such as shaking speed and mass transport. The HPLC traces, which were obtained with a 1 mL/min elution gradient consisting of 2 min 100% A, a 10 min ramp to 100% B, a 2 min ramp to 100% A for a 2 min hold are shown in Figure 3.14.

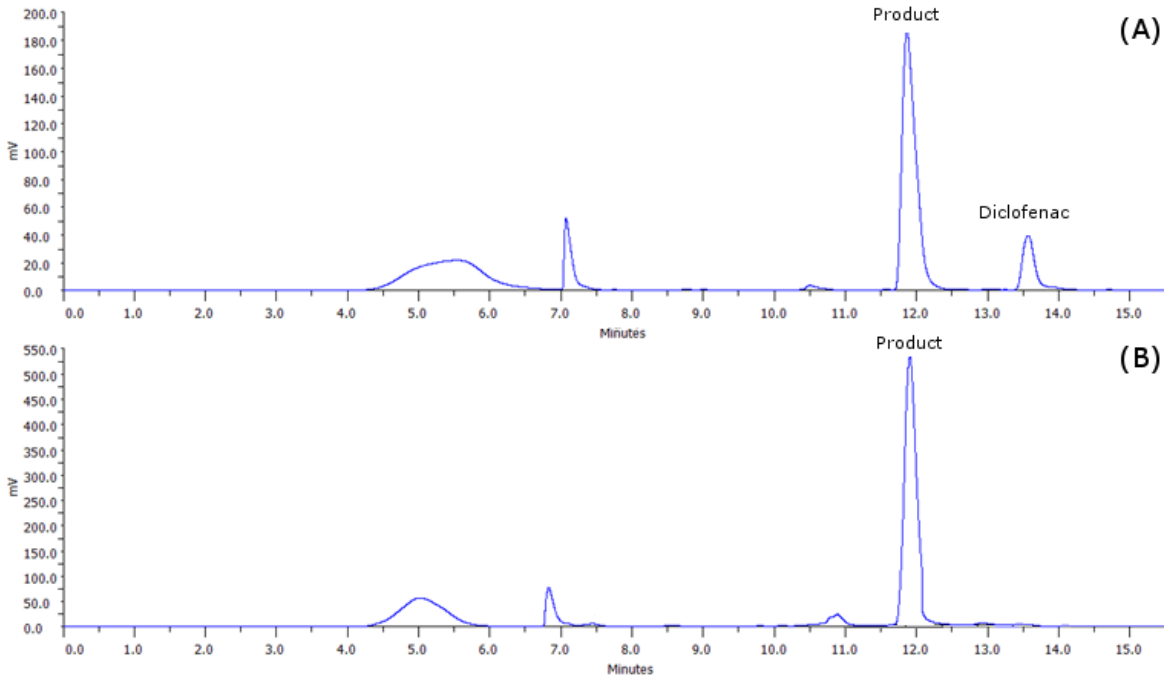

Figure 3.14. HPLC traces 2 mM diclofenac metabolized over 24 h at pH 7.4 by 5 µM **(A)** RP/FV/EV; **(B)** RP/FV/EV/F81W.

The total conversion of diclofenac by the RP/FV/EV/F81W variant is the first report of a $P450_{BM3}$ variant completely converting a drug compound to its human metabolites. The products of the RP/FV/EV/F81W were isolated and characterized by high resolution mass spectroscopy and ^{1}H NMR. Mass spectral data (Appendix 3) confirmed that RP/FV/EV/F81W also gives singly hydroxylated metabolites of diclofenac, with an accurate mass of 310.0046 Da. The NMR spectrum and peak assignments are shown in Figure 3.15.

NMR analysis of the RP/FV/EV/F81W reaction products also show that a mixture of 4′- and 5-hydroxydiclofenac are produced by this variant. While this is the first report of total conversion by a $P450_{BM3}$ variant of a drug compound, total turnover for the enzyme remained low, at only 400 in the 5 μM enzyme, 2 mM substrate case, and further work is needed to optimize reaction conditions.

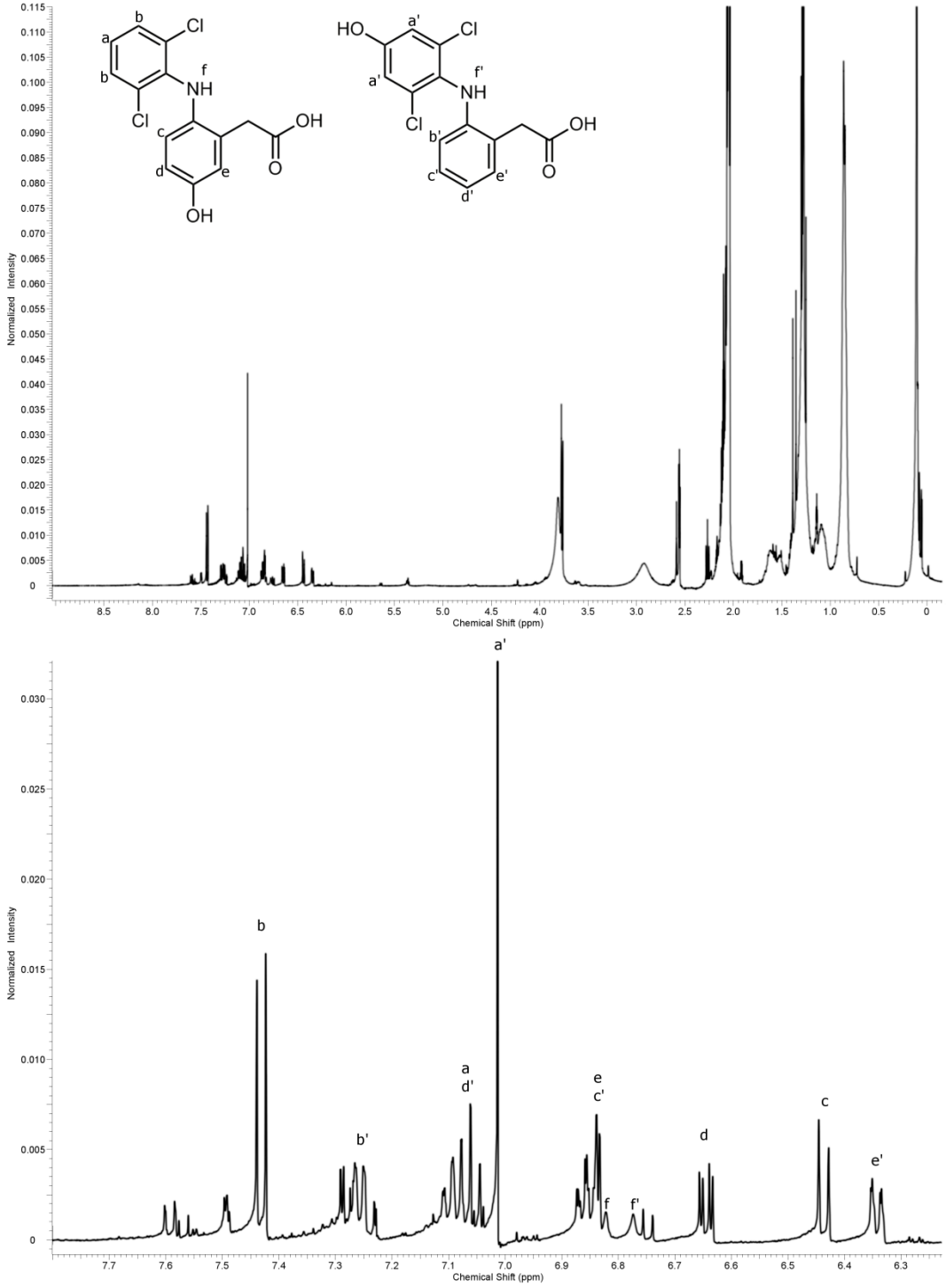

Figure 3.15. The NMR spectrum of the RP/FV/EV/F81W metabolites of diclofenac (top), with peak assignments in the aromatic region (bottom).

3.3.5 Testosterone oxidation

Testosterone is oxidized by aromatase (CYP19A1) to oestradiol, though it is also metabolized by the primary drug metabolizing P450 CYP3A4 to 6β-, 15β- and 2β-hydroxytestosterone and by CYP2C19 to 6β-, 15β- and 16β-hydroxytestosterone[243]. Testosterone, as a large, neutral compound is a contrast to the anionic diclofenac, so the RP/FV/EV variant, as well as the second generation variants, were tested for activity towards testosterone. $P450_{BM3}$ has been studied with testosterone as a substrate (Section 1.2.3.4), and several studies were published while this work was in progress[137, 138]. Figure 3.16 shows the conversion of testosterone to 2β-, 15β- and 16β-hydroxytestosterone, the reported products of oxidation by $P450_{BM3}$[136, 138].

The results of the conversion tests are shown in Table 3.7. Reactions were performed under the same conditions as the diclofenac turnovers, varying enzyme concentration as noted in Table 3.7. As testosterone is not soluble to 1 mM, substrate concentration was 500 μM for all experiments. Comparison to literature reports and HPLC retention times suggest that these variants also generate 2β-, 15β- and 16β-hydroxytestosterone[137], though products were not isolated in sufficient quantity to confirm this with ^{1}H NMR. The HPLC traces of RP/FV/EV and RP/FV/EV/A328I with testosterone are shown in Figure 3.17. These traces were obtained using the 0.8 mL/min method described above.

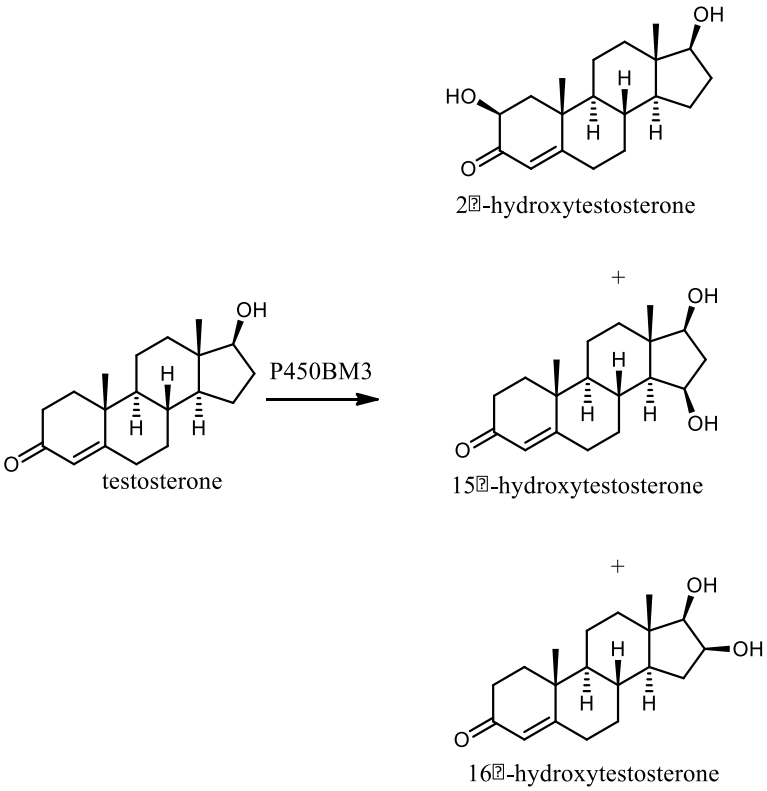

Figure 3.16. The oxidation of testosterone to 2β-, 15β- and 16β-hydroxytestosterone by $P450_{BM3}$.

Table 3.7. *In vitro* oxidation of 500 μM testosterone to 2β-, 15β- and 16β-hydroxytestosterone by $P450_{BM3}$ variants over 24 h, pH 7.4.

$P450_{BM3}$ variant	P450 concentration (μM)	Reaction volume (μL)	Conversion to 2β-OH (%)	Conversion to 15β-OH (%)	Conversion to 16β-OH (%)	Total conversion (%)
RP	2	1000	11.0	3.1	1.0	15.0
RP/FV/EV	0.25	1000	14.0	35.0	48.0	97.0
	1	1000	17.0	36.0	46.0	>99.0
RP/FV/EV /A328I	0.25	1000	3.7	30.0	2.3	36.0
RP/FV/EV /V78F	0.25	1000	15.0	28.0	36.5	79.5
RP/FV/EV / F81W	0.25	1000	16.0	9.6	16.5	42.0

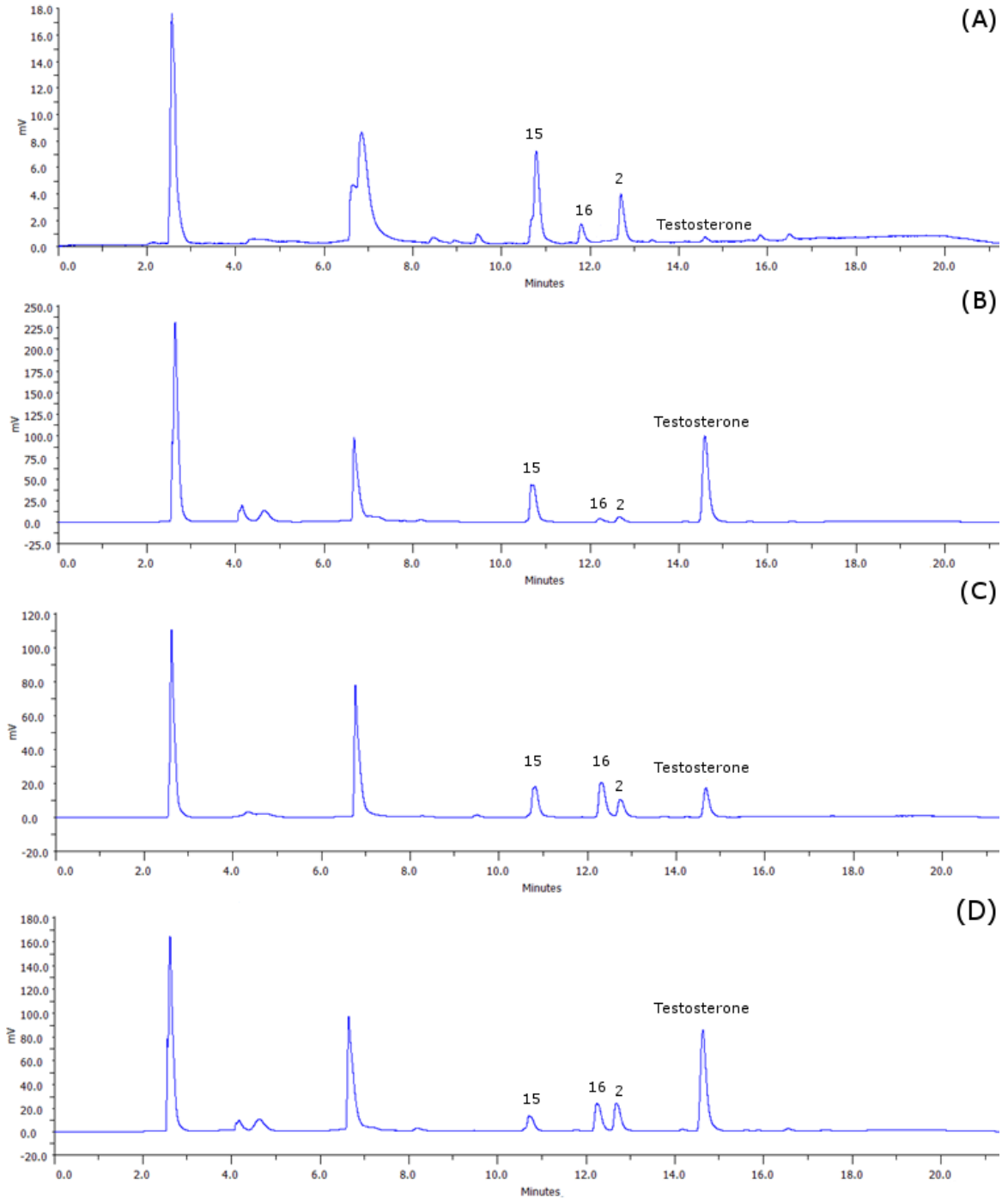

Figure 3.17. HPLC of 500 µM testosterone oxidation over 24 h, pH 7.4, by 0.25 µM **(A)** RP/FV/EV; **(B)** RP/FV/EV/A328I; **(C)** RP/FV/EV/V78F; **(D)** RP/FV/EV/F81W. 15, 16 and 2 represent 15β-, 16β-, and 2β-hydroxytestosterone, respectively.

The RP/FV/EV variant proved to be the most active towards testosterone, converting 97% of the substrate after 1 h. Selectivity of this variant is not the same as the F87V-containing M11 variant which gave a 18:53:29 mixture of 2β-,15β- and 16β-hydroxytestosterone[136], while the RP/FV/EV variant gives 14:35:48. The residue at position 87 can cause large changes in product selectivity, with M11/V87N giving solely 2β-hydroxytestosterone and M11/V87A giving a 10-fold excess of the 15β-product over the 16β-product[137], but the A328I, F81W and V78F variants also alter selectivity of the template variant. The addition of the A328I mutation once again lowered activity, though selectivity was shifted to favour 15β-hydroxylation, generating a 11:81:8 mixture of 2β-, 15β- and 16β-hydroxytestosterone. The addition of the V78F mutation slightly favoured 2β-hydroxylation as a percentage of total activity more than the RP/FV/EV variant, and RP/FV/EV/V78F had the highest activity of the second generation variants tested.

The RP/FV/EV/F81W variant had lower activity towards testosterone than RP/FV/EV, while shifting selectivity away from 15β-hydroxylation. The decrease in activity of this variant with testosterone compared to the RP/FV/EV variant highlights a difference between testosterone and diclofenac oxidation.

3.3.6 Oxidation of Lidocaine

The small RP/FV/EV-based library was shown to be active towards the anionic NSAID diclofenac and the neutral steroid testosterone. To test the range of drugs oxidized by this small library, a positively charged drug compound was also tested. Lidocaine is a topical anaesthetic primarily de-ethylated by CYP3A4 (Figure 3.18) [160]. Lidocaine is of particular interest in this study, as it has not yet been reported as a substrate for $P450_{BM3}$.

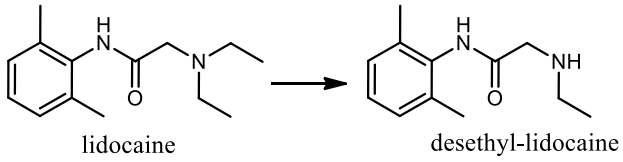

Figure 3.18. Metabolism of lidocaine to desethyl-lidocaine.

Reactions were performed under the same conditions as those used for diclofenac conversion over 24 h (5 μM enzyme, 2 mM substrate). Table 3.8 shows the conversion of lidocaine to desethyl-lidocaine by $P450_{BM3}$ variants RP/FV/EV and RP/FV/EV/F81W.

Table 3.8. Conversion of 2 mM Lidocaine by 5 μM RP/FV/EV and RP/FV/EV/F81W over 24 h, pH 7.4.

$P450_{BM3}$ variant	Conversion (%)
RP/FV/EV	66.5
RP/FV/EV/F81W	73.5

Figure 3.19 shows the HPLC traces of lidocaine with RP/FV/EV and RP/FV/EV/F81W, obtained using the 1 mL/min method described above. The F81W mutation improved activity of the RP/FV/EV variant towards lidocaine converting 73.5% of the substrate, compared to 66.5% by RP/FV/EV. Lidocaine was metabolized into a single product by RP/FV/EV/F81W, and this product was isolated as described above and characterized by NMR, shown in Figure 3.20. A sample of the reaction with F81W and lidocaine was also co-eluted with an authentic sample of desethyl-lidocaine, which confirmed that this compound elutes with the $P450_{BM3}$-generated lidocaine metabolite. NMR comparison of the product of lidocaine metabolism by RP/FV/EV/F81W with the authentic sample also reveals that the product generated is desethyl-lidocaine. This study is the first to report activity of a $P450_{BM3}$ variant towards lidocaine.

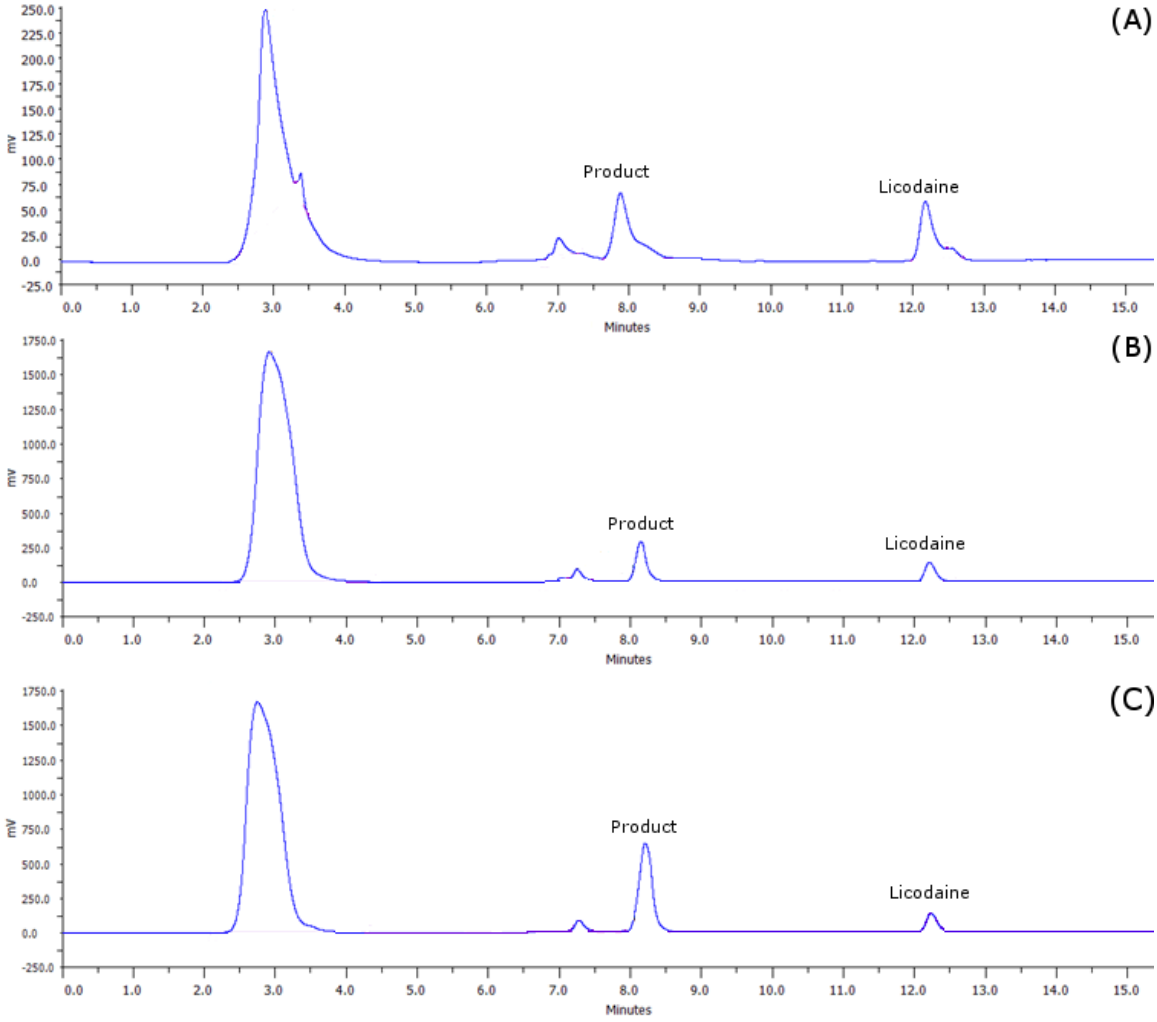

Figure 3.19. HPLC traces of 2 mM lidocaine metabolized over 24 h, pH 7.4, by 5 µM **(A)** RP/FV/EV; **(B)** RP/FV/EV/F81W; **(C)** RP/FV/EV/F81W with 0.8 mM desethyl-lidocaine added.

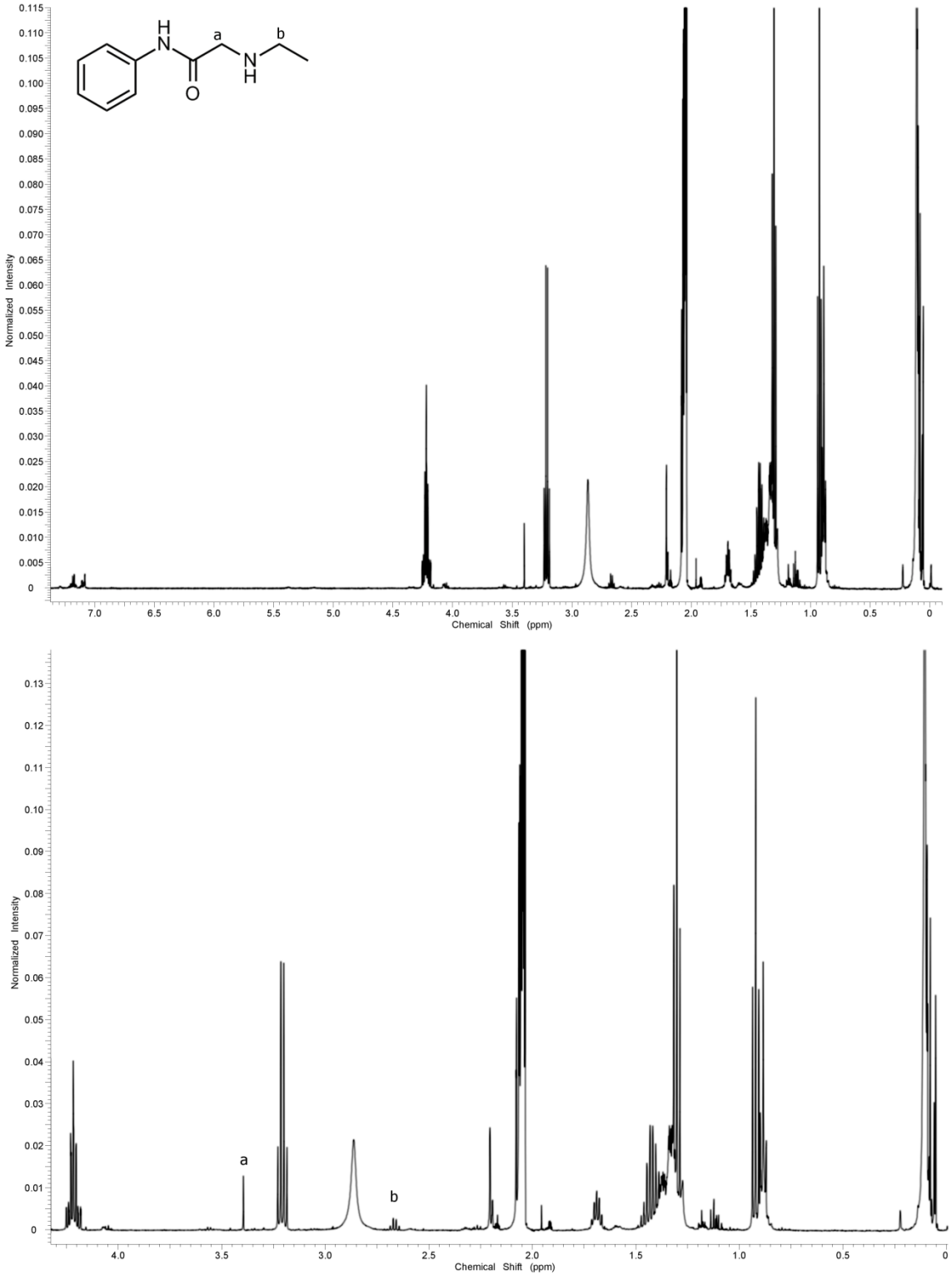

Figure 3.20. NMR spectrum of lidocaine metabolite of RP/FV/EV/F81W, with key peak assignments.

3.4 Conclusions and future work

The $P450_{BM3}$ variants RP/FV/EV, RP/FV/EV/F81W, RP/FV/EV/A328I and RP/FV/EV/V78F, which are based on the generic accelerator I401P, have been shown to be active towards the pharmaceuticals diclofenac and lidocaine and the steroid testosterone. The RP/FV/EV variant showed only a small type-II spin-state shift upon the binding of the anionic diclofenac but converted over 90% of 2 mM substrate in 24 h (5 μM enzyme, 1 mL volume), generating both of the predominant human metabolites. This enzyme was also active towards the neutral testosterone and cationic lidocaine. This range of activity and non-specific binding of substrates suggests that RP/FV/EV and the second generation variants based on it are active towards a range of compounds including those with an anionic carboxylate group, a feature which led Arnold *et al.* to report "There has been no report on a $P450_{BM3}$ variant exhibiting good activity on these charged molecules[149]." This shows that perhaps the best way to model human P450 behaviour is not to engineer a protein with high substrate specificity, but to develop systems, like the R47L/Y51F/F87V/E267V/I401P enzyme, which show activity towards a range of compounds and generate human metabolites.

Emily Taylor, a Part II student in this group, is currently working on testing RP/FV/EV and its related variants with a wider range of drug compounds, including propranolol and warfarin, with the aim of demonstrating that this system is capable of oxidizing a large selection of drug compounds to human metabolites. Further work on this project would initially involve optimizing the reaction conditions and scaling up the system for large scale metabolite production, followed by improving the reaction coupling without losing activity across the broad range of substrates. Possible routes to large scale metabolite synthesis could include optimizing *in vivo* reactions or the use of cell lysate with a NADPH regeneration system, though as purifying the enzymes for *in vitro* reactions is

rapid and produces cleaner reaction mixtures, this is the likely route forward for immediate expansion of the work.

3.5 Valencene oxidation by KSK19 variants

3.5.1 General background

The oxidation of (+)-valencene (from oranges, *ca*. 600 USD/kg) to (+)-nootkatone (grapefruit flavouring and fragrance, *ca*. 4500 USD/ kg for 85% pure, naturally sourced) (Figure 3.21) is a value-added process which presents an interesting biotechnological problem, owing to low enzyme coupling, poor substrate solubility, mass transport, and further oxidation of (+)-nootkatone (Section 1.2.3.3). Engineering a $P450_{BM3}$ variant which selectively oxidizes (+)-valencene at C2 to give *cis/trans*-(+)-nootkatol or (+)-nootkatone is a markedly different challenge than engineering a drug metabolising enzyme. For engineering a drug metabolizing enzyme, the target was an enzyme which displayed high activity across a broad range of substrates and was capable of generating multiple metabolites. In this case, the goal is highly-specific binding of one substrate with selective oxidation at one position.

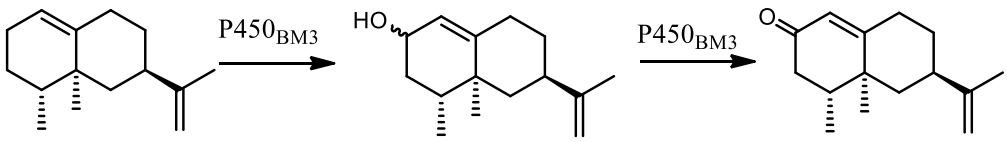

(+)-Valencene
ca. 600 USD/kg

cis/*trans*-nootkatol

(+)-Nootkatone
ca. 4500 USD/kg

Figure 3.21. Oxidation of (+)-valencene to *cis*/*trans*-nootkatol and (+)-nootkatone.

3.5.2 First generation variants

Sowden *et al*. showed that the I263A mutation improves C2 selectivity and F87A promotes further oxidation to (+)-nootkatone from the C2 alcohols[90]. KSK19 and variants of this generic accelerator were investigated for activity towards (+)-valencene and the production of (+)-nootkatol and (+)-nootkatone. Table 3.9 shows the *in vitro* activity of $P450_{BM3}$ variants towards (+)-valencene and Figure 3.22 shows GC traces of three KSK19 variants.

The reactions were performed as standard NADPH turnover assays, with 1250 μL of oxygenated 50 mM Tris, pH 7.4 containing 0.4 μM P450, 125 μg bovine liver catalase (added as a 10 mg/mL stock in 50% v/v Tris/glycerol) and 1 mM (+)-valencene added from a 100 mM stock in ethanol. This solution was equilibrated at 30 °C for 1 min, followed by the addition of 1 AU NADPH (ca. 160 μM). 1000 μL of the reaction mixture was removed and 3 μL of a 100 mM stock of *p*-benzylphenol in DMSO was added as an internal standard. 400 μL EtOAc was added and the mixture was vortexed to mix, then centrifuged at 21,100 *g* for 3 min. 250 μL of the organics was removed and dried over anhydrous $MgSO_4$ for 15 minutes. Solids were separated by centrifugation and the supernatant was analysed by GC, using a 15-m DB-1 column and the following oven conditions: 100 °C initial temperature held for 1 min, 15 °C/min ramp to 220 °C, hold for 4 min.

Table 3.9. *In vitro* activity of $P450_{BM3}$ variants towards (+)-valencene. NADPH consumption rates are given as nmol(nmol P450)$^{-1}$min^{-1}. Data for F87A/I401P obtained from Dr. Christopher Whitehouse[210]. Total products do not sum to 100% due to the presence of other minor products and represent percentage of product formed.

$P450_{BM3}$ variant	*N*	Coupling (%)	*cis*-(+)-nootkatol (%)	*trans*-(+)-nootkatol (%)	(+)-nootkatone (%)	Epoxides (%)
KSK19	753	21	29.5	3.1	25.5	29.0
RLYF/KSK19	761	25	28.3	2.3	23.8	28.8
KSK19/A82M	638	17	20.5	2.9	17.9	35.3
KSK19/I263A	252	24	31.1	1.3	38.6	19.5
KSK19/A328I	281	42	35.1	13.3	41.6	5.3
F87A/I401P[210]	1711	9.2	20	2.5	22	40

The KSK19 variant preferentially oxidizes (+)-valencene at the C2 position with 58.1% selectivity, though coupling is low at 21%. KSK19 gives a PFR for C2 oxidation products of 92 min^{-1}. The addition of the RLYF couplet did not have a large impact on selectivity, with 54.4% selectivity at C2 and a PFR for C2 oxidation products of 103 min^{-1}. The KSK19/A82M variant shows slightly less selectivity and activity for C2 oxidation, with 41.3% selectivity and a PFR of 45 min^{-1}.

Sowden *et al*. demonstrated that the I263A mutation shifts selectivity towards C2 oxidation with the RLYF/I263A variant, compared to the RLYF variant[90], while Seifert *et al.* demonstrated that the F87A/A328I variant gives 93% selectivity for C2 oxidation, albeit with a low (25.3 min^{-1}) NADPH consumption rate[97]. The addition of these mutations to KSK19 significantly improved selectivity towards C2 oxidation of (+)-valencene.

KSK19/I263A showed 71% selectivity for C2 oxidation, which is less than that reported for the F87A/I263A couplet alone, though still a significant improvement over the other

KSK19 variants. The oxidation rate has been lowered with this selectivity enhanced variant, with a PFR for C2 oxidation products of 43 min^{-1}. The KSK19/A328I variant showed the highest selectivity for C2 oxidation of the KSK19 variants investigated, at 90%. This variant also had the highest coupling of the tested variants, at 42%, and a PFR of C2 oxidation products of 106 min^{-1}, the highest among the tested variants.

The A328I and I263A mutations greatly improve the selectivity of KSK19 for C2 oxidation of (+)-valencene. This suggests that orienting the C2 position toward the heme iron is promoted by forcing the (+)-valencene molecule away from the 328 position and towards the 87 and 263 positions. The introduction of these mutations also caused the NADPH consumption rate to fall by nearly two-thirds, while the A328I mutation improved coupling by 100% over KSK19, suggesting that forcing the substrate towards the heme may reduce futile cycling of electrons while lowering overall NADPH consumption.

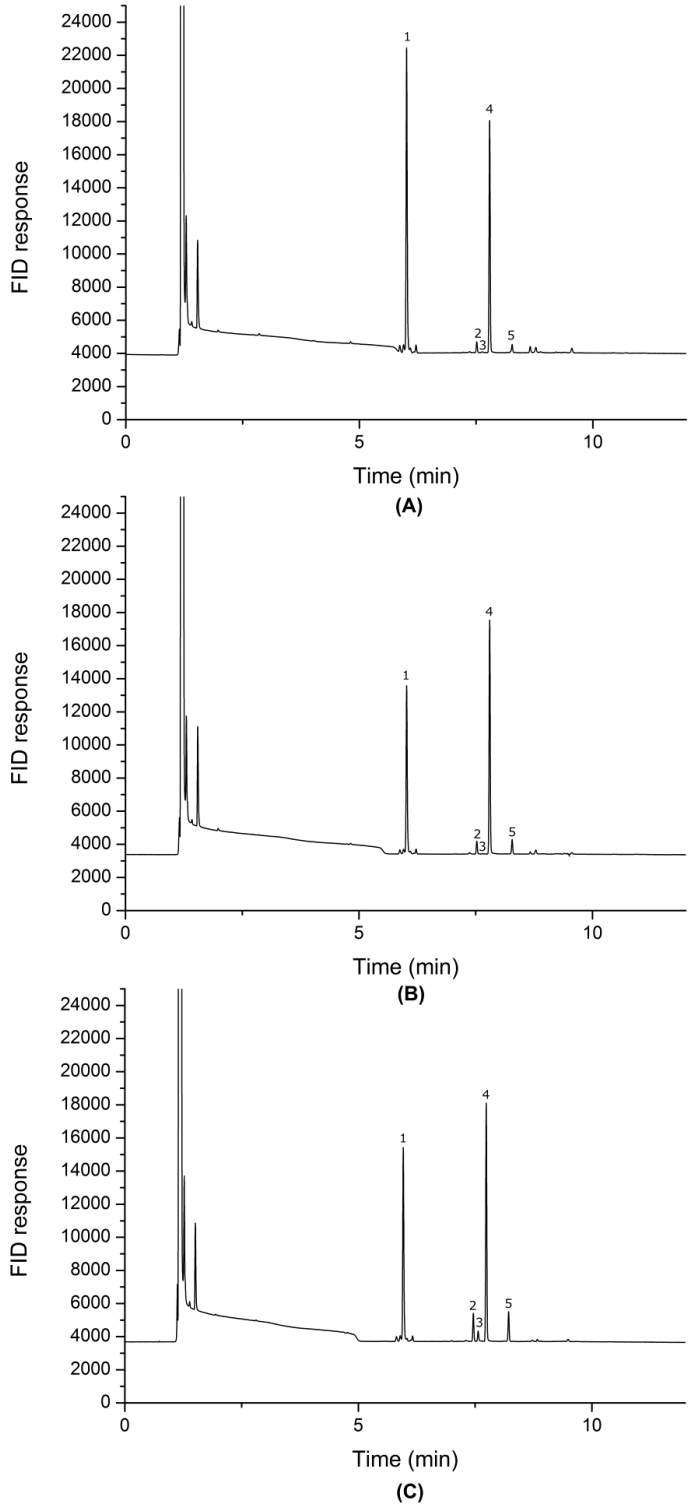

Figure 3.22. GC traces of valencene oxidation, pH 7.4, by **(A)** KSK19; **(B)** KSK19/I263A; **(C)** KSK19/A328I. Peak numbers are 1: valencene; 2: *cis*-(+)-nootkatol; 3: *trans*-(+)-nootkatol; 4: 4-benzylphenol (internal standard); 5: (+)-nootkatone.

The F87A/I401P variant was studied for activity towards (+)-valencene by Dr. Christopher Whitehouse[210] and is included for comparison. Coupling of this variant was halved compared to KSK19, whereas the NADPH consumption rate is nearly tripled. The selectivity of this variant is 45% for C2 oxidation, which is 10% less selective than KSK19. The rapid NADPH consumption rate partially overcomes the poor coupling, giving F87A/I401P a PFR for C2 oxidation products of 70 min^{-1}. This rapid NADPH consumption rate serves to further emphasize the impressive rate accelerating properties of I401P.

3.5.3 Second generation variants and improving total turnover

The A328I and I263A variants each improve the C2 selectivity of KSK19 towards (+)-valencene, though coupling and product formation remain low. Several methods for improving the total turnover of this system were explored, and these results are summarized in Table 3.10 with selected GC traces shown in Figure 3.23.

The methods tested for improved total turnover towards (+)-valence include the preparation of a second generation variant containing the I263A and A328I mutations in combination, KSK19/I263A/A328I.

As coupling with (+)-valencene was very low, lauric acid was employed as a decoy substrate (a substrate which partially fills the active site, forcing (+)-valencene towards the heme and initiates the catalytic cycle) to attempt to improve coupling, and subsequently total turnover, with KSK19/A328I. Watanabe *et al.* introduced the approach of using a decoy substrate with $P450_{BM3}$ for the oxidation of small alkanes while this work was in progress[121]. Sowden *et al.* demonstrated that (+)-nootkatone is actually a better substrate for $P450_{BM3}$ than (+)-valencene[90]. It is, therefore, important to remove the product from the reaction if possible. Using undecane as a second phase, KSK19/A328I

activity was tested. KSK19/A328I was also tested with undecane as a second phase and several surfactants, to determine if increasing mass transport between phases could increase total turnover and (+)-nootkatone production.

KSK19/I263A/A328I was engineered to utilize NADH, rather than NADPH, in an effort to determine if switching the electron source could improve total turnover. As NADH is significantly less expensive than NADPH, this system could also be more cost effective than a glucose dehydrogenase-based NADPH regeneration system. This was accomplished by adding the W1046A mutation, as described by Neeli *et at*[109].

Experiments were set up in 50 mM Tris, pH 7.4, in 7 mL glass vials with 1 mL total reaction volume. Enzyme and (+)-valencene concentrations were 0.4 μM and 2 mM respectively. Surfactants were added at 4.8% w/v of the aqueous phase. Reactions not involving undecane were worked up in the same manner described above. For reactions with undecane, the organic phase was removed from the aqueous phase and analysed directly by GC and the aqueous phase was extracted as above, though did not show any trace (+)-valencene or products. For reactions involving a surfactant, the phases were separated by centrifugation and analysed in the same manner as the undecane reactions. Concentration of C2 oxidation products was calculated using a calibration curve generated by Mr. Christopher Douse.

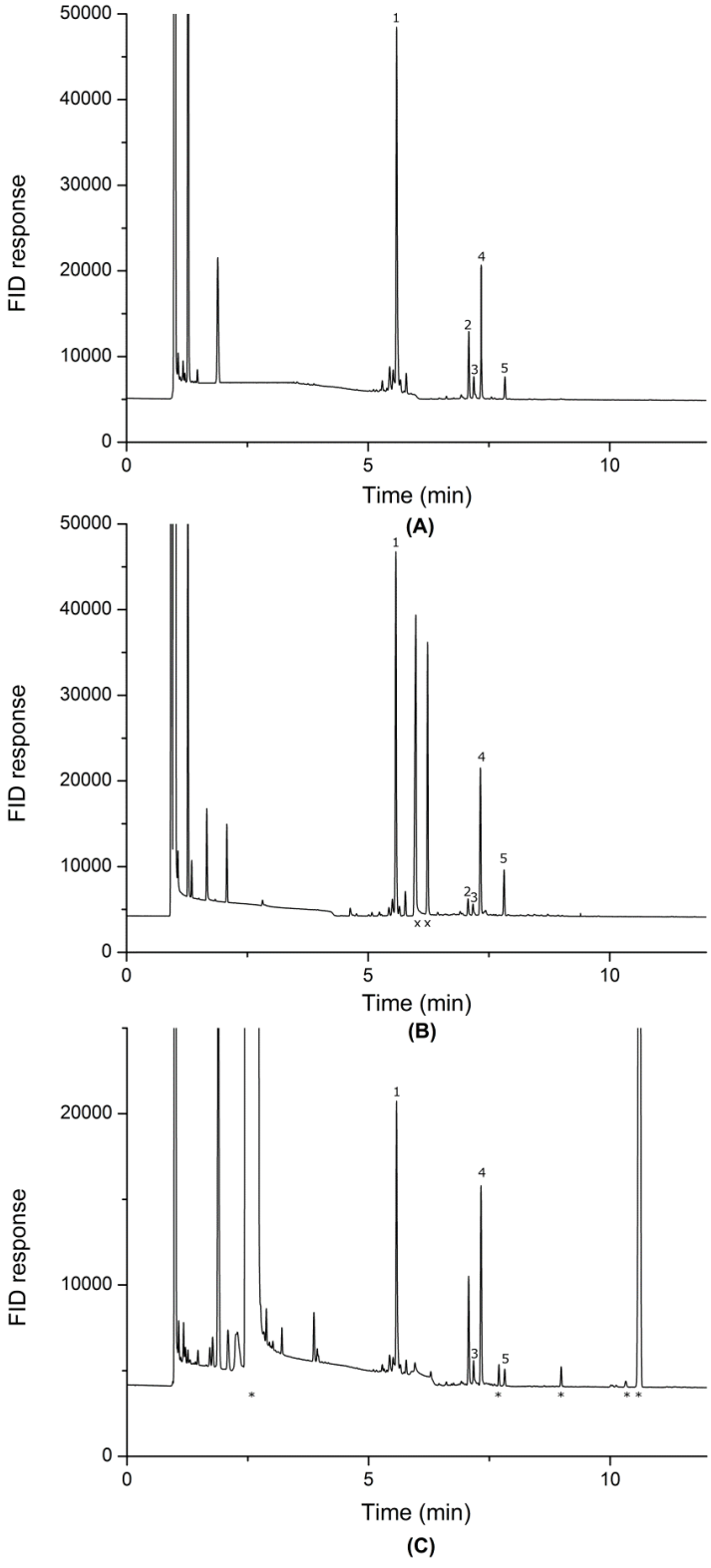

Figure 3.23. GC traces of valencene oxidation over 48 h, pH 7.4 by **(A)** KSK19/I263A/A328I; **(B)** KSK19/I263A/A328I in the presence of laurate, where **x** indicates a peak originating from laurate turnover; **(C)** KSK19/A328I with undecane as a second phase, where ***** indicates a peak arising from undecane. Peak numbers are 1: valencene; 2: *cis*-(+)-nootkatol; 3: *trans*-(+)-nootkatol; 4: 4-benzylphenol (internal standard); 5: (+)-nootkatone.

Table 3.10. Improving total turnover of 0.4 μM KSK19 variants with 2 mM (+)-valencene. GD – Glucose dehydrogenase with 100 mM glucose. YAD – Yeast alcohol dehydrogenase. **1** – *cis*-(+)-nootkatol. **2** – *trans*-(+)-nootkatol. **3** – (+)-nootkatone. CTAB - hexadecyltrimethylammonium bromide. DMDA: dimethyldioctadecylammonium, bromine salt. [*] – 2 mM laurate added. [†] – ethanol added to 5% of the reaction volume. [‡] – hexanol added to 5% of the reaction volume.

Variant	RS	Undecane (v/v%)	Surfactant	Time (h)	**1** (%)	**2** (%)	**3** (%)	Others	C2 oxidation products (μM)
KSK19/ I263A	GD	0	0	48	70.0	3.3	18.0	12.0	140
KSK19/A328I	GD	0	0	48	44.0	12.0	29.0	15.0	130
	GD[*]	0	0	48	32.5	19.5	28.0	4.0	195
	GD	40	0	48	61.5	19.0	7.9	10.5	385
	GD	200	0	48	54.0	12.5	17.5	8.8	335
	GD	20	CTAB	48	2.0	0	0	98.0	200
	GD	40	CTAB	48	2.6	0	0	97.4	205
	GD	20	DMDA	48	0	43.0	37.0	20.0	55
	GD	40	DMDA	48	0	45.5	36.0	18.5	60
KSK19/I263A/A328I	GD	0	0	48	55.0	19.0	19.0	6.5	150
	GD[*]	0	0	48	24.0	14.5	47.5	14.5	210
KSK19/ I263A/ A328I/W1046A	YAD[†]	0	0	48	19.5	12.5	50.5	17.5	145
	YAD[†]	0	0	100	16.5	10.5	59.5	14.5	180
	YAD[‡]	0	0	48	36.0	14.0	35.0	15.5	90
	YAD[‡]	0	0	100	32.0	14.5	24.5	28.5	100

When the conversion of (+)-valencene takes place over 48 h with glucose dehydrogenase as an NADPH regeneration system there seems to be a build-up of the *cis*-(+)-nootkatol over the observed selectivity reported for the KSK19/I263A and KSK19/A328I variants when an aliquot of NADPH is added and is not regenerated. This could indicate that the *trans*- product is a more favourable substrate for further oxidation. The total activity of the enzymes was low, with the second generation variant KSK19/I263A/A328I having the highest total turnover number of 150.

The addition of laurate as a decoy substrate improved the TTN of the variants tested by over 40%. It also appears that further oxidation of *cis*-(+)-nootkatol is promoted by the presence of the decoy substrate, with the KSK19/I263A/A328I variant showing at 31.3% drop in *cis*-(+)-nootkatol and a corresponding 28.1% increase in (+)-nootkatone.

Altering the electron source did not appear to increase total turnover of (+)-valencene by KSK19/I263A/A328I. Indeed, total turnover was the same after 48 h as when NADPH was used. This experiment did indicate that after 48 h the enzyme has nearly lost activity, as incubation for 100 h only slightly increased turnover.

The use of undecane as a second organic phase nearly tripled the total turnover of KSK19/A328I with (+)-valencene. Removal of the oxidation products also altered the product profile of the reaction, with these turnovers generating primarily the *cis*-product. Reactions involving undecane and a surfactant proved difficult to extract and analyse. It appeared that, while the total turnover with KSK19/I263A was increased with the surfactant CTAB, less than 3% of the products formed were C2 oxidation products, with *cis*-(+)-nootkatol being exclusively formed. Conversely, no *cis*-(+)-nootkatol was isolated from turnovers with DMDA, though total turnover was depressed to less than 20% of the activity observed when undecane alone was employed. The surfactant DSS was also tried, though the reaction mixtures proved impossible to extract and analyse.

3.5.4 Conclusions and future work

The initial screen of KSK19 variants showed that $P450_{BM3}$ could be engineered to selectively oxidize (+)-valencene at the C2 position. However, coupling with substrate was very low, as was total turnover. The generic accelerator variant I401P displayed rapid NADPH consumption with (+)-valencene (when used in combination with the F87A mutation). Coupling was even lower using this enzyme, however, so this variant was not explored in more detail.

The use of a decoy substrate did improve total turnover of (+)-valencene, as did employing undecane as a second phase to remove oxidation products from the reaction mixture. These tests showed that, though coupling remains low, it is possible that this system can be optimized to convert (+)-valencene to (+)-nootkatone. The KSK19 variants could most likely be improved by the substitution of valine in place of alanine at position 87, as Seifert *et al.* have demonstrated[97]. The addition of the selectivity enhancing mutations A328I and I263A, as well as F87V to I401P could also lead to a $P450_{BM3}$ variant capable of more rapid, selective oxidation of (+)-valencene to (+)-nootkatone.

Chapter Four

Spectroelectrochemistry

4.1 Potentiometric titrations

4.1.1 General background

Two methods can be employed in order to set and maintain the potential of the protein solution: chemical titrants or a three-electrode system used to both set potential and measure current. Each method has advantages, disadvantages and practical considerations.

A common method of potentiometric titrations employs chemical titrants to set the potential and two electrodes to measure the potential. Sodium dithionite is the most commonly used reductant and potassium ferricyanide is the oxidant. In 1978 Dutton described several methods for spectrochemical analysis of biological systems using chemical titrants and the challenges presented by proteins and enzymes[244].

Figure 4.1 shows a spectroelectrochemical cell, as described by Dutton[244]. The cell is designed to maintain an oxygen-free atmosphere, to prevent unwanted oxidation of the analyte, while the screw caps with septa allow for the addition of the titrant. In order to promote rapid equilibrium the solution is stirred throughout, while two electrodes monitor the potential set by the chemical titrants.

This method has been successfully applied to measure the redox properties of several proteins, including cytochrome *c*[245], cytochrome *b*-559[246], mitochondrial respiratory chain cytochromes[247] and several P450s[83, 248, 249]. The advantages of this method include a long path length, which allows small changes to be detected or the use of a smaller amount of enzyme, and rapid equilibration times.

Though this method has been successfully applied and has advantages, it is not without drawbacks. For one, it requires the use of specialized equipment to stir the solution during analysis, which may prohibit implementation. Secondly, and most importantly, the use of chemical titrants can have limitations or alter the reduction potential of the enzyme being studied.

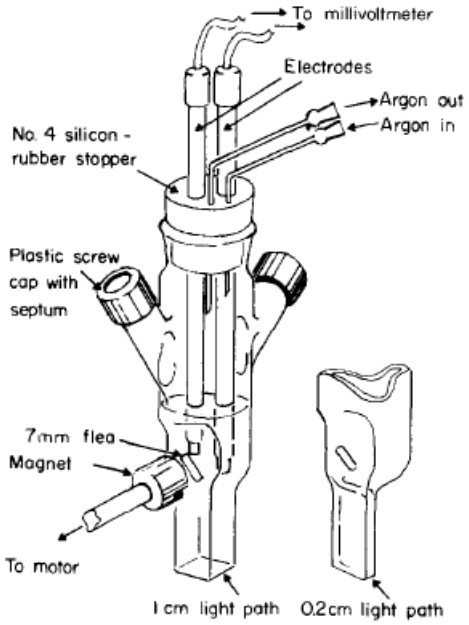

Figure 4.1. Spectroelectrochemical cell described by Dutton.

Potassium ferricyanide, a common titrant used to oxidize metalloproteins and mediators (Section 4.1.2) is known to bind to horse heart cytochrome c[250-253]. As binding of a small molecule can alter the reduction potential of a metalloprotein, the use of ferricyanide can give misleading results.

A second problem caused by using chemical titrants is the limited range of potentials available for analysis. The active reductant in dithionite solutions is the dissociation product SO_2^-, and the redox couple SO_2^-/HSO_3^- has a very negative potential (–660 mV. All potentials reported in this thesis are relative to SHE). For conditions typically used for enzymatic titrations its reducing capacity is limited, as at concentrations above 10 nM the

SO_2^- dimerizes to $S_2O_4^{2-}$, which has a reduction potential of 29 mV[254]. Thus, as concentration of dithionite increases, its reducing capacity decreases, limiting the available potentials. The calculated potential for 1 M $S_2O_4^{2-}$/2M HSO_3^- at pH 7 is –387 mV. As the reduction potentials of many metalloproteins including P450s are near or below this value, it may not be possible to achieve full reduction of the protein with sodium dithionite.

4.1.2 Mediated potentiometric titrations

The redox-active centres in metalloproteins are often buried within polypeptide chains. Since electrons cannot tunnel well over distances longer than *ca.* 14 Å[255], direct transfer of electrons from an electrode to a redox centre in a protein is difficult and slow. It is therefore often useful to add electrochemical mediators to facilitate electron transfer between the electrode and the protein.

Electrochemical mediators are small, often organic, molecules (though some metal complexes are used, such as the ferrocene derivative 1,1′-dimethyl-3-(2-amino-1-hydroxyethyl)ferrocene, which acts as a redox mediator for glucose oxidase in a commercial blood glucose level biosensor[256, 257] and cobalt metal complexes used by de Voss *et al.* in the potentiometric titration of cindoxin[258]) which can act as electron acceptors and donors, shuttling electrons between the electrode surface and the biological redox centre. The addition of mediators also serves to increase the rate of the protein reaching potential equilibrium, as they diffuse much faster through the bulk solution than the large protein molecules. There are several considerations when selecting an appropriate mediator for use in an electrochemical titration.

Firstly, the mediator should have a reduction potential within 60 mV of the desired potential. This ensures the mediator will efficiently accept and donate electrons at the

potential applied. Secondly, redox mediators must not decompose upon oxidation or reduction, or in other experimental conditions. While this may seem obvious, many common mediators may decompose at a potential far from their midpoint, which may occur if the mediator is part of a cocktail of mediators. Also, some mediators, such as methyl viologen, irreversibly react with oxygen when reduced, which must be taken into consideration during experiments.

A third consideration when using electrochemical mediators is that they must not chemically modify the redox protein, or act as a substrate. As substrate binding can significantly alter reduction potentials of proteins, a mediator which acts as a ligand or chemically modifies the enzyme should not be used. A final consideration, and a situation which is often difficult to avoid, is that mediators should not interfere with the measurement of either the reduced or oxidized state of the couple being analysed. That is to say, if the protein is being analysed spectrophotometrically it is key to use mediators that, in the oxidized or reduced forms, do not absorb at the same wavelengths as the analyte. This is sometimes difficult, as many of the best mediators absorb strongly in the visible region.

4.1.3 Optically Transparent Thin Layer Electrodes

Potentiometric titrations can also be carried out using a three electrode system to directly control potential and measure current. While cells using three electrode systems have been constructed for use with fiber-optic cells and microsamples[259], the most common method employs optically transparent thin layer electrodes (OTTLE). OTTLE cells have been used to measure the reduction potential of several proteins, including cytochrome *c*[260], $P450_{cam}$[261], $P450_{BM3}$[262, 263], and copper laccases[264]. Similar to electrochemical investigations using cyclic voltammetry, potentiometric titrations using OTTLE cells

often use surface modified electrodes[265-268] though many P450 enzymes[269-273] as well as several others[274-276] have been successfully analysed using unmodified electrodes.

The first OTTLE cell was described by O'Dom and co-workers in 1964[277] and is shown in Figure 4.2. The working electrode is a 45% transparent gold mesh sandwiched between two quartz plates separated by an adhesive spacer. The cell is slightly customizable with respect to sample volume by altering the spacer thickness. Section 4.2 describes the design of a custom-made OTTLE cell that has been used to investigate the reduction potential of a variety of P450s and redox partners.

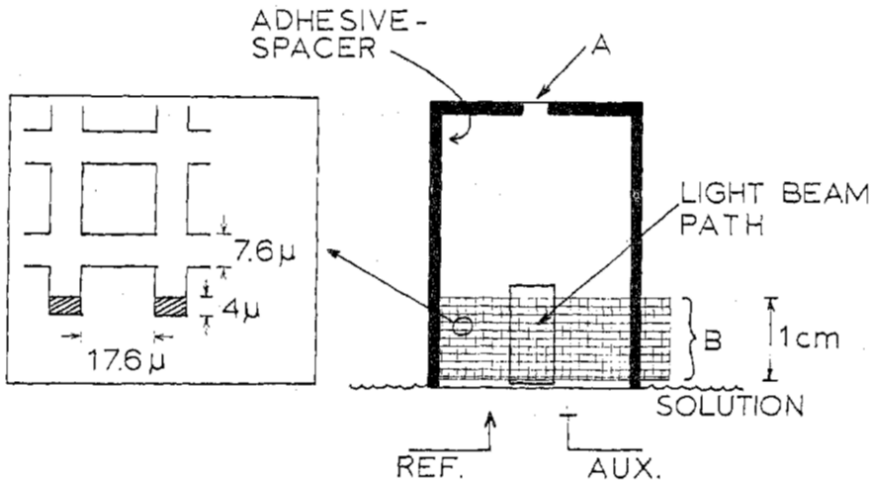

Figure 4.2. Spectroelectrochemical cell for use with an optically transparent thin layer electrode.

4.2 Design of a spectroelectrochemical cell

4.2.1 Selection of mediators for potentiometric titrations

As selection of mediators is of the utmost importance for potentiometric titrations, the properties of a range of mediators were analysed. Eight mediators were investigated, with the aim of choosing a mixture of mediators that would cover a range of potentials for application in spectroelectrochemical analysis of a variety of P450s and their redox partners. Table 4.2 shows the mediators investigated, their reported midpoint potentials

and the midpoint potentials determined using cyclic voltammetry. The cyclic voltammograms obtained from these studies are shown in Appendix 4.

From these, five mediators were selected: methylene blue, 9,10-anthraquinone-2-sulfonate, 9,10-anthraquinone-2,6-disulfonate, 9,10-anthraquinone-1,5-disulfonate and methyl viologen. These mediators were selected as they allow for a range of potentials (11 to –450 mV) to be covered while not interacting with $P450_{BM3}$, i.e. the mediators do not induce a spin-state shift (data not shown).

The selected mediators are not without issues. Methyl viologen absorbs strongly in the reduced form, with λ_{max} = 395 nm which interferes with the Soret band of P450s. However, as substrate-free P450s have reduction potentials well below that accessible using other mediators, methyl viologen is necessary. At the concentrations used during a potentiometric titration (*ca.* 5 μM), interference from the mediator absorbance is low, but to fully avoid it, reduction of P450s can also be monitored by an increase of absorbance at 465 nm[83], where none of the selected mediators show absorbance, though monitoring at this wavelength is less sensitive due to a smaller absorbance change, requiring higher protein concentrations (*ca*. 30 μM P450, for example).

Table 4.1. Mediators selected for use in the spectroelectrochemical titrations. [a]Present work, at pH 7.4 in 50 mM Tris using a platinum wire counter electrode and a graphite working electrode. In all cases, the literature reduction potentials were obtained at pH 7.

Mediator	Structure	Reduction Potential	
		Reported	Observed[a]
Methylene blue	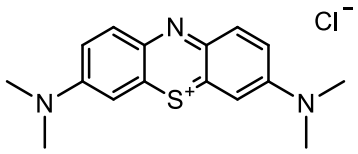	11[278]	37
Potassium indigo tetrasulfonate	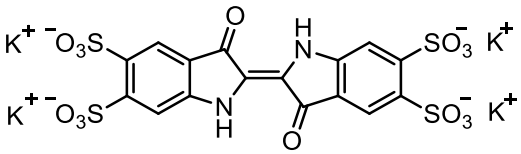	–46[278]	–149.5
2-hydroxy-1,4,naphthoquinone	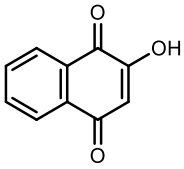	–152[278]	–182
9,10-Anthraquinone-1,5-disulfonate	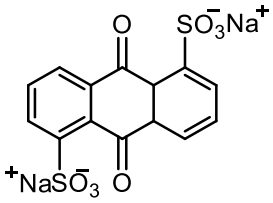	–174[278]	–146.5
9,10-Anthraquinone-2,6-disulfonate	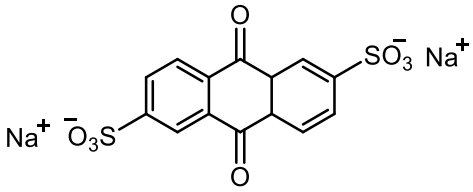	–184[278]	–234
9,10-Anthraquinone-2-sulfonate	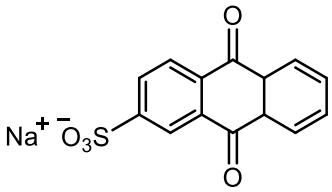	–225[278]	–287
Benzyl viologen	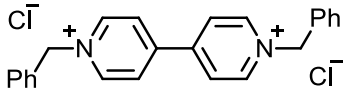	–358[279]	–319
Methyl viologen	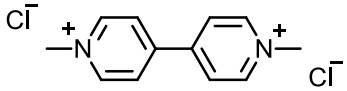	–449[279]	–372

4.2.2 Design considerations

Spectroelectrochemical cells are typically designed with the following points under consideration:

1. The molar absorptivity of the analyte – Some proteins have very strongly absorbing chromophores, like chlorophyll *a*, with a molar absorptivity of 6.4×10^4 M^{-1} cm^{-1} [280] or heme. These may be used in lower concentrations during an experiment and still produce a strong signal.

2. Cell volume and distance to the electrodes – In order to minimize the amount of analyte used, cell volume should be minimized. Minimizing cell volume should also allow for the distances to the electrodes to be minimized, providing faster equilibration.

3. Availability of proteins – While minimizing use of analyte is important, it is less so if the enzymes studied are easily expressed and purified on large scales.

4. Light path length – As absorbance increases with path length, shorter path lengths will require more concentrated solutions to achieve strong signals.

5. Electrode placement – The working, reference and counter electrodes must all contact the same solution, and ideally be placed near each other to avoid potential gradients.

6. Gold mesh working electrode – The working electrode will be a thin transparent mesh of gold, as this is a readily available material that is transparent and electrically conducting, but this material is fragile.

7. Oxygen – The cell must be anaerobic to prevent re-oxidation of the analyte. This means it must be able to be assembled in an anaerobic environment such as a glove box and be constantly purged with oxygen-free Ar or N_2.

8. Temperature control – Since redox potentials are temperature dependent, the cell must be able to be thermostatically controlled. Ideally, the cell would fit into a standard, temperature-controlled cuvette holder, to maximise usability and minimize cost.

4.2.3 Previous designs

In her 2008 thesis[264], Dr. Rachel Heath describes the design of a spectroelectrochemical cell addressing many of the considerations stated in secton 4.2.1. Later, Dr. Domenico Caprotti improved upon this design, leading to the cell shown in Figure 4.3[281].

The arms extending from the three-way neck are used as outlets for the wiring for the working and counter electrodes (Gold mesh, 500 wires per in, wire width 4.5×10^{-4} in, 60% transmission and a platinum wire respectively), while a Luggin capillary for the saturated calomel electrode (SCE) reference electrode can be inserted into the top. The arms are also used as an inlet and outlet for argon, which is blown over the head space of the cell to prevent air entering the reservoir. A ground glass joint connects the three-way neck to a polymethylmethacrylate (PMMA) reservoir, where the counter and reference electrodes contact the buffer solution. The PMMA reservoir is milled to fit a cuvette holder in a Cary-50 UV-vis spectrophotometer, and a cuvette with a 1 mm path length is fitted into the reservoir using a silicone sealant.

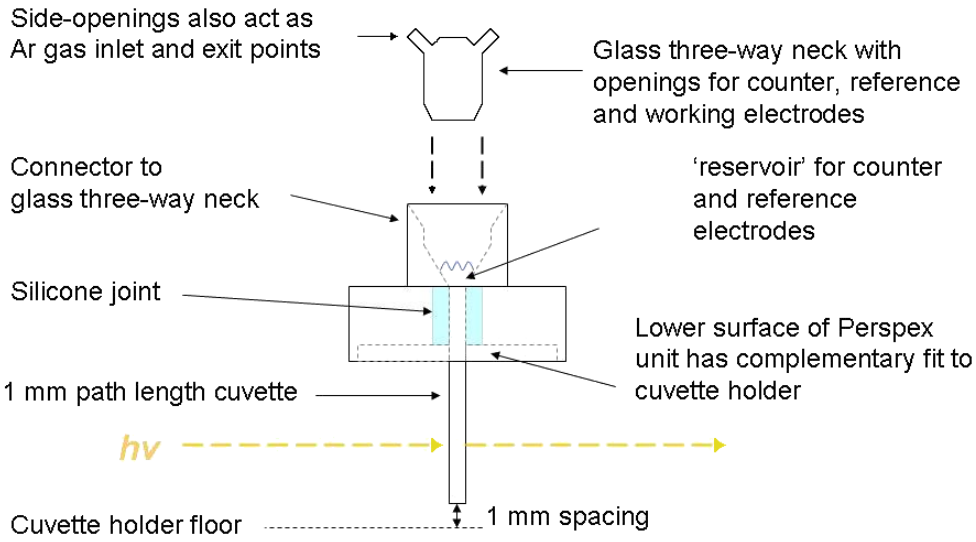

Figure 4.3. Schematic of the OTTLE cell designed by Dr. Domenico Caprotti. Reprinted from the thesis of Dr. Caprotti[261].

Dr. Caprotti also described a method of supporting the gold mesh electrode on an acetate backing, shown in Figure 4.4[281]. The gold mesh and acetate backing are cut to the full width and length of the cuvette (8.5 mm × 44 mm). The acetate backing is cut with a window to ensure full exposure of the solution to the working electrode. Cyanoacrylate adhesive ("Superglue") attaches the gold mesh to the acetate backing, while paraffin film wound tightly around the top of the electrode helps form an electrical contact between the gold wire and the gold mesh. In the present work this design was successfully used to measure the reduction potential of WT and the I401P variant of $P450_{BM3}$, which will be described in detail in Chapter 5.

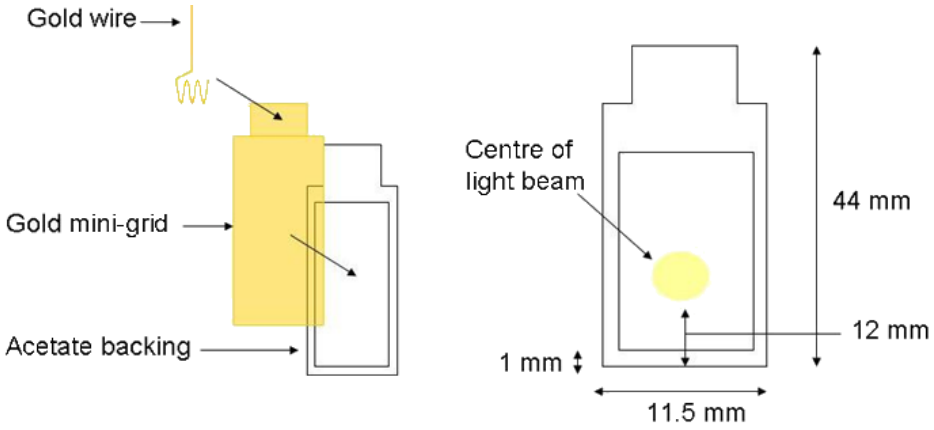

Figure 4.4. Schematic of the gold mesh electrode. Reprinted from the thesis of Dr. Caprotti[261].

Though this cell and electrode design was successfully implemented in the study of several P450s including variants of $P450_{cam}$[281], and WT and the I401P variant of $P450_{BM3}$[218], there were several problems with the design that led to many failed experiments. Firstly, the counter electrode, a piece of platinum wire, is submerged in the solution only in the reservoir. This means the distance between the counter electrode and working electrode is large, while the counter electrode area is very small compared to the working electrode. The distance between the electrodes and the small counter electrode area, combined with the large current produced during the titration, led to a positive potential to be applied to the counter electrode. The over-potential applied could exceed 1 V (data not shown), at which water is oxidized to oxygen. This was, in effect, generating oxygen within the cell, which was obviously problematic. In fact, bubbles could sometimes be seen forming at the counter electrode surface.

4.2.4 OTTLE cell and electrode redesign

In an effort to prevent the generation of this over-potential, the location and size of the counter electrode were reconsidered. A platinum mesh (100 mesh, wire diameter 3×10^{-3} in) counter electrode was added, greatly increasing the surface area of the counter

electrode, while being thin enough to be moved closer to the working electrode. Placing the counter electrode closer to the working electrode required a redesign of the acetate backing and working electrode, which is shown in Figure 4.5.

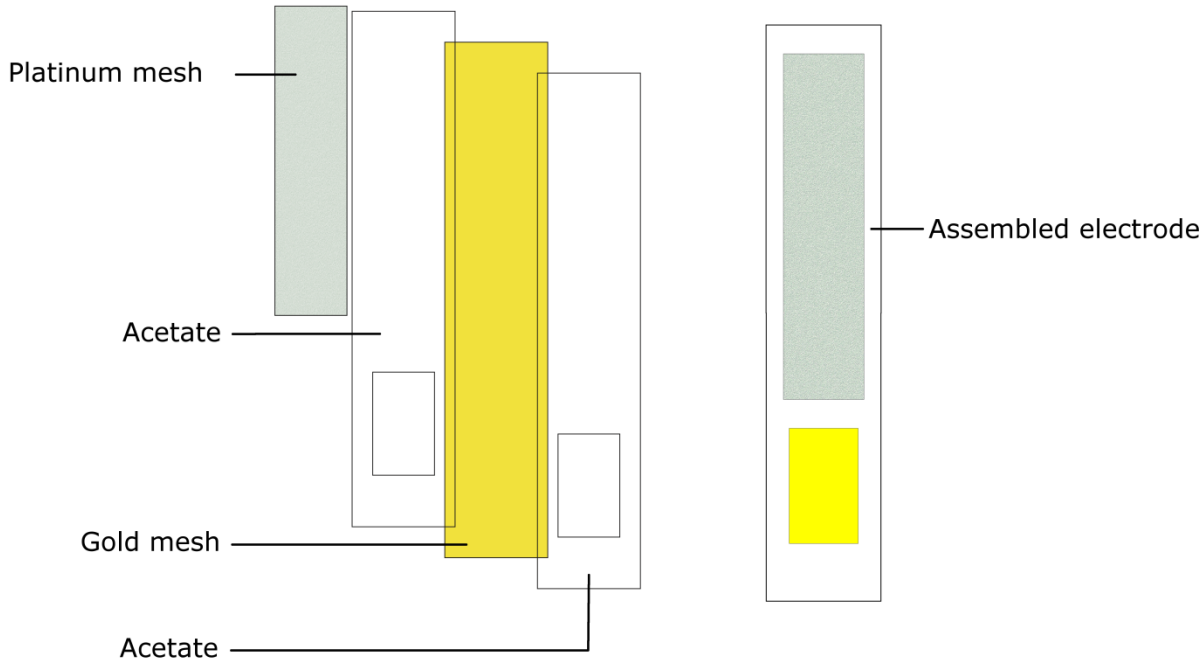

Figure 4.5. Schematic of new gold mesh electrode design.

The working electrode area has been limited, now encompassing solely the area where the beam of the spectrometer passes. This ensures that the protein being observed is sufficiently reduced, while lowering the total exposed surface area of the working electrode, allowing the counter electrode to be placed directly adjacent to the working electrode, while greatly increasing the area of the counter electrode relative to the working electrode.

Once these modifications were made, the over-potential was greatly reduced, and bubbles were no longer observed at the counter electrode surface. This solution, however, exposed a second issue with the original design: the argon purge is not sufficient to prevent oxygen from entering the cell. This is perhaps due to the fact that, though the cell is

assembled in the glove box, the cell is not sealed during transport from the glove box and the spectrometer, potentially allowing some oxygen to enter the cell. Thus, a new neck piece was designed and fabricated and is shown in Figure 4.6.

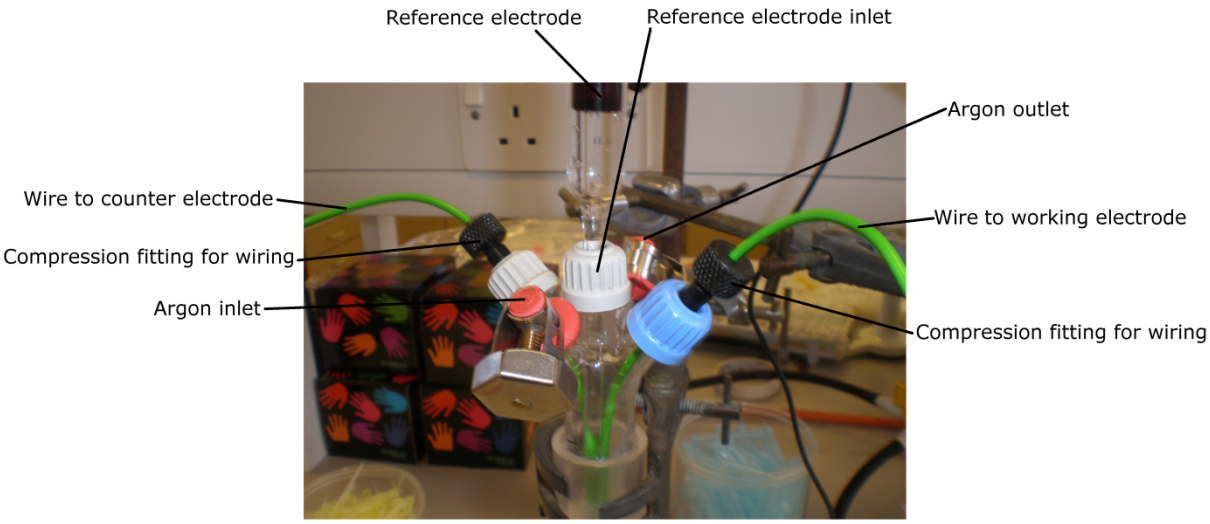

Figure 4.6. New 4-way adapter.

The new four-neck design has several advantages over the previous three-way neck. Firstly, the ground glass joint connecting the neck piece to the reservoir has a larger diameter, which allows for more space for the Luggin capillary, helping to prevent breakages. Secondly, the wires connecting the counter and working electrodes are insulated and threaded through custom O-ring compression fittings, preventing oxygen from entering through the wire outlets. A second pair of arms was added to allow argon to be purged through the cell, though they are sealed using rubber septa, increasing the anaerobicity of the cell.

To further decrease the amount of oxygen in the cell, three components were added to the analyte solution: glucose, glucose oxidase and catalase. Glucose oxidase uses dissolved oxygen to oxidize glucose, though forms potentially harmful hydrogen peroxide as a product. Hydrogen peroxide is subsequently decomposed into water and dioxygen by

catalase. This glucose oxidase/catalase system for removing oxygen limits the amount of dissolved oxygen available to react with other species.

The gold mesh electrode was cleaned by performing cyclic voltammetry in a 0.1 M H_2SO_4 solution. The potential was scanned at 50 mV/s for 15 cycles between –0.5 V and 1.15 V, which cleaned the surface of the gold and removed any adsorbed protein reside. The platinum mesh was similarly maintained. This common method of cleaning gold electrodes[282] helps to rid the gold surface of adsorbed organics or contaminants[283]. The method has also been shown to clean platinum electrodes[284].

4.3 Experimental details

4.3.1 Solution preparation

To prepare the analyte enzyme solution, the previously prepared enzyme stock solutions, which are 50:50 glycerol:phosphate buffer, was eluted on a 5-mL PD-10 gel filtration column, which serves to remove the glycerol and exchange the buffer with 50 mM Tris, pH 7.4. The resulting Tris solution was then concentrated to a volume of *ca*. 200 μL in a centricon. This concentrated solution was transferred to a glove box. A fresh analyte solution was used for each titration.

To prepare the cocktail of electrochemical mediators, appropriate amounts of solid mediators were weighed into a vial, and transferred to the glove box. Using 50 mM Tris, pH 7.4, which was stored in the glove box, a 1 mM solution of the mediators was prepared. 10 μL of this mixture was then added to a 310 mM solution of NaCl, which is used as the supporting electrolyte. 830 μL of the resulting mediator/salt solution was added to the enzyme solution. A fresh mediator solution was prepared for most experiments.

A 1 M stock of glucose was prepared by weighing solid glucose and adding 50 mM Tris, pH 7.4 in the glove box. This solution was sealed and stored in a freezer. 130 μL of this solution was added to the mediator/protein solution prepared above. A solution containing 1 mg mL^{-1} glucose oxidase and 2 mg mL^{-1} catalase was also prepared and stored in a freezer. 13 μL of this solution was added to the protein mixture, and the final volume of the protein solution was made up to 1300 μL. This gives final concentrations of 5 μM for each of the five mediators, 10 mM glucose, 0.1 mg mL^{-1} glucose oxidase, 0.2 mg mL^{-1} catalase, 200 mM NaCl and *ca.* 30 μM P450. Enzyme concentration was *ca.* 70 μM for ferredoxins.

4.3.2 Cell Assembly

The SCE reference electrode was assembled into the Luggin capilary outside of the glovebox, with the capilary containing a 0.1 M KCl solution. All other cell assembly is carried out in the glovebox, to minimize the presence of oxygen in the cell. The fully assembled cell is shown in Figure 4.7.

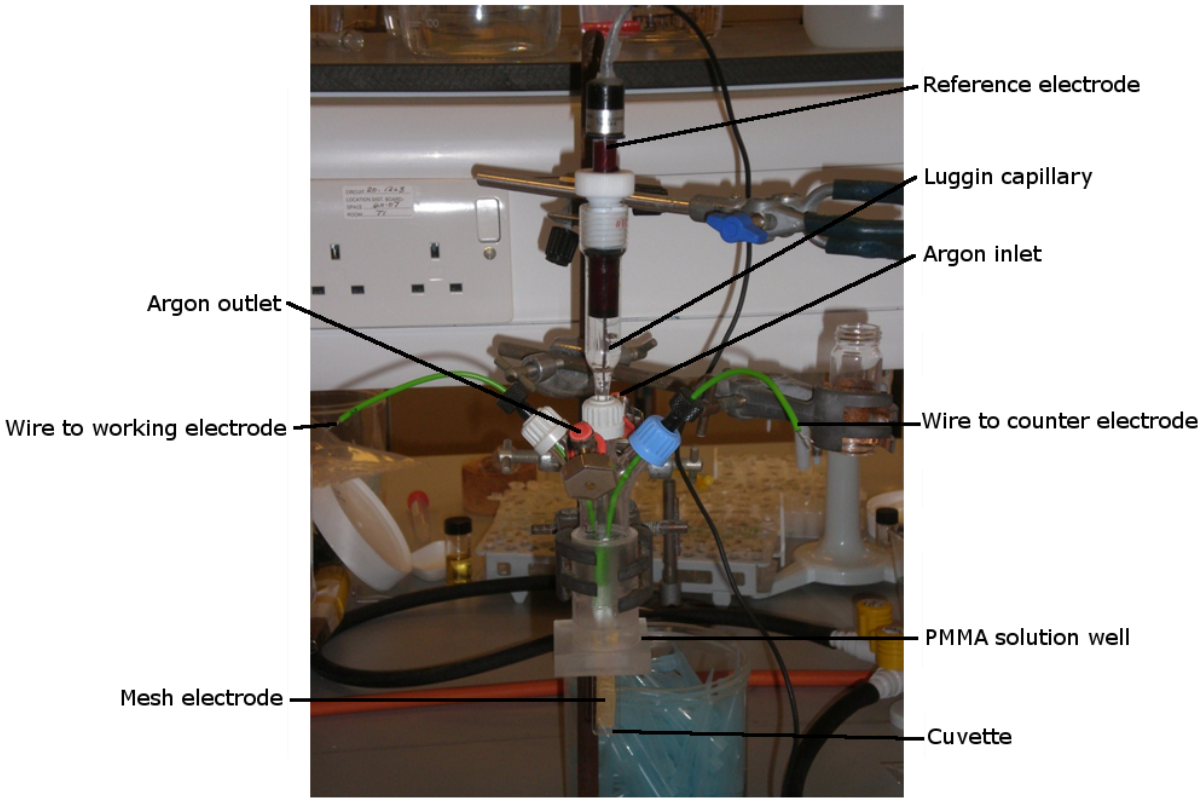

Figure 4.7. Assembled spectroelectrochemical cell.

The assembled cell was removed from the glove box, placed in the cuvette holder in the Cary 50 UV-Vis spectrophotometer and held steady using clamps attached to a ring stand. Argon gas was used to purge the cell after first being sparged through *ca*. 10 cm of deionized water. The purge outlet is also submerged to prevent any possible oxygen backflow. The cell was held at 25 ^{o}C with a recirculating water temperature regulator.

4.3.3 Determining equilibration time

With the OTTLE described in 4.2.3, equilibration times at each potential were 80 min, while the newer design allowed this to be reduced to 40 min. Figure 4.8 shows changes in the absorbance at 450 nm in SF WT over the course of an equilibration step with the redesigned mesh electrode. This shows that after 40 min equilibration time, between –300 and –460 mV, the absorbance had reached >99% of its final value. As this is a large

potential step (a typical step in a potentiometric titration is 20 mV), the fact that >99% of the observed absorbance change occurs after 40 minutes allows this to be used for the standard equilibration time in a potentiometric titration.

Using a 40 min equilibration time allowed for far more points to be obtained in a single experiment. A typical experiment lasts 16–20 hours, which requires the protein to be stable over long periods. Stability could be improved by performing the titration at a lower temperature, though the proteins studied in this work were stable for this duration.

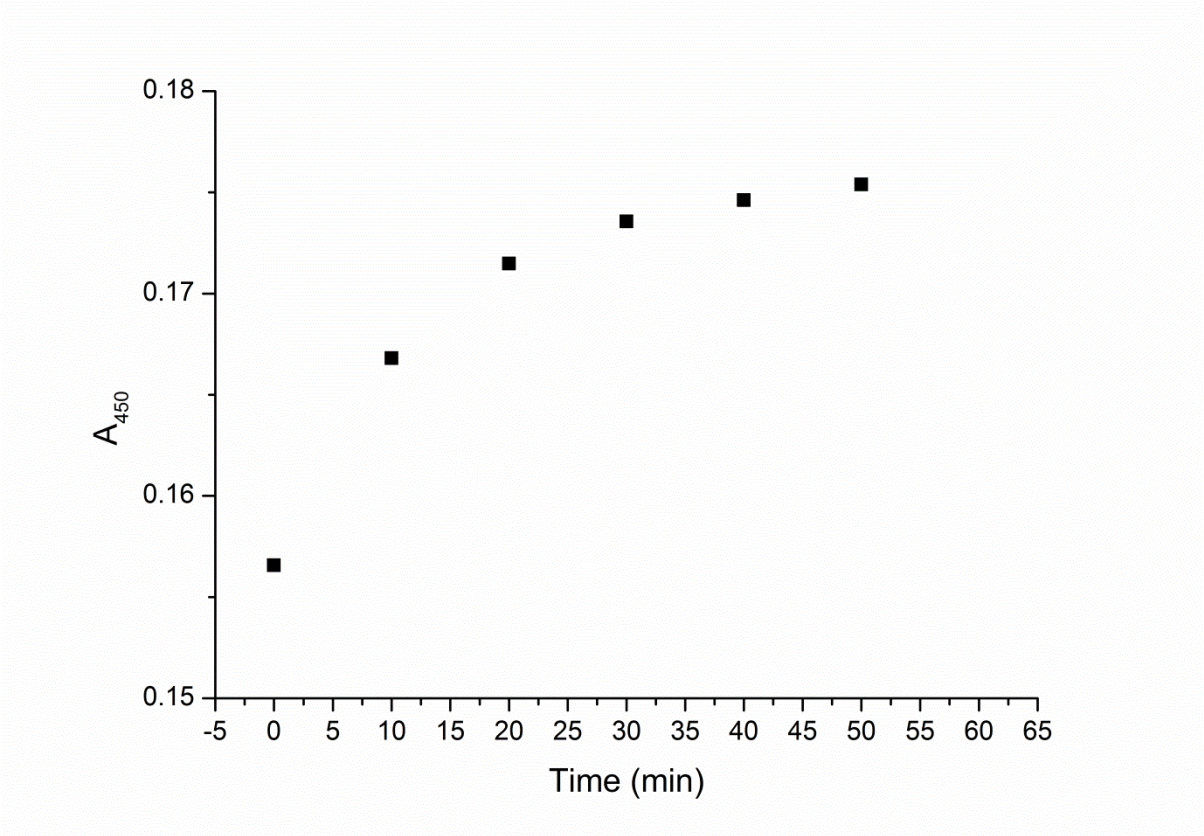

Figure 4.8. Absorbance at 450 nm for SF WT $P450_{BM3}$. Potential was stepped from –300 mV to –460 mV at t=0.

A typical experiment involved equilibrating the protein at 10–25 potentials and measuring spectral changes. Spectra were collected automatically every five minutes on a Cary 50 spectrophotometer over a window of 200–800 nm, with a scan rate of 300 nm/min. This

slow scan rate increased the precision of the spectra, which was important given that some of the spectral changes involved are small.

For the substrate-free and palmitate-bound forms of the WT $P450_{BM3}$ and the I401P variant, as well as the substrate-free A330P variant, potentials were set and currents measured using an Ivium CompactStat. For all other cases, an Autolab analogue potentiostat with a UE9 computer interface from LabJack was used. The use of the CompactStat or UE9 computer interface allowed the automation of potential setting and data collection.

4.3.4 Data analysis

Spectra were acquired every 5 minutes during the titration, to allow spectral changes to be monitored for the full duration of the experiment. After data collection was complete, the final spectra obtained at each potential were compiled, as these represented the fully equilibrated end-point for the applied potential. A 0^{th} order baseline correction was applied, based on the average absorbance from 775–800 nm, as no component of the solution absorbs in this region. Since reduced methyl viologen has a λ_{max}= 395 nm, data analysis was carried out at 450 nm, 465 nm and 570 nm. The absorbances at these wavelengths were plotted against applied potential, and fitted to a sigmoid derived from the Nernst equation (Eq. 4.1, see Appendix 5 for derivation), where $A(E)$ is the absorbance for a given potential, $A(E_{max})$ and $A(E_{min})$ are the optical densities for the fully oxidized and fully reduced chromophore, E_m and E_{appl} are the midpoint and applied potentials, R the gas constant, T the cell temperature, n the number of electrons transferred for the redox couple, and F Faraday's constant. The values of $A(E_{max})$, $A(E_{min})$ and E_m were determined by minimising the square of the difference between the measured

value and the predicted value, assuming equal weighting of the data. The value of *n* was fixed to 1.

$$A(E) = \frac{A(E_{\max}) - A(E_{\min})}{1 + \exp[(E_{\mathrm{m}} - E_{\mathrm{appl}})/(RT/nF)]} + A(E_{\min})$$

Equation 4.1.

The obtained midpoint potentials from analysis at all wavelengths were averaged, giving an experimental value for the titration. Unless otherwise noted, reported values are the average and standard deviation of three such titrations. Quality of the obtained data was checked by allowing *n* to vary, with values between 0.8 and 1.25 being typical.

4.3.5 Frequently encountered problems

Though the OTTLE cell allowed for the successful measurement of the reduction potential of over 25 enzymes (or enzyme/substrate complexes) there were several problems that were encountered frequently.

One of the most common problems was precipitation of the protein. This typically occurred in one of two ways: a large current resulted from the initial application of potential across the electrodes which caused the protein to precipitate, or precipitation of the protein after many hours exposed to the potential.

Precipitations that resulted from prolonged exposure were possibly the result of the electrode not being properly cleaned. Small amounts of protein adsorbed on the surface of the electrode can act as aggregation sites, causing the protein to precipitate out of solution over time. This issue was mostly addressed by a more rigorous cleaning routine.

The problem of precipitation caused by a current spike seemed to stem from a short circuit between the working and counter electrodes, a hazard of having the two electrodes so close together. Though the electrode connections were checked prior to use, it was

possible for a loose wire from the platinum mesh to make contact with the gold mesh only after it was placed into the cuvette, which is a tight space for the electrode assembly. When this happened, the large resulting current caused immediate precipitation of the protein.

A second problem that was observed in several attempted titrations with $P450_{BM3}$ was the generation of an alternate species of the enzyme that was not reduced in the same way as a typical P450. An example of this is shown in Figure 4.9. The initial scan of the protein (black) is typical for a substrate-free P450 (in this case the A330P variant). However, after 240 minutes the spectrum changes to one with the Soret band at 425 nm and the peaks at 535 nm and 565 nm remain separated rather than converging, and indeed the peak at 565 nm grows in intensity throughout the remainder of the experiment.

This shift in the spectrum of the enzyme was observed in both the KT2 and A330P variants. The spectral shift may result from the enzyme having an alternant heme binding ligand. The inactive form of P450s, dubbed P420 owing to the shift in the Soret band of the CO-bound enzyme to 420 nm, is known and has been studied[201, 285]. It is possible that this P420 inactive form may result from the ligating cysteine being replaced with a histidine, a suggestion which stems from the comparison of the P420 spectral properties with those of heme proteins such as myoglobin which have histidine as the heme ligating residue naturally[286].

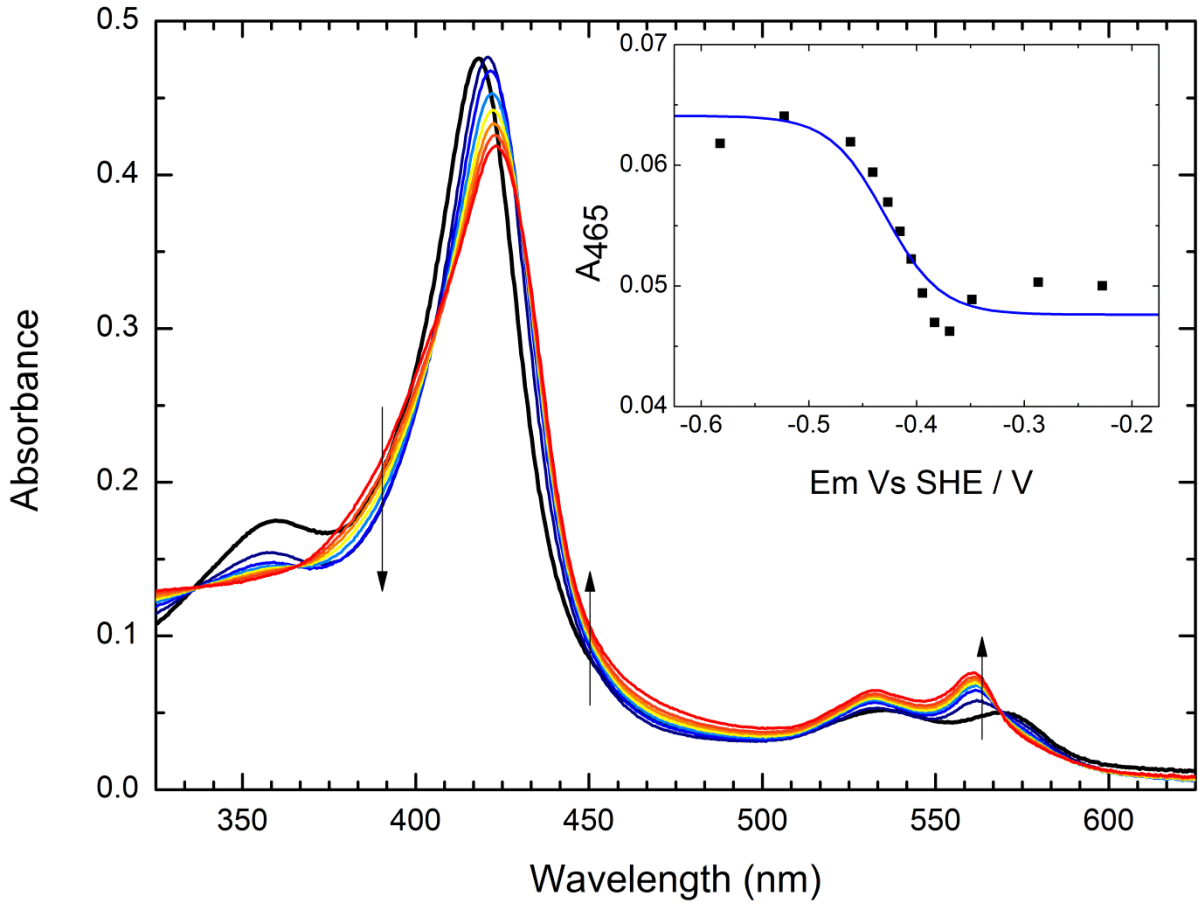

Figure 4.9. Spectroelectrochemical titration of A330P illustrating the Soret shift to 425 nm. The inset shows a non-linear least-squares fit of absorbance at 465 nm to a sigmoidal form of the Nernst equation with the number of electrons fixed at 1.

However, many P450s which exhibit a P420 form do not have histidines located near the heme and it is unlikely that the large scale conformational changes to allow for histine ligation of the heme iron are responsible for the P420 form in these cases. It is difficult to characterise the P420 'inactive' form of P450s because of the similar spectral properties of neutral thiol- and imidazole-bound heme[287, 288]. iNOS is an example of a protein that exhibts a P420 form but does not have a histidine readily available for ligation. It is believed that the inactive P420 may actually result from the electronic environment of the ligating thiol (that is to say, the thiol is negatively charged in the active form and protonation causes a shift to the P420 form)[287]. This is supported by the observation that

some P450s are reversibly converted to the P420 form by controlling pH[289] and by ligation experiments with myoglobin[289].

A sample of an enzyme which produced this peculiar spectrum in potentiometric titrations was recovered and tested in a P450 assay (not shown). Interestingly, this showed the enzyme was still in a P450 form, and had not been denatured to a P420 form. This form of the enzyme then, is not the so-called P420 form, but a different form of the enzyme which has been denatured or structurally changed in some other manner.

One of the most curious aspects of this form of the enzyme is that though the spectra are altered, the midpoint potential of the enzyme appears unchanged. In each case where this was observed, regardless of the point in the titration at which the change occurs, the midpoint potential determined was the same as in those titrations where a normal reduced protein is observed. For example, the protein shown in Figure 4.9, A330P, has a reduction potential of –405 ± 13 mV. Of the titrations with A330P which demonstrated this spectral shift, the average reduction potential was determined to be –420 ± 9 mV, within experimental error of the value for A330P. For KT2 the obtained reduction potential of the altered form was –410 mV, which is nearly identical to the determined reduction potential for the KT2 variant, –405 ± 8 mV.

However, given that KT2 and A330P have reduction potentials that are nearly identical, it is unclear if it is merely coincidence that the alternate form also has this potential, or if indeed the reduction potential has not been altered by the changes responsible for the spectral shift. Cyclic voltammetry studies on the P420 form of $P450_{BM3}$ have shown the reduction potential of the P420 form of the enzyme to be *ca*. –385 ± 10 mV[201], suggesting that the inactive form of the enzyme may indeed have a potential coincidentally equal to the active mutant variants.

The fact that the electronic environment of the heme is altered sufficiently to cause a shift in the Soret band and yet the potential is not shifted out of the range typically expected for SF P450s is interesting. Perhaps this is further evidence that, while the local electronic environment of the heme is no doubt important in P450 activity, it is actually larger scale structural changes induced by the addition of substrate that effect the shift in reduction potential to more oxidizing values.

4.4 Patterned gold electrodes

4.4.1 Initial design and fabrication

Gold mesh is fragile and often difficult to handle, making its repeated use as a working electrode potentially problematic, as tearing could eventually disrupt electrical contacts, requiring the costly fabrication of a new electrode. It was therefore desirable to design and produce an electrode that was both more robust, easy to handle and relatively inexpensive, while maintaining the positive aspects of the minigrid, including the transparency and ability to have a large counter electrode area. Design and fabrication of the new electrodes was assisted by Dr. Peter Leigh of the Department of Engineering and Dr. Christopher Blanford of the Department of Chemistry.

The new electrode design (Figure 4.10) features both the working and counter electrodes patterned onto a fused silica strip (4.3 mm × 80 mm × 0.5 mm). Fused silica is transparent in the UV-vis spectral window, so is ideal for this application. Both the counter and working electrodes are a thin (<100 nm) layer of gold which is etched into the required pattern using photolithographic techniques. Gold will not adhere directly to silica, so an initial layer of chromium (<10 nm) was deposited to permit gold adhesion. Metals were deposited using Chemical Vapour Deposition (CVD).

Since the metals can only easily be deposited on one side of the silica strip, the design calls for two strips, placed back to back, per electrode. Thus, the full protein solution will be exposed to the electrode surface. One side of the electrode features vertical working electrode bars, while the other features horizontal bars, mimicking the gold mini-grid. The bars are 20 nm thick and spaced 65 nm apart, which should maximize working electrode surface area while allowing for transmission of light. The electrode sides are chiral, ensuring that when placed back to back the electrodes connections are easier to make.

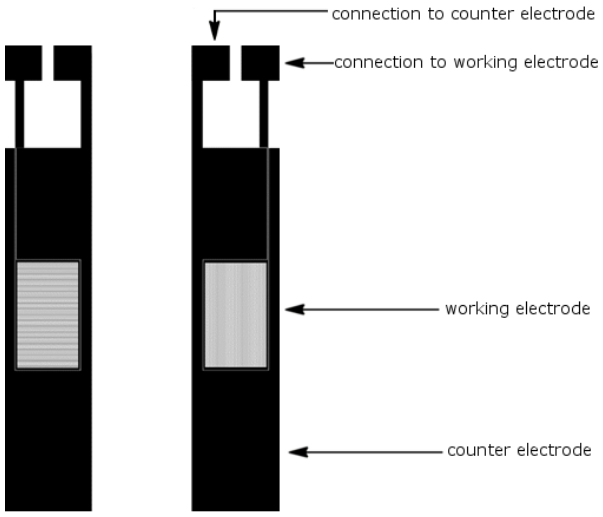

Figure 4.10. First generation patterned OTTLE design.

Photolithography was used to pattern the electrode onto the gold surface. Using a negative photolithographic dye the electrode mask was imprinted onto the surface. The metal not required in the electrode was etched away, preventing contacts from forming between the working and counter electrodes. The etchant for the gold layer was gold Etchant from Sigma-Aldrich and the chromium etchant was Etch 18 from Crytech.

This design showed a great deal of promise for use as an OTTLE. The mini-grid was 40% transparent, similar to the gold mini-grid, and the deposited gold showed excellent

conductivity. However, in several of the test electrodes, a connection existed between the working and counter electrodes. This prevented the initial set of electrodes from being used in potentiometric titrations or other electrochemical investigations.

Careful examination of the electrode surface uncovered a potential reason for the short-circuit. Some of the particularly fine details of the electrode, such as the small gap between the working electrode mesh and counter electrode, still had some of the chromium adhesion layer that was not etched away. This suggests that the spacing may be too small to allow the etch to fully remove the chromium, while leaving the slide in the etch for a longer period of time led to undercutting the gold (i.e. the chromium adhesion layer below the gold was etched away, removing the gold from the slide). The design of the electrode, including the thickness of the metal layers, was revisited in order to address these issues.

4.4.2 Design and fabrication improvements

The updated design of the patterned electrode is shown in Figure 4.11. It focuses on making the spacing of the fine details slightly larger, as well as using a thinner chromium layer, in an effort to make the etching more efficient and complete while avoiding undercutting the gold. The minimum line spacing was changed to 150 nm with 125 nm bar thickness, while the thickness of the chromium and gold layers were 7 nm and 80 nm respectively. The thicker bars and spacing allowed for more complete etching and helped to prevent undercutting of the gold. The gap separating the working and counter electrodes was also widened, to allow for more complete etching and prevent undercutting.

When fabrication was completed the new electrodes showed no connectivity between the working and counter electrodes, while the electrodes showed no resistance across the

length of the gold electrode. The electrodes were then connected to wiring for use in the electrochemical cell described in section 4.2.3, though the cell was equipped with a 2 mm path length cuvette. Given the 1 mm thickness of the electrode, a 2 mm cell provides an effective path length of 1 mm, as in the standard cell.

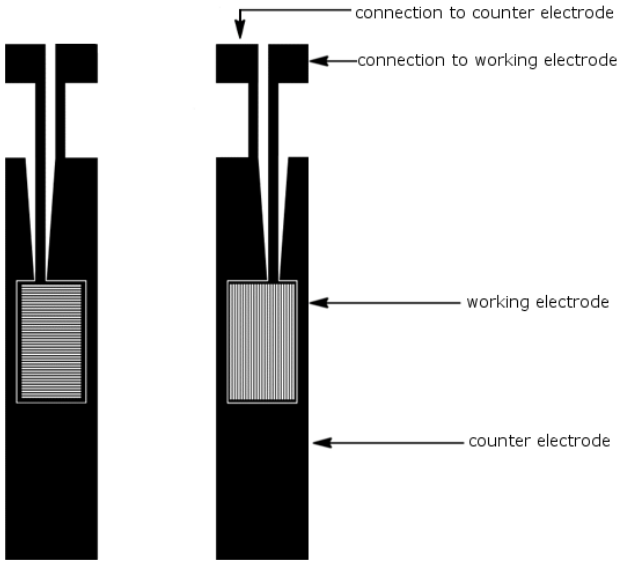

Figure 4.11. Second generation patterned OTTLE design.

These electrodes required different maintenance procedures than the gold mesh electrodes. Since the gold electrode is adhered to the fused silica with a chromium adhesion layer, applying a positive potential in an acidic solution causes the gold to flake off, as the chromium is dissolved. Thus, the electrode is washed thoroughly with acetone after use and is stored in deionized water.

4.4.3 Wiring of the patterned gold electrodes

Connecting wiring to the patterned electrodes proved difficult. In order for a connection to be maintained, constant pressure was required, which led to the design of a custom wire housing which could maintain the electrode connection. The wire housing was fabricated by Mr. Keith Waters of the Department of Chemistry workshop and is shown in Figure 4.12.

Even using the custom wire housing, the wiring often scratched the gold and chromium from the surface of the fused silica strips. As the connection area of the electrodes is not submerged in the analyte solution, silver paint was used to provide a contact point between the patterned electrodes and the wiring, though the connection between electrode and wiring was unreliable. Copper conductive tape from 3M was also used to affix the wiring to the gold surface, though this too failed to provide reliable, low resistance connections. The adhesive tape solution was both the easiest to implement and most cost effective, and was therefore used to provide the connection between patterned electrode and the wiring throughout the experiments described in this work.

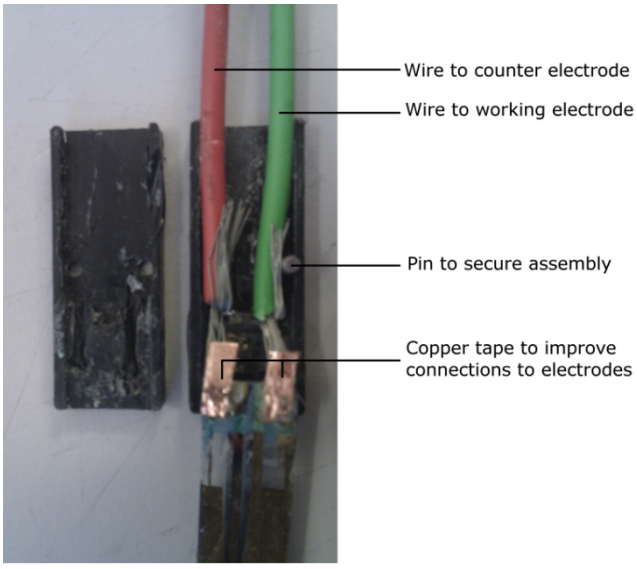

Figure 4.12. Custom wire housing. The top of the housing has been removed to show the inside of the housing.

4.5 Use of the patterned electrodes

4.5.1 Cyclic voltammetry of mediators

To determine the electrochemical viability of the electrode system, several tests were performed using small molecules commonly used as mediators. Cyclic voltammetry was performed on 9,10-anthraquinone-2-sulfonate, anthraquinone-2,6-disulfonate and methylene blue in order to confirm that the experimentally determined reduction potential using the patterned electrodes matches that determined with a conventional graphite working electrode and platinum counter electrode. Figures 4.13 shows the cyclic voltammograms obtained from these experiments.

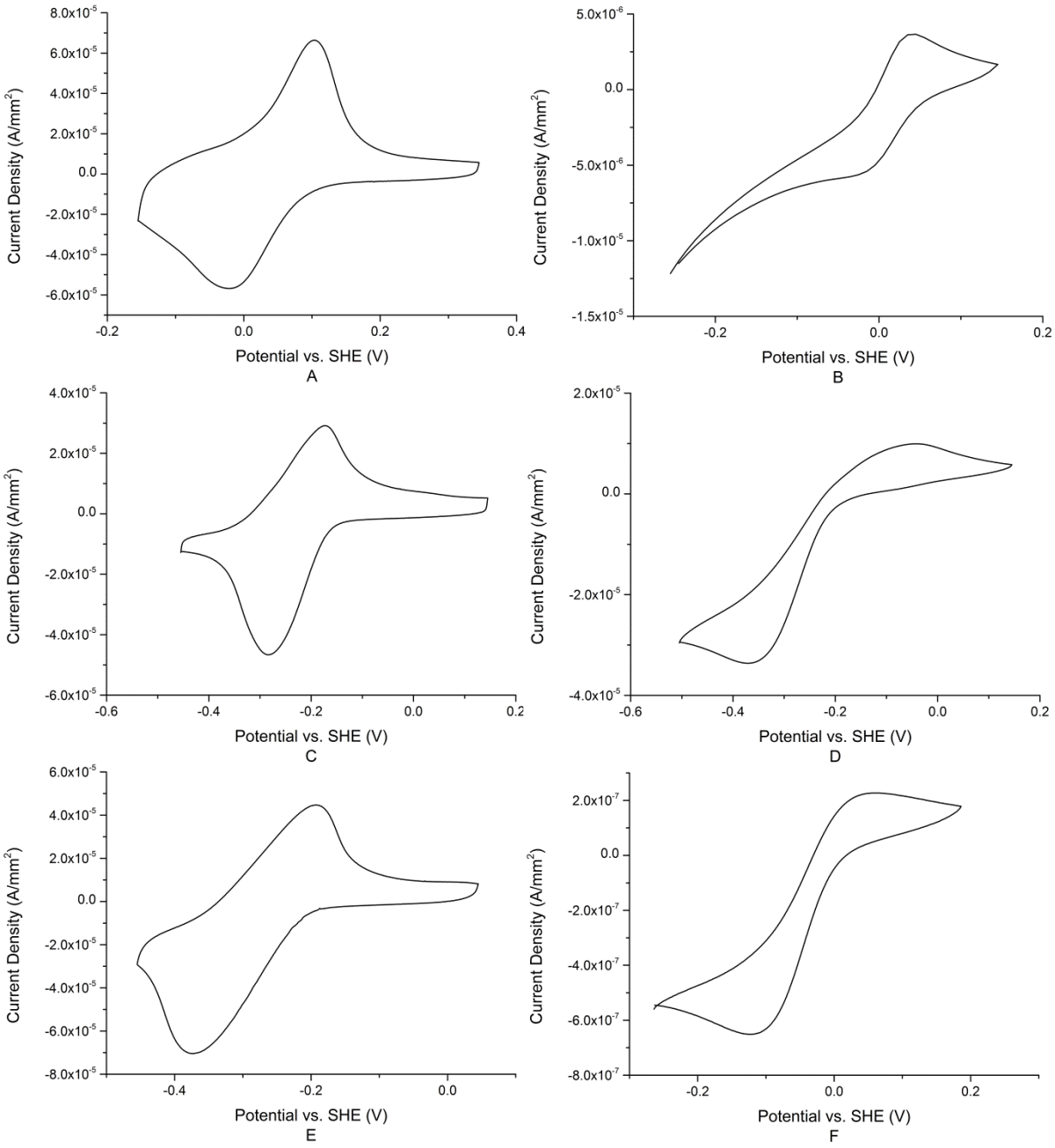

Figure 4.13. CV taken at 50 mV/s scan rate, pH 7.4, of 1 mM of the mediator methylene blue with the graphite working electrode **(A)** and new electrodes **(B)**; 9,10-anthraquinone-2,6-disulfonate with the graphite working electrode **(C)** and new electrodes **(D)**; 9,10- anthraquinone-2-sulfonate with the graphite working electrode **(E)** and new electrodes **(F)**.

With a graphite working electrode, platinum wire counter electrode and SCE reference electrode the reduction potential determined for methylene blue was +37 mV, and with the patterned gold electrodes the reduction potential was determined to be –10 mV. The reduction potential determined for 9,10- anthraquinone-2,6-disulfonate with the graphite working electrode was –234 mV and –202 mV when determined with the patterned gold electrodes. Reduction potentials of –287 mV and –275 mV were obtained for 9,10-anthraquinone-2-sulfonate with the graphite and patterned gold electrodes respectively.

The experimentally measured reduction potentials were in good agreement, and showed that the patterned gold electrodes can be successfully used in electrochemical experiments. However, the CVs obtained from the patterned gold electrodes have much steeper slopes than those obtained using the graphite working electrode. This indicates that there is a higher resistance in the gold electrode system, likely a result of the difficult-to-maintain connections to the wire assembly noted above. The oxidation and reduction peaks in the CVs obtained with the patterned gold electrodes are also broad compared to those obtained with the graphite working electrode, which is likely a result of slow electron transfer from the surface of the electrode to the mediators in solution[290, 291].

Peak separations obtained for the mediators are summarized in Table 4.2. The oxidation and reduction peaks in a CV should be separated by 59/*n* mV in a reversible process. As peaks are separated by more than this, even when using the graphite electrode, these systems are, under the conditions of these experiments, only quasi-reversible. An increase in peak separation also indicates increased resistance between the working and reference electrodes which can arise with increased spatial separation in the electrochemical cell. In these CV experiments the distance between working and reference electrodes was

constant, so variations in peak separation are mainly due to slow electron transfer kinetics and resistance across the working electrode.

With 9,10-anthraquinone-2-sulfonate, peak separation was similar for each system at 171 mV for the graphite working electrode and 186 mV for the patterned gold electrode. With 9,10-anthraquinone-2,6-disulfonate however, there was a very large difference in the two systems, with the gold electrode peak separation (323 mV) being three-fold larger than that of the graphite system (108 mV). This variation highlights that the gold electrode system has slow electron-transfer kinetics and high resistance in the electrode connections. With methylene blue the gold electrode system give a peak separation much closer to the theoretical value for a reversible process, at 70 mV, while the graphite system had peak separation of 126 mV. This serves to highlight that the connections between the patterned gold electrodes and the wiring are unreliable and perhaps the bulk of the variation in peak shape and separation is due to the high resistance and variable connections in this system.

Table 4.2. Peak separations for electrochemical mediators using a graphite working electrode and the patterned gold electrode.

Mediator	Working electrode	Peak separation (mV)
9,10-anthraquinone-2-sulfonate	graphite	171
	patterned gold	186
9,10-anthraquinone-2,6-disulfonate	graphite	108
	patterned gold	323
methylene blue	graphite	126
	patterned gold	70

4.5.2 Spectroelectrochemistry of mediators

Since the electrodes were capable of reducing and oxidizing the mediators through cyclic voltammetry, they were tested for use in spectroelectrochemistry. Potentiometric titrations were performed on methylene blue and methyl viologen, and these are shown in Figure 4.14.

The potentiometric titrations were performed in 50 mM Tris, pH 7.4, using 5 min equilibration time between potential steps. A shorter equilibration time was used for the mediators than for a protein as the mediators are more rapidly reduced by the electrodes. For methylene blue, the obtained reduction potential was –11 mV which is a slight deviation from the reported value of 10 mV at pH 7, though consistent with the value obtained by cyclic voltammetry with the patterned electrodes. When *n* is allowed to vary the fitted value is low, at 0.52. For methyl viologen, the reduction potential determined using this method was –457 mV, which is very near to the published value of –449 mV[279]. However, as with the methylene blue titration, the *n*-value is again low, at 0.78. The low *n*-values further reflect the slower electron transfer between the patterned electrode surface and the bulk solution observed with the cyclic voltammetry experiments (i.e. the system may have not reached equilibrium in the time allotted).

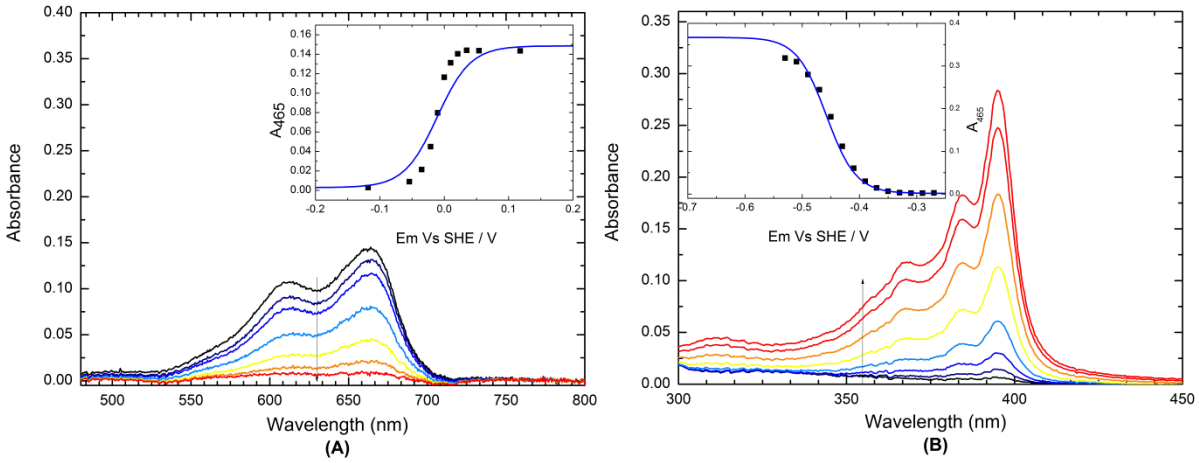

Figure 4.14. Spectroelectrochemical titration of **(A)** methylene blue using patterned gold electrodes. The inset shows a non-linear least-squares fit of absorbance at 665 nm to a sigmoidal form of the Nernst equation with the number of electrons fixed at 1; **(B)** methyl viologen using patterned gold electrodes. The inset shows a non-linear least-squares fit of absorbance at 395 nm to a sigmoidal form of the Nernst equation with the number of electrons fixed at 1.

4.6 Spectroelectrochemistry of proteins using the patterned electrodes

Though the electrodes displayed a higher than desired resistance, they nonetheless were used successfully in potentiometric titrations with the mediators methylene blue and methyl viologen. Three proteins which had been analysed using the gold mesh electrode described in section 4.2.4 were also examined spectrophotometrically using the patterned electrodes. The significance of the reduction potential data obtained for these three enzymes, palmitate-bound WT $P450_{BM3}$, SF KT2 and the ferredoxin PuxB/M66D/A105V, will be discussed in chapter 5; the titrations using the patterned gold electrodes are presented here. For the titrations using a gold mesh electrode, the results are the mean of three titrations and the standard deviation is <5% of the mean. For those titrations using the patterned gold electrodes, the results presented are from a single experiment.

4.6.1 Palmitate-bound WT $P450_{BM3}$

Figure 4.15 shows the potentiometric titration of the palmitate-bound form of WT $P450_{BM3}$. With the gold mesh electrode, the potential was determined to be –317 mV with n = 1.32. When determined using the patterned gold electrodes, these values were –300 mV and 2.46, respectively.

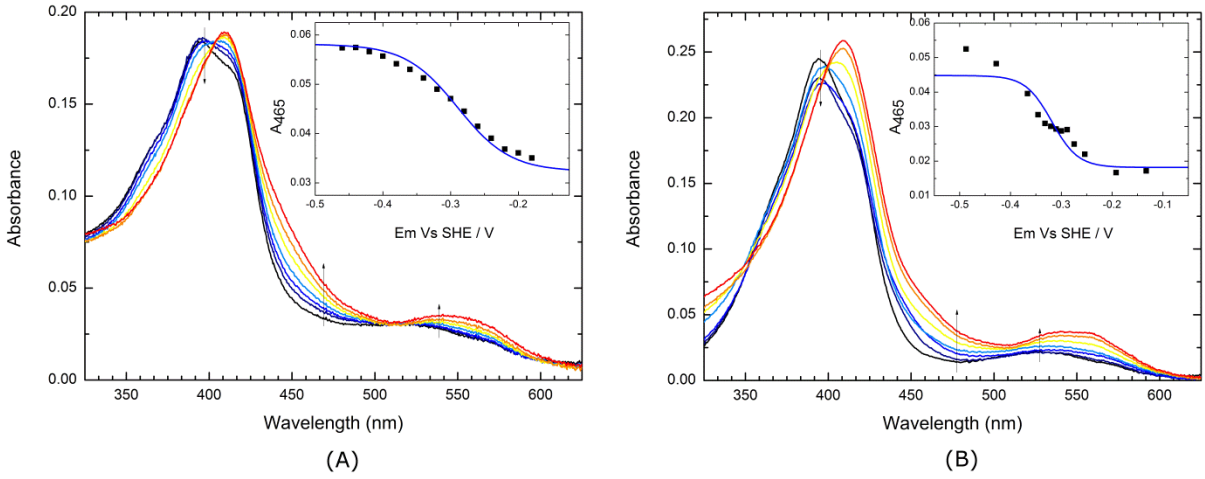

Figure 4.15. Spectroelectrochemical titration of palmitate-bound WT $P450_{BM3}$ using **(A)** the gold mesh electrode and **(B)** the patterned gold electrodes. The fully oxidized spectrum is black, while the fully reduced spectrum is in red. The inset shows a non-linear least-squares fit of absorbance at 465 nm to a sigmoidal form of the Nernst equation with the number of electrons fixed at 1.

The fully oxidized spectrum is mixed spin, as the 200 μM palmitate is not sufficient to induce a full spin-state shift in the WT. For the titration using the gold mesh electrode, the fully oxidized spectrum has a λ_{max} = 395 nm, while the fully reduced form has a λ_{max} = 414 nm. The sigmoidal fit of the absorbance change at 465 nm for this titration is not perfect with n = 1.32.

The titration performed with the patterned gold electrodes shows several differences. The λ_{max} of the fully oxidized and reduced forms remain unchanged. The most striking difference between the titration using the gold mesh electrode and the patterned gold electrodes is the sigmoidal fit at 465 nm. From –290 mV to –330 mV the spectrum does

not change significantly, which leads to the plateau observed in the sigmoidal fit. The fit of the sigmoid is also poor at the low potential end. In spite of the poor fit when using the patterned gold electrodes, the midpoint potential determined using this method was nearly equal to the value determined using the gold mesh electrode.

4.6.2 Substrate-free KT2

Shown in Figure 4.16 are the potentiometric titrations performed on SF KT2. The reduction potentials determined were –405 mV with the gold mesh electrodes and –391 mV for the patterned gold electrodes. The *n*-values determined with each electrode system were 1.19 and 1.02 respectively.

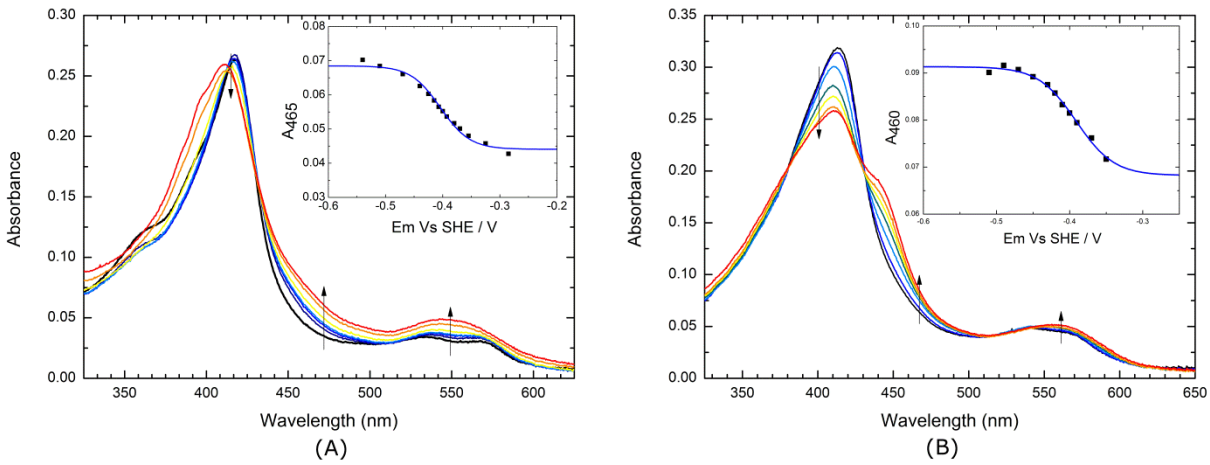

Figure 4.16. Spectroelectrochemical titration of SF KT2 using **(A)** the gold mesh electrode and **(B)** the patterned gold electrodes. The fully oxidized spectrum is black, while the fully reduced spectrum is in red. The inset shows a non-linear least-squares fit of absorbance at 465 nm to a sigmoidal form of the Nernst equation with the number of electrons fixed at 1.

The spectra obtained using the patterned gold electrodes have two isosbestic points, one at 416 nm and one at 432 nm. The fully oxidized spectrum had a λ_{max} = 418 nm while that of the fully reduced form was 414 nm. The fully reduced spectrum obtained using the gold electrodes shows a slight shoulder at 395 nm, which is due to the mediator methyl viologen, which when fully reduced absorbs strongly at this wavelength. The sigmoidal

fit for this experiment was good, with n = 1.19, though the absorbance at 465 nm of the fully reduced form is higher than the fit, which again could be due to slight baseline drift over the length of the experiment.

The sigmoidal fit for the titration using the patterned gold electrodes is good, with n = 1.02, though more points at the higher potential end would have been useful. The spectra obtained have equivalent λ_{max} values as those obtained with the gold mesh electrode, though there is a striking absorbance decrease as the titration progresses which could be a result of heme loss during the titration. The isosbestic at 432 nm is still present, though a shoulder has formed at 439 nm. Studies on chloroperoxidase (CPO) have shown that it too has a shoulder at *ca.* 440 nm in the reduced form[292]. In CPO, this shoulder was ascribed to reversible ligation of histidine to the heme iron, though $P450_{BM3}$ does not have an active site histidine which could act in this way. While the sigmoidal fit of the absorbance at 465 nm was better for the patterned gold electrodes, the spectral anomaly at 440 nm and the apparent heme loss which occurs during the titration with the patterned electrodes suggests that the gold mesh electrodes provide more reliable data.

4.6.3 PuxB/M66D/A105V

The patterned gold electrodes were also used to determine the reduction potential of the electron transfer protein PuxB, a [2Fe-2S] ferredoxin from *Rhodopseudomonas plaustris* which is described in Chapter 5. The reduction potential of a PuxB mutant, PuxB/M66D/A105V, was determined using the gold mesh electrode and the patterned gold electrodes, and the potentiometric titrations are shown in Figure 4.17. Using the gold mesh electrode the reduction potential was determined to be –299 mV and n = 1.02, the values obtained using the patterned electrodes were –296 mV and 1.24 respectively.

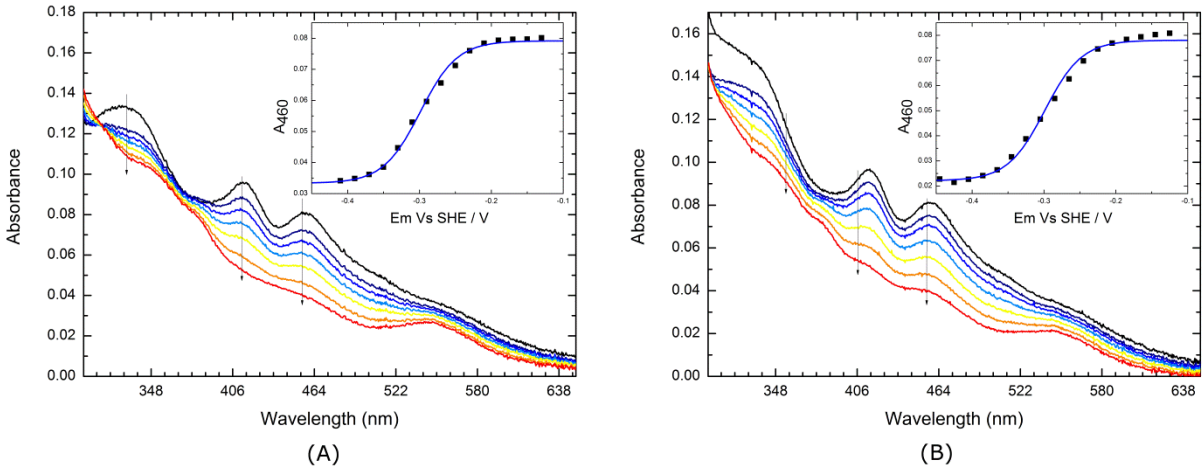

Figure 4.17. Spectroelectrochemical titration of the ferredoxin PuxB/M66D/A105V using **(A)** the gold mesh electrode and **(B)** the patterned gold electrodes. The fully oxidized spectrum is black, while the fully reduced spectrum is in red. The inset shows a non-linear least-squares fit of absorbance at 460 nm to a sigmoidal form of the Nernst equation with the number of electrons fixed at 1.

The titration of the ferredoxin variant PuxB M66D/A105V gave similar spectra and sigmoidal fits, regardless of the electrode system used. In the gold mesh electrode titration all spectra nearly overlap at 360 nm, while they remain more spread-out with the patterned gold electrodes. The fully oxidized spectrum is slightly different below 350 nm as well, with a defined peak being present in the gold mesh electrode titration and a more broad feature in the patterned gold electrodes, though similar variations have been noticed in spinach ferredoxin[293].

4.7 Conclusions

This study showed that the patterned gold electrodes were suitable candidates for use in spectroelectrochemical titrations and midpoint potentials determined using this system were equal to those determined using a gold mesh electrode, within experimental error. However, the large resistance observed in the cyclic voltammetry experiments with mediators and the slow electron transfer rates observed with the spectroelectrochemical titrations of mediators, combined with the spectral anomalies and poor sigmoidal fits

observed in the titrations of SF KT2 and palmitate-bound WT show that further development is required.

Practically, the patterned gold electrodes are difficult to handle compared to the gold mesh electrodes because the connection between the electrodes and the wiring was unreliable, difficult to maintain and caused a large resistance. While connectivity was checked using a potentiometer before the electrode was assembled into the cuvette, since the connections were easily lost either during assembly or in the course of the titration, the unreliable connections led to many failed experiments. It was decided that, while the patterned electrodes are an interesting possible method for spectroelectrochemical titrations worthy of further development, the remaining potentials determined in this work would be obtained using the gold mesh electrode described in section 4.2.4.

Chapter Five

Thermodynamic and Kinetic Origins of Generic Accelerating Effects in $P450_{BM3}$ Activity

5.1 General background

The mutations in the $P450_{BM3}$ variants KSK19 (F87A/H171L/Q307H/N319Y)[1], KT2 (A191T/N239H/I259V/A276T/L353I)[1], A330P[1] and I401P[2] have been dubbed generic accelerators since the variants show accelerated rates of substrate oxidation compared to the WT form of the enzyme for a wide range of substrates and, except for the A330P variant, the product profile of the precursor is maintained.

Table 5.1 summarizes the resting spin-state and leak rate of $P450_{BM3}$ variants and generic accelerators. The leak rate is the rate at which NADPH is consumed in the absence of substrate, measured in nmol (nmol P450)$^{-1}$ s^{-1}, henceforth abbreviated to s^{-1}.

Table 5.1. Resting spin-state and leak rates of various $P450_{BM3}$ variants.

$P450_{BM3}$ variant	Resting spin-state (% high-spin)	Leak rate (nmol (nmol P450)$^{-1}$ s^{-1})	References
WT	0	0.47 ± 0.01	3
F87A	0	0.32	4
KSK19	25	0.73	4, 5
A330P	0	0.48 ± 0.02	3
KT2	10	0.82 ± 0.03	6
I401P	50	7.58 ± 0.62	3

The WT enzyme is low-spin in the resting state (SF), and has a low leak rate of 0.47 ± 0.01 s^{-1}. The F87A variant shows that the leak rate, 0.32 s^{-1}, is unaffected by the alanine substitution, as is the spin-state. KSK19 displays a leak rate comparable to the F87A variant on its own at 0.73 s^{-1}, while the spin-state has shifted to 25%.

KT2 is predominantly low-spin (90%) in the absence of substrate and, like the WT enzyme has a low leak rate ($0.82 \pm 0.03\ s^{-1}$)

A330P is similar to WT $P450_{BM3}$ in that it is low-spin in the absence of substrate and has an identical leak rate, at $0.48 \pm 0.02\ s^{-1}$. Unlike the WT enzyme, however, A330P shows no spin-state shift upon the addition of palmitic acid and NADPH consumption rate also does not increase.

I401P is unlike the other generic accelerator mutants discussed here, as in the resting state it is 50% high-spin and the leak rate is high, at $7.58 \pm 0.62\ s^{-1}$. Though the leak rate is high, I401P is actually highly coupled with many substrates compared to the WT. Indeed, I401P is more highly coupled with many non-natural substrates and even lauric acid[7]. These variations in resting spin-state and leak rate show that, although the variants all impact substrate oxidation rate, they likely do so in different ways.

This chapter aims to detail the investigation into the origin of the rate accelerating effects by determining the heme reduction potential (BMP domains only) and rate constant of the first electron transfer, as well as the kinetic parameters. These properties were determined for the WT and the mutants in their substrate-free form as well as in the presence of palmitate, a fatty acid natural substrate, and propylbenzene, a non-natural substrate with which WT displays rapid NADPH consumption and high coupling. The results presented in the following section have been published[2, 3, 6].

5.2 Spectroelectrochemical and kinetic studies

5.2.1 The substrate-free form

Heme reduction potentials were determined in the absence of substrate for the WT, A330P, I401P and KT2 variants, and the resulting titrations are shown in Figure 5.1. The

first electron rate constant was determined using stopped-flow spectrophotometry, which measures the rate constant of formation of the $Fe^{II}(CO)$ complex, k_f, an acceptable proxy. The obtained time courses for $Fe^{II}(CO)$ complex formation for the SF WT, A330P, I401P and KT2 are shown in Figure 5.2, and the results are collected in Table 5.2.

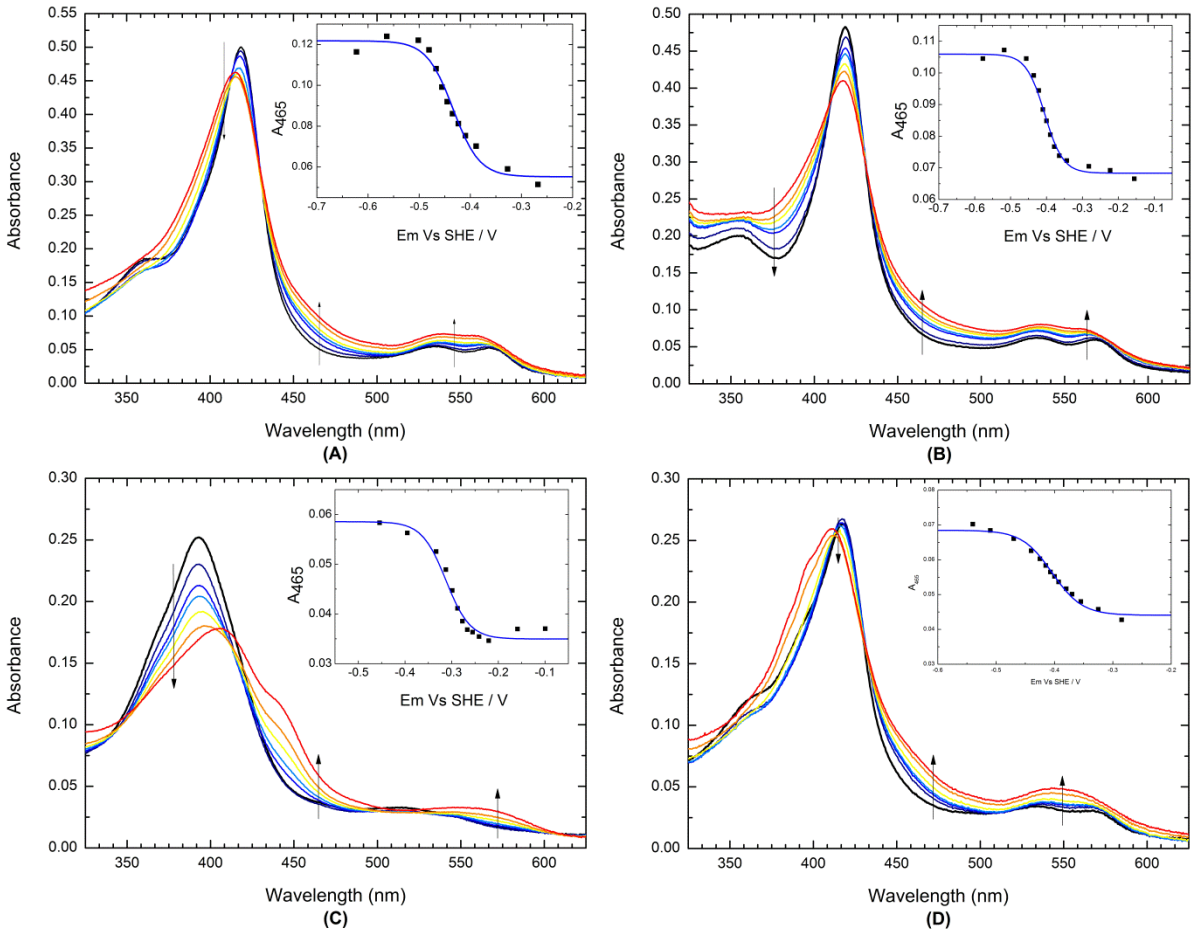

Figure 5.1. Potentiometric titrations for **(A)** SF WT; **(B)** SF A330P; **(C)** SF I401P; **(D)** SF KT2. The insets show non-linear least-squares fits of absorbance at 465 nm to a sigmoidal form of the Nernst equation with *n*, the number of electrons fixed at 1.

The potentiometric titrations of SF WT, SF A300P and SF KT2 are all similar, with λ_{max} = 418 nm in the fully oxidized form, λ_{max} = 414 nm in the fully reduced form and an isosbestic point at 432 nm. When allowed to vary, *n* values for these four titrations were 1.15, 0.80, 1.33 and 1.19 respectively but the potentials determined do not change significantly (<1%) from those with *n* fixed at 1. The *n* value varies slightly across the

experiments with a single protein. For example, the three A330P titrations used to obtain the experimental midpoint potential have *n* values in the range 0.8–1.2. The fully reduced SF KT2 spectrum has a small shoulder at 395 nm, owing to the mediator methyl viologen, which absorbs strongly at this wavelength when reduced.

The spectra of the SF I401P titration are different from those of the other SF enzymes studied. The enzyme is fully high-spin in the fully oxidized form owing to the high salt concentration in the spectroelectrochemical cell, with a λ_{max} = 395 nm. The fully reduced form has a λ_{max} = 414 nm, and the absorbance change from fully oxidized to fully reduced is large, at nearly 30 % of the starting absorbance. The most unusual feature of the fully reduced SF I401P is the shoulder at 440 nm. Shortly after we reported the I401P variant, another variant of $P450_{BM3}$ with a substitution at Ile401 was reported[8]. This variant, I401E, was also studied spectroelectrochemically and, like I401P, displayed a largely shifted reduction potential (–219 ± 4 mV) and in the fully reduced form showed a shoulder at 440 nm. Thus, this shoulder may be due to the altered environment near the heme which results from the substitution at the residue adjacent to the ligating cysteine. The I401P titration had an *n* value of 1.33, which is slightly high.

Stopped-flow experiments were set up by preparing components in a 15 mL plastic centrifuge tube in 50 mM Tris, pH 7.4. The solution was then saturated with CO by gently bubbling for 5 min and then purging the headspace for a further 5 min. One tube was prepared with NADPH (200 μM), and the other the appropriate $P450_{BM3}$ variant in *ca.* 4 μM concentration. In SB enzyme measurements, each tube also contained 2% (v/v) DMSO and the two syringes also contained palmitic acid or propylbenzene (200 μM). The tubes were transferred to a glove box and syringes used to remove the solutions from the tubes, maintaining CO saturation. The syringes were loaded into the stopped-flow apparatus and components were mixed in a 1:1 ratio.

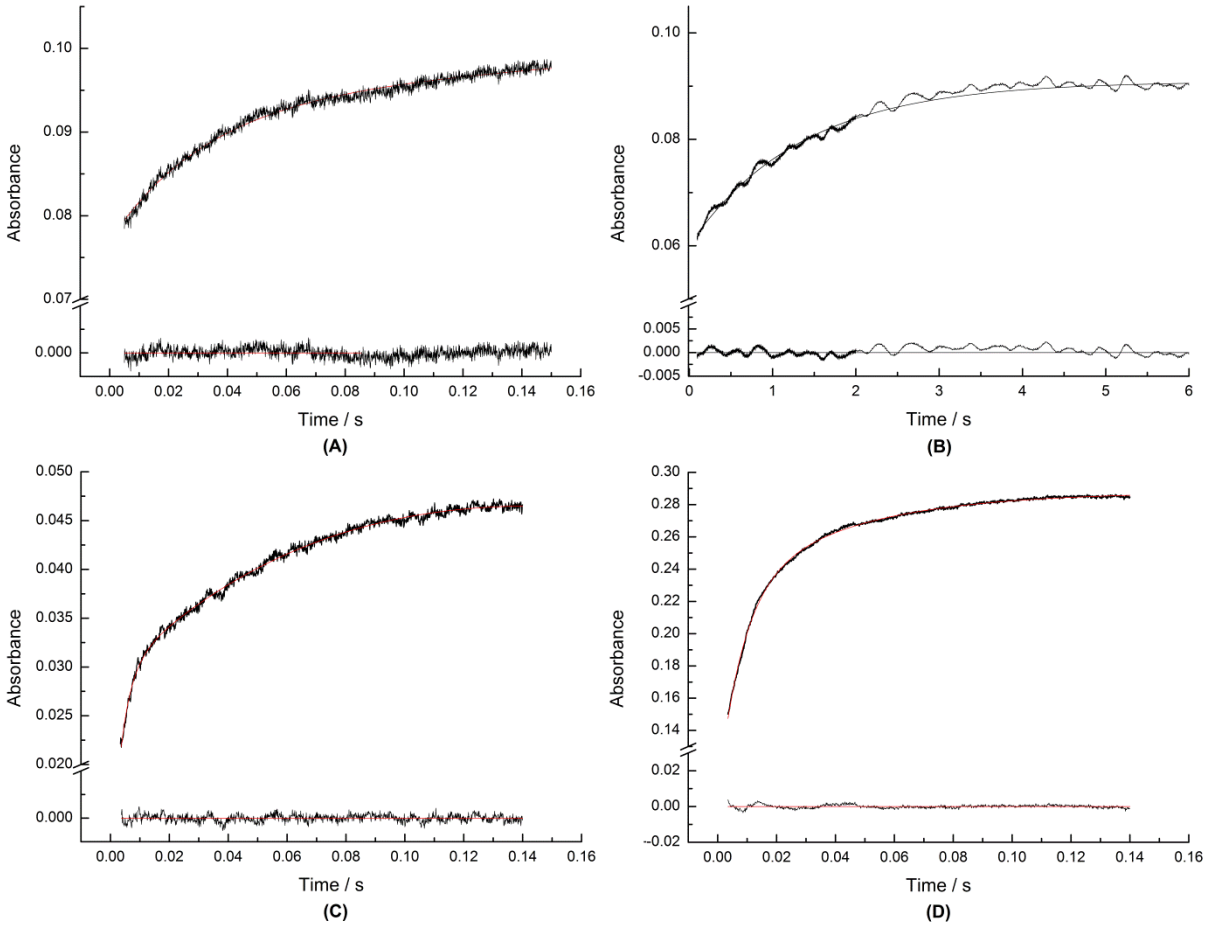

Figure 5.2. Time courses for $Fe^{II}(CO)$ complex formation monitored at 450 nm for **(A)** SF WT, which required a double exponential to fit contributions from the fast (55%) and denatured (45%) phases; **(B)** SF A330P, which required a single exponential to fit; **(C)** SF I401P, which required a triple exponential to fit contributions from the fast (27%), slow (29%) and denatured (44%) phases; **(D)** SF KT2, which required a triple exponential to fit the contributions from the fast, (53%), slow (21%) and denatured (26%) phases.

The SF A330P experiment has two apparently unusual features, namely the apparent oscillation in the signal and the thinning of the experimental data after 2 s. The oscillation is likely an artefact of the long time scale of the experiment and slow electron transfer in this variant, though does not seem to impact the fit or experimental value of k_f. The experiment is set up to acquire more data points from 0–2 s than 2–6 s, which is why the line appears darker at the beginning of the experiment. There are slight variations in the ΔA_{max} values in the stopped-flow experiments, owing to small variations in the protein sample concentrations and likely the presence of the denatured phase.

The stopped-flow time courses showed the presence of a phase with a rate constant of *ca*. 30 s^{-1} in the WT, I401P and KT2 variants. This phase was observed in other stopped-flow experiments (see below) and had a consistent rate constant of *ca*. 30 s^{-1}. To investigate the origin of this phase, which has a rate constant inconsistent with the SF or SB forms of the enzyme (see below), a sample of the SF KT2 variant was prepared where the CO bubbling step in the experimental set up was overly vigorous. A side-by-side comparison of this experiment with a more typical SF KT2 experiment is shown in Figure 5.3. This test showed that upon intentionally bubbling the CO through the enzyme solution vigorously, the phase with a rate constant of *ca*. 30 s^{-1} became the dominant phase in the sample (Figure 5.3 B), and so the phase was labelled a 'denatured' phase. It should be noted that as the stopped-flow experiment monitors absorbance at 450 nm this denatured form is not the P420 form of the enzyme, which does not absorb at 450 nm. Perhaps this denatured form is the same which was observed in several unsuccessful potentiometric titrations and was described in Section 4.3.5.

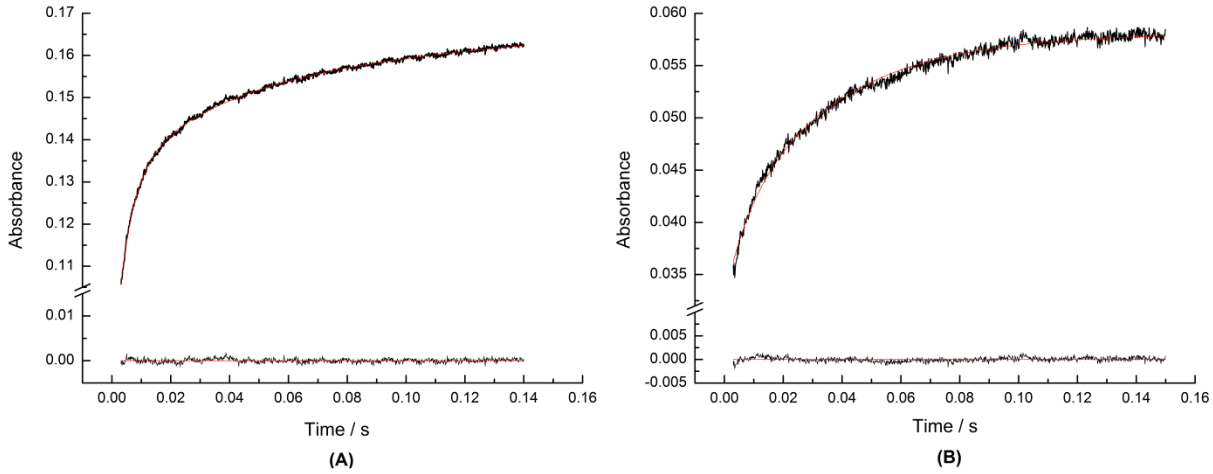

Figure 5.3. Time courses for $Fe^{II}(CO)$ complex formation monitored at 450 nm for **(A)** SF KT2, prepared in the usual manner, which required a triple exponential to fit the contributions from the fast, (53%), slow (21%) and denatured (26%) phases; **(B)** SF KT2, purposely exposed to vigorous bubbling of CO, which requires a double exponential to fit the fast (24%) and the denatured (76%) phases.

Table 5.2. Midpoint potentials for the heme domains of substrate-free $P450_{BM3}$ variants (E), rate constants for the formation of the $Fe^{II}(CO)$ complexes of the full-length proteins (k_f) with relative amplitudes for the fastest phase observed in parentheses.

	WT	KT2	I401P	A330P
E (mV)	–449 ± 14	–405 ± 8	–302 ± 9	–408 ± 13
k_f (s^{-1})	1.5 ± 0.3 (95%)	209 ± 19 (53%)	254 ± 36 (27%)	0.74 ± 0.4 (95%)
Leak rate (nmol (nmol-P450)$^{-1}$ s^{-1})	0.47 ± 0.01	0.82 ± 0.03	7.58 ± 0.62	0.48 ± 0.02
% High-spin	0	10	50	0

There appears to be a correlation between the resting heme spin-state equilibrium and the heme reduction potential. The WT enzyme is fully low-spin in the resting state and has a reduction potential of –449 ± 14 mV. The KT2 and A330P variants have reduction potentials of –405 ± 8 mV and –408 ± 13 mV respectively. A330P is fully low-spin and KT2 is 10% high-spin in the resting state. The I401P variant is 50% high-spin in the resting state and the heme reduction potential is shifted by 147 mV to –302 ± 9 mV, similar to the 138 mV shift induced by arachidonate binding in the WT[9]. However, the I401P variant was 100% high-spin under the conditions of the spectroelectrochemical titration and so such a large shift is perhaps not unexpected and it is possible that the 50% high-spin form has a reduction potential which is more oxidizing than the WT, but less than the 100% high-spin form.

The leak rates of the enzymes also correlate to the heme reduction potentials and spin-states of the enzymes, with the WT, A330P and KT2 variants having low (<1 s^{-1}) leak rates and that of I401P being accelerated at 7.58 ± 0.62 s^{-1}. In the WT and A330P variants the k_f values are also low at 1.5 ± 0.3 s^{-1} and 0.74 ± 0.4 s^{-1} respectively. In the KT2 and I401P variants however, even in the absence of substrate the first electron transfers are fast at 209 ± 19 s^{-1} and 254 ± 36 s^{-1}, respectively.

From Marcus theory (Equation 5.1), the two major contributing factors to the rate of electron transfer in an outer-sphere process are the thermodynamic driving force, ΔG, and the reorganization energy, λ. The reduction potential of the heme is a major contributor to ΔG: the more oxidizing the potential the higher the driving force. A large driving force is not a requirement for fast electron transfer, however, and a reduction in the reorganization energy will overcome a smaller driving force. In P450s, the reorganization energy is associated with the transition from substrate-free form to the substrate-bound form and as the protein assumes a substrate-bound or substrate-bound-like conformation, it is activated towards electron transfer.

$$k_{et} = \frac{2\pi}{\hbar}(H_{AB})^2 \frac{1}{\sqrt{4\pi\lambda kT}} \exp - \frac{(\Delta G + \lambda)^2}{4kT}$$

Equation 5.1. The Marcus equation. k_{et} is the electron transfer rate constant, $\hbar$ is the reduced Planck's constant, H_{AB} is the electronic overlap, k is the Boltzmann constant, T is the temperature, ΔG is the driving force and λ is the reorganization energy.

In the WT and A330P, it seems that the catalytic cycle remains 'gated' by the first electron transfer. In KT2, the first electron transfer 'gate' is open, and the fact that the leak rate of catalytic consumption of NADPH remains low indicates the presence of one or more other 'gates' beyond oxygen binding to the ferrous form. In the I401P variant, each of these 'gates' is open, at least partially, and the enzyme catalyses NADPH oxidation even in the absence of substrate. The higher k_f values in KT2 and I401P indicate that, for these enzymes, the onus on substrates to induce conformational changes required to facilitate the first electron transfer is essentially eliminated, which is consistent with the structural similarities between I401P, KT2 and the SB WT (Sections 5.3 and 5.4).

5.2.2 The palmitate-bound form

The heme reduction potentials (Figure 5.4) and first electron transfer rate constants (Figure 5.5) were determined in the presence of palmitate for the WT and the I401P and KT2 variants. A330P was not studied, as palmitate binding does not induce a spin-state shift in this variant. These results are collected in Table 5.3. The K_M and k_{cat} of KT2 with palmitate were determined in 50 mM Tris, pH 7.4 (Figure 5.6).

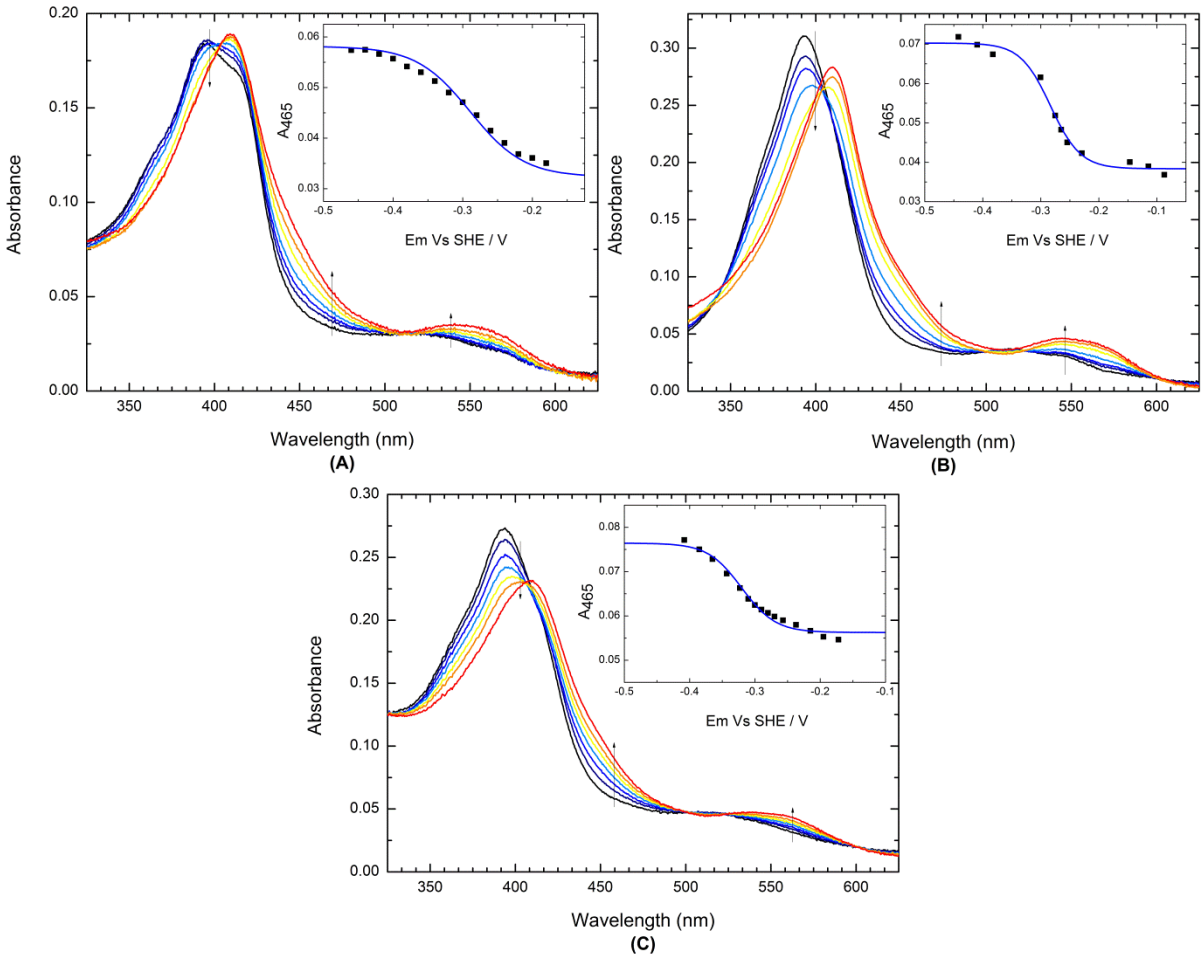

Figure 5.4. Potentiometric titrations for palmitate-bound forms of **(A)** WT; **(B)** I401P; **(C)** KT2. The insets show non-linear least-squares fits of absorbance at 465 nm to a sigmoidal form of the Nernst equation with *n*, the number of electrons fixed at 1.

The spectrum of the fully oxidized form of palmitate-bound WT shows that the heme has a mixed spin state (*ca.* 90% high-spin), as the 200 μM palmitate is not sufficient to induce a full spin-state shift in the WT. λ_{max} = 395 nm for the fully oxidized form, while the fully reduced form has a λ_{max} = 414 nm. There is an isosbestic point at 404 nm, with the exception of the fully oxidized spectrum, which is slightly below the other spectra in this region owing to the mixed spin-state. The sigmoidal fit of the absorbance change at 465 nm for this titration is not ideal, with n = 1.32, though the potential was unaffected by the large n value.

Palmitate-bound I401P and KT2 are broadly similar to the palmitate-bound WT, with the exception that they are fully high-spin in these conditions, and so have an isosbestic point at 404 nm. The n values for these titrations are 0.86 and 1.19 respectively. Once again in the I401P spectrum there is a hint of a shoulder at 440 nm, though this is much less pronounced than the SF form.

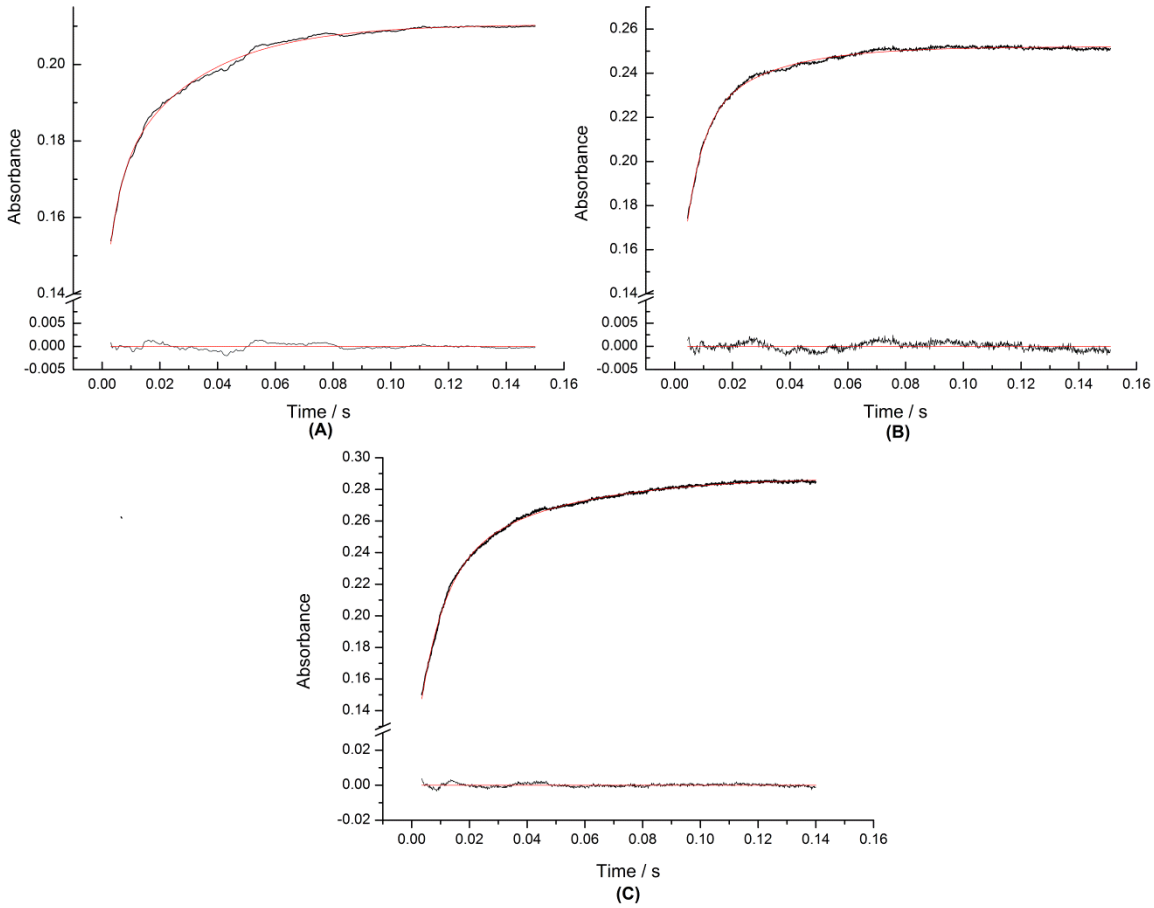

Figure 5.5. Time courses for $Fe^{II}(CO)$ complex formation monitored at 450 nm for palmitate-bound forms of **(A)** WT, which required a double exponential to fit contributions from the fast (47%) and denatured (53%) phases; **(B)** I401P, which required a double exponential to fit contributions from fast (70%) and denatured (30%) phases; **(C)** KT2, which required a double exponential to fit contributions from the fast (72%) and denatured (28%) phases.

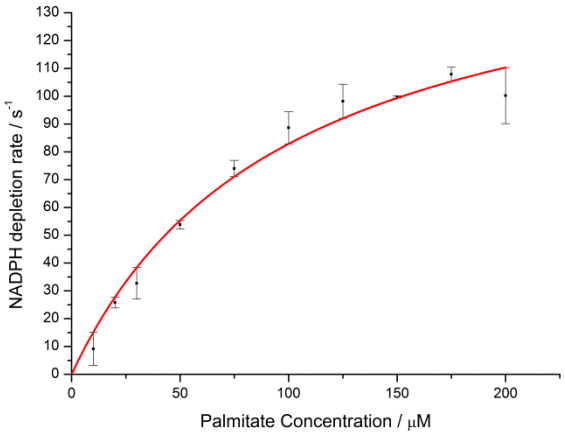

Figure 5.6. Hyperbolic fit of the NADPH consumption rate against substrate concentration for the determination of K_M and k_{cat} of palmitate with KT2.

Table 5.3. Midpoint potentials for the heme domains of palmitate-bound $P450_{BM3}$ variants (E), rate constants for the formation of the Fe^{II}—CO complexes of the full-length proteins (k_f) with relative amplitudes for the fastest phase observed in parentheses. Spin-state shifts and N values for all variants, as well as K_M and k_{cat} for WT and I401P obtained by Dr. Christopher Whitehouse.

	WT	KT2	I401P
E (mV)	–317 ± 17	–303 ± 19	–274 ± 8
k_f (s^{-1})	226 ± 15 (60%)	277 ± 26 (72%)	191 ± 6 (70%)
k_{cat} (s^{-1})	91.4 ± 8.9	111 ± 10	76.3 ± 1.7
K_M (μM)	42.4 ± 8.5	66.0 ± 13	17.2 ± 1.4
N (nmol (nmol-P450)$^{-1}$ s^{-1})	72.2 ± 3.9	87.9 ± 0.47	69.3 ± 0.48
% High-spin	90	100	100

Palmitate binding induces a 90% spin-state shift in the WT and both I401P and KT2 are fully high-spin in the presence of the fatty acid. The heme reduction potential of WT shifts by 132 mV upon palmitate binding to –317 ± 17 mV. A similar shift is observed in KT2, where the palmitate-bound heme reduction potential is –303 ± 19 mV, and the potential of I401P is slightly more oxidizing in the presence of palmitate at –274 ± 8 mV.

The binding of palmitate promotes electron transfer in the WT, which has a k_f of 226 ± 15 s^{-1} in the palmitate-bound form. Though the first electron transfer was already fast in SF KT2, palmitate binding slightly accelerates it to 277 ± 26 s^{-1}, while palmitate binding reduces the k_f of I401P slightly to 191 ± 6 s^{-1}.

The K_M and k_{cat} values for WT with palmitate are 42.4 ± 8.5 μM and 91.4 ± 8.9 s^{-1} respectively, which allows for a high N value of 72.2 ± 3.9 s^{-1}. KT2 has a larger K_M, at 66 ± 13 μM and a higher k_{cat} of 110 ± 10 s^{-1} which leads to N = 87.9 ± 0.47 s^{-1}. The I401P has a lower K_M (17.2 ± 1.4 μM) than the WT enzyme, though the k_{cat} is decreased in this variant (76.3 ± 1.7 s^{-1}) and thus the NADPH consumption rate is also decreased, at 69.3 ± 0.48 s^{-1}. This is because under standard turnover conditions for a natural substrate, 200 μM palmitate and 250 nM $P450_{BM3}$, each variant is fully saturated and so with palmitate NADPH consumption rates are most reflective of the k_{cat}, with I401P being the slowest variant with palmitate and KT2 being the fastest.

5.2.3 Propylbenzene-bound

Propylbenzene is a non-natural substrate towards which WT $P450_{BM3}$ is particularly active, with a PFR >10 s^{-1}, while the substrate induces a 10% spin-state shift in the enzyme[4]. KT2 is highly active towards this substrate, with a PFR of 2244 min^{-1} and a spin-state shift to 25%[4]. The reduction potentials (Figure 5.7) and first electron transfer rate constants (Figure 5.8) of WT and KT2 in the presence of propylbenzene were determined, as were the K_M and k_{cat} of the enzymes with propylbenzene (Figure 5.9) in 50 mM Tris, pH 7.4. This marks the first report of the reduction potential and first electron transfer rate constant being determined for a $P450_{BM3}$ variant for a non-natural substrate. These results are summarized in Table 5.4.

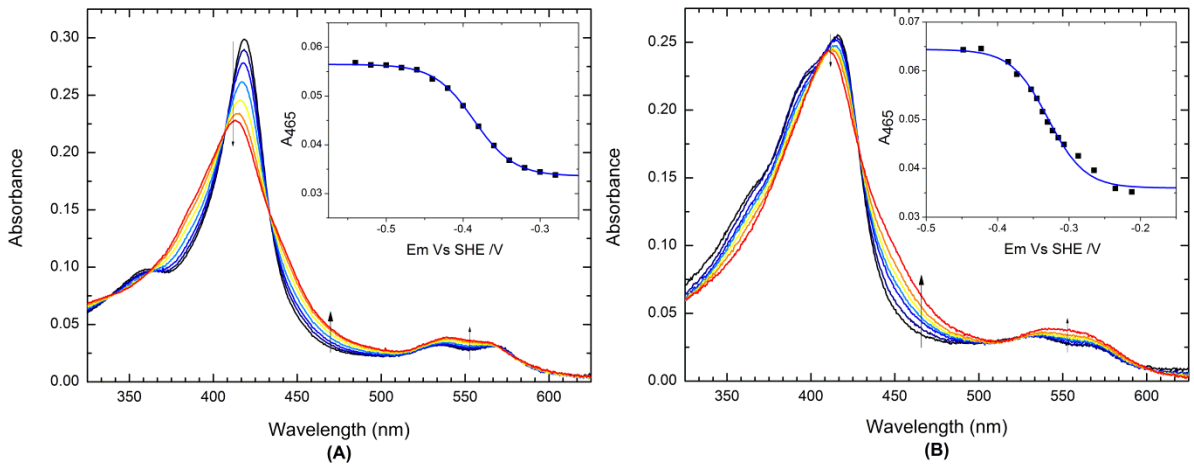

Figure 5.7. Potentiometric titrations for propylbenzene-bound forms of **(A)** WT; **(B)** KT2. The inset shows a non-linear least-squares fit of absorbance at 465 nm to a sigmoidal form of the Nernst equation with the number of electrons fixed at 1.

λ_{max} = 418 nm for the fully oxidized form of the propylbenzene-bound WT, and the substrate induces a small spin-state shift in the enzyme (*ca.* 10%). There are two clear isosbestic points, at 404 nm and 435 nm. There is a relatively large absorbance drop from the fully-oxidized to fully-reduced forms and the absorbance change at 550 nm is small. The heme reduction potential of propylbenzene-bound WT was determined to be –400 ± 15 mV. The *n* value for this experiment was 1.02. Propylbenzene-bound KT2 is broadly similar to the WT, with isosbestic points at 404 and 435 nm, but the heme is *ca.* 25% high-spin in the fully oxidized form and *n* = 1.15. The heme reduction potential, however, was shifted to a significantly more oxidizing value of –334 ± 6 mV which was slightly more reducing than that of the palmitate-bound form. This indicates that larger reduction potential shifts result from substrates which induce larger spin-state shifts and towards which the enzyme is more active. This has also been noted in the drug metabolising enzyme CYP3A4, where the erythromycin bound form has a spin-state shift of 11% and the reduction potential is 10 mV more oxidizing, and testosterone induces an 81% spin-state shift and the reduction potential is 80 mV more positive[10].

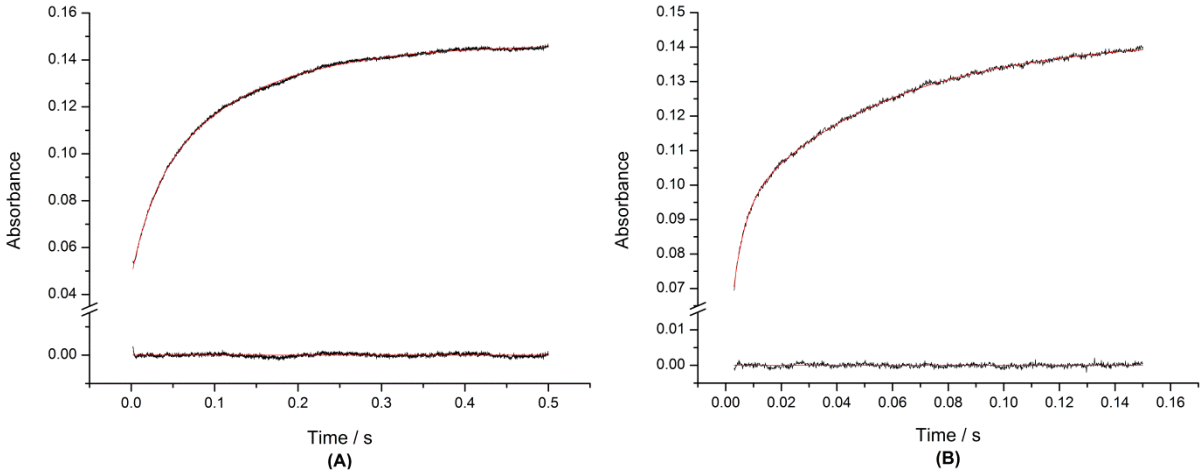

Figure 5.8. Time courses for $Fe^{II}(CO)$ complex formation monitored at 450 nm for propylbenzene-bound forms of **(A)** WT, which required a double exponential to fit contributions from the fast (30%) and slow (70%) phases; **(B)** KT2, which required a double exponential to fit contributions from the fast (51%) and denatured (49%) phases.

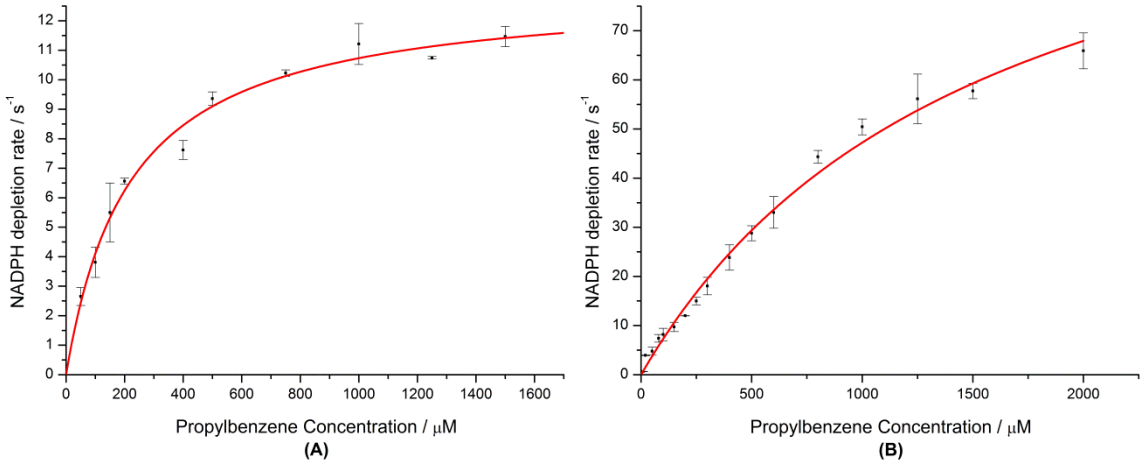

Figure 5.9. Determination of K_M and k_{cat} of propylbenzene with **(A)** WT; **(B)** KT2.

The k_f of WT increases from 1.5 s^{-1} to 38.5 ± 4.7 s^{-1} upon the binding of propylbenzene, sufficient to allow the observed NADPH depletion rate of *ca.* 15 s^{-1} in turnover assays. As propylbenzene also induces a more substantial change in heme reduction potential in KT2 than WT, the k_f of KT2 with propylbenzene is similarly affected, increasing to 200 ± 15 s^{-1}.

Table 5.4. Midpoint potentials for the heme domains of propylbenzene-bound $P450_{BM3}$ variants (E), rate constants for the formation of the Fe^{II}—CO complexes of the full-length proteins (k_f) with relative amplitudes for the fastest phase observed in parentheses. Spin-state shifts and N values obtained by Dr. Christopher Whitehouse.

	WT	KT2
E (mV)	–400 ± 15	–334 ± 6
k_f (s^{-1})	38.5 ± 4.7 (30%)	200 ± 15 (50%)
k_{cat} (s^{-1})	13.1 ± 0.6	121 ± 7
K_M (μM)	218 ± 34	1560 ± 160
N (nmol (nmol-P450)$^{-1}$ s^{-1})	14.9 ± 0.5	46.8 ± 0.55
% High-spin	10	25

WT has a significantly lower K_M with propylbenzene than KT2, with respective K_M values of 218 ± 34 μM and 1560 ± 160 μM. The k_{cat} values also vary greatly, with KT2 having a k_{cat} nearly 10-times as high as the WT, 121 ± 7 s^{-1} *vs.* 13.1 ± 0.6 s^{-1}. Standard turnover conditions for a non-natural substrate such as propylbenzene are 1000 μM substrate and 250 nM P450; sufficient to ensure saturation of the WT, but not KT2. The lack of saturation is overcome, however, by the vastly improved k_{cat} of KT2.

As a general observation, it appears that the rate enhancement effect of KT2 is solely a result of the increased k_{cat}, while the rate enhancement of I401P may be, at least in part, due to a decrease in K_M as observed with palmitate. This may extend to other substrates, allowing for tighter binding of non-natural substrates by I401P. As the first electron transfer rate of WT, I401P and KT2 would allow for a higher oxidation rates than are observed, the first electron transfer does not appear to be rate limiting in the $P450_{BM3}$ catalytic cycle. A step (or steps) further along the catalytic cycle (Section 1.1.2), such as the second electron transfer, O—O bond cleavage, or product release, contribute significantly to the overall rate of the catalytic process.

5.3 Crystal structures of generic accelerators

Of critical importance to the investigation of the rate accelerating properties of A330P, I401P and KT2 was the determination of the X-ray crystal structures. This was accomplished by the group of Professor Zihe Rao, Nankai University in China, while Dr. Christopher Whitehouse completed structural analysis. The results presented in this section have been published[2, 3, 6].

5.3.1 A330P (PDB code: 3M4V)

In molecule A of the two in the asymmetric unit, all residues from 5 onwards are resolved, but residues 189–201, in the F/G loop, are unresolved in molecule B, though this is common in P450 structural biology[11-13]. The 271 'structurally invariant' residues[14] align well with the SF WT structure[15] (PDB code: 1BU7), as does the I-helix. However, there is significant perturbation in the substrate recognition site[16-18], in the region of A330P. The backbone atoms in the mutated residue align well with their WT counterparts, with an average deviation of 0.8 Å, while the backbone atoms of Pro329 have moved on average 2.3 Å. The introduction of a proline at residue 330 has forced Pro329 into the lumen of the substrate access channel, restricting access to the heme iron (Figure 5.10).

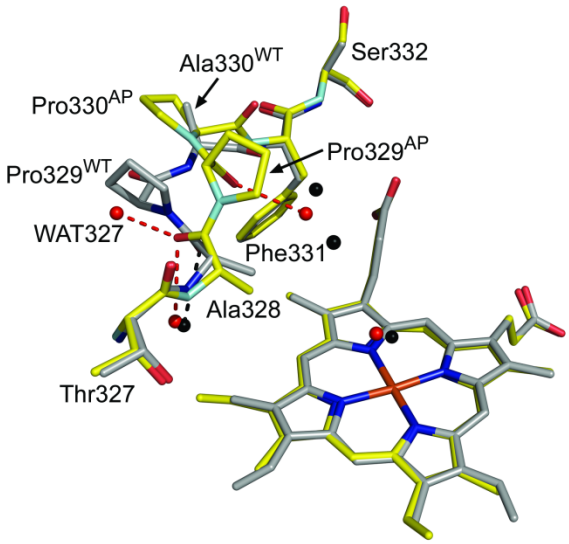

Figure 5.10. Active site of the A330P variant overlaid with SF WT. A330P (PDB code: 3M4V) is shown in yellow, with waters and hydrogen bonds in red and SF WT (PDB code: 1BU7) is shown in grey, with waters and hydrogen bonds in black.

The relocation of Pro329 into the active site also disrupts the water content. At the entrance to the active site, as in WT, a chain of water molecules extends towards the heme iron. In the WT enzyme, the chain terminates with the axial water ligand, which is stabilized through this hydrogen-bond network and through a hydrogen-bond to the carbonyl oxygen of Ala264. In A330P, however, the chain of water molecules extending through the active site terminates 5.5 Å from the axial water ligand, with a water molecule bound to the carbonyl oxygen of Pro329. Thus, the axial water ligand is stabilized only by a hydrogen-bond to the carbonyl oxygen of Ala264.

As a result of the constricted access to the heme iron, A330P possesses unusual activity, notably the elimination of activity towards medium- to long-chain fatty acids. The more restricted active site does, however, improve activity towards small molecules such as propane (Chapter 3) and alters product profiles, such as giving 30% *o*-propylphenol from propylbenzene, compared to 1% from the WT[3, 19].

5.3.2 I401P (PDB code: 3HF2)

Unlike the A330P variant, which generally aligned well with the WT structure with the exception of the region of the mutation, the single proline mutation in I401P caused a number of complex changes. Figure 5.11 shows the active site of the SF I401P variant overlaid with the substrate-free WT structure, as well as with the *N*-palmitoylglycine (NPG)-bound WT structure (PDB code: 1JPZ)[14]. As in the A330P structure, the 'structurally invariant' residues align well with the WT (1BU7) structure, while parts of the F-helix and the F/G and G/H loops are unresolved. This suggests that the shift between the open and closed conformations is facile.

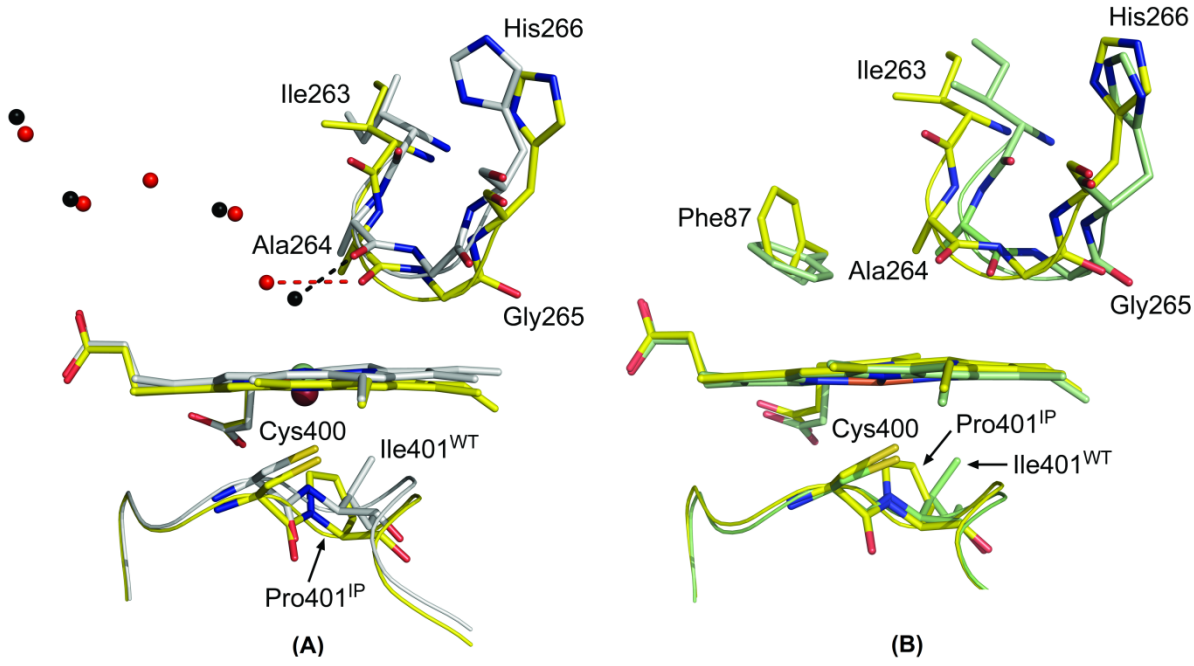

Figure 5.11. Active site of the I401P variant. I401P shown in yellow, with the iron in brown and waters and hydrogen bonds in red. **(A)** Overlay with SF WT (PDB code: 1BU7), which is shown in grey, including the iron atom, with waters and hydrogen bonds in black. **(B)** Overlay with NPG-bound WT (PDB code: 1JPZ) shown in green.

The heme iron in I401P is slightly below the plane of the porphyrin ring owing to a 0.6 Å drop in the C_α and C_β atoms of the ligating cysteine. The axial water ligand is located

more than 1 Å further from the heme iron, at 3.65 Å, compared to 2.6 Å in the WT structure, and is off-axial (S-Fe-O bond angle is 161.5^{o}), which is consistent with the partially high-spin characteristic of the enzyme. The off-axial water remains hydrogen-bonded to the carbonyl oxygen of Ala264. This SF I401P feature is similar to the NPG-bound WT structure[14], as illustrated in Figure 5.10.

The crystal structure of I401P displays further similarities to the SB WT form of the enzyme. Four consecutive inter-helical hydrogen bonds in the oxygen bonding region of the I-helix fail to form as a result of the reorientation of the carbonyl oxygen in Gly265 and the side chain of His266, compared to two in the SF WT. This reduces the kink angle in the I-helix which may facilitate oxygen binding and activation. Although the imidazole ring of $His266_{I401P}$ overlays more closely onto the NPG-WT equivalent, it is not rotated through 180°. The Ile263 side chain overlays more closely onto its SF WT equivalent because there is no substrate present to push it away from the active site.

These changes in the I-helix region resemble the SB WT enzyme, though other portions of the I-helix remain SF-like. The side chain of Phe87 is not rotated through 90^{o} and does not lie parallel to the heme[20].

5.3.3 KT2 (PDB code: 3PSX)

The crystal structure of SF KT2 has been solved to 1.9-Å resolution. Like the crystal structure of SF I401P and several other P450s[21, 22], portions of the highly mobile F-helix, F/G loop and G-helix are unresolved. Also like the I401P structure, the structure of KT2 more closely resembles the SB WT than the SF WT enzyme.

When the backbone C_{α} atoms of the 411 resolved residues in KT2 are compared to those of the SF WT enzyme (1BU7), the root mean squared deviation (r.m.s.d.) is 0.79–1.09 Å, which is much higher than the comparable value with the SB WT structure, which is

0.49 Å. Many of the similarities between SF KT2 and SB WT are a result of a translation of the G-helix towards the E-helix. The side chain of Ile219 impacts Phe158, which must rotate *ca.* 90° about the C_α—C_β bond to avoid steric crowding, in turn causing the rotation of Phe261 by *ca.* 90° about the C_α—C_{ipso} bond. The functional role of this 'phenylalanine cascade' (Figure 5.12) is unclear. Though there has been speculation that non-natural substrate oxidation products may exit the active site through an opening beside Phe261[23], this opening is not enlarged by the induced Phe261 rotation.

A second structural similarity between SF KT2 and SB WT which also results from the relocation of the G-helix is that one of the two ion-pairs usually linking the G-helix to the I-helix, Lys224-Asp251, is broken and the other Asp217-Arg255 remains intact only as a result of the side chain of Arg255 lying in a more extended conformation. This ion-pair breaking disrupts the turn pattern of the I-helix and reduces the kink angle of the dioxygen binding region. This new I-helix conformation is the same observed in SB WT.

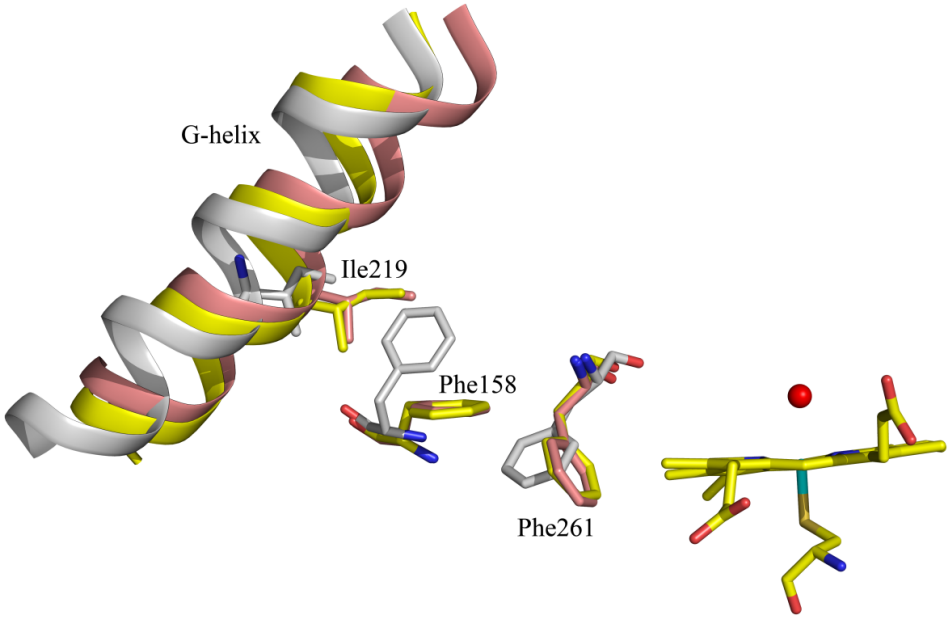

Figure 5.12. The 'phenylalanine cascade.' KT2 is shown in yellow, SF WT (PDB code: 1BU7) in grey and NPG-bound WT (PDB code: 1JPZ) in salmon.

An interesting result of the I-helix adopting the same conformation as in SB WT is that the axial water ligand in KT2 is not hydrogen-bound to the carbonyl oxygen of Ala264. Instead, this oxygen is bound to a water molecule found in the dioxygen binding groove which is absent in SF WT, but present in the NPG-bound form. The failure of the axial water ligand to form a stabilizing hydrogen bond to Ala264 is unusual in $P450_{BM3}$ structures and indeed one of the more interesting aspects of the SF KT2 structure is the location of this water molecule. This is shown in Figure 5.13. The axial water ligand does not relocate to the SB type position upon the shift in the I-helix. Indeed, it remains 2.6 Å from the heme iron, which has dropped 0.2 Å below the plane of the porphyrin in response to a drop of the ligating cysteine by 0.3 Å (half the distance in SB WT).

There are several key differences between molecule A and B of the asymmetric unit. In molecule A, as in the SF WT enzyme, the aromatic ring of Phe87 is perpendicular to the heme, while in the SB WT form it rotates 90^{o} to lie parallel to the heme and displacing the axial water (Section 1.2.2). In molecule B of SF KT2, the aromatic side chain of Phe87 has rotated *ca.* 60^{o}, to a position closer to the SB form than the SF form, though not far enough to displace the axial water ligand. Phe87 tends to move in tandem with Leu437[24], and in molecule B Leu437 has been retracted into the SB WT position, while it remains in the SF WT position in molecule A.

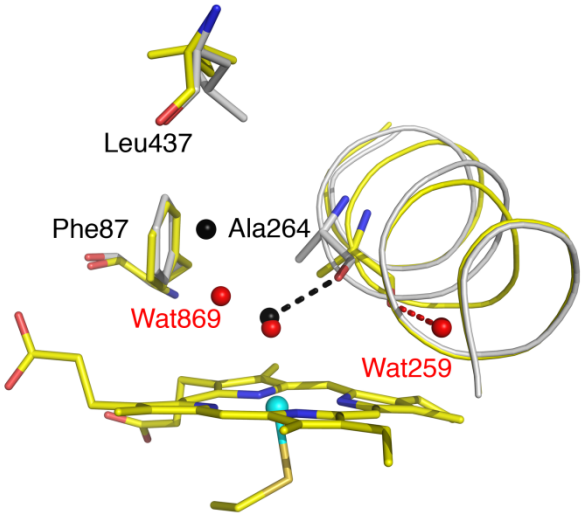

Figure 5.13. Active site of KT2 overlaid with SF WT (PDB code: 1BU7). KT2 is shown in yellow with waters and hydrogen bonds in red, SF WT is shown in grey with waters and hydrogen bonds in black.

It is not immediately obvious why the five mutations in KT2 cause these structural alterations. Ala191 is in the often unresolved F/G loop, though it can be imagined that the substitution of a polar threonine alters the behaviour of this region. There are no structural deviations in the regions of three of the substitutions I259V, A276T and L353I, so their impact is unknown. A histidine mutation at Asn239 is also present in the 21B3 variant, which also displays increased oxidation rates[25]. Asn239 lies at the protein surface and in the SB WT form fails to form a hydrogen-bond with the Gln229 side-chain which is found in SF WT. This hydrogen-bond, which constricts the movement of the G/H loop, also fails to form when histidine is introduced at position 239. The lack of this hydrogen-bond may also explain the relocation of the G-helix and resulting loss of the Lys224-Asp251 ion-pair, as Lys224 is the third residue in the G-helix from the G/H loop. Though this residue is important, it is not solely responsible for the enhanced activity of KT2, as upon reversing the mutation the enzyme retains 60–80% of its enhanced product formation rates[6].

5.4 Structural comparisons between the generic accelerator variants

A330P shares more in common with the SF WT structure than with SF I401P, SF KT2 or the SB WT. I401P and KT2 however, have several structural similarities to SB WT, although there are structural differences which may account for the differences in their properties.

The proximal loop drop is more pronounced in the I401P versus KT2. In I401P the nearest water molecule to the heme iron is 3.6 Å away and off-axial, lending I401P a partially high-spin character. In KT2, however, the water remains axial and 2.6 Å from the heme iron, despite lacking the typical stabilizing hydrogen bond to Ala264. Thus, KT2 remains low-spin in the resting state.

The I-helix region in KT2 overlays much better with the NPG-bound WT than I401P. In I401P the Phe87 side chain lies perpendicular to the heme as in SF WT, and Phe158 and Phe261, those involved in the 'phenylalanine cascade' are also in their SF WT positions. The side-chain of His266 is not rotated and, though residue Lys224 is unresolved, it appears that the Lys224-Asp251 ion pair is intact, judging from the positioning of Asp251.

The crystal structures of both SF I401P and SF KT2 each bear resemblance to SB WT (Section 5.2.2 and 5.2.3). No substrate is required to induce the conformational changes required to promote fast first electron transfer, yet in KT2 the leak rate is low. Thus, another conformational change is required to promote the catalytic consumption of electrons from NADPH and both palmitate and propylbenzene are able to induce this change in KT2. It is possible that, as I401P has an accelerated leak rate, this change is present in the SF structure of this variant.

Of the features of the SB WT crystal structure present in I401P and not fully so in KT2, perhaps the most striking is the lack of the axial water ligand in I401P. Though the axial water ligand in KT2 is lacking the stabilizing hydrogen bond to Ala264 found in most P450 structures, the water ligand remains axial, and KT2 is mostly low-spin. With I401P, the water ligand is off-axial and far from the iron centre, imparting I401P with mixed-spin characteristics. As KT2 features more extensive disruption in the I-helix, including a significant reduction in the kink angle and the failure of 2 ion-pairs to form, yet still has a slow leak rate and a SF WT-like reduction potential, the displacement of this axial water ligand is an integral step in altering the heme reduction potential.

In addition to the displacement of the axial water ligand, the increased drop of the heme iron below the plane of the porphyrin ring also likely plays a role in activating the enzyme towards catalytic activity. This is because electron transfer and heme reduction are impacted by the positioning of the proximal loop, which contains both the ligating Cys400 and Ile401. This drop was more complete in I401P than KT2, relative to SB WT.

5.5 Conclusions from generic accelerators

The rate accelerating properties of these enzymes seem to lie in the catalytically ready conformation the enzymes adopt in the resting state. It is likely that the off-axial water ligand in the I401P variant accounts for the shifted reduction potential of the SF I401P, as this is the most prominent feature in the I401P crystal structure not present in the KT2 structure, and heme spin-state broadly correlates to reduction potential.

The catalytically ready conformation the I401P variant adopts in the resting state means fewer substrate-induced structural changes are required to promote electron transfer and initiate the catalytic cycle. This allows I401P, and variants based on this mutation, to be

more active towards a range of non-natural substrates, as illustrated by the metabolism of anionic, neutral and cationic drug compounds by the RP/FV/EV library (Chapter 3).

5.6 P450s and electron transfer proteins from *Rhodopseudomonas palustris*

The spectroelectrochemical titrations used to determine heme reduction potentials of $P450_{BM3}$ variants was also used to determine the reduction potentials of two P450s and several ferredoxin electron transfer proteins. These measurements, along with stopped flow and kinetic data, were used to investigate the support of P450 activity by an alien ferredoxin.

Rhodopseudomonas plaustris is a family of metabolically diverse purple photosynthetic bacteria[26]. Though bacteria classified into this family share some characteristics, each express a unique set of genes tailored to the specific environment in which the bacteria are found[27, 28].

Dr. Stephen Bell isolated two complete P450/ferredoxin/ferredoxin reductase systems and characterized their behaviour: CYP199A2/Pux/PuR from *R. plaustris* CGA009[29], and CYP199A4/HaPux/HaPuR from *R. plaustris* HaA2[30]. CYP199A2 is a *para*-substituted benzoic acid hydroxylase which can also accept electrons from the $P450_{cam}$ ferredoxin Pdx, albeit with only 6% the catalytic activity of its physiological partner. CYP199A4 also oxidizes *para*-substituted benzoic acids and whole cell turnovers with the CYP199A4 system are approximately five times as effective as those using the CYP199A2 system[30]. Though Pux and PuR are the physiological redox partners for CYP199A2, supporting the oxidative demethylation of 4-methoxybenzoate with k_{cat} = 37.9 s^{-1} and K_M = 0.45 μM, monooxygenase activity is also supported by HaPux and HaPuR, with k_{cat} and K_M values of 48.4 s^{-1} and 0.53 μM respectively.

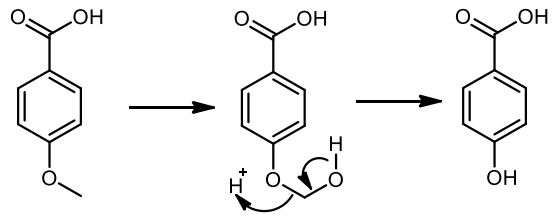

Figure 5.14. Oxidative dealkylation of *p*-methoxybenzoic acid by CYP199A2 or CYP199A4.

The heme reduction potentials of CYP199A2 and CYP199A4 were determined both in the absence of substrate and in the presence of 4-methoxybenzoate, a substrate which induces a >95% spin-state shift. The spectroelectrochemical titrations for the determination of these potentials are shown in Figure 5.15. The reduction potentials of the ferredoxins Pux and HaPux were also determined, and the titration data are shown in Figure 5.16.

The potentiometric titrations of the SF forms of CYP199A2 and A4 are nearly identical, with isosbestic points at 404 and 435 nm, a slight drop in absorbance from the fully oxidized (λ_{max} = 418 nm) to fully reduced (λ_{max} = 414 nm) form. The slight shoulder at 395 nm in the CYP199A2 titration is again due to methyl viologen. The *n* values for the titrations were 1.11 and 0.95 respectively. The substrate-bound forms titrations are similarly nearly identical, with isosbetic points at 404 and 518 nm and *n* = 0.94 for the CYP199A2 titration and 0.85 for the CYP199A4 experiment.

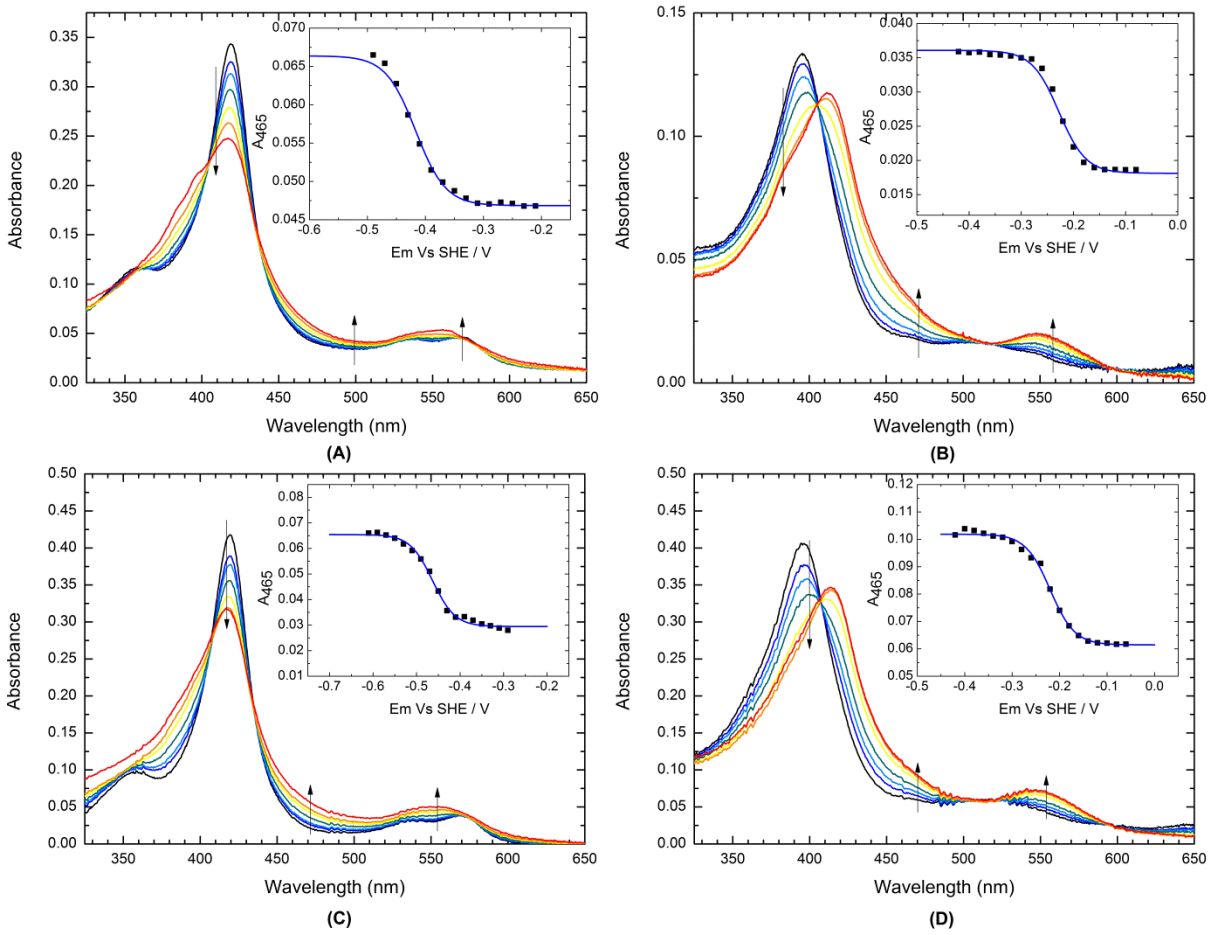

Figure 5.15. Potentiometric titrations for **(A)** SF CYP199A2; **(B)** SB CYP199A2; **(C)** SF CYP199A4; **(D)** SB CYP199A4. The inset shows a non-linear least-squares fit of absorbance at 465 nm to a sigmoidal form of the Nernst equation with the number of electrons fixed at 1.

The SF reduction potentials of both CYP199A2 and CYP199A4 are within the range expected for SF P450s at –432 ± 8 and –461 ± 6 mV respectively. The shift upon the binding of substrate is unexpectedly large for each of these enzymes. The heme reduction potential of CYP199A2 shifts by 218 mV to –227 ± 3 mV, while that of CYP199A4 shifts by 243 mV to –218 ± 3 mV. The reduction potentials of Pux (–251 ± 2 mV) and HaPux (–232 ± 15 mV) are similar to that of Pdx, the ferredoxin associated with $P450_{cam}$, which has a reduction potential of –245 mV[31]. The *n* values for the Pux and HaPux titrations were 0.98 and 0.87 respectively.

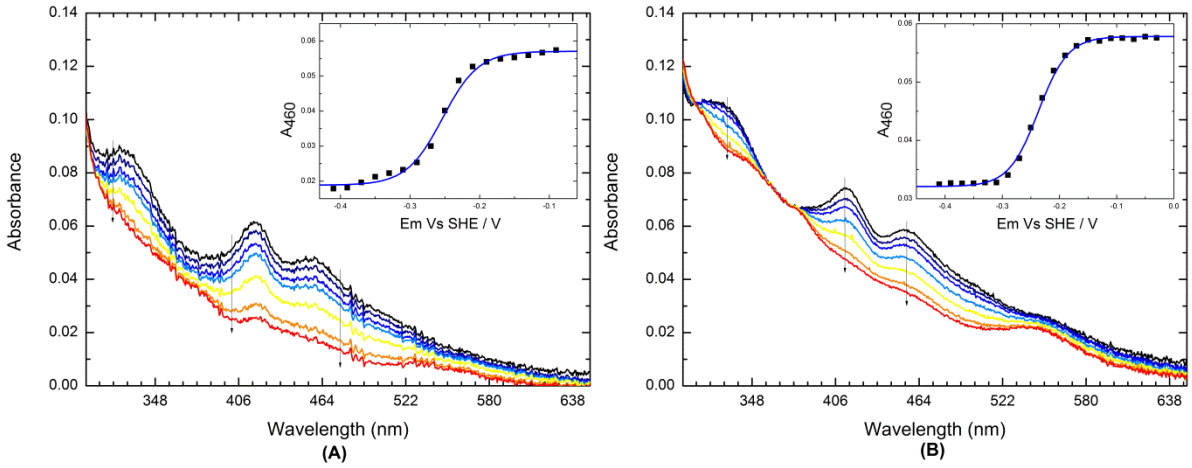

Figure 5.16. Potentiometric titrations for **(A)** Pux; **(B)** HaPux. The inset shows a non-linear least-squares fit of absorbance at 460 nm to a sigmoidal form of the Nernst equation with the number of electrons fixed at 1.

R. plaustris CGA009 has a second [2Fe-2S] ferredoxin, PuxB, which shares 50% sequence identity with Pux but is not associated with a *CYP* gene[31]. PuxB supports CYP199A2 activity, albeit with a reduced k_{cat} (19.1 s^{-1}) and much weaker binding (K_M = 34.3 μM). The increased K_M indicates poor complementarity between the interacting surfaces of the P450 and the ferredoxin. The disfavoured interactions lead to a low turnover rate of 1.65 s^{-1} in activity assays with a ten-fold excess of ferredoxin to P450, compared to 24.0 s^{-1} for Pux and 27.8 s^{-1} HaPux.

Mutagenesis experiments and computer modelling studies on the interactions between $P450_{cam}$ and Pdx as well as CYP11A1 and Adx identified several residues which are important in the P450/ferredoxin interface[32, 33]. Residues 42–44 are part of the iron-sulfur cluster binding loop, which shields the iron centre from the bulk solvent and is likely important in P450 recognition and electron transfer. The surface residues in the α3 helix, as well as those in the C-terminus of the α1 helix that flank the trio of residues from 42–44 are also important in P450 binding.

Sequence alignment of PuxB with Pux and HaPux (Figure 5.17), as well as analysis of the crystal structure of the PuxB/A105R variant have allowed PuxB to be engineered to more effectively support monooxygenase activity with CYP199A2. Previous work by Dr. Stephen Bell identified an engineered PuxB variant, PuxB-5 (A42N/C43A/A44V/M66D/A105V) which supports CYP199A2 activity with a k_{cat} nearly identical to Pux (37.2 s^{-1}) albeit with a K_M that remained high at 28.3 μM[31]. These five mutations all substitute to amino acids found in Pux. Along these lines, Mr. James McMillan, a Part II student in this group, worked to further engineer PuxB to support CYP199A2 activity like Pux.

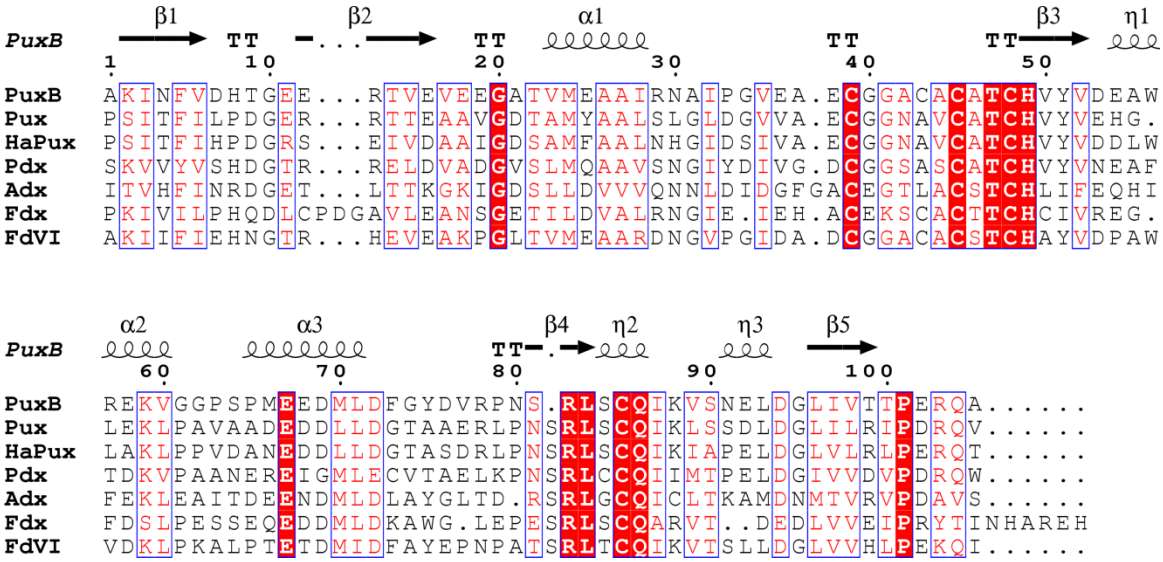

Figure 5.17. Structure-based sequence alignment of PuxB with Pux, HaPux, Pdx, Adx, and the ferredoxins Fdx and FdVI.

Glu36 and Phe73 in PuxB are Val and Gly, respectively, in Pux and HaPux. In the α3 helix, Met66 is Asp in Pux (and was targeted in PuxB-5), Met70 is Leu in Pux and HaPux, while Asp69 and Asp72 are conserved in the three ferredoxins. These residues are highlighted in Figure 5.18, which shows the X-ray crystal structure of PuxB/A105R. When the E36V mutation was added to the PuxB-5 variant, binding to CYP199A2 was tightened (K_M = 19.5 ± 2.3 μM), though k_{cat} was also lowered (28.6 ± 2.1 s^{-1}). In the

PuxB-5/F73G variant, K_M was reduced dramatically to 3.8 ± 0.4 μM, allowing the substrate oxidation rate under standard conditions to be raised to 13.5 ± 1.1 s^{-1}, as the enzyme is nearly saturated under these conditions, despite k_{cat} being reduced slightly to 30.9 ± 1.1 s^{-1}. The most significant improvement on substrate oxidation rate was with the PuxB-5/E36V/F73G variant, with *N* being increased to 19.4 ± 0.7 s^{-1}. This increase in *N* is a result of both tighter binding (K_M = 2.0 ± 0.2 μM) and a relatively high k_{cat} of 34.1 ± 0.8 s^{-1}.

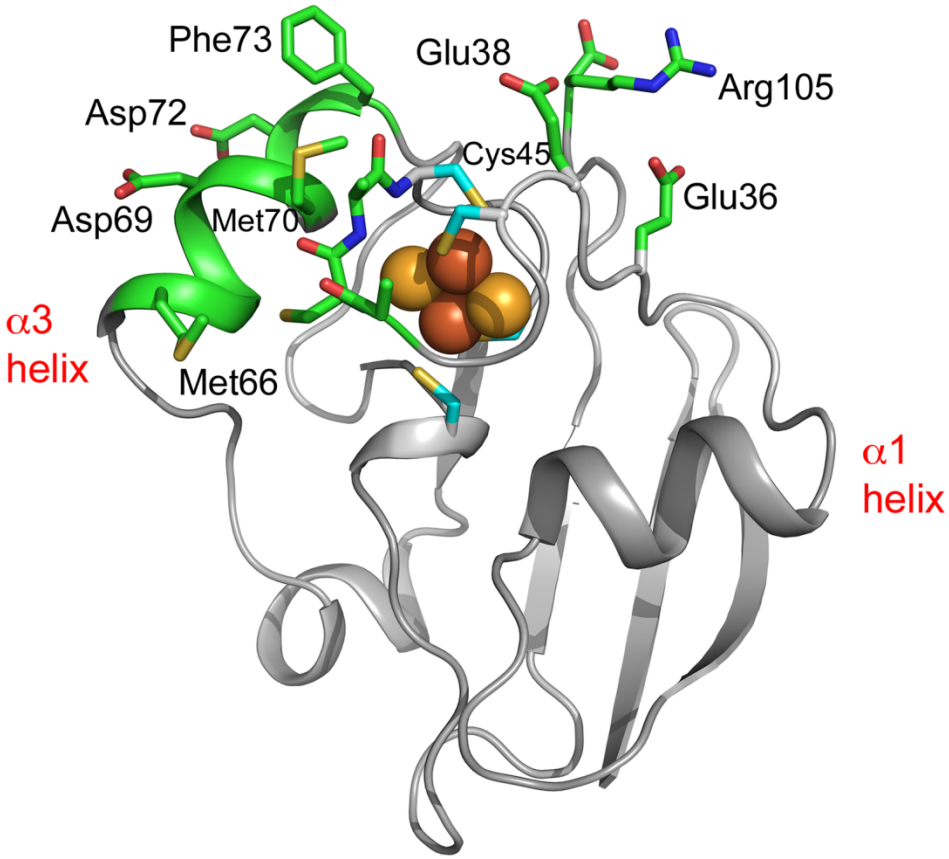

Figure 5.18. The crystal structure of the A105R mutant of PuxB (PDB code: 3HUI) highlighting residues in the likely P450 recognition surface.

In an effort to further understand the engineering of PuxB for the native-like CYP199A2 activity the reduction potentials of PuxB and several of the engineered variants were determined (Figure 5.19). In collaboration with Mr. James McMillian and Mr. Eachan Johnson the rate constant for ferredoxin (Fdx)–to–CYP199A2 intra-complex electron transfer was determined by stopped-flow spectrophotometry. The results of these studies are summarized in Table 5.5.

All six of the examined PuxB variants had very similar potentiometric titrations, with broad peaks at 340, 415 and 460 nm. The *n* values for PuxB, PuxB/M66D/A105V, PuxB-5, PuxB-5/F73G, PuxB-5/E36V/F73G and PuxB-5/E36V/F73G/M70L were 1.23, 1.02, 0.99, 0.97, 0.85 and 1.11 respectively.

The reduction potentials of PuxB, PuxB/M66D/A105V and PuxB-5 were *ca.* 50 mV more reducing than that of Pux, at –291 ± 4, –299 ± 2 and –293 ± 2 mV, respectively. The addition of the F73G mutation to PuxB-5 brings the potential to –257 ± 14 mV, in line with Pux. Interestingly, this variant has an increased k_f over Pux, at 44.4 ± 2.2 s^{-1}, compared to 30.9 ± 0.7 s^{-1}. That the addition of F73G shifts the potential by *ca.* 50 mV indicates that the α3 helix, which contains residue 73, exerts strong influence over the reduction potential of the [2Fe-2S] cluster. For the PuxB-5/F73G/E36V variant, the reduction potential again shifted to a more oxidizing value, similar to that of HaPux, at –225 ± 9 mV. The k_f, 36.0 ± 1.8 s^{-1}, is slightly depressed from that of PuxB-5/F73G, though more than sufficient to support the observed *N* value of 19.4 ± 0.7 s^{-1}. The reduction potential is shifted further, to –202 ± 13 mV, by the addition of the M70L mutation. This mutation also further slows the electron transfer, with k_f to 31.7 ± 1.7 s^{-1}.

Table 5.5. Midpoint potentials and kinetic parameters for CYP199A2-catalysed oxidation of 4-methoxybenzoate under conditions where the first electron transfer from a ferredoxin (Fdx) to CYP199A2 is rate limiting (0.1 μM CYP199A2, 0.5–20 μM Fdx, 0.2 μM PuR, 1 mM 4-methoxybenzoate). The apparent Michaelis-Menten parameters k_{cat} and K_m were obtained from hyperbolic fits of the NADH consumption rate to the Fdx concentration. The rate constant, k_f for the formation of the Fe^{II}—CO complex and K_s the dissociation constant for the formation of the Fdx/CYP199A2 complex were obtained from stopped-flow experiments. *N*: NADH consumption rate under normal activity assay conditions with 0.5 μM CYP199A2, 5 μM Fdx and 1 μM PuR. All data are given as mean ± S.D. for at least three independent experiments. *N*, k_{cat}, K_M, k_f and K_s values obtained by Mr. James MacMillian and Mr. Eachan Johnson. N.D. – Not determined.

Ferredoxin	N (s^{-1})	k_{cat} (s^{-1})	K_M (μM)	E (mV)	k_f (s^{-1})	K_S (μM)
Pux[34]	24.0 ± 0.8	37.9 ± 0.8	0.45 ± 0.1	–251 ± 2	30.9 ± 0.7	0.48 ± 0.08
HaPux[35]	27.8 ± 0.9	48.4 ± 1.9	0.53 ± 0.1	–232 ± 15	N.D.	N.D.
PuxB[36]	1.65 ± 0.03	19.1 ± 0.6	34.3 ± 2.2	–291 ± 4	N.D.	N.D.
PuxB/F73G	1.70 ± 0.1	18.4 ± 2.3	35.2 ± 3.6	N.D.	N.D.	N.D.
PuxB/M66D/A105V[36]	2.6 ± 03	22.7 ± 1.4	36.4 ± 3.6	–299 ± 2	N.D.	N.D.
PuxB/A42N/C43A/A44V/M66D/A105V = PuxB-5[36]	4.70 ± 0.04	37.2 ± 1.8	28.3 ± 2.5	–293 ± 2	N.D.	N.D.
PuxB-5/E36V	5.46 ± 0.8	28.6 ± 2.1	19.5 ± 2.3	N.D.	N.D.	N.D.
PuxB-5/F73G	13.5 ± 1.1	30.9 ± 1.1	3.8 ± 0.4	–257 ± 14	44.4 ± 2.2	2.1 ± 0.4
PuxB-5/E36V/F73G	19.4 ± 0.7	34.1 ± 0.8	2.0 ± 0.2	–225 ± 9	36.0 ± 1.8	1.7 ± 0.2
PuxB-5/E36V/F73G/M70L	14.1 ± 0.9	27.3 ± 0.5	1.4 ± 0.1	–202 ± 13	31.7 ± 1.7	1.0 ± 0.2
PuxB-5/E36V/F73G/R29S	13.4 ± 0.3	32.5 ± 0.5	3.5 ± 0.2	N.D.	N.D.	N.D.

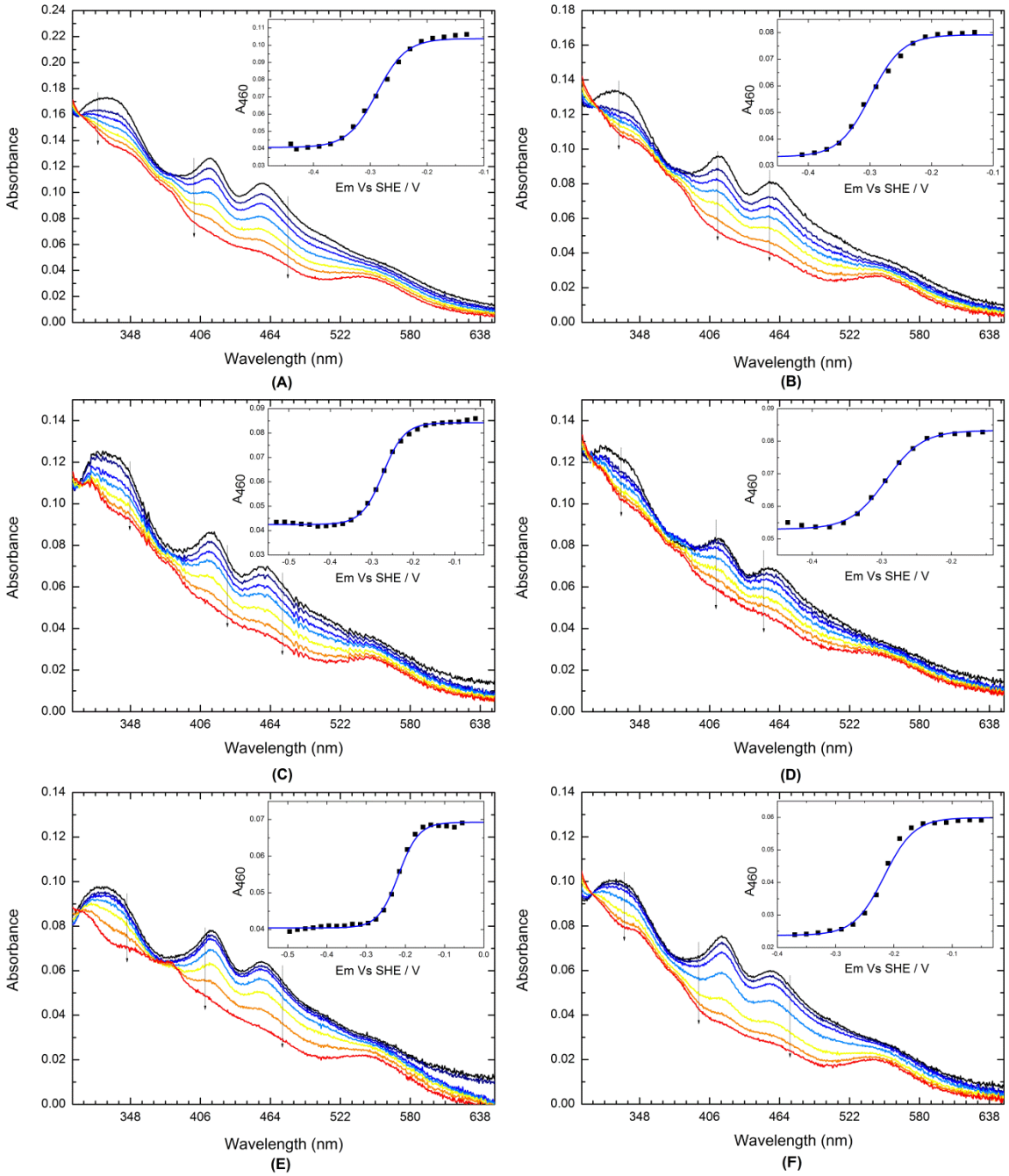

Figure 5.19. Potentiometric titrations for **(A)** PuxB WT; **(B)** PuxB/M66D/A105V; **(C)** PuxB-5; **(D)** PuxB-5/F73G; **(E)** PuxB-5/E36V/F73G; **(F)** PuxB-5/E36V/F73G/M70L. The inset shows a non-linear least-squares fit of absorbance at 460 nm to a sigmoidal form of the Nernst equation with the number of electrons fixed at 1.

It is known that the reduction potential of the ferredoxin may alter on complex-formation with the P450[37, 38]. However, the uncomplexed equilibrium values provide an indication of the thermodynamic driving force. Both the ferredoxin FDVI from *Rhodobacter capsulatus*[39] and Etp1 from *Schizosaccharomyces pombe*[38] also have more negative reduction potentials like PuxB and PuxB-5, at –306 mV and –353 mV respectively. The higher driving force that results from the larger difference between the reduction potentials of the ferredoxins and substrate-bound P450s is likely a significant factor in raising k_f and k_{cat}. The fact that there is a corresponding decrease in k_f with the shift to more oxidizing potentials caused by the addition of the E36V, F73G and M70L suggests that this thermodynamic driving force is the most important factor in determining k_f. Indeed, that HaPux supports higher activity with CYP199A2 than Pux would suggest that even the physiological redox partner can be improved. Indeed, this has been demonstrated with the truncated Adx variants Adx (4-108) and Adx (4-114) showing increased rates of electron transfer to CYP11B1 by Bernhardt *et al*[40]. While reduction potential is an important factor in determining k_f, K_M is a more important parameter in promoting electron transfer to the P450. Unless the ferredoxin binds sufficiently tightly to the P450 to achieve the k_f saturation value, overall activity of the system will remain low. For example, PuxB-5 has a k_{cat} similar to Pux (37.2 ± 1.8 s^{-1} *vs.* 37.9 ± 0.8 s^{-1}) but a K_M over 60 times higher (28.3 ± 2.5 μM *vs.* 0.45 ± 0.1 μM). The much weaker binding prevents the ferredoxin from efficiently transferring electrons to the P450 and the NADH consumption rate drops from 24.0 ± 0.8 min^{-1} with Pux to 4.70 ± 0.04 min^{-1} with PuxB-5.

5.7 Conclusions from redox partner protein engineering

This is the first example of an alien ferredoxin being tailored to overcome the protein recognition barrier and efficiently transfer electrons to a P450 enzyme with turnover activity approaching that of the physiological ferredoxin. This study demonstrated the collective role of the surface residues in the α3 helix and iron-sulfur binding loop in protein binding and electron transfer. Given that PuxB has been engineered to support Pux-like CYP199A2 turnover, it is possible that a P450 enzyme could be tailored to enable practical substrate oxidation rates with non-physiological redox partner proteins.

Chapter Six

Thesis Summary and Future Prospects

The aim of this thesis was to engineer cytochrome $P450_{BM3}$ variants capable of metabolising pharmaceuticals and other chemicals which yield value-added products. A screen of the KSK19/I263A, I401P, F87A/I401P and RLYF/I401P (RP) variants for activity with propranolol, resveratrol, diclofenac and chlorzoxazone showed that a small amount of product was formed in reactions of RP with diclofenac, and so this enzyme was selected as a base variant for further mutagenesis. Second generation variants based on the RP enzyme were engineered to oxidize diclofenac to the two human metabolites, 4′-hydroxydiclofenac from CYP2C9 and 5-hydroxydiclofenac from CYP3A4. The RLYF/F87V/E267V/I401P 'RP/FV/EV' variant was shown to convert >90% of 2 mM diclofenac over 24 h, at 5 μM concentration, while the second generation variant RP/FV/EV/F81W totally converted 2 mM diclofenac at the same concentration. Though this means the total turnover for the enzyme was at best 400, sufficient product was produced from these reactions to allow for complete characterization of the metabolites. It was confirmed that both the RP/FV/EV and RP/FV/EV/F81W variants produced both human primary human metabolites, 4′ and 5-hydroxydiclofenac, though the products could not be separated by HPLC. These variants were also used to hydroxylate testosterone to 15β-, 16β- and 2β-hydroxytestosterone, and lidocaine, to desethyl-lidocaine. The activity of the RP/FV/EV library towards these diverse (anionic, neutral and cationic) compounds serves to highlight the range of compounds this enzyme is capable of oxidizing and establishes it as an excellent template for further studies in drug metabolism. In reactions with RP/FV/EV and related variants there is a trade-off between high coupling and range of substrates oxidized. RP/FV/EV and the related variants are CYP3A4-like, in that they are active towards a range of compounds and produce multiple oxidation products from some substrates, though coupling is low. Engineering enzymes

with higher coupling towards drug compounds could improve total turnover of the system towards a particular drug, though this could lead to enzymes more similar to $P450_{cam}$, which would lack the desired range of accepted substrates and product profiles. Future work should include expanding the range of pharmaceuticals screened for oxidation by this system, a project which is currently underway.

Using the directed evolution variant KSK19, which was developed by Whitehouse *et al*., the oxidation of (+)-valencene was explored, as this presents a different engineering challenge than the oxidation of drugs. The addition of the A328I mutation to KSK19 gave >90% selectivity for C2 oxidation, though the enzyme's total turnover remained low. The second generation variant KSK19/I263A/A328I improved activity and selectivity slightly, though the addition of laurate as a co-substrate nearly doubled activity towards (+)-valencene. The largest improvement in activity was achieved by adding undecane as a second phase, with which total concentration of C2 oxidation products was increased to nearly 400 μM. Future work on this project would include replacing the F87A mutation in KSK19 with F87V, which does not limit turnover in the same way as F87A. Variants based on the I401P variant would also be a potentially interesting avenue to achieving (+)-nootkatone production from (+)-valencene.

A second aim of this thesis was to investigate the origin of the rate enhancing properties of the generic accelerator variants. Heme reduction potentials are a key factor in the P450 catalytic cycle and an important parameter for investigating the origin of the rate enhancing effects, and these can be determined using potentiometric titrations. A custom electrochemical cell was designed, based on the design of Dr. Caprotti, as was an improved gold-mesh based optically transparent thin layer electrode. In addition to improving upon existing designs, a custom electrode system was designed and fabricated, using gold deposited onto a fused-silica strip and patterned using photolithography. The

properties of these patterned gold electrodes were investigated by cyclic voltammetry of small molecule mediators as well as by spectroelectrochemical titrations of mediators and proteins. The experiments revealed that, while the electrodes are viable for use in spectroelectrochemical investigations, they displayed a high resistance across the electrode, as well as slow electron transfer. The high resistance likely results from the connections to the electrodes from the wiring, which were difficult to maintain. These difficult connections, combined with the slow electron transfer, led the electrodes to be abandoned for use in determining the reduction potentials of the generic accelerator variants.

The heme reduction potentials, as well as first electron transfer rate constants and K_M and k_{cat} values were determined for the generic accelerator variants A330P, KT2 and I401P, as well as the WT. In addition, X-ray crystal structures were determined by the group of Professor Zihe Rao at Nankai University. This body of data provided valuable insight into the rate enhancing effects of these variants. It seems that the resting states of the enzymes are in a catalytically ready conformation, and the reorganization energies associated with substrate binding are lower. Thus, the onus on substrate to induce conformational changes required to promote electron transfer is lower which allows the enzymes to be more active to substrates not normally accepted by the WT.

The gold mesh electrode system and electrochemical cell designed for use with the generic accelerator variants was also used to investigate the reduction potentials of CYP199A2 and A4 from *Rhodopseudomonas plaustris*, as well as several ferredoxin electron transport proteins. These investigations were part of a study into the engineering of PuxB, a [2Fe-2S] ferredoxin not associated with a P450 system, to transfer electrons to CYP199A2 as efficiently as the physiological ferredoxin Pux. It can be imagined that, as PuxB has been engineered to support CYP199A2 turnover, it is possible to tailor the

proximal surface of a P450 enzyme to resemble that of CYP199A2, enabling Pux and HaPux to efficiently transfer electrons at rates which would allow for practical turnover and potentially even biotechnical applications. Extensive mutagenesis studies on the residues in CYP199A2 important for protein recognition, as well as analysis of the structure of the Pux/CYP199A2 complex, would be required for this to be accomplished.

References

1. Teoh, K. H.; Polichuk, D. R.; Reed, D. W.; Nowak, G.; Covello, P. S., *FEBS Letters* **2006,** *580*, 1411-1416.
2. Guengerich, F. P., *Chem Res Toxicol* **2001,** *14*, 611-50.
3. Damsten, M. C.; van Vugt-Lussenburg, B. M.; Zeldenthuis, T.; de Vlieger, J. S.; Commandeur, J. N.; Vermeulen, N. P., *Chem Biol Interact* **2008,** *171*, 96-107.
4. Makino, M.; Sugimoto, H.; Shiro, Y.; Asamizu, S.; Onaka, H.; Nagano, S., *P Natl Acad Sci USA* **2007,** *104*, 11591-11596.
5. Whitehouse, C. J.; Bell, S. G.; Wong, L. L., *Chem-Eur J* **2008,** *35*, 10905-10908.
6. Whitehouse, C. J. C.; Rees, N. H.; Bell, S. G.; Wong, L.-L., *Chem-Eur J* **2011,** *17*, 6862-6868.
7. de Montellano, O., *Cytochrome P450: Structure, Mechanizm and Biochemistry.* 3rd ed.; Plenum Publishers: New York, **2005**.
8. Rupasinghe, S.; Schuler, M. A.; Kagawa, N.; Yuan, H.; Lei, L.; Zhao, B.; Kelly, S. L.; Waterman, M. R.; Lamb, D. C., *FEBS Lett* **2006,** *580*, 6338-42.
9. Denisov, I. G.; Shih, A. Y.; Sligar, S. G., *J Inorg Biochem* **2012,** *108*, 150-158.
10. Gotoh, O., *J Biol Chem* **1992,** *267*, 83-90.
11. Nelson, D. R., Cytochrome P450 Nomenclature, 2004. In *Cytochrome P450 Protocols*, 2005; Vol. 320, pp 1-10.
12. Sevrioukova, I. F.; Li, H.; Zhang, H.; Peterson, J. A.; Poulos, T. L., *P Natl Acad Sci USA* **1999,** *96*, 1863-8.
13. Poulos, T. L.; Finzel, B. C.; Howard, A. J., *J Mol Biol* **1987,** *195*, 687-700.
14. Williams, P. A.; Cosme, J.; Ward, A.; Angove, H. C.; Matak Vinkovic, D.; Jhoti, H., *Nature* **2003,** *424*, 464-468.
15. Yano, J. K.; Wester, M. R.; Schoch, G. A.; Griffin, K. J.; Stout, C. D.; Johnson, E. F., *J Biol Chem* **2004,** *279*, 38091-38094.
16. Matsunaga, I.; Yokotani, N.; Gotoh, O.; Kusunose, E.; Yamada, M.; Ichihara, K., *J Biol Chem* **1997,** *272*, 23592-23596.
17. Omura, T.; Sanders, E.; Estabrook, R. W.; Cooper, D. Y.; Rosenthal, O., *Arch Biochem Biophys* **1966,** *117*, 660-673.
18. Lu, A. Y. H.; Coon, M. J., *J Biol Chem* **1968,** *243*, 1331-1332.
19. Lu, A. Y. H.; Junk, K. W.; Coon, M. J., *J Biol Chem* **1969,** *244*, 3714-3721.
20. Hannemann, F.; Bichet, A.; Ewen, K. M.; Bernhardt, R., *BBA-Gen Subjects* **2007,** *1770*, 330-344.
21. Annalora, A. J.; Goodin, D. B.; Hong, W.-X.; Zhang, Q.; Johnson, E. F.; Stout, C. D., *J Mol Biol* **2010,** *396*, 441-451.
22. Yang, W.; Bell, S. G.; Wang, H.; Zhou, W.; Hoskins, N.; Dale, A.; Bartlam, M.; Wong, L.-L.; Rao, Z., *J Biol Chem* **2010,** *285*, 27372-27384.
23. Capdevila, J. H.; Wei, S.; Helvig, C.; Falck, J. R.; Belosludtsev, Y.; Truan, G.; Graham-Lorence, S. E.; Peterson, J. A., *J Biol Chem* **1996,** *271*, 22663-71.
24. Matson, R. S.; Hare, R. S.; Fulco, A. J., *BBA-Lipid Lipid Met* **1977,** *487*, 487-494.
25. Govindaraj, S.; Poulos, T. L., *Biochemistry-US* **1995,** *34*, 11221-11226.
26. Black, S. D.; Martin, S. T., *Biochemistry-US* **1994,** *33*, 12056-62.
27. Girvan, H. M.; Dunford, A. J.; Neeli, R.; Ekanem, I. S.; Waltham, T. N.; Joyce, M. G.; Leys, D.; Curtis, R. A.; Williams, P.; Fisher, K.; Voice, M. W.; Munro, A. W., *Arch Biochem Biophys* **2011,** *507*, 75-85.
28. Gorren, A. C. F.; Mayer, B., *BBA-Gen Subjects* **2007,** *1770*, 432-445.
29. Griffith, O. W.; Stuehr, D. J., *Annu Rev Physiol* **1995,** *57*, 707-736.
30. Hevel, J. M.; White, K. A.; Marletta, M. A., *J Biol Chem* **1991,** *266*, 22789-22791.

31. Bell, S.; Xu, F.; Johnson, E.; Forward, I.; Bartlam, M.; Rao, Z.; Wong, L.-L., *J Biol Inorg Chem* **2010,** *1*, 315-328.
32. Pochapsky, T. C.; Lyons, T. A.; Kazanis, S.; Arakaki, T.; Ratnaswamy, G., *Biochimie* **1996,** *78*, 723-733.
33. Bell, S. G.; Wong, L.-L., *Biochem Biophys Res Co* **2007,** *360*, 666-672.
34. Marohnic, C. C.; Huber Iii, W. J.; Patrick Connick, J.; Reed, J. R.; McCammon, K.; Panda, S. P.; Martásek, P.; Backes, W. L.; Masters, B. S. S., *Arch Biochem Biophys* **2011,** *513*, 42-50.
35. Guengerich, F. P., *Mol Interv* **2003,** *3*, 194-204.
36. Sem, D. S.; Kasper, C. B., *Biochemistry-US* **1995,** *34*, 12768-12774.
37. Enoch, H. G.; Strittmatter, P., *J Biol Chem* **1979,** *254*, 8976-8981.
38. Ilan, Z.; Ilan, R.; Cinti, D. L., *J Biol Chem* **1981,** *256*, 10066-10072.
39. Schacter, B. A.; Nelson, E. B.; Marver, H. S.; Masters, B. S. S., *J Biol Chem* **1972,** *247*, 3601-3607.
40. Whitehouse, C. J. C.; Bell, S. G.; Wong, L.-L., *Chem Soc Rev* **2012,** *41*, 1218-1260.
41. Kühnel, K.; Derat, E.; Terner, J.; Shaik, S.; Schlichting, I., *P Natl Acad Sci USA* **2007,** *104*, 99-104.
42. Rittle, J.; Green, M. T., *Science* **2010,** *330*, 933-937.
43. Luthra, A.; Denisov, I. G.; Sligar, S. G., *Arch Biochem Biophys* **2011,** *507*, 26-35.
44. Jung, C.; Vries, S. d.; Schünemann, V., *Arch Biochem Biophys* **2011,** *507*, 44-55.
45. Porro, C. S.; Sutcliffe, M. J.; de Visser, S. P., *J Phys Chem A* **2009,** *113*, 11635-11642.
46. Woggon, W.-D.; Wagenknecht, H.-A.; Claude, C., *J Inorg Biochem* **2001,** *83*, 289-300.
47. Hollenberg, P. F., *FASEB J* **1992,** *6*, 686-694.
48. Winterbourn, C. C.; Vissers, M. C. M.; Kettle, A. J., *Curr Opin Hematol* **2000,** *7,* 53-58.
49. Warman, A. J.; Roitel, O.; Neeli, R.; Girvan, H. M.; Seward, H. E.; Murray, S. A.; McLean, K. J.; Joyce, M. G.; Toogood, H.; Holt, R. A.; Leys, D.; Scrutton, N. S.; Munro, A. W., *Biochem Soc Trans* **2005,** *33*, 747-53.
50. Munro, A. W.; Leys, D. G.; McLean, K. J.; Marshall, K. R.; Ost, T. W. B.; Daff, S.; Miles, C. S.; Chapman, S. K.; Lysek, D. A.; Moser, C. C.; Page, C. C.; Dutton, P. L., *Trends Biochem Sci* **2002,** *27*, 250-257.
51. Munro, A.; Maclean, K.; Noble, M.; Ost, T.; Green, A.; Robledo, L.; Miles, C.; Murdoch, J.; Chapman, S., *Eds. Springer US*, **2002,** *35*, 297-315.
52. Li, H.; Poulos, T. L., *BBA-Mol Cell Biol L* **1999,** *1441*, 141-149.
53. Peterson, J. A.; Sevrioukova, I.; Turan, G.; Graham-Lorence, S. E.; *Steroids* **1997,** *62*, 117.
54. Li, H.; Poulos, T. L., *Biochim Biophys Acta* **1999,** *1441*, 141-9.
55. Eiben, S.; Kaysser, L.; Maurer, S.; Kuhnel, K.; Urlacher, V. B.; Schmid, R. D., *J Biotechnol* **2006,** *124*, 662-9.
56. Yun, C. H.; Kim, K. H.; Kim, D. H.; Jung, H. C.; Pan, J. G., *Trends Biotechnol* **2007,** *25*, 289-98.
57. Narhi, L. O.; Fulco, A. J., *J Biol Chem* **1986,** *261*, 7160-9.
58. Narhi, L. O.; Fulco, A. J., *J Biol Chem* **1987,** *262*, 6683-90.
59. Miura, Y.; Fulco, A. J., *J Biol Chem* **1974,** *249*, 1880-1888.
60. Shirane, N.; Sui, Z.; Peterson, J. A.; Ortiz de Montellano, P. R., *Biochemistry-US* **1993,** *32*, 13732-41.
61. Miura, Y.; Fulco, A. J., *Biochim Biophys Acta* **1975,** *388*, 305-17.

62. Ahmed, F.; Al-Mutairi, E. H.; Avery, K. L.; Cullis, P. M.; Primrose, W. U.; Roberts, G. C. K,; Willis, C.L.; *Chem Commun* **1999,** *6*, 2049-2050.
63. Cryle, M. J.; Espinoza, R. D.; Smith, S. J.; Matovic, N. J.; De Voss, J. J., *Chem Commun* **2006,** *22*, 2353-5.
64. Ravichandran, K. G.; Boddupalli, S. S.; Hasermann, C. A.; Peterson, J. A.; Deisenhofer, J., *Science* **1993,** *261*, 731-6.
65. Li, H.; Poulos, T. L., *Nat Struct Biol* **1997,** *4*, 140-6.
66. Haines, D. C.; Tomchick, D. R.; Machius, M.; Peterson, J. A., *Biochemistry-US* **2001,** *40*, 13456-65.
67. Stjernschantz, E.; van Vugt-Lussenburg, B. M.; Bonifacio, A.; de Beer, S. B.; van der Zwan, G.; Gooijer, C.; Commandeur, J. N.; Vermeulen, N. P.; Oostenbrink, C., *Proteins* **2007,** *71*, 336-52.
68. Modi, S.; Sutcliffe, M. J.; Primrose, W. U.; Lian, L. Y.; Roberts, G. C., *Nat Struct Biol* **1996,** *3*, 414-7.
69. Jovanovic, T.; Farid, R.; Friesner, R. A.; McDermott, A. E., *J Am Chem Soc* **2005,** *127*, 13548-52.
70. Jovanovic, T.; McDermott, A. E., *J Am Chem Soc* **2005,** *127*, 13816-21.
71. Haines, D. C., *Protein Pept Lett* **2006,** *13*, 977-80.
72. Farinas, E. T.; Alcalde, M.; Arnold, F., *Tetrahedron* **2004,** *60*, 525-528.
73. Huang, W. C.; Westlake, A. C.; Marechal, J. D.; Joyce, M. G.; Moody, P. C.; Roberts, G. C., *J Mol Biol* **2007,** *373*, 633-51.
74. Oliver, C. F.; Modi, S.; Primrose, W. U.; Lian, L. Y.; Roberts, G. C., *Biochem J* **1997,** *327*, 537-544.
75. Cowart, L. A.; Falck, J. R.; Capdevila, J. H., *Arch Biochem Biophys* **2001,** *387*, 117-24.
76. Dietrich, M.; Do, T. A.; Schmid, R. D.; Pleiss, J.; Urlacher, V. B., *J Biotechnol* **2009,** *139*, 115-7.
77. Cirino, P. C.; Arnold, F. H., *Adv Synth Catal* **2002,** *344*, 932-937.
78. Whitehouse, C. J.; Bell, S. G.; Yang, W.; Yorke, J. A.; Blanford, C. F.; Strong, A. J.; Morse, E. J.; Bartlam, M.; Rao, Z.; Wong, L. L., *ChemBioChem* **2009,** *10*, 1654-6.
79. Yeom, H.; Sligar, S. G.; Li, H.; Poulos, T. L.; Fulco, A. J., *Biochemistry-US* **1995,** *34*, 14733-40.
80. Volz, T. J.; Rock, D. A.; Jones, J. P., *J Am Chem Soc* **2002,** *124*, 9724-5.
81. Cryle, M. J.; De Voss, J. J., *Angew Chem Int Edit* **2006,** *45*, 8221-3.
82. Kim, D.-H.; Kim, K.-H.; Kim, D.-H.; Liu, K.-H.; Jung, H.-C.; Pan, J.-G.; Yun, C.-H., *Drug Metab Dispos* **2008,** *36*, 2166-70.
83. Ost, T. W.; Miles, C. S.; Munro, A. W.; Murdoch, J.; Reid, G. A.; Chapman, S. K., *Biochemistry-US* **2001,** *40*, 13421-9.
84. Ost, T. W.; Clark, J.; Mowat, C. G.; Miles, C. S.; Walkinshaw, M. D.; Reid, G. A.; Chapman, S. K.; Daff, S., *J Am Chem Soc* **2003,** *125*, 15010-20.
85. Boddupalli, S. S.; Hasemann, C. A.; Ravichandran, K. G.; Lu, J. Y.; Goldsmith, E. J.; Deisenhofer, J.; Peterson, J. A., *P Natl Acad Sci USA* **1992,** *89*, 5567-71.
86. Gillam, E. M. J., *Clin Exp Pharmacol P* **2005,** *32*, 147-52.
87. Gillam, E. M. J., *Chem Res Toxicol* **2007,** *21*, 220-31.
88. Carmichael, A. B.; Wong, L. L., *Eur J Biochem* **2001,** *268*, 3117-25.
89. Farinas, E. T.; Schwaneberg, U.; Glieder, A.; Arnold, F. H., *Adv Synth Catal* **2001,** *343*, 601-6.
90. Sowden, R. J.; Yasmin, S.; Rees, N. H.; Bell, S. G.; Wong, L. L., *Org Biomol Chem* **2005,** *3*, 57-64.

91. Vugt-Lussenburg, B. M.; Stjernschantz, E.; Lastdrager, J.; Oostenbrink, C.; Vermeulen, N. P.; Commandeur, J. N., *J Med Chem* **2007,** *50*, 455-61.
92. Oliver, C. F.; Modi, S.; Sutcliffe, M. J.; Primrose, W. U.; Lian, L. Y.; Roberts, G. C., *Biochemistry-US* **1997,** *36*, 1567-72.
93. Otey, C. R.; Bandara, G.; Lalonde, J.; Takahashi, K.; Arnold, F. H., *Biotechnol Bioeng* **2006,** *93*, 494-9.
94. Bloom, J. D.; Meyer, M. M.; Meinhold, P.; Otey, C. R.; MacMillan, D.; Arnold, F. H., *Curr Opin Struct Biol* **2005,** *15*, 447-52.
95. Kubo, T.; Peters, M. W.; Meinhold, P.; Arnold, F. H., *Chemistry* **2006,** *4*, 1216-20.
96. Meinhold, P.; Peters, M. W.; Hartwick, A.; Hernandez, A. R.; Arnold, F. H., *Adv Synth Catal* **2006,** *348*, 763–72.
97. Seifert, A.; Vomund, S.; Grohmann, K.; Kriening, S.; Urlacher, V. B.; Laschat, S.; Pleiss, J., *Chembiochem* **2009,** *10*, 853-861.
98. Li, Q. S.; Schwaneberg, U.; Fischer, P.; Schmid, R. D., *Chemistry* **2000,** *6*, 1531-6.
99. Li, Q. S.; Ogawa, J.; Schmid, R. D.; Shimizu, S., *Appl Environ Microbiol* **2001,** *67*, 5735-9.
100. Schulze, H.; Schmid, R. D.; Bachmann, T. T., *Anal Chem* **2004,** *76*, 1720-5.
101. Waibel, M.; Schulze, H.; Huber, N.; Bachmann, T. T., *Biosens Bioelectron* **2006,** *21*, 1132-40.
102. Budde, M.; Morr, M.; Schmid, R. D.; Urlacher, V. B., *ChemBioChem* **2006,** *7*, 789-94.
103. Feenstra, K. A.; Starikov, E. B.; Urlacher, V. B.; Commandeur, J. N.; Vermeulen, N. P., *Protein Sci* **2007,** *16*, 420-31.
104. Branco, R. J.; Seifert, A.; Budde, M.; Urlacher, V. B.; Ramos, M. J.; Pleiss, J., *Proteins* **2008,** *73*, 597-607.
105. Urlacher, V. B.; Makhsumkhanov, A.; Schmid, R. D., *Appl Microbiol Biotechnol* **2006,** *70*, 53-9.
106. Li, H. M.; Mei, L. H.; Urlacher, V. B.; Schmid, R. D., *Appl Biochem Biotechnol* **2008,** *144*, 27-36.
107. Klein, M. L.; Fulco, A. J., *J Biol Chem* **1993,** *268*, 7553-61.
108. Neeli, R.; Girvan, H. M.; Lawrence, A.; Warren, M. J.; Leys, D.; Scrutton, N. S.; Munro, A. W., *FEBS Lett* **2005,** *579*, 5582-8.
109. Neeli, R.; Roitel, O.; Scrutton, N. S.; Munro, A. W., *J Biol Chem* **2005,** *280*, 17634-44.
110. Xu, F.; Bell, S. G.; Lednik, J.; Insley, A.; Rao, Z.; Wong, L. L., *Angew Chem Int Ed* **2005,** *44*, 4029-32.
111. Lipscomb, J. D., *Annu Rev Microbiol* **1994,** *48*, 371-99.
112. Leahy, J. G.; Colwell, R. R., *Microbiol Rev* **1990,** *54*, 305-15.
113. Sumita, T.; Iida, T.; Hirata, A.; Horiuchi, H.; Takagi, M.; Ohta, A., *FEMS Microbiol Lett* **2002,** *214*, 31-38.
114. Stevenson, J.-A.; Westlake, A. C. G.; Whittock, C.; Wong, L.-L., *J Am Chem Soc* **1996,** *118*, 12846-47.
115. Stevenson, J.-A.; K. Bearpark, J.; Wong, L.-L., *New J Chem* **1998,** *22*, 551-2.
116. Bell, S. G.; Stevenson, J.-A.; Boyd, H. D.; Campbell, S.; Riddle, A. D.; Orton, E. L.; Wong, L.-L., *Chem Commun* **2002,** 490-1.
117. Munro, A. W.; Lindsay, J. G.; Coggins, J. R., *Biochem Soc Trans* **1993,** *21*, 412S.
118. Appel, D.; Lutz-Wahl, S.; Fischer, P.; Schwaneberg, U.; Schmid, R. D., *J Biotechnol* **2001,** *88*, 167-71.

119. Fasan, R.; Meharenna, Y. T.; Snow, C. D.; Poulos, T. L.; Arnold, F. H., *J Mol Biol* **2008,** *383*, 1069-80.
120. Meinhold, P.; Peters, M. W.; Chen, M. M.; Takahashi, K.; Arnold, F. H., *ChemBioChem* **2005,** *6*, 1765-8.
121. Kawakami, N.; Shoji, O.; Watanabe, Y., *Angew Chemie Int Edit* **2011,** *50*, 5315-8.
122. Zilly, F. E.; Acevedo, J. P.; Augustyniak, W.; Deege, A.; Häusig, U. W.; Reetz, M. T., *Angew Chem Int Ed* **2011,** *50*, 2720-4.
123. Chappell, J., *Trend Plant Sci* **2004,** *9*, 266-9.
124. Karp, F.; Mihaliak, C. A.; Harris, J. L.; Croteau, R., *Arch Biochem Biophys* **1990,** *276*, 219-26.
125. Fraatz, M.; Berger, R.; Zorn, H., *Appl Microbiol Biot* **2009,** *83*, 35-41.
126. Davies, A. G.; Davison, I. G. E., *J Chem Soc Perk T 2* **1989,** *7*, 825-30.
127. Shaffer, G. W.; Eschinasi, E. H.; Purzycki, K. L.; Doerr, A. B., *J Org Chem* **1975,** *40* , 2181-5.
128. Bombarda, I.; Gaydou, E. M.; Smadja, J.; Faure, R., *J Agr Food Chem* **1996,** *44*, 217-22.
129. Bell, S. G.; Chen, X.; Sowden, R. J.; Xu, F.; Williams, J. N.; Wong, L.-L.; Rao, Z., *J Am Chem Soc* **2002,** *125*, 705-14.
130. Kim, D.; Ortiz de Montellano, P., *Biotechnol Lett* **2009,** *31*, 1427-31.
131. Hu, M.-C.; Hsu, H.-J.; Guo, I.-C.; Chung, B.-C., *Mol Cell Endocrinol* **2004,** *215*, 95-100.
132. Pikuleva, I. A., *Pharmacol Therapeut* **2006,** *112*, 761-73.
133. Pellissier, H.; Santelli, M., *Org Prep Proced Int* **2001,** *33*, 1-58.
134. Wong, L.-L., *ChemBioChem* **2011,** *12*, 2537-9.
135. Lewis, J. C.; Mantovani, S. M.; Fu, Y.; Snow, C. D.; Komor, R. S.; Wong , C.-H.; Arnold, F. H., *ChemBioChem* **2010,** *11*, 2502-5.
136. van Vugt-Lussenburg, B. M.; Damsten, M. C.; Maasdijk, D. M.; Vermeulen, N. P.; Commandeur, J. N., *Biochem Biophys Res Commun* **2006,** *346*, 810-8.
137. Vottero, E.; Rea, V.; Lastdrager, J.; Honing, M.; Vermeulen, N.; Commandeur, J., *J Biol Inorg Chem* **2011**, *16*, 899-912.
138. Kille, S.; Zilly, F. E.; Acevedo, J. P.; Reetz, M. T., *Nat Chem* **2011,** *3*, 738-43.
139. Powell, K. A.; Ramer, S. W.; del Cardayré, S. B.; Stemmer, W. P. C.; Tobin, M. B.; Longchamp, P. F.; Huisman, G. W., *Angew Chem Int Edit* **2001,** *40*, 3948-59.
140. Gillam, E. M.; Aguinaldo, A. M.; Notley, L. M.; Kim, D.; Mundkowski, R. G.; Volkov, A. A.; Arnold, F. H.; Soucek, P.; DeVoss, J. J.; Guengerich, F. P., *Biochem Biophys Res Commun* **1999,** *265*, 469-72.
141. Park, S.-H.; Kim, D.-H.; Kim, D.; Kim, D.-H.; Jung, H.-C.; Pan, J.-G.; Ahn, T.; Kim, D.; Yun, C.-H., *Drug Metab Dispos* **2010,** *38*, 732-9.
142. Celik, A.; Speight, R. E.; Turner, N. J., *Chem Commun* **2005,** 3652-4.
143. Bloom, J. D.; Labthavikul, S. T.; Otey, C. R.; Arnold, F. H., *P Natl Acad Sci USA* **2006,** *103*, 5869-74.
144. Lussenburg, B. M.; Babel, L. C.; Vermeulen, N. P.; Commandeur, J. N., *Anal Biochem* **2005,** *341*, 148-55.
145. Tsotsou, G. E.; Cass, A. E. G.; Gilardi, G., *Biosens Bioelectron* **2002,** *17*, 119-31.
146. Tsotsou, G. E.; Sideri, A.; Goyal, A.; Di Nardo, G.; Gilardi, G., *Chem Eur Jl* **2012,** *18*, 3582-8.
147. Glieder, A.; Meinhold, P., *Methods Mol Biol* **2003,** *230*, 157-70.
148. Reetz, M. T.; Bocola, M.; Carballeira, J. D.; Zha, D.; Vogel, A., *Angew Chem Int Edit* **2005,** *44*, 4192-6.

149. Rentmeister, A.; Brown, T. R.; Snow, C. D.; Carbone, M. N.; Arnold, F. H., *ChemCatChem* **2011**, *6*, 1065-71.
150. Reetz, M. T.; Carballeira, J. D.; Peyralans, J.; Höbenreich, H.; Maichele, A.; Vogel, A., *Chem Euro J* **2006,** *12*, 6031-8.
151. Reinen, J.; van Leeuwen, J. S.; Li, Y.; Sun, L.; Grootenhuis, P. D. J.; Decker, C. J.; Saunders, J.; Vermeulen, N. P. E.; Commandeur, J. N. M., *Drug Metab Dispos* **2011,** *39*, 1568-76.
152. Komatsu, T.; Yamazaki, H.; Shimada, N.; Nakajima, M.; Yokoi, T., *Drug Metab Dispos* **2000,** *28*, 1457-63.
153. Cohen, M. B.; Berenbaum, M. R.; Schuler, M. A., *J Chem Ecol* **1989,** *15*, 2347-55.
154. Freeman, J. J.; Hayes, E. P., *Toxicol Sci* **1987,** *8*, 263-71.
155. Lewis, D. F. V.; Ito, Y., *Expert Opin Drug Met* **2008,** *4*, 1181-6.
156. Testa, B., *Chem Biodivers* **2009,** *6*, 2055-70.
157. Lewis, D. F. V.; Dickins, M., *Drug Discov Today* **2002,** *7*, 918-25.
158. Kaminsky, L. S.; Zhang, Z.-Y., *Pharmacol Therapeut* **1997,** *73*, 67-74.
159. Lewis David, F. V., *Curr Med Chem* **2003,** *10*, 1955-72.
160. Rendic, S., *Drug Metab Rev* **2002,** *34*, 83-448.
161. Lewis, D. F. V., *Pharmacogenomics* **2004,** *5*, 305-18.
162. John W, R., *Steroids* **1966,** *7*, 261-71.
163. Soars, M. G.; Gelboin, H. V.; Krausz, K. W.; Riley, R. J., *Brit J Clin Pharmaco* **2003,** *55*, 175-81.
164. Rettie, A. E.; Jones, J. P., *Annu Rev Pharmacol*, **2005,** *45*, 477-94.
165. Ullrich, V., *Arznei-Forschung* **1977,** *27*, 1821-7.
166. Galetin, A.; Houston, J. B., *J Pharmacol Exp Ther* **2006,** *318*, 1220-9.
167. Raeissi, S. D.; Guo, Z.; Dobson, G. L.; Artursson, P.; Hidalgo, I. J., *Pharm Res* **1997,** *14*, 1019-1025.
168. Russell, W. M. S.; Burch, R. L., *The principles of humane experimental technique*. Methuen: London, **1959,** 238.
169. May, J. E.; Xu, J.; Morse, H. R.; Avent, N. D.; Donaldson, C., *Br J Biomed Sci* **2009,** *66*, 160-5.
170. Varga, O.; Hansen, A. K.; Sandoe, P.; Olsson, I. A. S., *EMBO Rep* **2010,** *11*, 500-3.
171. Guengerich, F., *AAPS J* **2006,** *8*, 101-11.
172. Jia, L.; Liu, X., *Curr Drug Metab* **2007,** *8*, 822-9.
173. Drăgan, C.-A.; Peters, F.; Bour, P.; Schwaninger, A.; Schaan, S.; Neunzig, I.; Widjaja, M.; Zapp, J.; Kraemer, T.; Maurer, H.; Bureik, M., *Appl Biochem Biotechnol* **2011,** *163*, 965-80.
174. Van Booven, D.; Marsh, S.; McLeod, H.; Carrillo, M. W.; Sangkuhl, K.; Klein, T. E.; Altman, R. B., *Pharmacogenet Genom* **2010,** *20*, 277-81.
175. Anzenbacher, P.; Anzenbacherová, E., *Cell Mol Life Sci* **2001,** *58*, 737-47.
176. Pirmohamed, M.; Park, B. K., *Toxicology* **2003,** *192*, 23.
177. Lewis, D. F. V., *Biochem Pharmacol* **2000,** *60*, 293-306.
178. Tang, W.; Stearns, R. A., *Curr Drug Metab* **2001,** *2*, 185-98.
179. Hutzler, J. M.; Hauer, M. J.; Tracy, T. S., *Drug Metab Dispos* **2001,** *29*, 1029-34.
180. Matthew Hutzler, J.; Wienkers, L. C.; Wahlstrom, J. L.; Carlson, T. J.; Tracy, T. S., *Arch Biochem Biophys* **2003,** *410*, 16-24.
181. Rowlatt, B.; Yorke, J.; Strong, A.; Whitehouse, C.; Bell, S.; Wong, L.-L., *Protein & Cell* **2011,** *2*, 656-71.

182. Wester, M. R.; Yano, J. K.; Schoch, G. A.; Yang, C.; Griffin, K. J.; Stout, C. D.; Johnson, E. F., *J Biol Chem* **2004,** *279*, 35630-7.
183. Warrington, J. S.; Shader, R. I.; von Moltke, L. L.; Greenblatt, D. J., *Drug Metab Dispos* **2000,** *28*, 392-7.
184. Bu, H. Z., *Curr Drug Metab* **2006,** *7*, 231-49.
185. Thummel, K. E.; Wilkinson, G. R., *Annu Rev Pharmacol* **1998,** *38*, 389-430.
186. Schmider, J.; Brockmöller, J.; Arold, G.; Bauer, S.; Roots, I., *Pharmacogenetics* **1999,** *9*, 725-34.
187. Williams, P. A.; Cosme, J.; Matak Vinković, D.; Ward, A.; Angove, H. C.; Day, P. J.; Vonrhein, C.; Tickle, I. J.; Jhoti, H., *Science* **2004,** *305*, 683-6.
188. Ekroos, M.; Sjögren, T., *P Natl Acad Sci USA* **2006,** *103*, 13682-7.
189. Khan, K. K.; He, Y. Q.; Domanski, T. L.; Halpert, J. R., *Mol Pharmacol* **2002,** *61*, 495-506.
190. Nave, C., *Radiat Phys Chem* **1995,** *45*, 483-490.
191. Scott, E. E.; Halpert, J. R., *Trends Biochem Sci* **2005,** *30*, 5-7.
192. Nath, A.; Koo, P. K.; Rhoades, E.; Atkins, W. M., *J Am Chem Soc* **2008,** *130*, 15746-7.
193. Dong, S.; Niu, J.; Cotton, T. M., *Method Enzymol*, **1995,** *246*, 701-732.
194. Kono, T.; Nakamura, S., *Bull. Agric. Chem. Soc. Jpn.* **1958,** *22*, 399.
195. Udit, A. K.; Hill, M. G.; Gray, H. B., *J Inorg Biochem* **2006,** *100*, 519-23.
196. Yang, M.; Kabulski, J. L.; Wollenberg, L.; Chen, X.; Subramanian, M.; Tracy, T. S.; Lederman, D.; Gannett, P. M.; Wu, N., *Drug Metab Dispos* **2009,** *37*, 892-9.
197. Krishnan, S.; Rusling, J. F., *Electrochem commun* **2007,** *9*, 2359-63.
198. Krishnan, S.; Schenkman, J. B.; Rusling, J. F., *J Phys Chem B* **2011,** *115*, 8371-80.
199. Udit, A. K.; Hill, M. G.; Gray, H. B., *Langmuir* **2006,** *22*, 10854-7.
200. Udit, A. K.; Hagen, K. D.; Goldman, P. J.; Star, A.; Gillan, J. M.; Gray, H. B.; Hill, M. G., *J Am Chem Soc* **2006,** *128*, 10320-5.
201. Panicco, P.; Astuti, Y.; Fantuzzi, A.; Durrant, J. R.; Gilardi, G., *J Phys Chem B* **2008,** *112*, 14063-8.
202. Sadeghi, S. J.; Fantuzzi, A.; Gilardi, G., *BBA-Proteins Proteom* **2011,** *1814*, 237-48.
203. Guengerich, F. P., *Biochemistry-US* **1983,** *22*, 2811-20.
204. Nakano, H.; Yamazaki, T.; Miyatake, S.; Nozaki, N.; Kikuchi, A.; Saito, T., *J Biol Chem* **1996,** *271*, 6483-9.
205. Sligar, S. G.; Cinti, D. L.; Gibson, G. G.; Schenkman, J. B., *Biochem Bioph Res Co* **1979,** *90*, 925-32.
206. Das, A.; Grinkova, Y. V.; Sligar, S. G., *J Am Chem Soc* **2007,** *129*, 13778-9.
207. Douse, C. Engineering altered selectivity in cytochrome P450BM-3. *Part II Thesis*, University of Oxford, **2009**.
208. Kern, W., *Handbook of Semiconductor Wafer Cleaning Technology - Science, Technology, and Applications*. William Andrew Publishing/Noyes.: **1993**.
209. Whitehouse, C. J.; Bell, S. G.; Tufton, H. G.; Kenny, R. J.; Ogilvie, L. C.; Wong, L. L., *Chem Commun* **2008,** 966-8.
210. Whitehouse, C. Structure-Function Studies of Cytochrome $P450_{BM3}$ by Directed Evolution. *DPhil Thesis*, University of Oxford, 2010.
211. Farinas, E. T.; Glieder, A.; Arnold, F. H.; Schwaneberg, U., *US patent WO 2003008563, Registry Number: 494230-85-2* **2003**.
212. Cirino, P. C.; Arnold, F. H., *Angew Chem Int Ed* **2003,** *42*, 3299-301.
213. Bloom, J. D.; Romero, P. A.; Lu, Z.; Arnold, F. H., *Biol Direct* **2007,** *2*, 17.

214. Bloom, J. D.; Lu, Z.; Chen, D.; Raval, A.; Venturelli, O. S.; Arnold, F. H., *BMC Biol* **2007,** *5*, 29.
215. Glieder, A.; Farinas, E. T.; Arnold, F. H., *Nat Biotechnol* **2002,** *20*, 1135-9.
216. Whitehouse, C. J. C.; Yang, W.; Yorke, J. A.; Tufton, H. G.; Ogilvie, L. C. I.; Bell, S. G.; Zhou, W.; Bartlam, M.; Rao, Z.; Wong, L.-L., *Dalton T* **2011,** *40*, 10383-96.
217. Sulistyaningdyah, W. T.; Ogawa, J.; Li, Q. S.; Maeda, C.; Yano, Y.; Schmid, R. D.; Shimizu, S., *Appl Microbiol Biotechnol* **2005,** *67*, 556-62.
218. Whitehouse, C. J. C.; Bell, S. G.; Yang, W.; Yorke, J. A.; Blanford, C. F.; Strong, A. J. F.; Morse, E. J.; Bartlam, M.; Rao, Z.; Wong, L.-L., *ChemBioChem* **2009,** *10*, 1654-6.
219. Leys, D.; Mowat, C. G.; McLean, K. J.; Richmond, A.; Chapman, S. K.; Walkinshaw, M. D.; Munro, A. W., *J Biol Chem* **2003,** *278*, 5141-7.
220. Kühnel, K.; Maurer, S. C.; Galeyeva, Y.; Frey, W.; Laschat, S.; Urlacher, V. B., *Adv Synth Catal* **2007,** *349*, 1451-61.
221. Johnson, M.; Zuo, H.; Lee, K.-H.; Trebley, J.; Rae, J.; Weatherman, R.; Desta, Z.; Flockhart, D.; Skaar, T., *Breast Cancer Res Tr* **2004,** *85*, 151-9.
222. Vail, R. B.; Homann, M. J.; Hanna, I.; Zaks, A., *J Ind Microbiol Biot* **2005,** *32*, 67-74.
223. Parikh, A.; Gillam, E. M. J.; Guengerich, F. P., *Nat Biotech* **1997,** *15*, 784-8.
224. Rushmore, T. H.; Reider, P. J.; Slaughter, D.; Assang, C.; Shou, M., *Metab Eng* **2000,** *2*, 115-25.
225. Guengerich, F. P.; Gillam, E. M. J.; Shimada, T., *Crit Rev Toxicol* **1996,** *26*, 551-83.
226. Sawayama, A. M.; Chen, M. M. Y.; Kulanthaivel, P.; Kuo, M.-S.; Hemmerle, H.; Arnold, F. H., *Chem Eur J* **2009,** *15*, 11723-9.
227. Fairhead, M.; Giannini, S.; Gillam, E.; Gilardi, G., *J Biol Inorg Chem* **2005,** *10*, 842-53.
228. Dodhia, V.; Fantuzzi, A.; Gilardi, G., *J Biol Inorg Chem* **2006,** *11*, 903-16.
229. Di Nardo, G.; Fantuzzi, A.; Sideri, A.; Panicco, P.; Sassone, C.; Giunta, C.; Gilardi, G., *J Biol Inorg Chem* **2007,** *12*, 313-323.
230. Chen, W.; Koenigs, L. L.; Thompson, S. J.; Peter, R. M.; Rettie, A. E.; Trager, W. F.; Nelson, S. D., *Chem Res Toxicol* **1998,** *11*, 295-301.
231. Peter, R.; Boecker, R.; Beaune, P. H.; Iwasaki, M.; Guengerich, F. P.; Yang, C. S., *Chem Res Toxicol* **1990,** *3*, 566-73.
232. Lussenburg, B. M. A.; Babel, L. C.; Vermeulen, N. P. E.; Commandeur, J. N. M., *Anal Biochem* **2005,** *341*, 148-55.
233. van Leeuwen, J. S.; Vredenburg, G.; Dragovic, S.; Tjong, T. F. J.; Vos, J. C.; Vermeulen, N. P. E., *Toxicol Lett* **2011,** *200*, 162-8.
234. Damsten, M. C.; de Vlieger, J. S. B.; Niessen, W. M. A.; Irth, H.; Vermeulen, N. P. E.; Commandeur, J. N. M., *Chem Res Toxicol* **2008,** *21*, 2181-7.
235. Boerma, J. S.; Vermeulen, N. P. E.; Commandeur, J. N. M., *Chem Res Toxicol* **2011,** *24*, 1263-74.
236. Reinen, J.; Ferman, S.; Vottero, E.; Vermeulen, N. P. E.; Commandeur, J. N. M., *J Biomol Screen* **2011,** *16*, 239-50.
237. Kim, D.-H.; Ahn, T.; Jung, H.-C.; Pan, J.-G.; Yun, C.-H., *Drug Metab Dispos* **2009,** *37*, 932-6.
238. Kim, K.-H.; Kang, J.-Y.; Kim, D.-H.; Park, S.-H.; Park, S. H.; Kim, D.; Park, K. D.; Lee, Y. J.; Jung, H.-C.; Pan, J.-G.; Ahn, T.; Yun, C.-H., *Drug Metab Dispos* **2011,** *39*, 140-50.

239. Kenny, R. P. F., Forced evolution of P450 enzymes for terpene oxidation. *Part II thesis*, University of Oxford, **2004**.
240. Morse, E.; Drug Metabolism by Engineered Cytochrome P450(BM3). *Part II thesis*, University of Oxford, **2008**.
241. Kenny, J. R.; Maggs, J. L.; Meng, X.; Sinnott, D.; Clarke, S. E.; Park, B. K.; Stachulski, A. V., *J Med Chem* **2004,** *47*, 2816-25.
242. Whitehouse, C. J. C.; Yang, W.; Yorke, J. A.; Rowlatt, B. C.; Strong, A. J. F.; Blanford, C. F.; Bell, S. G.; Bartlam, M.; Wong, L.-L.; Rao, Z., *ChemBioChem* **2010,** *11*, 2549-56.
243. Yamazaki, H.; Shimada, T., *Arch Biochem Biophys* **1997,** *346*, 161-9.
244. Dutton, P. L., *Methods Enzymol* **1978,** *54*, 411-35.
245. Bloch, D.; Belevich, I.; Jasaitis, A.; Ribacka, C.; Puustinen, A.; Verkhovsky, M. I.; Wikström, M., *P Natl Acad Sci USA* **2004,** *101*, 529-33.
246. Arnon, D. I.; Tang, G. M. S., *P Natl Acad Sci USA* **1988,** *85*, 9524-8.
247. Kusel, J. P.; Storey, B. T., *J Bacteriol* **1976,** *127*, 812-6.
248. Murugan, R.; Mazumdar, S., *ChemBioChem* **2005,** *6*, 1204-11.
249. Reipa, V.; Mayhew, M. P.; Holden, M. J.; Vilker, V. L., *Chem Commun* **2002,** 318-9.
250. Butler, J.; Davies, D. M.; Sykes, A. G., *J Inorg Biochem* **1981,** *15*, 41-53.
251. Miller, W. G.; Cusanovich, M. A., *Biophys Struct Mech* **1975,** *1*, 97-111.
252. Stellwagen, E.; Cass, R. D., *J Biol Chem* **1975,** *250*, 2095-8.
253. Elly, C. G. S.; Moore, G. R.; Williams, G.; Williams, R. J. P., *Eur J Bioch* **1982,** *124*, 295-303.
254. Mayhew, S. G., *Eur J Bioch* **1978,** *85*, 535-47.
255. Page, C. C.; Moser, C. C.; Chen, X.; Dutton, P. L., *Nature* **1999,** *402*, 47-52.
256. Forrow, N. J.; Walters, S. J., *Biosens Bioelectron* **2004,** *19*, 763-70.
257. Forrow, N. J.; Sanghera, G. S.; Walters, S. J., *Dalton T* **2002,** 3187-3194.
258. Hawkes, D. B.; Slessor, K. E.; Bernhardt, P. V.; De Voss, J. J., *ChemBioChem* **2010,** *11*, 1107-14.
259. Larsson, T.; Lindgren, A.; Ruzgas, T., *Bioelectrochemistry* **2001,** *53*, 243-9.
260. Eddowes, M. J.; Hill, H. A. O.; Uosaki, K., *J Electroanal Chem* **1980,** *116*, 527-37.
261. Caprotti, D. Control of Electron Transfer in Cytochrome P450 Enzymes. *DPhil Thesis*, University of Oxford, **2009**.
262. Clark, J. P.; Miles, C. S.; Mowat, C. G.; Walkinshaw, M. D.; Reid, G. A.; Daff, S. N.; Chapman, S. K., *J Inorg Biochem* **2006,** *100*, 1075-90.
263. Hanley, S. C.; Ost, T. W.; Daff, S., *Biochem Biophys Res Commun* **2004,** *325*, 1418-23.
264. Heath, R. Studies of a 'Blue' Copper Oxidase Electrocatalyst. *DPhil Thesis*, University of Oxford, **2008**.
265. Lei, C.; Wollenberger, U.; Jung, C.; Scheller, F. W., *Biochem Biophys Res Commun* **2000,** *268*, 740-4.
266. Iwuoha, E. I.; Smyth, M. R., *Biosens Bioelectron* **2003,** *18*, 237-44.
267. Zhang, Z.; F. Nassar, A.-E.; Lu, Z.; B. Schenkman, J.; F. Rusling, J., *J Chem Soc Faraday T* **1997,** *93*, 1769-74.
268. Iwuoha, E. I.; Joseph, S.; Zhang, Z.; Smyth, M. R.; Fuhr, U.; Ortiz De Montellano, P. R., *J Pharmaceut Biomed* **1998,** *17*, 1101-10.
269. Hara, M.; Yasuda, Y.; Toyotama, H.; Ohkawa, H.; Nozawa, T.; Miyake, J., *Biosens Bioelectron* **2002,** *17*, 173-9.

270. Estavillo, C.; Lu, Z.; Jansson, I.; Schenkman, J. B.; Rusling, J. F., *Biophys Chem* **2003,** *104*, 291-6.
271. Shumyantseva, V. V.; Bulko, T. V.; Usanov, S. A.; Schmid, R. D.; Nicolini, C.; Archakov, A. I., *J Inorg Biochem* **2001,** *87*, 185-90.
272. Joseph, S.; Rusling, J. F.; Lvov, Y. M.; Friedberg, T.; Fuhr, U., *Biochem Pharmacol* **2003,** *65*, 1817-26.
273. Faulkner, K. M.; Shet, M. S.; Fisher, C. W.; Estabrook, R. W., *P Natl Acad Sci USA* **1995,** *92*, 7705-09.
274. Zhu, Y.; Cheng, G.; Dong, S., *Biophys Chem* **2002,** *97*, 129-38.
275. Durliat, H.; Comtat, M., *J Biol Chem* **1987,** *262*, 11497-500.
276. Kong, J.; Mbindyo, J. N.; Wu, X.; Zhou, J. X.; Rusling, J. F., *Biophys Chem* **1999,** *79*, 219-29.
277. Murray, R. W.; Heineman, W. R.; O'Dom, G. W., *Anal Chem* **1967,** *39*, 1666-8.
278. Clarke, W. M., *Oxidation-Reduction Potentials of Organic Systems*. Williams and Wilkins: Baltimore, MD, **1960**.
279. Steckhan, E.; Kuwana, T., *Ber. Bunsenges. Phys. Chem* **1974,** *78*, 253.
280. Hiyama, T.; Ke, B., *BBA-Bioenergetics* **1972,** *267*, 160-71.
281. Caprotti, D. Control of Electron Transfer in Cytochrome P450 Enzymes. *DPhil Thesis*, University of Oxford, **2009**.
282. Fischer, L. M.; Tenje, M.; Heiskanen, A. R.; Masuda, N.; Castillo, J.; Bentien, A.; Émneus, J.; Jakobsen, M. H.; Boisen, A., *Microelectron Eng* **2009,** *86*, 1282-5.
283. Noh, M.; Tothill, I., *Anal Bioanal Chem* **2006,** *386*, 2095-106.
284. Spégel, C.; Heiskanen, A.; Acklid, J.; Wolff, A.; Taboryski, R.; Emnéus, J.; Ruzgas, T., *Electroanal* **2007,** *19*, 263-71.
285. Manna, S. K.; Mazumdar, S., *J Inorg Biochem* **2008,** *102*, 1312-21.
286. Chang, C. K.; Traylor, T. G., *Biochem Biophys ResCommun* **1975,** *62*, 729-35.
287. Sabat, J.; Stuehr, D. J.; Yeh, S.-R.; Rousseau, D. L., *J Am Chem Soc* **2009,** *131*, 12186-92.
288. Perera, R.; Sono, M.; Sigman, J. A.; Pfister, T. D.; Lu, Y.; Dawson, J. H., *P Natl Acad Sci USA* **2003,** *100*, 3641-6.
289. Dunford, A. J.; McLean, K. J.; Sabri, M.; Seward, H. E.; Heyes, D. J.; Scrutton, N. S.; Munro, A. W., *J Biol Chem* **2007,** *282*, 24816-24.
290. Aurbach, D.; Levi, M. D.; Lev, O.; Gun, J.; Rabinovich, L., *J Appl Electrochem* **1998,** *28*, 1051-9.
291. Bowyer, W. J.; Geiger, W. E., *J Electroanal Chem* **1988,** *239*, 253-71.
292. Gruia, F.; Ionascu, D.; Kubo, M.; Ye, X.; Dawson, J.; Osborne, R. L.; Sligar, S. G.; Denisov, I.; Das, A.; Poulos, T. L.; Terner, J.; Champion, P. M., *Biochemistry* **2008,** *47*, 5156-67.
293. Garbett, K.; Gillard, R. D.; Knowles, P. F.; Stangroom, J. E., *Nature* **1967,** *215*, 824-8.
294. Girvan, H. M.; Levy, C. W.; Williams, P.; Fisher, K.; Cheesman, M. R.; Rigby, S. E.; Leys, D.; Munro, A. W., *Biochem J* **2010,** *427*, 455-66.
295. Whitehouse, C. J. C.; Bell, S. G.; Wong, L.-L., *Chem Eur J* **2008,** *14*, 10905-8.
296. Hasemann, C. A.; Ravichandran, K. G.; Peterson, J. A.; Deisenhofer, J., *J Mol Biol* **1994,** *236*, 1169-85.
297. Seifert, A.; Pleiss, J., *Proteins* **2009,** *74*, 1028-35.
298. Chen, C.-K.; Berry, R.; Shokhireva, T.; Murataliev, M.; Zhang, H.; Walker, F., *J Biol Inorg Chem* **2010,** *15*, 159-74.
299. Girvan, H. M.; Seward, H. E.; Toogood, H. S.; Cheesman, M. R.; Leys, D.; Munro, A. W., *J Biol Inorg Chem* **2007,** *282*, 564-72.

300. Stjernschantz, E.; van Vugt-Lussenburg, B. M. A.; Bonifacio, A.; de Beer, S. B. A.; van der Zwan, G.; Gooijer, C.; Commandeur, J. N. M.; Vermeulen, N. P. E.; Oostenbrink, C., *Proteins* **2008,** *71*, 336-52.
301. Larimer, F. W.; Chain, P.; Hauser, L.; Lamerdin, J.; Malfatti, S.; Do, L.; Land, M. L.; Pelletier, D. A.; Beatty, J. T.; Lang, A. S.; Tabita, F. R.; Gibson, J. L.; Hanson, T. E.; Bobst, C.; Torres, J. L. T. y.; Peres, C.; Harrison, F. H.; Gibson, J.; Harwood, C. S., *Nat Biotech* **2004,** *22*, 55-61.
302. Oda, Y.; Larimer, F. W.; Chain, P. S. G.; Malfatti, S.; Shin, M. V.; Vergez, L. M.; Hauser, L.; Land, M. L.; Braatsch, S.; Beatty, J. T.; Pelletier, D. A.; Schaefer, A. L.; Harwood, C. S., *P Natl Acad Sci USA* **2008,** *105*, 18543-8.
303. Oda, Y.; Meijer, W. G.; Gibson, J. L.; Gottschal, J. C.; Forney, L. J., *Microbial Ecology* **2004,** *47*, 68-79.
304. Bell, S. G.; Hoskins, N.; Xu, F.; Caprotti, D.; Rao, Z.; Wong, L.-L., *Biochem Biophys Res Commun* **2006,** *342*, 191-6.
305. Bell, S. G.; Tan, A. B. H.; Johnson, E. O. D.; Wong, L.-L., *Mol BioS* **2010,** *6*, 206-14.
306. Kuznetsov, V. Y.; Poulos, T. L.; Sevrioukova, I. F., *Biochemistry* **2006,** *45*, 11934-44.
307. Ewen, K. M.; Kleser, M.; Bernhardt, R., *BBA-Proteins* **2011,** *1814*, 111-25.
308. Xu, F.; Bell, S. G.; Peng, Y.; Johnson, E. O.; Bartlam, M.; Rao, Z.; Wong, L. L., *Proteins Struct. Funct. Bioinf.* **2009,** *77*, 867-880.
309. Bell, S. G.; Tan, A. B.; Johnson, E. O.; Wong, L. L., *Mol. Biosyst.* **2010,** *6*, 206-214.
310. Bell, S. G.; Xu, F.; Johnson, E. O.; Forward, I. M.; Bartlam, M.; Rao, Z.; Wong, L. L., *J. Biol. Inorg. Chem.* **2010,** *15*, 315-328.
311. Sligar, S. G.; Gunsalus, I. C., *Pro Natl Acad Sci U S A* **1976,** *73*, 1078-82.
312. Schiffler, B.; Bureik, M.; Reinle, W.; Müller, E. C.; Hannemann, F.; Bernhardt, R., *J Inorg Biochem* **2004,** *98*, 1229-37.
313. Sainz, G.; Jakoncic, J.; Sieker, L.; Stojanoff, V.; Sanishvili, N.; Asso, M.; Bertrand, P.; Armengaud, J.; Jouanneau, Y., *J Biol Inorg Chem* **2006,** *11*, 235-46.
314. Salazar, O.; Cirino, P. C.; Arnold, F. H., *ChemBioChem* **2003,** *4*, 891-3.
315. Dragovic, S.; Boerma, J. S.; van Bergen, L.; Vermeulen, N. P. E.; Commandeur, J. N. M., *Chem Res Toxicol* **2010,** *23*, 1467-76.
316. Kang, J.-Y.; Kim, S.-Y.; Kim, D.; Kim, D.-H.; Shin, S.-M.; Park, S.-H.; Kim, K.-H.; Jung, H.-C.; Pan, J.-G.; Joung, Y.; Chi, Y.-T.; Chae, H.; Ahn, T.; Yun, C.-H., *AMB Express* **2011,** *1*, 1.
317. Kim, D.-H.; Kim, K.-H.; Kim, D.; Jung, H.-C.; Pan, J.-G.; Chi, Y.-T.; Ahn, T.; Yun, C.-H., *J Mol Catal B-Enzym* **2010,** *63*, 179-87.
318. Landwehr, M.; Carbone, M.; Otey, C. R.; Li, Y.; Arnold, F. H., *Chem Biol* **2007,** *14*, 269-78.
319. Landwehr, M.; Hochrein, L.; Otey, C. R.; Kasrayan, A.; Backvall, J. E.; Arnold, F. H., *J Am Chem Soc* **2006,** *128*, 6058-9.
320. Li, X.-Q.; Björkman, A.; Andersson, T. B.; Ridderström, M.; Masimirembwa, C. M., *J Pharmacol Exp Ther* **2002,** *300*, 399-407.
321. Dubey, K. K.; Jawed, A.; Haque, S., *Eng Life Sci* **2011,** *11*, 598-606.
322. O'Brien, S. G.; Meinhardt, P.; Bond, E.; Beck, J.; Peng, B.; Dutreix, C.; Mehring, G.; Milosavljev, S.; Huber, C.; Capdeville, R.; Fischer, T., *Br J Cancer **2003**,* *89*, 1855-9.
323. Wang, R. W.; Kari, P. H.; Lu, A. Y.; Thomas, P. E.; Guengerich, F. P.; Vyas, K. P., *Arch Biochem Biophys* **1991,** *290*, 355-61.

324. Lewis, D. F.; Ito, Y.; Eddershaw, P. J.; Dickins, M.; Goldfarb, P. S., *Drug Metab Lett* **2010,** *4*, 25-30.
325. Grobe, N.; Zhang, B.; Fisinger, U.; Kutchan, T. M.; Zenk, M. H.; Guengerich, F. P., *J Biol Chem* **2009,** *284*, 24425-31.
326. Lasker, J. M.; Huang, M. T.; Conney, A. H., *Science* **1982,** *216*, 1419-21.
327. Conney, A. H.; Trousof, N.; Burns, J. J., *J Pharmacol Exp Ther* **1960,** *128*, 333-9.
328. Majumdar, A. K.; McCrea, J. B.; Panebianco, D. L.; Hesney, M.; Dru, J.; Constanzer, M.; Goldberg, M. R.; Murphy, G.; Gottesdiener, K. M.; Lines, C. R.; Petty, K. J.; Blum, R. A., *Clin Pharmacol Ther* **2003,** *74*, 150-156.
329. Hendset, M.; Hermann, M.; Lunde, H.; Refsum, H.; Molden, E., *Eur J Clin Pharmacol* **2007,** *63*, 1147-51.
330. Urichuk, L.; Prior, T. I.; Dursun, S.; Baker, G., *Curr Drug Metab* **2008,** *9*, 410-8.
331. Padhi, D.; Salfi, M.; Emery, M., *Drugs in R&D* **2008,** *9*, 335-43.
332. De Francia, S.; D'Avolio, A.; De Martino, F.; Pirro, E.; Baietto, L.; Siccardi, M.; Simiele, M.; Racca, S.; Saglio, G.; Di Carlo, F.; Di Perri, G., *J Chromatog B* **2009,** *877*, 1721-6.
333. Keating, G. M.; Santoro, A., *Drugs* **2009,** *69*, 223-40.
334. Li, F.; Wang, L.; Guo, G. L.; Ma, X., *Drug Metab Dispos* **2010,** *38*, 871-8.

Appendices

Appendix 1. $P450_{BM3}$ variants reported to be active towards pharmaceuticals

$P450_{BM3}$ variant	Mutations present vs. WT $P450_{BM3}$
WT[82, 229, 237]	none
R47L/F87V/L188Q[144]	R47L, F87V, L188Q
21B3[212]	F87A, I58V, H100R, F107L, A135S, M145V, N239H, S274T, K434E, V446I
9C1[93]	21B3 + I102T, V145A, L324I, I366V, E442K
DE10[93, 226]	9C1 + A72V, A82L, A87G
D6H10[93]	9C1 + L75H, V78E, A82P
2C11[93]	9C1 + K24R, R47H, A72V, A82L, A87G
5H6[314]	21B3 + L52I, , S106R, V145M, A184V, L324I, V340M, I366V, E442K
21B3-14C10[143]	21B3 + F205L, H239R, K306N
21B3-27B2[143]	21B3 + S106R, A319C, F205S, E434A
21B3-31B12[143]	21B3 + A82T, G247A, A295S
5H6-13C9[143]	5H6 + L75R
5H6-27G12[143]	5H6 + E35D, K98R, F173V, L437P, K451E, P461S, H468R
5H6-27G8[143]	5H6 + F173L
5H6-30B10[143]	5H6 + M118V, I357T, F444L
5H6-32F7[143]	5H6 + S108G, D214Y, V366A, I433F
5H6-36G11[143]	5H6 + K113E, F173L, E430G
5H6-37F4[143]	5H6 + F173L, D338N
5H6-38F11[143]	5H6 + F173l, D217G, E430G
139-3[226]	V78A, H138Y, T175I, V178I, A184V, H236Q, E252G, R255S, A290V, A295T, L353V
J[226]	139-3 + Y138H, I178V, F205C, S226R, A290V
9-10A[226]	J + R47C, K94I, P142S

9-10A L75I[226]	9-10A +L75I
9-10A A78F[226]	9-10A + A78F
9-10A A78S[226]	9-10A + A78S
9-10A A78T[226]	9-10A + A78T
9-10A A82C[226]	9-10A + A82C
9-10A A82I[226]	9-10A + A82I
9-10A A82F[226]	9-10A + A82F
9-10A A82G[226]	9-10A + A82G
9-10A A82L[226]	9-10A + A82L
9-10A A82S[226]	9-10A + A82S
9-10A A82T[226]	9-10A + A82T
9-10A F87A[226]	9-10A + F87A
9-10A F87I[226]	9-10A + F87I
9-10A F87L[226]	9-10A + F87L
9-10A F87V[226]	9-10A + F87V
9-10A T88L[226]	9-10A + T88L
9-10A T260S[226]	9-10A + T260S
9-10A A328M[226]	9-10A + A328M
8C7	9-10A F87V + L75A, L181A
4H5	8C7 + M177A
1-12G[226]	9-10A + A82L, A328V
7-11D[226]	9-10A + A82F, A328V
12-10C[226]	9-10A + A82G, F87V, A328V
41-5B[226]	9-10A + A78F, A82G, A328L
9-10A T260L[226]	9-10A + T260L
9-10A T260N[226]	9-10A + T269N
11-8E[226]	9-10A + F87V, A328L
23-11B[226]	9-10A + A78T, A82G, F87V, A328L

49-9B[226]	9-10A + A82G, F87L, A328L
13C9R1[149]	L52I, I58V, L75R, F87A, H100R, S106R, F107L, A135S, A184V, N239H, S274T, L324I, V340M, I366V, K434E, E442K, V446I
22A3[149]	13C9R1 + F162I
16G2[149]	22A3 + Q109L, E140G
W7D8[149]	16G2 + V286A, R398H
X3H1[149]	W7D8 + M185K
A2[146]	D251G, Q307H
R47L/F87V/L188Q[82, 136, 232, 237, 238]	R47L, F87V, L188Q
M01[67, 82, 91, 151]	R47L, F87V, L188Q, E267V, G415S
M02[67, 91, 151, 236]	R47L, F87V, L188Q, L86I, N319T
M05[67, 91, 151]	R47L, F87V, L188Q, F81I, E267V, G415S
M11[82, 91, 151, 233, 236, 237]	R47L, F87V, L188Q, E64G, F81I, E143G, E267V, G415S
M01a[91, 238]	R47L, F87V, L188Q, E267V
M02a[91, 238]	R47L, F87V, L188Q, L86I
M02b[91]	R47L, F87V, L188Q, N319T
$M01_{his}$[3]	M01 + G1049E, His tag
$M02_{his}$[3]	M02 + A964V, His tag
$M05_{his}$[3]	M05 + His tag
$M11_{his}$[3, 234, 315]	M11 + Y198C, H258Y, His tag
M11 V87A[236]	$M11_{his}$ + V87A
MT35[151, 236]	$M11_{his}$ + L437S
MT43[151, 236]	$M01_{his}$ + S72D
MT80[236]	$M01_{his}$ + A74E, A82W
M11 87SS[137]	$M11_{his}$ + site saturation at position 87
MT32[151]	$M11_{his}$ + L437E
MT33[151]	$M11_{his}$ + L437N

MT34[151]	$M11_{his}$ + A74E, C198Y, Y285H
MT35[151]	$M11_{his}$ + L437S
MT36[151]	$M11_{his}$ + L437T
MT37[151]	$M11_{his}$ + A74D, C198Y, Y285H
MT38[151]	$M11_{his}$ + S72D
MT41[151]	$M01_{his}$ + A74E
MT44[151]	$M01_{his}$ + S72E
F87A[82, 237]	F87A
RLFY[82, 237]	R47L, Y51F
A264G[82, 237]	A264G
FAAG[82, 237, 238]	F87A, A264G
RLYFFAAG[82, 237, 238]	R47L, Y51F, F87A, A264G
RLYFFA[82, 237]	R47L, Y51F, F87A
RLYFAG[82, 237]	R47L, Y51F, A264G
Schmid[82, 237, 238]	A74G, F87V, L188Q
R47L/L86I/L188Q[82, 237]	R47L, L86I, L188Q
R47L/L86I/L188Q/E267V[82, 237, 238]	R47L, L86I, L188Q, E267V
R47L/F87V/E143G/L188Q/E267V[82, 237, 238]	R47L, F87V, E143G, L188Q, E267V
M#15[82, 237, 238]	R47L, E64G, F87V, E143G, L188Q, E267V
M#16[82, 237, 238]	R47L, F81I, F87V, E143G, L188Q, E267V
M#17	M#16 + E64G
F162I/M237I[141]	F162I, M237I
F162I[141]	F162I
L148I/F162I[141]	L148I, F162I
F1621/K187E[141]	F1621, K187E
F162I/E228K[141]	F162I, E228K
F162I/H236R[141]	F162I, H236R

F162I/M185V/M237I[141]	F162I, M185V, M237I
F162I/K187E/M237I[141, 238]	F162I, K187E, M237I
F162I/F165L/M177T/M237I[141]	F162I, F165L, M177T, M237I
F162I/M185T/L188P/M237I[141]	F162I, M185T, L188P, M237I

Appendix 2. Pharmaceuticals towards which $P450_{BM3}$ variants have shown activity

Structure and oxidation sites of pharmaceutical compounds towards which $P450_{BM3}$ shows activity. The human enzymes responsible for metabolism are also shown, with the enzyme in bold being primarily responsible for metabolism. * indicates sites of oxidation by human P450s. ` indicates oxidation sites by $P450_{BM3}$, if known. Variants shown in italics are chimeras of $P450_{BM3}$ and other CYP102A enzymes or human drug metabolising enzymes.

Pharmaceutical structure	Name	Human P450 responsible for metabolism ([160], unless otherwise noted)	Most active $P450_{BM3}$ variant	Reference for $P450_{BM3}$ activity
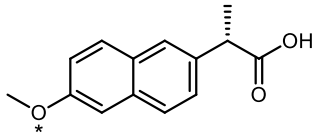	Naproxen	CYP1A2 CYP2C8 CYP2C9	X3H1[149]	143, 149
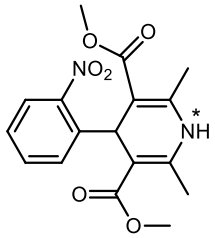	Nifedipine	CYP2D6 CYP3A4	MT43[151]	151, 229, 236
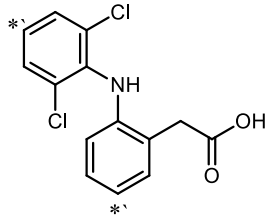	Diclofenac	CYP1A1 CYP1A2 CYP2B6 CYP2C18 CYP2C19 CYP2C8 CYP2C8 CYP2C9 CYP2J2 CYP3A4	MT35[151]	3, 141, 144, 151, 228, 229, 233
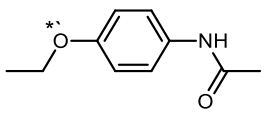	Phenacetine	CYP1A1 CYP1A2 CYP2A6 CYP2C9 CYP2D6 CYP2E1 CYP3A4	MT43[151]	141, 151, 229, 316, 317
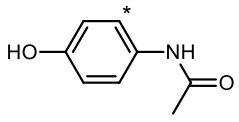	Acetaminophen	CYP1A2 CYP2A6 CYP2C9 CYP2D6 CYP2E1 CYP3A4	$M11_{his}$[3]	3, 136, 141

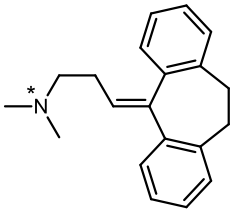	Amitryptiline	CYP1A2 CYP2C19 CYP2C9 CYP2D6 CYP3A4	MT35[151]	151, 236
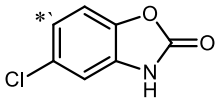	Chlorzoxazone	CYP1A1 CYP1A2 CYP2A6 CYP2D6 CYP2E1 CYP3A4	WT[229]	141, 144, 227, 229, 316, 318
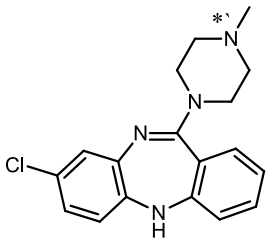	Clozapine	CYP1A2 CYP2C19 CYP2C8 CYP2C9 CYP2D6 CYP3A4	R47L/F87V/L188Q [144]	3, 144
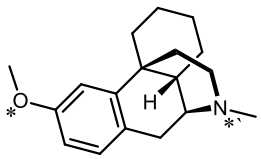	Dextromethorphan	CYP2B6 CYP2C19 CYP2C9 CYP2D6 CYP3A4 CYP3A5 CYP3A7	MT35[151]	67, 91, 135, 136, 144, 151
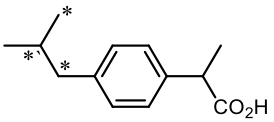	Ibuprofen	CYP2C19 CYP2C8 CYP2C9	W7D8[149]	149, 229
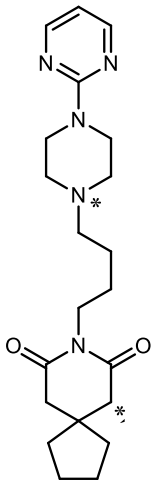	Buspirone	CYP3A4	M11[151]	151, 236, 319

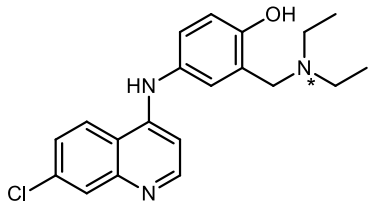	Amodiaquine	CYP1A1 CYP1B1 CYP2C8[320]	R47L/F87V/L188Q [144]	136, 144
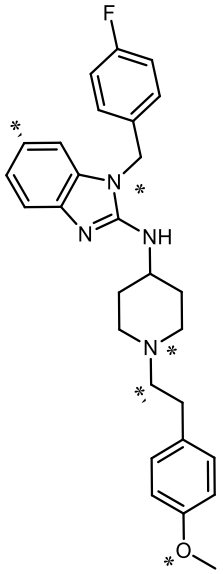	Astemizole	CYP3A4	M01[151]	151, 226
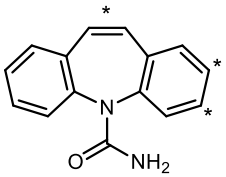	Carbamazepine	CYP1A2 CYP2C8 CYP3A4	MT35[151]	144, 151
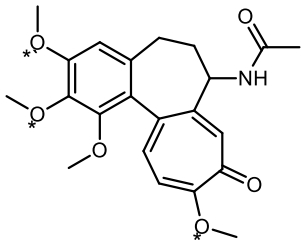	Colchicine	CYP3A4	WT[321]	321
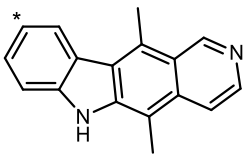	Ellipticine	CYP1A1 CYP1A2 CYP1B1 CYP2C9 CYP3A4	R47L/F87V/ L188Q [144]	144

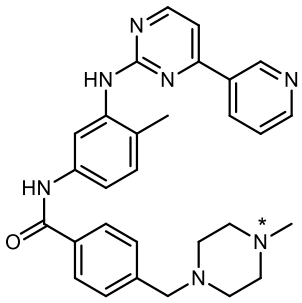	Imatinib	CYP3A4[322]	M11[151]	151
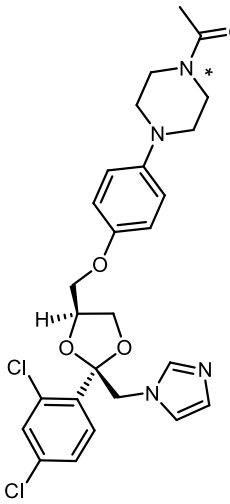	Ketoconazole	CYP3A4	M11[137]	137, 144
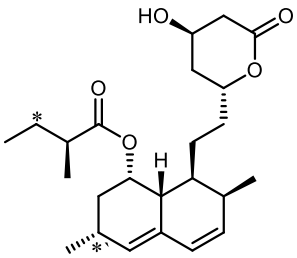	Lovastatin	CYP3A4[323]	M#17[238]	238
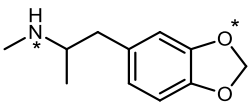	MDMA	CYP1A2 CYP2B6 CYP2D6 CYP3A4	M02[67]	67, 91, 136
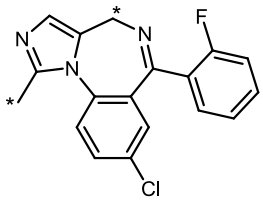	Midazolam	CYP2B6 CYP3A4 CYP3A5 CYP4B1	MT35[151]	151, 236
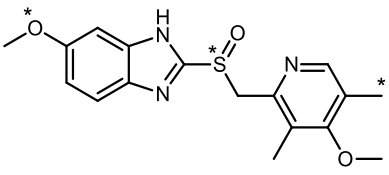	Omeprazole	CYP2A6 CYP2C18 CYP2C19 CYP2C8 CYP2C9 CYP2D6 CYP3A4	*CYP3A4/BMR*[228]	228, 236

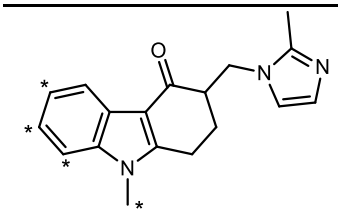	Ondansetron	CYP1A2 CYP2C9 CYP2D6 CYP2E1[324] CYP3A4	MT43[151]	151, 236
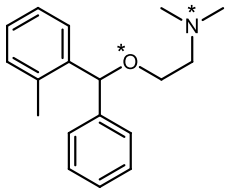	Orphenadrine	CYP3A4	R47L/F87V/ L188Q [144]	144
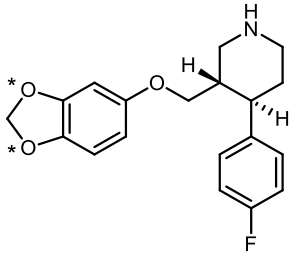	Paroxetine	CYP2D6	MT38[151]	151, 236
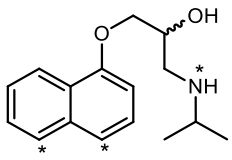	Propranolol	CYP1A1 CYP1A2 CYP2C19 CYP2D6	*22213132 R2*[318]	93, 143, 229, 318
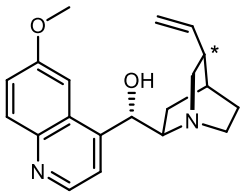	Quinidine	CYP2C9 CYP231 CYP3A4	MT35[151]	144, 151
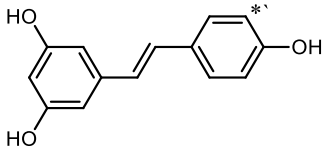	Resveratrol	CYP3A4	WT[237]	236, 237
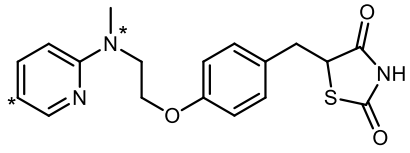	Rosiglitazone	CYP2C8 CYP2C9	M02[151]	151, 236
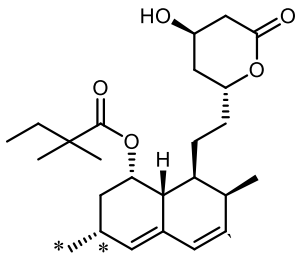	Simvastatin	CYP3A4	M#17[238]	238

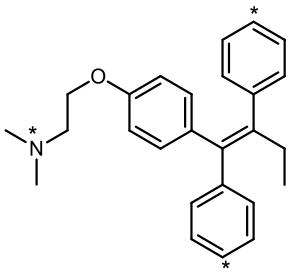	Tamoxifen	CYP2A6 CYP2B6 CYP2C9 CYP2D6 CYP2E1 CYP3A4	MT43[151]	144, 151
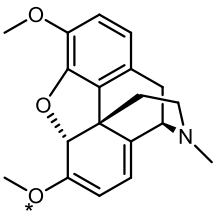	Thebaine	CYP2D6 CYP3A4[325]	8C7[135]	135
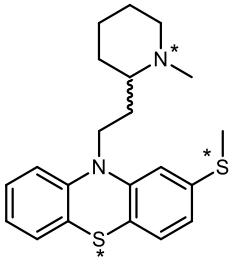	Thioridazine	CYP2D6	M01[151]	151, 236
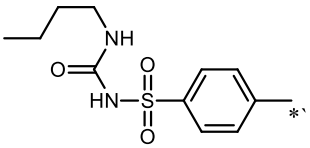	Tolbutamide	CYP2C18 CYP2C19 CYP2C8 CYP2C9	WT[229]	229, 318
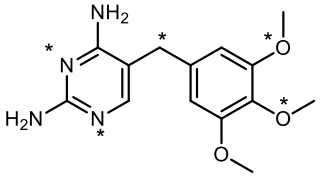	Trimethoprim	CYP2C8 CYP2C9 CYP3A4	$M11_{his}$[234]	234
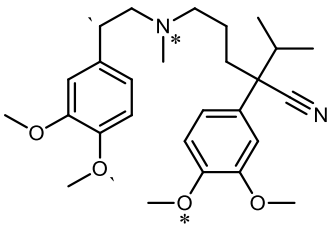	Verapamil	CYP1A2 CYP2B6 CYP2C18 CYP2C19 CYP2C8 CYP2C9 CYP2E1 CYP3A4 CYP3A5	D6H10[226]	151, 226
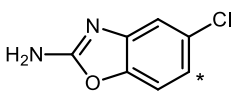	Zoxazolamine	CYP1A2 CYP3A4[326, 327]	*32313233 R1*[318]	318
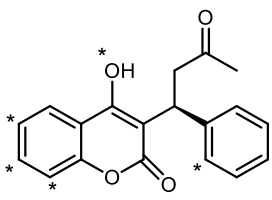	(*R*)-Warfarin	CYP1A1 CYP1A2 CYP2C18 CYP2C19 CYP2C8 CYP2C9 CYP3A4	M01[151]	151

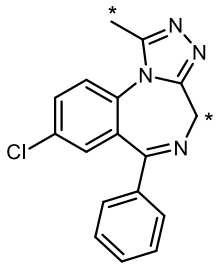	Alprazolam	CYP3A4	MT35[151]	[151]
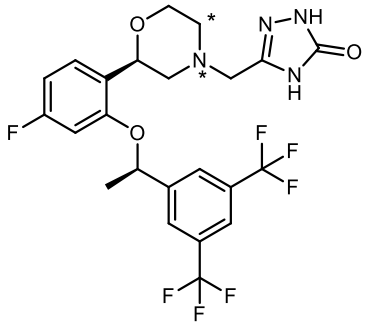	Aprepitant	CYP3A4[328]	MT43[151]	[151]
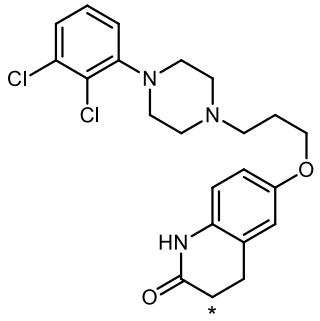	Aripiprazole	CYP2D6[329] CYP3A4[330]	M11[151]	[151]
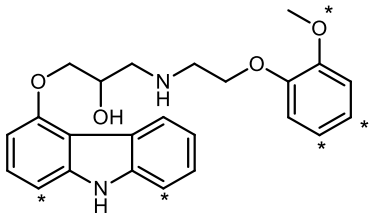	Carvedilol	CYP1A1 CYP1A2 CYP2C9 CYP2D6 CYP2E1 CYP3A4	M01[151]	[151]
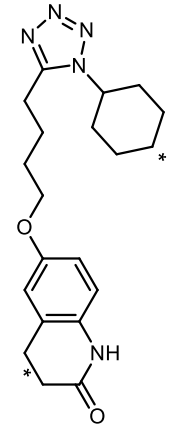	Cilostazol	CYP1A2 CYP2C19 CYP2D6 CYP3A4	MT43[151]	[151]

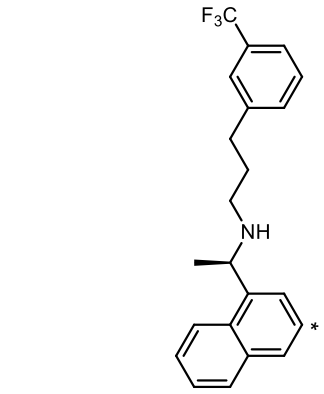	Cinacalcet	CYP3A4[331]	M01[151]	[151]
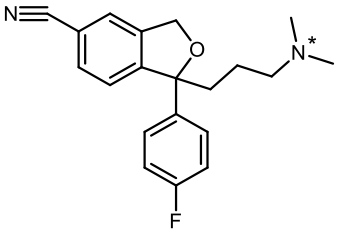	Citalopram	CYP2C19 CYP2D6	MT35[151]	[151]
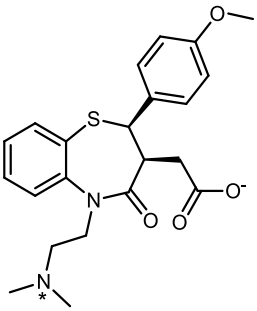	Diltiazem	CYP2C8 CYP2C9 CYP3A4	MT35[151]	[151]
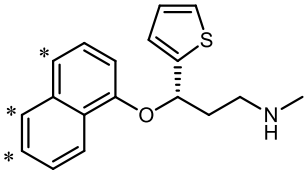	Duloxetine	CYP1A2 CYP2D6	MT38[151]	[151]
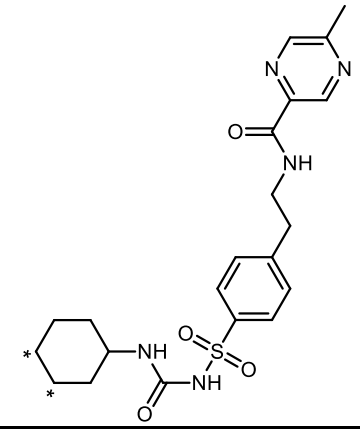	Glipizide	CYP2C9 CYP3A4	MT35[151]	[151]

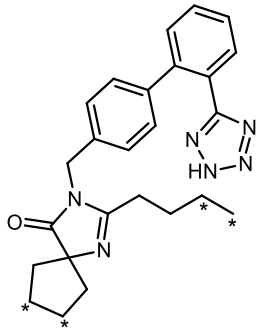	Irbesartan	CYP2C9	MT35[151]	[151]
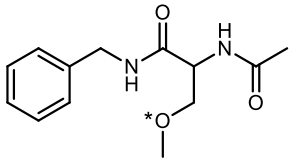	Lacosamide	CYP2C19	MT38[151]	[151]
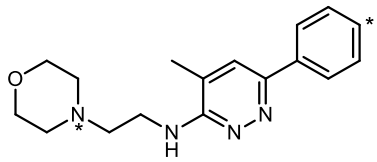	Minaprine	CYP1A1 CYP2D6	MT35[151]	[151]
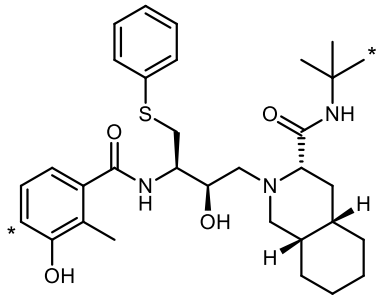	Nelfinavir	CYP2C9 CYP2C19 CYP3A4	MT43[151]	[151]
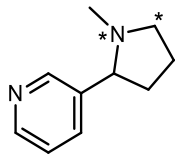	Nicotine	CYP1A1 CYP1A2 CYP2B6 CYP2C19 CYP2C8 CYP2C9 CYP2D6 CYP3A4	MT35[151]	[151]

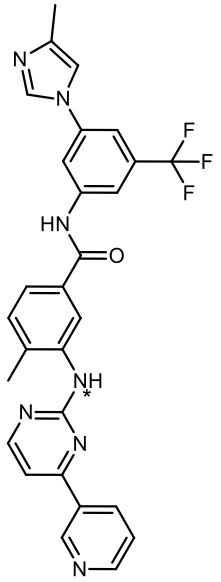	Nilotinib	CYP2C9[332] CYP3A4[332]	M02[151]	[151]
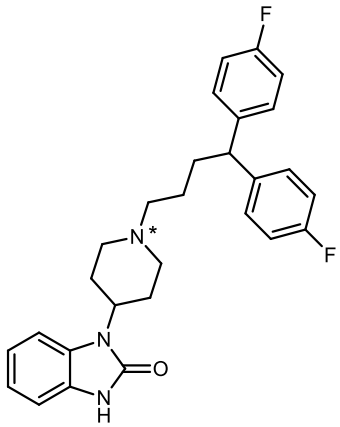	Pimozide	CYP1A2 CYP3A4	M02[151]	[151]
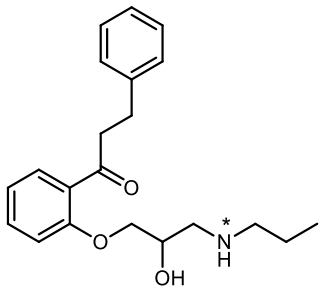	Propafenone	CYP1A2 CYP2D6 CYP3A4	MT35[151]	[151]

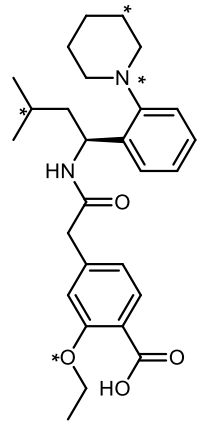	Repaglinide	CYP2C8 CYP3A4	MT35[151]	[151]
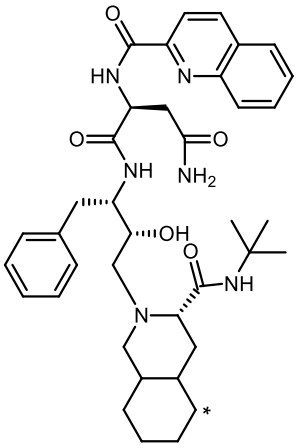	Saquinavir	CYP2D6 CYP3A4	MT35[151]	[151]
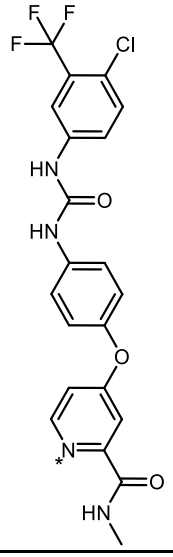	Sorafenib	CYP3A4[333]	MT38[151]	[151]

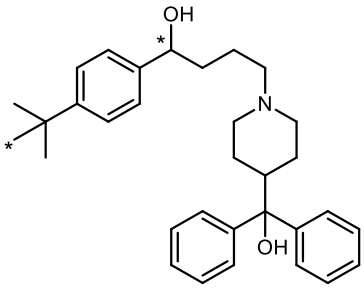	Terfenadine	CYP2C8 CYP2D6 CYP3A4	MT38[151]	[151]
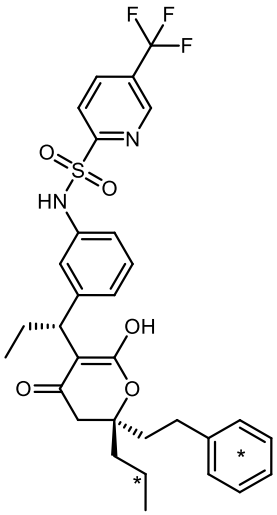	Tipranavir	CYP2D6[334] CYP2C9[334] CYP3A4[334]	MT43[151]	[151]
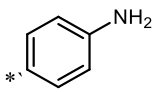	Analine	CYP2E1[229]	WT[229]	[229]
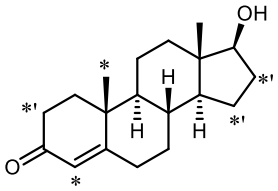	Testosterone	CYP19A1 CYP2C19 CYP3A4	M11[137]	[137]

Appendix 3. Mass Spectrometry Data

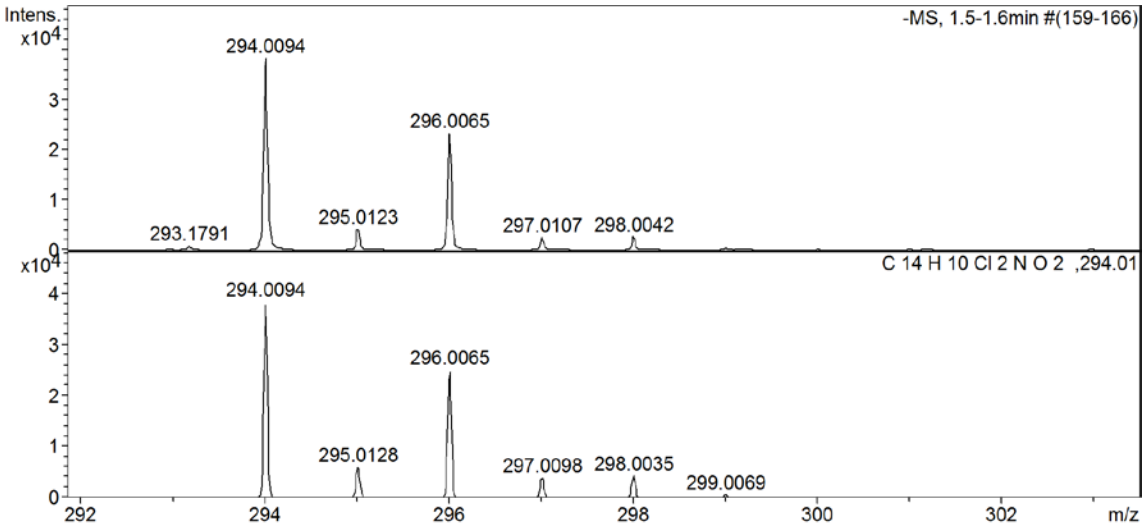

Figure A3.1. Accurate mass spectrum of diclofenac (top) and the theoretical isotope model (bottom).

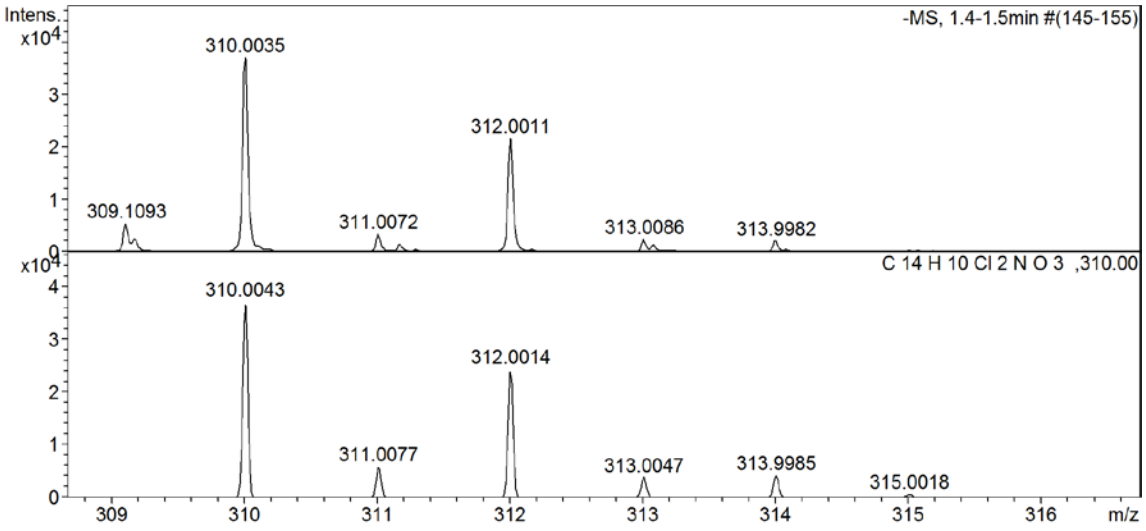

Figure A3.2. Accurate mass spectrum of the product of diclofenac metabolism by RP/FV/EV (top) and the theoretical isotope model (bottom).

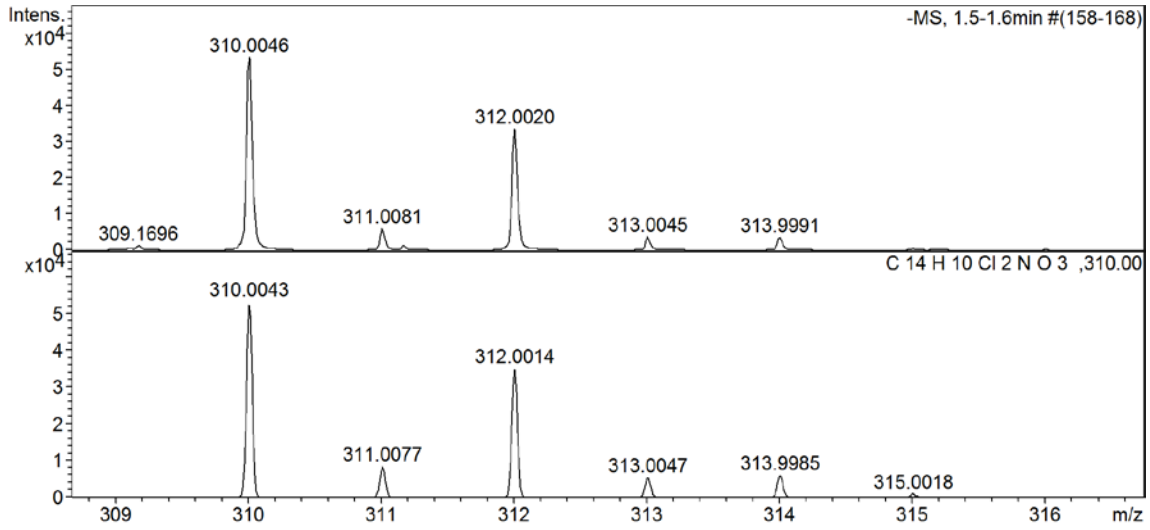

Figure A3.3. Accurate mass spectrum of the product of diclofenac metabolism by RP/FV/EV/F81W (top) and the theoretical isotope model (bottom).

Appendix 4. Cyclic voltammograms of potential mediators.

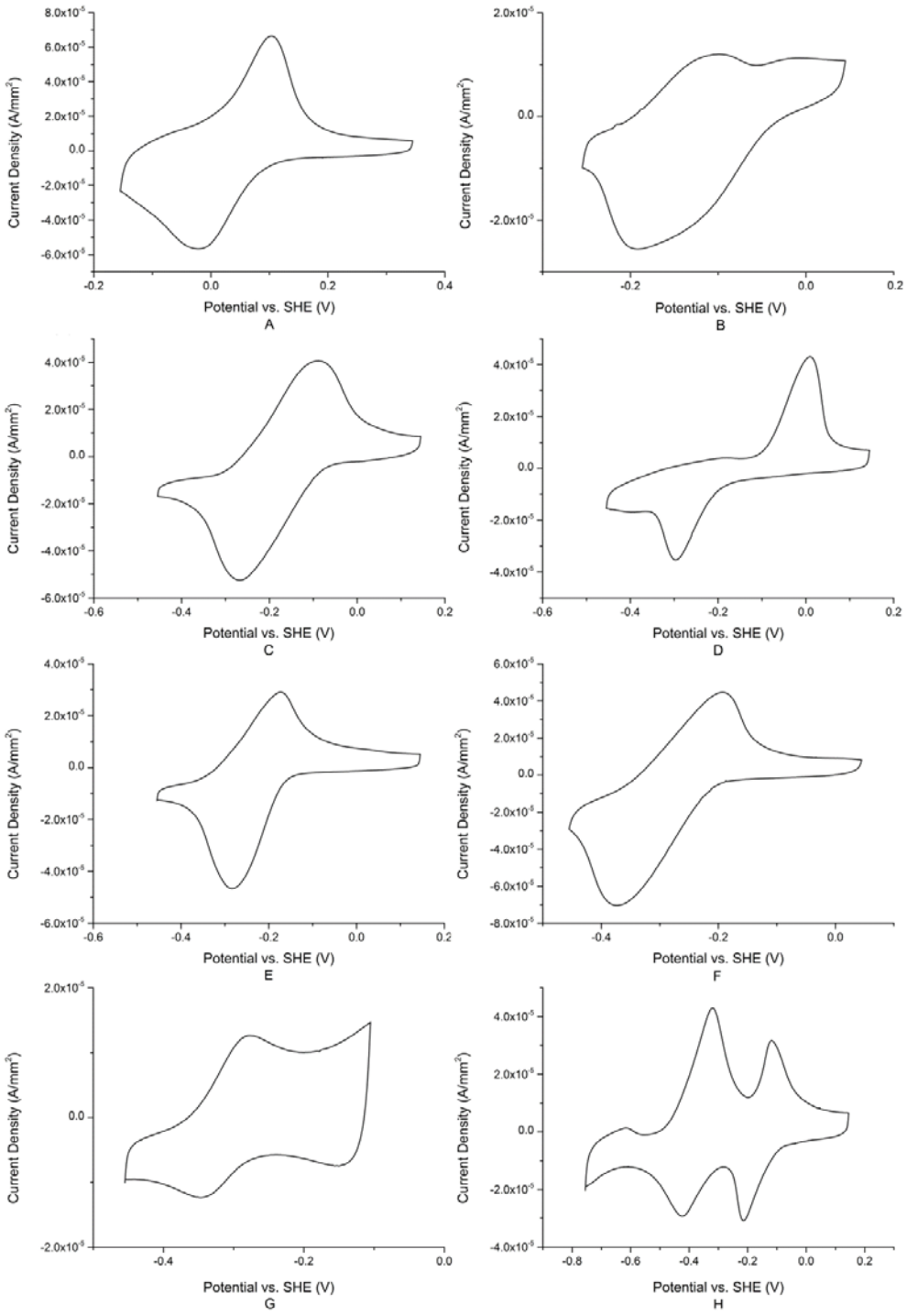

Figure A4.1. CVs taken using a graphite working electrode, platinum wire counter electrode and saturated calomel reference electrode in 50 mM Tris, pH 7.4 of 1 mM **(A)** methylene blue; **(B)** potassium indigo tetrasulfonate; **(C)** 2-hydroxy-1,4,naphthoquinone; **(D)** 9,10-anthraquinone-1,5-disulfonate; **(E)** 9,10-anthraquinone-2,6-disulfonate; **(F)** 9,10-anthraquinone-2-sulfonate; **(G)** benzyl viologen; **(H)** methyl viologen

Appendix 5. Sigmoid derived from the Nernst equation.

The Nernst equation is:

$$E_{app} = E_m + \frac{RT}{nF}\ln\frac{[\mathrm{O}]}{[\mathrm{R}]}$$

At any applied potential the absorbance is given by:

$$A(E_{app}) = \frac{[\mathrm{O}]}{[\mathrm{T}]}A_{\max} + \frac{[\mathrm{R}]}{[\mathrm{T}]}A_{\min} \qquad \mathbf{1}$$

where $A_{\max}$ is the absorbance of the oxidised form and $A_{\min}$ is that of the reduced form and

$$[\mathrm{T}] = [\mathrm{O}] + [\mathrm{R}] \qquad \mathbf{2}$$

Substituting **2** into **1**:

$$A(E_{app}) = \frac{[\mathrm{O}]}{[\mathrm{T}]}A_{\max} + \frac{[\mathrm{T}]-[\mathrm{O}]}{[\mathrm{T}]}A_{\min}$$

$$A(E_{app}) = \frac{[\mathrm{O}]}{[\mathrm{T}]}\left(A_{\max} - A_{\min}\right) + A_{\min} \qquad \mathbf{3}$$

From the Nernst equation we have:

$$\frac{[R]}{[O]} = \exp\left[\frac{nF\left(E_m - E_{app}\right)}{RT}\right] \qquad \mathbf{4}$$

Substituting **3** into **4**:

$$[\mathrm{T}] = [\mathrm{O}] + [\mathrm{O}]\exp\left[\frac{nF\left(E_m - E_{app}\right)}{RT}\right]$$

$$[\mathrm{T}] = [\mathrm{O}]\left\{1 + \exp\left[\frac{nF\left(E_m - E_{app}\right)}{RT}\right]\right\} \qquad \mathbf{5}$$

Substituting **5** into **3** gives the sigmoid derived from the Nernst equation:

$$A(E_{app}) = \frac{A_{\max} - A_{\min}}{1 + \exp\left[nF\left(E_m - E_{app}\right)/RT\right]} + A_{\min}$$